Complexity

Dynamical Analysis of Biological Systems 2021

Lead Guest Editor: George V. Popescu
Guest Editors: Eberhard O. Voit and Constantin Udriste

Dynamical Analysis of Biological Systems 2021

Complexity

Dynamical Analysis of Biological Systems 2021

Lead Guest Editor: George V. Popescu
Guest Editors: Eberhard O. Voit and Constantin Udriste

Contents

Hindawi
Complexity
Volume 2022, Article ID 9055480, 8 pages
https://doi.org/10.1155/2022/9055480

Research Article

Pattern Dynamics in a Predator-Prey Model with Diffusion Network

Wenjie Yang,[1] Qianqian Zheng,[1] Jianwei Shen,[2] and Qing Hu[2]

[1]*School of Science, Xuchang University, Xuchang, Henan 461000, China*
[2]*School of Mathematics and Statistics, North China University of Water Resources and Electric Power, Zhengzhou 450046, China*

Correspondence should be addressed to Jianwei Shen; phdshen@126.com

Received 30 July 2021; Revised 21 October 2021; Accepted 19 June 2022; Published 31 July 2022

Academic Editor: Eberhard O. Voit

Diffusion plays an essential role in the distribution of predator and prey. We mainly research the diffusion network's effect on the predator-prey model through bifurcation. First, it is found that the link probability and diffusion parameter can cause Turing instability in the network-organized predator-prey model. Then, the Turing stability region is obtained according to the sufficient condition of Turing instability and the eigenvalues' distribution. Finally, the biological mechanism is explained through our theoretical results, which are also illustrated by numerical simulation.

1. Introduction

Turing instability was first investigated in the reaction-diffusion system [1], and it is constantly being promoted to explain the dynamical mechanism [2, 3]. Asllani et al. pointed out that the directed network could induce Turing instability when an indirect network does not work [4, 5]. Meanwhile, tuning the topology structure of the system can create or destroy patterns in a reaction-diffusion system [6]. Mimar et al. proved that the pattern formation's topological properties are determined by complex interaction [7]. Although spontaneous patterns [8] are associated with the dominance of eigenvectors and eigenvalues [9–11], the dynamical mechanism of the random network in pattern formation remains to be uncovered.

Since the Lotka–Volterra model was proposed in the early twentieth century, some biological mechanisms were explained in the predator-prey system [12–18]. Chang et al. researched the dynamics in the predator-prey system on complex networks and found that Turing instability caused by delay can generate spiral waves [19]. Liu et al. showed the effect of network and diffusion on the ecological balance of the predator-prey system [20]. Upadhyay and Bhattacharya studied the differences between the aqueous and terrestrial environments in predator-prey networks and tried to explain their biological mechanism [21]. Astarloa et al. tried to use the joint species distribution modeling to reveal the coexistence problem of prey and predator in the Bay of Biscay [22]. Although previous work shows that diffusion and randomness influence the Turing pattern significantly, the random network's effect on the distribution of predator and prey should be carefully evaluated.

To reveal the natural mechanism of biological invasion, we intend to investigate the random diffusion network's effect on the network-organized predator-prey model's stability. First, we obtain the conditions under which Turing bifurcation arises. Second, we find an estimated region of all the eigenvalues of the Laplacian matrix, the sufficient stability conditions in the network-organized predator-prey model. Third, we explain the network-organized Turing instability by the mean-field approximation and comparison principle. Also, we estimate the Turing instability range about link probability and diffusion and try to explain the mechanism of biological invasion. Last, we illustrate our theoretical results through numerical simulation.

2. A Network-Organized Predator-Prey Model

For the convenience of subsequent research, we first give some necessary symbolic rules. The network Laplacian

matrix $L = \{L_{ij}\}$ can be treated as $L_{ij} = A_{ij} - k_i\delta_{ij}$, and all the eigenvalues of L are $\Lambda = \{\Lambda_i\}$. The eigenvectors $\phi_i \in R^n$ of Λ_i satisfy $L\phi_i = \Lambda_i\phi_i, i = 1, \ldots, n$. L is real symmetric, and we choose an orthonormal basis for $\phi_i\phi_j = \delta_{ij}$, where the degree of node i is k_i, and δ_{ij} is the Kronecker delta function.

We consider the following predator-prey system:

$$\begin{aligned}\frac{dx}{dt} &= x[r_1 - a_{11}x - a_{12}y],\\ \frac{dy}{dt} &= y[r_2 + a_{21}x - a_{22}y],\end{aligned} \tag{1}$$

where x and y are prey and predator, respectively. r_1 represents the intrinsic growth rate, a_{12} is the proportionality coefficient of predator and prey, and a_{21} is the growth rate of the predator; the predator increases exponentially with ratio r_2 (actually $r_2 < 0$ means the number of predators decreases exponentially). According to Samuelson's assumptions [23], a_{11} and a_{22} represent increasing returns or decreasing returns, respectively. Among them, $a_{ii} > 0\,(<0), (i = 1, 2)$ correspond to increasing returns (decreasing returns). System (1) correspond to the mixed-income when $a_{11}a_{22} \le 0$.

System (1) always has three equilibria $E_0 \triangleq (0, 0), E_1 \triangleq (r_1/a_{11}, 0)$, and $E_2 \triangleq (0, r_2/a_{22})$. System (1) also have fourth equilibrium point $E_3 \triangleq (x^*, y^*) \triangleq (r_1a_{22} - r_2a_{12}/a_{11}a_{22} + a_{12}a_{21}, r_1a_{21} + r_2a_{11}/a_{11}a_{22} + a_{12}a_{21})$ when $r_1a_{22} - r_2a_{12}/a_{11}a_{22} + a_{12}a_{21} > 0, r_1$ $a_{21} + r_2a_{11}/a_{11}a_{22} + a_{12}a_{21} > 0$. On the basis of Hopf bifurcation's definition, we need to satisfy $tr(J_{E_3}) = 0, \det(J_{E_3}) > 0$. The critical value for bifurcation is a positive root of $tr(J_{E_3}) = 0$ and the bifurcation parameter is $a_{12} = a_{12}^*$ which satisfies $\det(J_{E_3}) > 0$,

$$\begin{aligned}a_{12} &= \frac{(r_1 + r_2)a_{11}a_{22} + r_1a_{21}a_{22}}{r_2a_{11}} \triangleq a_{12}^*,\\ &\frac{r_2(r_1a_{21} + r_2a_{11})}{a_{11} + a_{21}} < 0.\end{aligned} \tag{2}$$

Then, we give the condition of Hopf bifurcation. Firstly, we verify the transversality condition [24].

$$\begin{aligned}\frac{d}{da_{12}} tr\left(J_{(x^*,y^*)}\right)\Big|_{a_{12}=a_{12}^*} &= -\frac{a_{22}(a_{11} + a_{21})(r_1a_{21} + r_2a_{11})}{(a_{11}a_{22} + a_{12}a_{21})^2}\Big|_{a_{12}=a_{12}^*}\\ &= -\frac{(r_2a_{11})^2}{a_{22}(a_{11} + a_{21})(r_1a_{21} + r_2a_{11})} \neq 0.\end{aligned} \tag{3}$$

Then, we compute the first Lyapunov coefficient [25]. Let $a_{12} = a_{12}^*$, then $(x^{*c}, y^{*c}) = (-(r_2/a_{11} + a_{21}), (r_2a_{11}/a_{22}(a_{11} + a_{21})))$. Making the following shift

$$\begin{aligned}X &= x - x^{*c},\\ Y &= y - y^{*c}.\end{aligned} \tag{4}$$

(1) becomes

$$\begin{aligned}\dot{X} &= \alpha_{10}X + \alpha_{01}Y + \alpha_{20}X^2 + \alpha_{11}XY,\\ \dot{Y} &= \beta_{10}X + \beta_{01}Y + \beta_{11}XY + \beta_{02}Y^2,\end{aligned} \tag{5}$$

where $\alpha_{10} = -a_{11}x^{*c}, \alpha_{01} = -a_{12}x^{*c}, \alpha_{20} = -a_{11}$, $\alpha_{11} = -a_{12}$, $\beta_{10} = a_{21}y^{*c}$, $\beta_{01} = -a_{22}y^{*c}, \beta_{11} = a_{21}, \beta_{02} = -a_{22}$.

The first Lyapunov coefficient at $a_{12} = a_{12}^*$ can be computed by the formula

$$\begin{aligned}l_1 &= \frac{-3\pi}{2\alpha_{01}\Delta^{3/2}}\left\{\left[\begin{array}{c}\alpha_{10}\alpha_{01}\left(\beta_{11}^2 - 2\alpha_{20}^2 + \alpha_{20}\beta_{11} + \alpha_{11}\beta_{02}\right) + \alpha_{10}\beta_{10}\left(\alpha_{11}^2 - 2\beta_{02}^2 + \alpha_{11}\beta_{02}\right)\\ +\alpha_{01}\beta_{10}(\beta_{11}\beta_{02} - \alpha_{11}\alpha_{20})\end{array}\right] - 2\alpha_{10}^2\beta_{11}\beta_{02} + 2\alpha_{10}^2\alpha_{11}\alpha_{20}\right\}\\ &= \frac{-3\pi}{2}\left(-\frac{a_{11} + a_{21}}{r_2(r_1a_{21} + r_2a_{11})}\right)^{3/2}\frac{(r_1a_{21} + r_1a_{11} + r_2a_{11})a_{22}^2}{a_{11} + a_{21}},\end{aligned} \tag{6}$$

where $\Delta = \alpha_{10}\beta_{01} - \alpha_{01}\beta_{10} > 0, \alpha_{10} + \beta_{01} = 0$, and if $l_1 < 0\,(>0)$, the Hopf bifurcation is supercritical (*resp.* subcritical).

When $r_1a_{22} - r_2a_{12}/a_{11}a_{22} + a_{12}a_{21} > 0, r_1 \;\; a_{21} + r_2a_{11}/a_{11}a_{22} + a_{12}a_{21} > 0$, E_3 changes its stability, and Hopf bifurcation occurs if $a_{12} = a_{12}^*$.

Typically, the distribution of individuals is spatially heterogeneous. So, we research (1) with a reaction-diffusion and network as follows:

$$\begin{aligned}\frac{dx_i}{dt} &= x_i[r_1 - a_{11}x_i - a_{12}y_i] + d_1\nabla^2x_i,\\ \frac{dy_i}{dt} &= y_i[r_2 + a_{21}x_i - a_{22}y_i] + d_2\nabla^2y_i,\end{aligned} \tag{7}$$

where d_1, d_2 are the diffusion constants.

Generally, we can regard diffusion as an interplay between network nodes. In this article, we consider a distinctive interaction between nodes. So the network-organized system (7) is

$$\frac{dx_i}{dt} = x_i[r_1 - a_{11}x_i - a_{12}y_i] + d_1\sum_j L_{ij}x_i,$$
$$\frac{dy_i}{dt} = y_i[r_2 + a_{21}x_i - a_{22}y_i] + d_2\sum_j L_{ij}y_i. \quad (8)$$

The linearized network-organized system of the system (8) is

$$\frac{dx_i}{dt} = \alpha_{10}x_i + \alpha_{01}y_i + d_1\sum_j L_{ij}x_i,$$
$$\frac{dy_i}{dt} = \beta_{10}x_i + \beta_{01}y_i + d_2\sum_j L_{ij}y_i. \quad (9)$$

The general solution of the linear network-organized system can be expressed as [3].

$$x_i = \sum_{k=1}^{N} c_k\beta_k e^{\lambda_k t}\phi_i^k,$$
$$y_i = \sum_{k=1}^{N} c_k e^{\lambda_k t}\phi_i^k, \quad (10)$$

where $\sum_j L_{ij}\phi_j^k = \Lambda_i\phi_i^k$.

Substituting the general solution into system (9), the Jacobian matrix $B_i\,(i = 1, \ldots, n)$ is

$$B_i = \begin{pmatrix} \alpha_{10} + d_1\Lambda_i & \alpha_{01} \\ \beta_{10} & \beta_{01} + d_2\Lambda_i \end{pmatrix}, \quad (11)$$

where all the eigenvalues of matrix L can be represented as $\Lambda_i\,(0 = \Lambda_1 > \Lambda_2 > \cdots > \Lambda_N)$. Then, system (8) has the following characteristic function:

$$\lambda^2 + p_{\Lambda_i}\lambda + q_{\Lambda_i} = 0, \quad (12)$$

where $p_{\Lambda_i} = -(\alpha_{10} + \beta_{01}) - (d_1 + d_2)\Lambda_i$, $q_{\Lambda_i} = d_1d_2\Lambda_i^2 + (\alpha_{10}d_2 + \beta_{01}d_1)\Lambda_i + \alpha_{10}\beta_{01} + \alpha_{01}\beta_{10}$. Turing instability occurs when there is a Λ_i with $\mathrm{Re}\lambda > 0$. From (12),

$$4d_1d_2(\alpha_{10}\beta_{01} + \alpha_{01}\beta_{10}) + (\alpha_{10}d_2 + \beta_{01}d_1)^2 = 0. \quad (13)$$

We can get the Turing instability's critical value about Λ (Skim $d_1 = 0.1562d_2$) in the reaction-diffusion system Figure 1. Note $k_{1c}^2, k_{2c}^2\,(k_{1c}^2 < k_{2c}^2)$ as two solutions of $\mathrm{Re}\lambda(k^2) = 0$, $\mathrm{Re}\lambda(k^2) > 0$ holds if $k^2 \in B = \{\lambda | k_{1c}^2 < \lambda < k_{2c}^2\}$ Figure 2 $(d_2 = 2)$. Turing instability of the reaction-diffusion system is the Turing instability's prerequisite in the network-organized system. Based on the Gershgorin circle theorem [9, 10], we have.

(i) Result 1: $k_{\max} = \max\{k_i\}, k_{\min} = \min\{k_i\}$ and Λ_i is the eigenvalue of the Laplacian matrix L, then, $\Lambda_i \in C = \{\Lambda_i | -2k_{\max} < \Lambda_i \le 0\}$.

(ii) Result 2: in a network-organized system, a system remains stable when no eigenvalue of L stays at the instability range $\Lambda \cap B = \Phi$, Turing instability occurs when $\Lambda \cap B \neq \Phi$, and $B \cap C \neq \Phi$ (C is the set of the eigenvalues of Laplacian matrix) induces the occurring of instability.

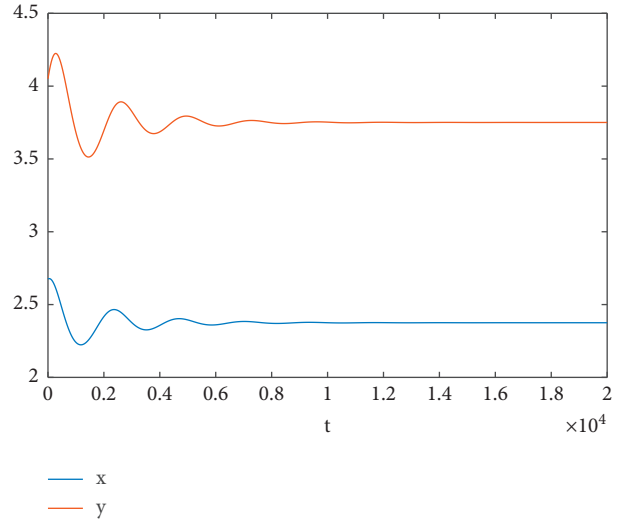

Figure 1: The stability of the system (1) without diffusion when $r_1 = 1, r_2 = -1, a_{11} = -1.158, a_{12} = 1, a_{21} = 2, a_{22} = 1$.

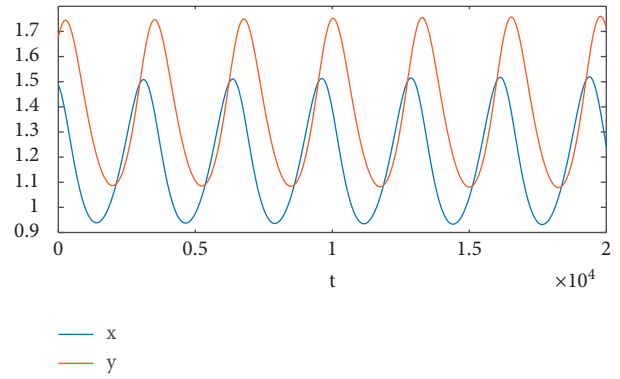

Figure 2: The stability of the system (1) without diffusion when $r_1 = 1, r_2 = -1, a_{11} = -1.158, a_{12} = 1.7271, a_{21} = 2, a_{22} = 1$.

To study the mechanism of the network-organized system's stability, we research (8) through the comparison principle: let $x_i = x^* + \varepsilon\hat{x}_i$ and $y_i = y^* + \varepsilon\hat{y}_i$, where $0 < \varepsilon \ll 1$. Substituting x_i, y_i in (9), expanding in ε, we can get the linearized system:

$$\frac{d\hat{x}_i}{dt} = \alpha_{10}\hat{x}_i + \alpha_{01}\hat{y}_i + d_1L\hat{x}_i,$$
$$\frac{d\hat{y}_i}{dt} = \beta_{10}\hat{x}_i + \beta_{01}\hat{y}_i + d_2L\hat{y}_i. \quad (14)$$

We resolve the first-order perturbations into ϕ_i's eigenfunction expansions, to consider the system's stability. Let

$$\hat{x}_i = \hat{X}_i\phi_i, \hat{Y}_i = \hat{Y}_i\phi_i, \text{for each} \quad i = 1, \ldots, n. \quad (15)$$

Substituting (15) into (20) and noting the properties of ϕ_i, we obtain

$$\frac{d\widehat{X}_i}{dt} = \alpha_{10}\widehat{X}_i + \alpha_{01}\widehat{Y}_i + d_1\Lambda_i\widehat{X}_i,$$
$$\frac{d\widehat{Y}_i}{dt} = \beta_{10}\widehat{X}_i + \beta_{01}\widehat{Y}_i + d_2\Lambda_i\widehat{Y}_i. \quad (16)$$

Using the comparison principle from [26], we note

$$\frac{d^2Y}{dt^2} + P(t)\frac{dY}{dt} + Q(t)Y = 0, \quad (17)$$

where $Q(t) < 0$. We eliminate one of $\widehat{X}_i$ or $\widehat{Y}_i$ from (16), then

$$\frac{d^2\widehat{X}_i}{dt^2} + p_{\Lambda_i}\frac{d\widehat{X}_i}{dt} + q_{\Lambda_i}\widehat{X}_i = 0,$$
$$\frac{d^2\widehat{Y}_i}{dt^2} + p_{\Lambda_i}\frac{d\widehat{Y}_i}{dt} + q_{\Lambda_i}\widehat{X}_i = 0, \quad (18)$$

where $p_{\Lambda_i}, q_{\Lambda_i}$ are as in (12). Then, we obtain the generalized condition:

$$\alpha_{10}\beta_{01} + \alpha_{01}\beta_{10} + (d_1\beta_{01} + d_2\alpha_{10})\Lambda_i + d_1d_2\Lambda_i^2 < 0. \quad (19)$$

Assume that the instability condition (19) holds. Then, the homogeneous state $(x_k, y_k) = (x^*, y^*)$ is unstable under the ith Turing mode (15).

We also consider the system (8) through the mean-field theory:

$$\frac{dx_i}{dt} = f(x_i, y_i) + d_1(H^x - k_ix_i),$$
$$\frac{dy_i}{dt} = g(x_i, y_i) + d_2(H^y - k_iy_i), \quad (20)$$

where $H^x = \sum_{j=1}^n A_{ij}x_j, H^y = \sum_{j=1}^n A_{ij}y_j$ and k_i is the network's degree. We let other nodes stay at equilibrium (x^*, y^*), and rewrite the single-node system,

$$\frac{dx_i}{dt} = x_i[r_1 - a_{11}x_i - a_{12}y_i] + d_1(x^* - k_ix_i),$$
$$\frac{dy_i}{dt} = y_i[r_2 + a_{21}x_i - a_{22}y_i] + d_2(y^* - k_iy_i). \quad (21)$$

Therefore, it is easy to obtain the characteristic equation:

$$\lambda^2 + p_{k_i}\lambda + q_{k_i} = 0, \quad (22)$$

where $p_{k_i} = -(\alpha_{10} + \beta_{01}) + d_1k_i + d_2k_i$, $q_{k_i} = \alpha_{10}\beta_{01} + (\alpha_{10}d_2 + \beta_{01}d_1)k_i + d_1d_2k_i^2$. Assume λ_1 and λ_2 are two eigenvalues of system (22). Then system (21) is stable when $d_1 = d_2 = 0$, namely $p_{k_i} > 0$, so $\lambda_1 + \lambda_2 = -p_{k_i} < 0$. If $q_{k_i} > 0$ ($q_{k_i} < 0$). Then, the system (21) is stable(unstable). To sum up, we can use the comparison principle(the mean-field theory) to conclude that the system (8) is unstable when $q_{\Lambda_i} < 0$ ($q_{k_i} < 0$).

3. Numerical Simulation

We give some numerical analysis based on the earlier theoretical analysis. From Figure 3, if we choose

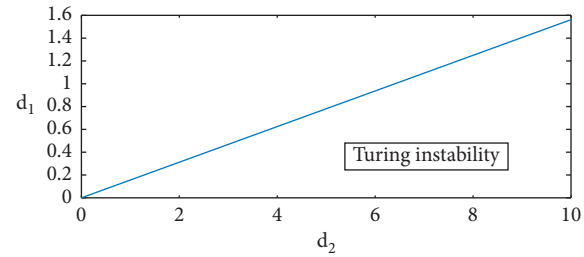

Figure 3: Turing bifurcation about d_2 and d_1 in the continuous system.

$r_1 = 1, r_2 = -1, a_{11} = -1.158, a_{12} = 1, a_{21} = 2, a_{22} = 1$, the equilibrium point (x^*, y^*) is asymptotically stable, namely, ecological balance persists as long as there is no biological invasion. That means the predator and the prey can coexist. The equilibrium $(x^{*c}, y^{*c}) = (1.1326, 1.2651)$ is unstable, and Hopf bifurcation occurs Figure 4, when a_{12} passes through the critical value $a_{12}^* = 1.7271$. Because $l_1 = 8.2123 > 0$, the Hopf bifurcation is subcritical, the prey-predator system shows periodic changes; thus, this state is easy to destroy. The equilibrium point (x^*, y^*) becomes unstable, when $a_{12} = 1.8271 > a_{12}^*$.

As diffusion is a vital factor in the distribution of predator and prey, we should not ignore migration. So we construct the random network and transform it into the Laplacian matrix L_{ij}. And we consider how the random network affects the equilibrium point's stability when (7) is stable.

Based on the above theoretical analysis, the Turing instability in the reaction-diffusion equation is a precondition for Turing instability in a network-organized system. Turing instability occurs in a reaction-diffusion equation when Turing bifurcation parameters d_2 and d_1 are in a certain range Figure 1. Namely, diffusion behavior is universal and allowed, but the relative diffusion rate needs to be within a specific range; otherwise, the ecosystem will be out of balance and destroyed.

To observe Turing instability in the network-organized, we should guarantee $d_1 < 0.1562d_2$ while changing p. However, the Laplacian matrix eigenvalues are $\Lambda_1, \Lambda_2, \ldots, \Lambda_N$, N is the number of nodes, and k^2 is continuous in a reaction-diffusion system. In other words, the distribution of $-\Lambda_i$ determines the system stability. The critical point is $d_{1c} = 0.3124$ when $d_2 = 2$. The range of eigenvalues Λ_i could be obtained by result 1. The eigenvalues of L are discrete and included in the continuous region Figure 2.

The red region shows the estimated range of Turing instability about (p, d_1) in Figure 5. Besides, we obtain the estimated range of p, $(d_2 \ln N/d_{1c}N) > p > (1/N^2)$, which determines the system dynamical behavior and network characteristics. Moreover, $p = \ln N/N$ is the critical value between the connected network and sparse network [27]. Anyway, the invasive rate of species and p in the predator-prey network play a vital role in balancing the native biological system.

Let the value of (p, d_1) lie in the blue region shown in Figure 5 (here, we set $p = 0.00006, d_1 = 0.1124$), then,

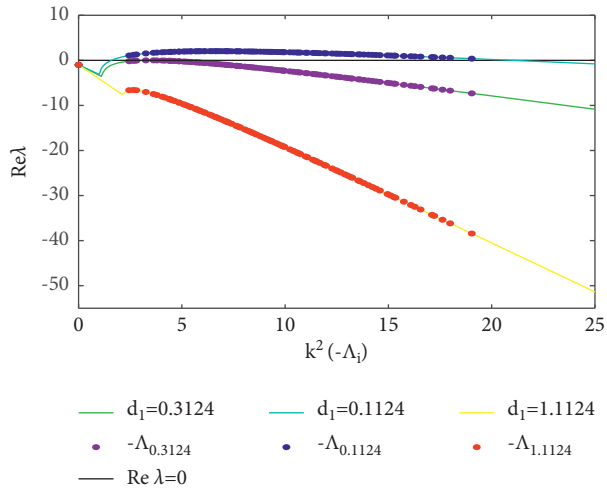

Figure 4: Linear stability analysis. The relationship between Reλ about $-\Lambda_i(k^2)$ when $r_1 = 1, r_2 = -1, a_{11} = -1.158, a_{12} = 1, a_{21} = 2, a_{22} = 1$, and $p = 0.1, d_2 = 2$. The critical values are $\Lambda_c = -3.35, d_{1c} = 0.3124$.

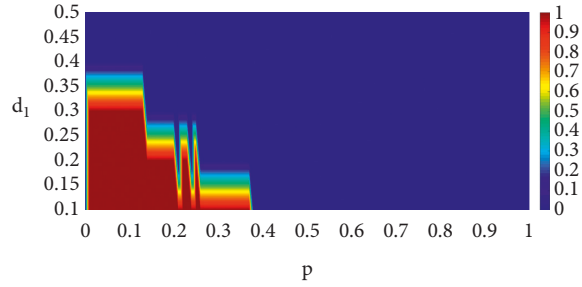

Figure 5: The region of instability about d_1 and p.

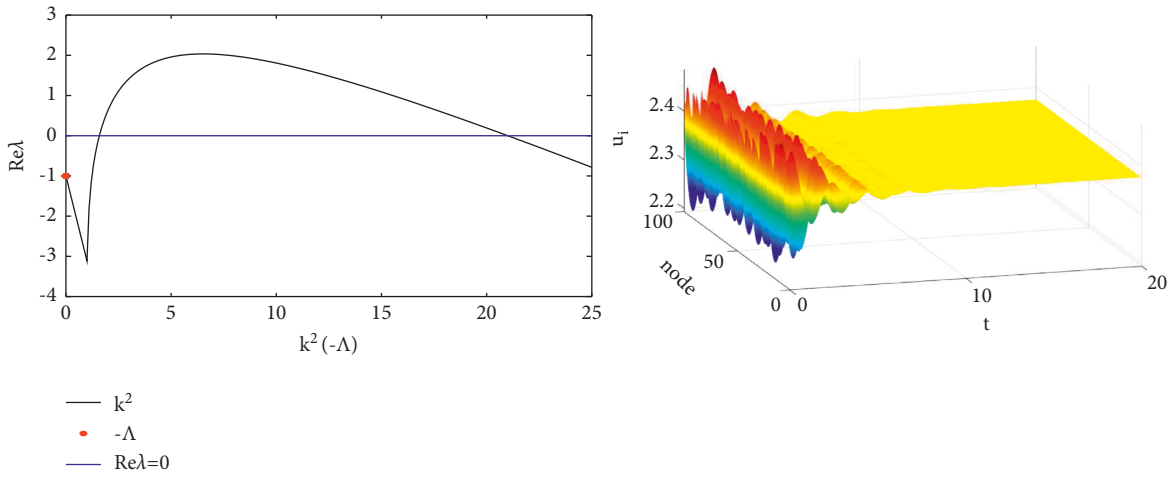

(a)

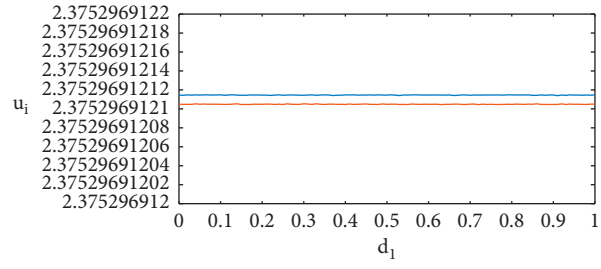

(b)

Figure 6: (a) Instability region (left) of random network and pattern formation (right) in random network when $p = 0.00006, d_1 = 0.1124$. (b) The bifurcation about d_1 when $p = 0.00006$.

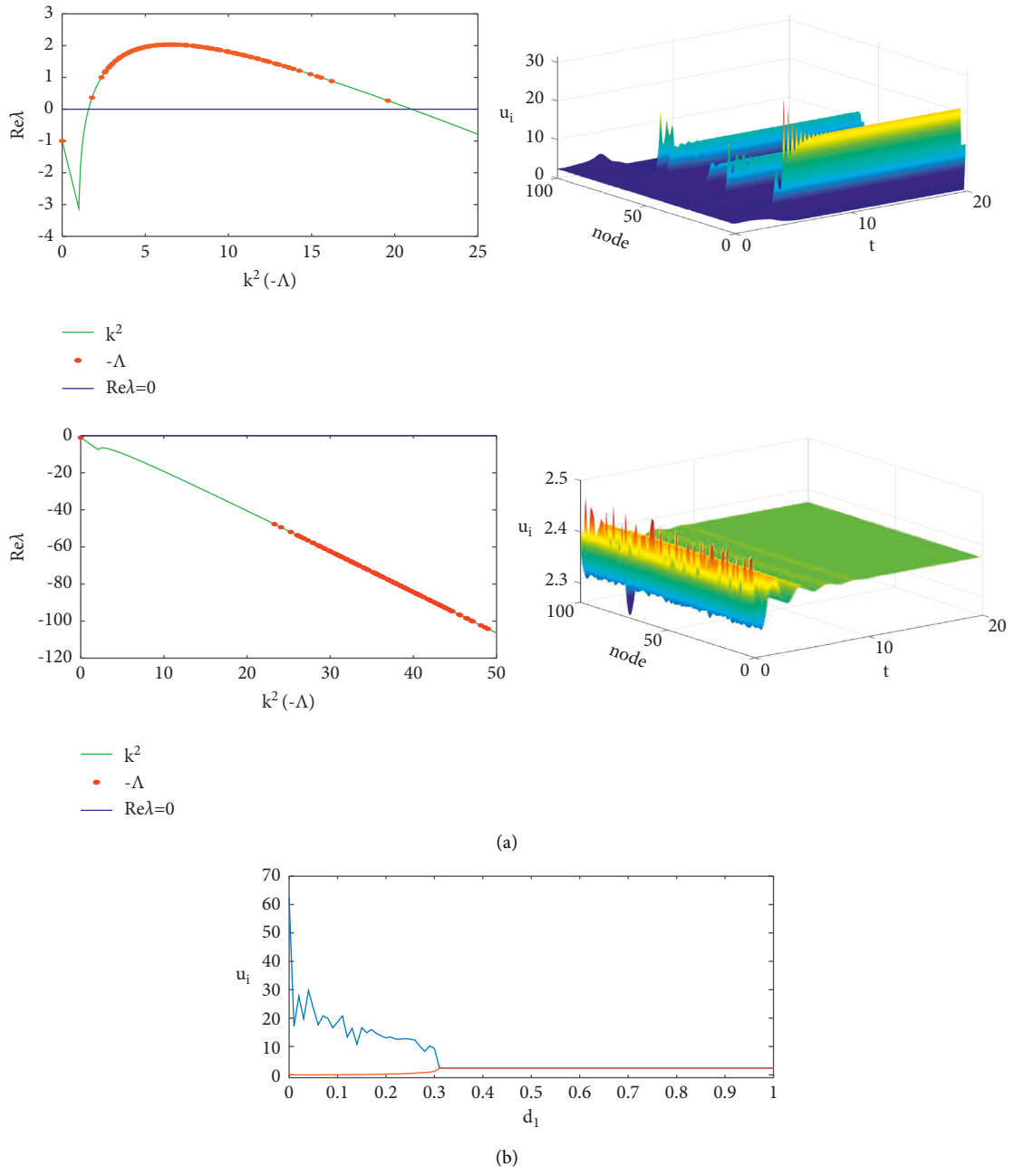

Figure 7: (a) The relationship between Reλ about $-\Lambda_i(k^2)$ (left) and the pattern formation of system (3) (right). Top: when $p = 0.08, d_1 = 0.1124$, almost all points $\Lambda_i(k^2)$ lie in the instability region and the Turing instability occurs. Bottom: when $p = 0.08, d_1 = 1.1124$, no point $\Lambda_i(k^2)$ lies in the instability region and the system is stable. (b) The bifurcation occurs about d_1 when $p = 0.08$.

there is no point Λ_i (k^2) in the instability region $\Lambda \cap (1.7, 21.1) = \Phi$ (result 2) (Figure 6(a)) and the equilibrium is stable (Figure 6(a)). We verified the correctness of the previous analysis with bifurcation diagrams (Figure 6(b)). We can conclude that with a fixed predator invasion rate and a fixed prey invasion rate, the link probability between two different systems will negatively impact the entire predator-prey network stability. Even the predator-prey network's diffusion induces the species extinction.

Figure 7 shows an example of p that belongs to the red region in Figure 5, such as $p = 0.08, d_1 = 0.1124 < d_{1c} = 0.3124$, almost all of $\Lambda_i(k^2)$ in instability region Figure 7(a) left(up) and 7(a) right(up) shows that Turing instability occurs. If $p = 0.08$ and $d_1 = 1.1124 > d_{1c} = 0.3124$ (i.e., (p, d_1) in the blue region in Figure 5), there is no point $\Lambda_i(k^2)$ in the instability region (Figure 7(a), left(down)), the system is stable (Figure 7(a), right(down)). We also verified the correctness of the previous analysis with a bifurcation diagram (Figure 7(b)).

The ecological interpretation is that the system is less stable when the invasion rate of the prey is lower when the link probability of predator-prey systems is fixed. Conversely, if we want to keep the predator-prey system stable, the invasion rate of the prey needs to be decreased.

4. Conclusion

This paper theoretically derives Turing instability conditions [28–31] in a predator-prey network and carries out a detailed numerical study. We study the effects of diffusion and link probability on pattern formation in a random system. The smaller the invasion rate d_1 of the prey undergoes, the easier the predator-prey network Turing instability. Meanwhile, Turing instability occurs when the link probability p falls in the approximate region $(d_2 \ln N/d_{1c}N) > p > (N^2/1)$, which depends on the system characteristics.

Regarding an explanatory biological mechanism, the link probability and the invasion rate significantly influence the entire predator-prey network stability. The lower the invasion rate of the prey is, the less stable it is. Conversely, the prey invasion rate can be increased if we want to keep the predator-prey system stable. That means we can find an equilibrium point between native and invasive species by adjusting the diffusion probability and species' invasion rate. Finally, we obtain the estimated region of p, $(d_2 \ln N/d_{1c}N) > p > (1/N^2)$. Thus, invasion rate of species and the link probability in the predator-prey network play a key role in balancing the native biological system.

Data Availability

All data and codes can be found on Baidu Wangpan (password: reff) and Baidu.

Conflicts of Interest

The authors declare that there are no conflicts of interest.

Acknowledgments

This work is supported by the National Natural Science Foundation of China (11772291,12002297), Basic research Project of Universities in Henan Province (21zx009), Young Talent Support Project of Henan (2020HYTP012), Key scientific research projects of Henan Institutions of Higher learning in 2021 (21B130004), and Program for Science and Technology Innovation Talents in Universities of Henan Province (22HASTIT018).

References

[1] A. Turing, "The chemical basis of morphogenesis," *Trans.-R.Soc.B*, vol. 237, pp. 37–72, 1952.

[2] H. G. Othmer and L. E. Scriven, "Instability and dynamic pattern in cellular networks," *Journal of Theoretical Biology*, vol. 32, no. 3, pp. 507–537, 1971.

[3] H. Nakao and A. S. Mikhailov, "Turing patterns in network-organized activator-inhibitor systems," *Nature Physics*, vol. 6, no. 7, pp. 544–550, 2010.

[4] M. Asllani, D. M. Busiello, T. Carletti, D. Fanelli, and G. Planchon, "Turing patterns in multiplex networks," *Physical Review A*, vol. 90, no. 4, Article ID 042814, 2014.

[5] M. Asllani, J. D. Challenger, F. S. Pavone, L. Sacconi, and D. Fanelli, "The theory of pattern formation on directed networks," *Nature Communications*, vol. 5, no. 1, p. 4517, 2014.

[6] M. Asllani, T. Carletti, and D. Fanelli, "Tune the topology to create or destroy patterns," *The European Physical Journal B*, vol. 89, no. 12, p. 260, 2016.

[7] S. Mimar, M. M. Juane, J. Park, A. P. Muñuzuri, and G. Ghoshal, "Turing patterns mediated by network topology in homogeneous active systems," *Physical Review A*, vol. 99, no. 6, 2019.

[8] Z. G. Song and J. Xu, "Stability switches and double Hopf bifurcation in a two-neural network system with multiple delays," *Cognitive Neurodynamics*, vol. 7, no. 6, pp. 505–521, 2013.

[9] S. Hata and H. Nakao, "Localization of Laplacian eigenvectors on random networks," *Scientific Reports*, vol. 7, no. 1, p. 1121, 2017.

[10] Q. Zheng, J. Shen, and Y. Xu, "Turing instability in the reaction-diffusion network," *Physical Review E*, vol. 102, no. 6, Article ID 062215, 2020.

[11] G. Cencetti, F. Battiston, T. Carletti, and D. Fanelli, "Turing-like patterns from purely reactive systems," 2019, https://arxiv.org/pdf/1909.05524.pdf.

[12] I. M. Bomze, "Lotka-Volterra equation and replicator dynamics: a two-dimensional classification," *Biological Cybernetics*, vol. 48, no. 3, pp. 201–211, 1983.

[13] J. Li, "Dynamics of age-structured predator-prey population models," *Journal of Mathematical Analysis and Applications*, vol. 152, no. 2, pp. 399–415, 1990.

[14] S. Ruan and D. Ruan, "Global analysis in a predator-prey system with nonmonotonic functional response," *SIAM Journal on Applied Mathematics*, vol. 61, no. 4, pp. 1445–1472, 2001.

[15] D. Pal and G. P. Samanta, "Effects of dispersal speed and strong Allee effect on stability of a two-patch predator-prey model," *International Journal of Dynamics and Control*, vol. 6, no. 4, pp. 1484–1495, 2018.

[16] S. Saha and G. P. Samanta, "Influence of dispersal and strong Allee effect on a two-patch predator-prey model," *International Journal of Dynamics and Control*, vol. 7, no. 4, pp. 1321–1349, 2019.

[17] G. P. Samanta, "Analysis of a nonautonomous delayed predator-prey system with a stage structure for the predator in a polluted environment," *International Journal of Mathematics and Mathematical Sciences*, vol. 2010, pp. 1–18, Article ID 891812, 2010.

[18] Y. S. Ji, J. W. Shen, and X. C. Mao, "Pattern formation of Brusselator in the reaction-diffusion system," *Discrete and Continuous Dynamical Systems - S*, 2022, in Press.

[19] L. Chang, C. Liu, G. Sun, Z. Wang, and Z. Jin, "Delay-induced patterns in a predator-prey model on complex networks with diffusion," *New Journal of Physics*, vol. 21, no. 7, Article ID 073035, 2019.

[20] C. Liu, L. Chang, Y. Huang, and Z. Wang, "Turing patterns in a predator-prey model on complex networks," *Nonlinear Dynamics*, vol. 99, no. 4, pp. 3313–3322, 2020.

[21] S. Upadhyay and S. Bhattacharya, "A spectral graph theoretic study of predator-prey networks," 2019, https://arxiv.org/abs/1901.02883.

[22] A. Astarloa, M. Louzao, G. Boyra et al., "Identifying main interactions in marine predator-prey networks of the Bay of Biscay," *ICES Journal of Marine Science*, vol. 76, no. 7, pp. 2247–2259, 2019.
[23] H. I. Freedman, *Deterministic mathematical models in population ecology*, Marcel Dekker, New York, NY, U.S.A, 1980.
[24] Y. Lv, Z. Zhang, R. Yuan, and Y. Pei, "Effect of harvesting and prey refuge in a prey-predator system," *Journal of Biological Systems*, vol. 22, no. 01, pp. 133–150, 2014.
[25] Y. Kuznetsov, *Elements of Applied Bifurcation Theory*, Springer-Verlag, New York, NY, U.S.A, 2nd ed edition, 1998.
[26] N. McCullen and T. Wagenknecht, "Pattern formation on networks: from localised activity to Turing patterns," *Scientific Reports*, vol. 6, no. 1, Article ID 27397, 2016.
[27] N. Iqbal, R. C. Wu, and B. Liu, "Pattern formation by super-diffusion in FitzHugh-Nagumo model," *Applied Mathematics and Computation*, vol. 313, pp. 245–258, 2017.
[28] Q. Zheng and J. Shen, "Turing instability induced by random network in FitzHugh-nagumo model," *Applied Mathematics and Computation*, vol. 381, no. 1, Article ID 125304, 2020.
[29] Q. Zheng, J. Shen, and Y. Xu, "Spontaneous activity induced by Gaussian noise in the modified FitzHugh-nagumo model," *Neural Plasticity*, vol. 2020, Article ID 6651441, 2020.
[30] Y. Ji and J. Shen, "Turing instability of Brusselator in the reaction-diffusion," *Complexity*, vol. 2020, Article ID 1572743, 2020.
[31] Q. Zheng, J. Shen, and Z. Wang, "pattern formation and oscillations in reaction-diffusion model with p53-mdm2 feedback loop," *International Journal of Bifurcation and Chaos*, vol. 29, no. 14, Article ID 1930040, 2019.

Hindawi
Complexity
Volume 2022, Article ID 7903450, 18 pages
https://doi.org/10.1155/2022/7903450

Research Article

A State-Dependent Impulsive Nonlinear System with Ratio-Dependent Action Threshold for Investigating the Pest-Natural Enemy Model

Ihsan Ullah Khan,[1] Saif Ullah,[2,3] Ebenezer Bonyah,[4] Basem Al Alwan,[5] and Ahmed Alshehri[6]

[1]*Department of Mathematics, Institute of Numerical Sciences, Gomal University, Dera Ismail Khan 29050, KPK, Pakistan*
[2]*Department of Mathematics, University of Peshawar, Peshawar, Pakistan*
[3]*Department of Mathematics, Faculty of Science and Technology, Universitas Airlangga, Surabaya 60115, Indonesia*
[4]*Department of Mathematics Education, Akenten Appiah Menka University of Skills Training and Entrepreneurial Development, Kumasi, Ghana*
[5]*Chemical Engineering Department, College of Engineering, King Khalid University, Abha 61411, Saudi Arabia*
[6]*Department of Mathematics, Faculty of Sciences, King Abdulaziz University, Jeddah 21589, Saudi Arabia*

Correspondence should be addressed to Ebenezer Bonyah; ebbonya@gmail.com

Received 20 September 2021; Accepted 17 December 2021; Published 18 January 2022

Academic Editor: George V. Popescu

Based on the Lotka–Volterra system, a pest-natural enemy model with nonlinear feedback control as well as nonlinear action threshold is introduced. The model characterizes the implementation of comprehensive prevention and control measures when the pest density reaches the nonlinear action threshold level depending on the pest density and its change rate. The mortality rate of the pest is a saturation function that strictly depends on their density while the release of natural enemies is also a nonlinear pulse term depending on the density of real-time natural enemies. The exact impulsive and phase sets are given. The definition and properties of the Poincaré map corresponding to the pulse points on the phase set are provided. We investigate the existence and stability of boundary and interior order-1 periodic solution. The theoretical analysis developed in the present paper combined with nonlinear controlling measures as well as nonlinear action threshold methods and techniques laid the foundation for the establishment and analysis of other state-dependent feedback control models.

1. Introduction

Pest control [1–6] is not only an ancient problem but also a new challenge faced by the modern world. Various scientific and effective methods [7–13] are needed to comprehensively prevent and control pest outbreaks and reinfestation. The most common early method was chemical control [14, 15], that is, the method of controlling pest by spraying pesticides during pest outbreaks. The main advantages of chemical control are quick effect and convenient use. It can eradicate or maintain the number of pests at a lower level within a short period of time. Therefore, chemical control is still one of the important means to control pest population. Biological control [16–18] is another important control method, which has the advantages of strong effect and long duration, and is also an environmental friendly control method. Maiti et al. [19] used a valuable technique known as sterile insect release method (SIRM) to manage the pest population. The authors discussed the effect of uncertain ecological variations on sterile and fertile insects. Other main methods are physical control and agricultural control. For example, the agricultural control method is a method to reduce or control pests through measures such as crop rotation, intercropping, and reasonable adjustment of cultivation procedures.

Each pest control method has its advantages and disadvantages. Due to long-term and high-dose use, pests can easily develop resistance to specific pesticides, resulting in pest control failure and pest reemergance. However, other control strategies cannot effectively reduce the number of pests in a short time because of their slow effectiveness. Therefore, how to effectively and reasonably use multiple methods is the best choice for pest control. Based on this, the Food and Agriculture Organization of the United Nations (FAO) proposed the concept of integrated pest management (IPM) [1, 20, 21] and defined it as follows: "IPM is a pest control system that comprehensively considers the population dynamics of the pest and its related environment and uses all appropriate control techniques and methods that work as closely as possible to maintain levels at which pest populations do not cause economic harm." Both experimentally [22, 23] and theoretically [24, 25], it has been proved that IPM is more practical than the classic approach. This is one of the most useful methods which minimizes damage to individuals and the environment in addressing pest control.

In this perspective, researchers have studied the mathematical problems based on impulsive differential equations in order investigate the dynamics of IPM and compass biped robotic systems. In numerous realistic problems, impulses often occur at state-dependent. Therefore, it is more feasible to apply the procedure of state-dependent feedback control to model real-world issues. Znegui et al. [26] used an impulsive hybrid nonlinear system to construct a passive biped robot model that demonstrates complicated behaviors. In [27], the authors constructed a Poincaré map which was further utilized to examine the existence and stability of order-1 periodic type solution of the problem under consideration. Many new systems on the design of specific analytical expression of the hybrid state-dependent Poincaré were studied in [28, 29]. The authors in [26–29] portrayed an expression of the controlled Poincaré map to discuss the stabilization of passive dynamic walking of the compass-gait biped robot. The compass-gait biped robot is a two-DoF legged mechanical system which is identified by its passive dynamic walking. The one-DoF mechanical systems are also of great importance. Some articles related to one-DoF state-feedback control with respect to different perspectives can be found in [30, 31].

The impulsive differential equations are also used proficiently in epidemic dynamics [32] and population dynamics [33–35]. A basic assumption of the above series of studies is that regardless of how huge the number of pests or the growth rate is, as long as the number of pest populations touches economic threshold (ET) [33–35], the IPM strategy can be implemented. However, there are two basic situations of actual pest growth that require high attention: first, the number of pests is comparatively large, and the rate of change is small; second, the population is small, but the rate of change is high. A fundamental problem illustrated by these two situations is that when the pest population is large (such as exceeding ET), the growth rate is small or even negative at this time. In this case, even if the IPM strategy is not implemented, the number of pests may not exceed economic injury level (EIL) [36]. Another situation is that the number of pests is not large, and the rate at which the pest population is growing is very large. In this case, if the control strategy is not implemented in time, it may lead to a large outbreak of pests. Next, in order to establish appropriate and effective integrated controlling strategies, the IPM process needs precise inspection of the pest quantity. The mortality rate should be fluctuated according to the saturating function which relies upon the density of pest, and the releasing quantity of natural enemies should be a function of their density. Therefore, keeping in mind the above factors, a feasible new state-feedback control pest-natural enemy ecosystem with nonlinear controlling measures as well as nonlinear action threshold system is proposed. The corresponding analytical techniques and numerical methods are developed to examine the dynamical aspects of the system under consideration.

The main research contents are reflected in the following aspects. We construct a Lotka–Volterra prey-predator model involving both nonlinear feedback and action threshold depending on the density of pest and its change rate. In the model, we use the action threshold instead of the economic threshold to characterize the implementation of control measures, that is, when the number of pests reaches the action threshold depending on the density of pest and its change rate, a comprehensive pest control tactic is applied so that the number of pests does not exceed the nonlinear ratio-dependent AT. On the other hand, the use of nonlinear controlling factors in the feedback control makes the model closer to reality. Properties of the nonlinear ratio-dependent AT are given. Then, the classification is performed according to the positional relationship between the action threshold level and the stable equilibrium point of the corresponding ordinary differential system. By using the definition and properties of Lambert W function, the analytical expression of the Poincaré map is given. Furthermore, by using the analytical properties of Poincaré map, the existence, uniqueness, and stability of the pest-free and interior-order one periodic solution of the pest-natural enemy system are given, and corresponding sufficient conditions are obtained. The main results are confirmed by numerical simulations.

2. Model Construction and Main Properties of Action Threshold

2.1. Construction of Model. In view of the above objective factors, we propose the following nonlinear state-dependent feedback control model combined with nonlinear ratio-dependent AT:

$$\begin{cases} \left.\begin{aligned} \frac{dx(t)}{dt} &= ax(t) - bx(t)y(t), \\ \frac{dy(t)}{dt} &= cx(t)y(t) - dy(t), \end{aligned}\right\} \theta_1 x(t) + \theta_2 \frac{dx(t)}{dt} < AT, \\ \left.\begin{aligned} x(t^+) &= \left(1 - \frac{\delta x(t)}{x(t)+\alpha}\right)x(t), \\ y(t^+) &= y(t) + \frac{v}{1+\beta y(t)}, \end{aligned}\right\} \theta_1 x(t) + \theta_2 \frac{dx(t)}{dt} = AT. \end{cases} \tag{1}$$

It can be seen that without pulse control measures, the model is simply based on the classical Lotka–Volterra type problem which is extensively used to describe the relation between the populations of pest and natural enemy shown by $x(t)$ and $y(t)$, respectively. Weighted parameters θ_1, θ_2, and AT are positive constants, which satisfy $\theta_1 + \theta_2 = 1$. The discontinuous mapping shown in the third and fourth equations in system (1) represents that the implementation of comprehensive control measures depends on the action level, that is, once the pest density reaches action threshold, the densities of pests as well as the natural enemies are immediately updated to $(1 - \delta x(t)/x(t) + \alpha)x(t)$ and $y(t) + v/1 + \beta y(t)$, respectively. $\alpha > 0$ represents the semisaturation constant, $\delta > 0$ is defined as the maximum instantaneous killing rate after the use of pesticides, and $v > 0$ is the maximum natural enemy when executing the control strategy. The amount $\beta > 0$ is the natural enemy density adjustment parameter. The nonlinear term $v/1 + \beta y(t)$ shows a function of $y(t)$ which decreases monotonically, and the maximum amount of natural enemy release does not exceed. The symbols $x(0^+)$ with $y(0^+)$, respectively, represent the initial populations of pests and natural enemies and satisfy $x(0^+) + y(0^+) < AT$. In model (1), there always exist a stable centre $E_0 = (d/c, a/b)$ and a saddle point $(0, 0)$ which is unstable.

The special cases of the above model for different parameters were considered in [37–39]. The biological significance and main properties of the corresponding ODE model can be seen in [37]. In [38], Tian et al. extended the classic pest-natural enemy model with linear state-dependent control measures to a model with nonlinear state-dependent impulsive control tactics. In [39], the authors for the first time introduced and provided the concept of action threshold depending on the density of pest and its rate of change. They used the definition and properties of the Lambert W function to construct the analytical expression of the Poincaré map. Furthermore, by using the analytical properties of Poincaré map, the existence, uniqueness, and stability of the natural enemy free periodic solution and internal periodic solution were discussed in detail. The results explain the significance of nonlinear ratio-dependent AT in integrated pest control and the important guiding role in IPM strategy.

2.2. Properties of Action Threshold. The quantities θ_1 and θ_2 are dependent weighted parameters. If $\theta_2 = 0$, then the ratio-dependent AT converts into ET. Therefore, we can say that ET is a special case of ratio-dependent AT for $\theta_2 = 0$. Combining the first equation of ODE model (1) with ratio-dependent AT, we get

$$\lim_{x \longrightarrow +\infty} \frac{(\theta_1 + a\theta_2)x - AT}{b\theta_2 x} = \frac{\theta_1 + a\theta_2}{b\theta_2}. \tag{2}$$

If we put $\theta_1 = 0$, then the ratio-dependent AT converts into $y = ax - AT/bx$. In this case, if $x \longrightarrow +\infty$, then y is bounded and reaches its highest value a/b. Further, with the utilization of the control actions on $y = (\theta_1 + a\theta_2)x - AT/b\theta_2 x$, we get another curve $y^+ = (\theta_1 + a\theta_2)x^+ - AT(1 - \delta x(t)/x(t) + \alpha)/b\theta_2 x^+ + v/1 + \beta y$. For $\theta_2 = 0$, the curve changes into $x^+ = (1 - \delta x/x + \alpha)AT$ showing a vertical straight line. Let $P_{AT} = \delta x/x + \alpha$; then, for convenience, we denote the two curves $y = (\theta_1 + a\theta_2)x - AT/b\theta_2 x$ and $y^+ = (\theta_1 + a\theta_2)x^+ - AT(1 - P_{AT})/b\theta_2 x^+ + v/1 + \beta y$ by Γ_{IS} and Γ_{PS}, respectively, as shown in Figure 1.

3. Impulsive and Phase Sets

This section is devoted to present the dynamical aspects of the system (1), and we can use the Poincaré map on the sequence of pulse points which will be formulated later. Let AT/θ_1 be the abscissa of the curves Γ_{IS} at $y = a/b$.

Then, we take the following cases based on the equilibrium E_0 and curve Γ_{IS}.

$$(A)\ \frac{AT}{\theta_1} \leq \frac{d}{c};\ (B)\ \frac{d}{c} < \frac{AT}{\theta_1}. \tag{3}$$

The necessary and primary component is to examine the section that is not used during the pulse effect process, which means that the trajectory initiating from Γ_{PS} cannot touch the curve Γ_{IS} in the case of maximum impulsive set. In the following part of the paper, we address the definition of impulsive sets.

3.1. Impulsive Set. In Case (A), the solution Γ_1 is tangent to the curve Γ_{PS} at point $T = (x_T, y_T)$. If we denote the impulsive set by $\mathscr{M}_1$, then it can be written as

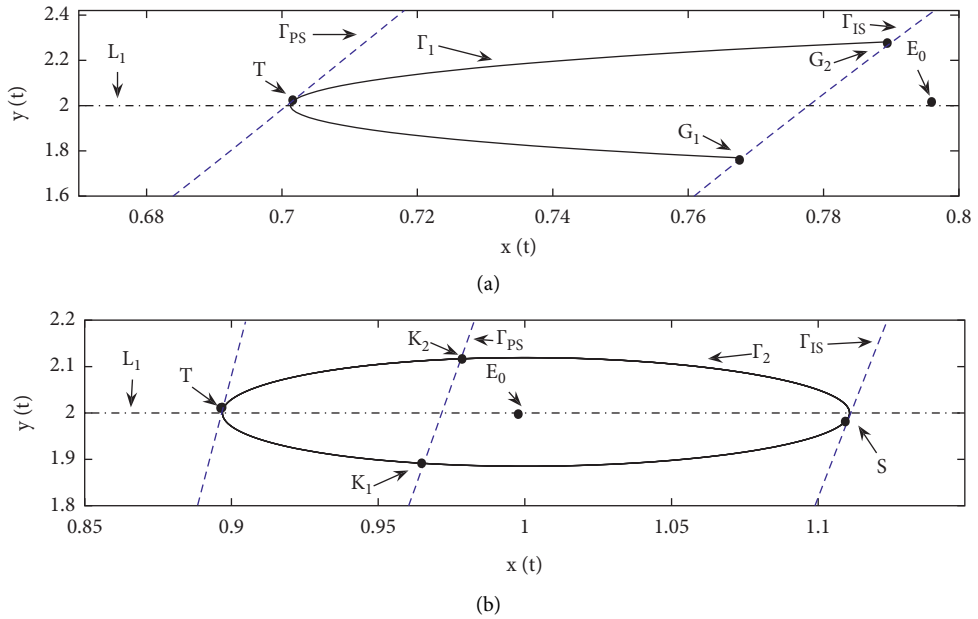

FIGURE 1: Detailed diagrams describing the impulsive along with phase sets where (a) $AT/\theta_1 \le d/c$ and $AT/\theta_1 > d/c$. In sub-plot (a), Γ_1 shows the tangent trajectory to the curve Γ_{PS} and touches the curve Γ_{IS} at (x_{G_2}, y_{G_2}). In sub-plot (b), Γ_2 touches the curve Γ_{PS} at two points (x_{K_1}, y_{K_1}) and (x_{K_2}, y_{K_2}), and tangent to the curve Γ_{IS} at point (x_S, y_S).

$$\mathcal{M}_1 = \left\{(x,y) \in \mathbb{R}^2_+ \middle| \frac{AT}{\theta_1 + a\theta_2} \le x \le x_{G_2}, 0 \le y \le y_{G_2}\right\}. \quad (4)$$

Now based on the corresponding horizontal coordinate, we search the exact value of y_{G_2} in the following lemma. The point y_{G_2} is actually the maximum value of the impulsive set $\mathcal{M}_1$ for Case (A).

Lemma 1. *For Case (A), the maximum impulsive set is defined as $\mathcal{M}_1$ with*

$$y_{G_2} = -\frac{a}{b} W\left(-\frac{b}{a} y_T e^{-b/a y_T + A_{G_2}/a}\right) \text{provided that } A^1_{G_2} \le 0. \quad (5)$$

Proof. Let Γ_1 be a trajectory tangent at $T = (x_T, y_T)$, and it touches the curve Γ_{IS} at point $G_2 = (x_{G_2}, y_{G_2})$. Then, T and G_2 must satisfy the following equation:

$$a \ln y_{G_2} - b y_{G_2} + d \ln x_{G_2} - c x_{G_2} = a \ln y_T - b y_T + d \ln x_T - c x_T. \quad (6)$$

Solving this equation for y_{G_2}, we get

$$\left(-\frac{b}{a} y_{G_2}\right) e^{-b/a y_{G_2}} = -\frac{b}{a} y_T e^{-b/a y_T + A_{G_2}/a}, \quad (7)$$

where $A_{G_2} = d(\ln x_T - \ln x_{Q_2}) + c(x_{G_2} - x_T)$. The above equation obviously gives two solutions when we solve it by using Lambert W function. The minimum solution can be written as follows:

$$y_{G_2} = -\frac{a}{b} W\left(-\frac{b}{a} y_T e^{-b/a y_T + A_{G_2}/a}\right), \quad (8)$$

which is well defined because $A_{G_2} \le 0$.

For Case (B), it is clear from Figure 1(b) that at point $S = (x_S, y_S)$, Γ_2 is tangent to the curve Γ_{IS} where $y_S \le a/b$. Then, taking into account the locations of equilibrium E_0 and the curve Γ_{IS}, we can write the maximum impulsive set for Case (B) as

$$\mathcal{M}_2 = \left\{(x,y) \in \mathbb{R}^2 \middle| \frac{AT}{\theta_1 + a\theta_2} \le x \le x_S, 0 \le y \le y_S\right\}. \quad (9)$$

The above information shows that for this case, the tangent point with Γ_{IS} varies due to small changes in θ_1 and θ_2.

If the weighted parameter θ_2 decreases, then the quantity y_S approaches its maximum value a/b. □

3.2. Phase Set. To determine the exact phase set of system (1) under different conditions, we need to know whether the solution from initial point (x_0^+, y_0^+) reaches the corresponding impulsive set and whether the pulse action occurs or not. To provide the exact domain of phase sets, we first discuss the interval which is free of impulsive effect.

Lemma 2. *For Case (B), any solution starting from the phase set with initial point (x_0^+, y_0^+) (where $y_0^+ \in (y_{K_2}, y_{K_1})$) will not reach the impulsive set $\mathcal{M}_2$, where*

$$y_{K_1} = -\frac{a}{b}W\left(-1, -\frac{b}{a}y_S e^{-b/ay_S - A_{K_1}/a}\right) \text{and } y_{K_2} = -\frac{a}{b}W\left(-\frac{b}{a}y_S e^{-b/ay_S - A_{K_2}/a}\right), \tag{10}$$

provided that $A_{K_1}, A_{K_2} \geq 0$.

Proof. Assume that the closed trajectory Γ_1 starts from $K_1 = (x_{K_1}, y_{K_1})$ and touches the curve Γ_{IS} at point $S = (x_S, y_S)$. Then, K_1 and S must satisfy the following relationship:

$$\begin{aligned} a\ln y_{K_1} - by_{K_1} + d\ln x_{K_1} - cx_{K_1} &= a\ln y_S - by_S \\ &+ d\ln x_S - cx_S. \end{aligned} \tag{11}$$

Rearranging this equation for y_{K_1}, we get

$$\left(-\frac{b}{a}y_{K_1}\right)e^{-b/ay_{K_1}} = -\frac{b}{a}y_S e^{-b/ay_S - A_{K_1}/a}, \tag{12}$$

where $A_{K_1} = d(\ln x_{K_1} - \ln x_S) + c(x_S - x_{K_1})$. The above equation can be easily solved utilizing the Lambert W function approach which clearly will result in two solutions of the problem. The maximum solution can be written as

$$y_{K_1} = -\frac{a}{b}W\left(-1, -\frac{b}{a}y_S e^{-b/ay_S - A_{K_1}/a}\right). \tag{13}$$

The value of y_{K_2} can be found in the similar way as above, i.e.,

$$y_{K_2} = -\frac{a}{b}W\left(-\frac{b}{a}y_S e^{-b/ay_S - A_{K_2}/a}\right), \tag{14}$$

with $A_{K_2} = d(\ln x_{K_2} - \ln x_S) + c(x_S - x_{K_2})$.

As a result, any solution curve initiating from (x_0^+, y_0^+) with $y_0^+ \in (y_{K_2}, y_{K_1})$ will be free from the effect of impulsive set.

For the case when $\theta_2 = 0$, the trajectory shown by Γ_2 becomes tangent at $y = a/b$. So, y_{K_2} and y_{K_1} become

$$y_{K_2} = -\frac{a}{b}W\left(-1, -e^{-1-A_{K_1}/a}\right), \text{and } y_{K_1} = -\frac{a}{b}W\left(-e^{-1-A_{K_2}/a}\right). \tag{15}$$

The impulsive function described by $y(t^+) = y(t) + v/1 + \beta y(t)$ satisfies some properties which are very important.

To do this, we indicate

$$F(u) = u + \frac{v}{1+\beta u}, \quad u \in \left[0, \frac{a}{b}\right], \tag{16}$$

and then we get $F'(u) = 1 - v\beta/(1+\beta u)^2$ and $F'(u) = 0$ at $u = \sqrt{v\beta} - 1/\beta$.

$(A)\mathrm{AT}/\theta_1 \leq d/c$. From Lemma 1, we can describe the impulsive set $\mathcal{M}_1$ as $\mathcal{M}_1 = \{(x, y) \in \mathbb{R}_+^2 | \mathrm{AT}/\theta_1 + a\theta_2 \leq x \leq x_{G_2}, 0 \leq y \leq y_{G_2}\}$. Further, we can take three subclasses as follows.

(i) $\sqrt{v\beta} - 1/\beta \leq 0$.

For this subcase, $F(u) \geq 0$ for all $u \in [0, y_{G_2}]$, which shows that $v \leq F(u) \leq y_{G_2} + v/1 + \beta y_{G_2}$. Then, the corresponding phase set to $\mathcal{M}_1$ can be expressed as

$$\mathcal{N}_{11} = \left\{(x^+, y^+) \in \mathbb{R}_+^2 | x^+ \in X_1^1, y^+ \in Y_1^1\right\}, \tag{17}$$

with

$$\begin{aligned} X_1^1 &= \left[\frac{\mathrm{AT}(1-P_{\mathrm{AT}})}{\theta_1 + a\theta_2}, (1-P_{\mathrm{AT}})x_{G_2}\right], \\ Y_1^1 &= \left[v, y_{G_2} + \frac{v}{1+\beta y_{G_2}}\right]. \end{aligned} \tag{18}$$

(ii) $\sqrt{v\beta} - 1/\beta \geq y_{G_2}$.

For this subcase, $F(u) \leq 0$ for $u \in [0, y_{G_2}]$, which denotes that $y_{G_2} + v/1 + \beta y_{G_2} \leq F(u) \leq v$. Then, the corresponding phase set to $\mathcal{M}_1$ is expressed as follows:

$$\mathcal{N}_{12} = \left\{(x^+, y^+) \in \mathbb{R}_+ \times \mathbb{R}_+ | x^+ \in X_2^1, y^+ \in Y_2^1\right\}, \tag{19}$$

with

$$\begin{aligned} X_2^1 &= \left[(1-P_{\mathrm{AT}})x_{G_2}, \frac{\mathrm{AT}(1-P_{\mathrm{AT}})}{\theta_1 + a\theta_2}\right], \\ Y_2^1 &= \left[y_{G_2} + \frac{v}{1+\beta y_{G_2}}, v\right]. \end{aligned} \tag{20}$$

(iii) $0 < \sqrt{v\beta} - 1/\beta < y_{G_2}$.

For the present subcase, the impulsive set $\mathcal{M}_1$ becomes $\mathcal{M}_1 = \mathcal{M}_{11} \cup \mathcal{M}_{12}$, where

$$\mathcal{M}_{11} = \left\{(x, y) \in \mathbb{R}_+^2 | x \in X_3^1, y \in Y_3^1\right\}, \tag{21}$$

with

$$\begin{aligned} X_3^1 &= \left[\frac{\mathrm{AT}}{\theta_1 + a\theta_2}, \frac{\mathrm{AT}\beta}{(\theta_1 + a\theta_2)\beta - (\sqrt{v\beta} - 1)b\theta_2}\right], \\ Y_3^1 &= \left[0, \frac{\sqrt{v\beta} - 1}{\beta}\right], \end{aligned} \tag{22}$$

$$\mathcal{M}_{12} = \left\{(x, y) \in \mathbb{R}_+^2 | < x \in X_4^1, y \in Y_4^1\right\}, \tag{23}$$

with

$$\begin{aligned} X_4^1 &= \left(\frac{\mathrm{AT}\beta}{(\theta_1 + a\theta_2)\beta - (\sqrt{v\beta} - 1)b\theta_2}, x_{G_2}\right], \\ Y_4^1 &= \left(\frac{\sqrt{v\beta} - 1}{\beta}, y_{G_2}\right]. \end{aligned} \tag{24}$$

Hence, the corresponding phase set to the impulsive set $\mathcal{M}_1 = \mathcal{M}_{11} \cup \mathcal{M}_{12}$ is $\mathcal{N}_{13} \cup \mathcal{N}_{14}$, where

$$\mathcal{N}_{13} = \left\{(x^+, y^+) \in \mathbb{R}_+^2 | x^+ \in X_5^1, y^+ \in Y_5^1\right\}, \tag{25}$$

with

$$X_5^1 = \left[\frac{\mathrm{AT}(1-P_{\mathrm{AT}})\beta}{(\theta_1 + a\theta_2)\beta - (\sqrt{v\beta} - 1)b\theta_2}, \frac{\mathrm{AT}(1-P_{\mathrm{AT}})}{\theta_1 + a\theta_2}\right],$$
$$Y_5^1 = \left[\frac{2\sqrt{v\beta} - 1}{\beta}, v\right], \tag{26}$$

$$\mathcal{N}_{14} = \left\{(x^+, y^+) \in \mathbb{R}_+^2 | x^+ \in X_6^1, y^+ \in Y_6^1\right\}, \tag{27}$$

with

$$X_6^1 = \left(\frac{\mathrm{AT}(1-P_{\mathrm{AT}})\beta}{(\theta_1 + a\theta_2)\beta - (\sqrt{v\beta} - 1)b\theta_2}, (1-P_{\mathrm{AT}})x_{G_2}\right],$$
$$Y_6^1 = \left(\frac{2\sqrt{v\beta} - 1}{\beta}, y_{G_2} + \frac{v}{1+\beta y_{G_2}}\right]. \tag{28}$$

(B) $d/c < \mathrm{AT}/\theta_1$. For this case, we express the impulsive set as follows.

$\mathcal{M}_2 = \{(x, y) \in \mathbb{R}_+ \times \mathbb{R}_+ | \mathrm{AT}/\theta_1 + a\theta_2 \le x \le x_S, 0 \le y \le y_S\}$. In order to give the exact domain of phase sets for Case (B), based on Lemma 2, we describe the following sets:

$$X_D^l = \left[\frac{\mathrm{AT}(1-P_{\mathrm{AT}})}{(\theta_1 + a\theta_2 + vb\theta_2)}, x_{K_2}\right] \cup \left[x_{K_1}, \infty\right),$$
$$Y_D^l = \left[0, y_{K_2}\right] \cup \left[y_{K_1}, \frac{(\theta_1 + a\theta_2)}{b\theta_2} + \frac{b\theta_2 v}{b\theta_2 + \beta(\theta_1 + a\theta_2)}\right). \tag{29}$$

The following three subcases can be taken based on the definition of the phase set.

(i) $\sqrt{v\beta} - 1/\theta \le 0$.

For this subcase, $F(u) \ge 0$ for all values of u belongs to $[0, y_S]$. This shows that $v \le F(u) \le y_S + v/1 + \beta y_S$. The corresponding phase set to $\mathcal{M}_2$ can be expressed as

$$\mathcal{N}_{21} = \left\{(x^+, y^+) \in \mathbb{R}_+ \times \mathbb{R}_+ | x^+ \in X_1^2, y^+ \in Y_1^2\right\}, \tag{30}$$

with

$$X_{21}^0 = \left[\frac{\mathrm{AT}(1-P_{\mathrm{AT}})}{\theta_1 + a\theta_2}, (1-P_{\mathrm{AT}})x_S\right],$$
$$X_1^2 = X_D^l \cap X_{21}^0, \tag{31}$$

$$Y_{21}^0 = \left[v, y_S + \frac{v}{1+\beta y_S}\right],$$
$$Y_1^2 = Y_D^l \cap Y_{21}^0. \tag{32}$$

(ii) $\sqrt{v\beta} - 1/\beta \ge y_S$.

For this subcase, $F(u) \le 0$ for $u \in [0, y_S]$, which denotes that $y_S + v/1 + \beta y_S \le F(u) \le v$. Hence, the phase set corresponding to $\mathcal{M}_2$ is given as

$$\mathcal{N}_{22} = \left\{(x^+, y^+) \in \mathbb{R}_+ \times \mathbb{R}_+ | x^+ \in X_2^2, y^+ \in Y_2^2\right\}, \tag{33}$$

with

$$X_{22}^0 = \left[(1-P_{\mathrm{AT}})x_S, \frac{\mathrm{AT}(1-P_{\mathrm{AT}})}{\theta_1 + a\theta_2}\right],$$
$$X_2^2 = X_D^l \cap X_{22}^0, \tag{34}$$

$$Y_{22}^0 = \left[y_S + \frac{v}{1+\beta y_S}, v\right],$$
$$Y_2^2 = Y_D^l \cap Y_{22}^0. \tag{35}$$

(iii) $0 < \sqrt{v\beta} - 1/\beta < y_S$.

If $0 \le u \le \sqrt{v\beta} - 1/\beta$, then $F(u) \le 0$ and $2\sqrt{v\beta} - 1/\beta \le F(u) \le v$. If $\sqrt{v\theta} - 1/\beta < u \le y_S$, then $F(u) > 0$ and $2\sqrt{v\beta} - 1/\beta < F(u) \le y_S + v/1 + \beta y_S$.

The impulsive set $\mathcal{M}_2$ is now can be explained in the form $\mathcal{M}_2 = \mathcal{M}_{21} \cup \mathcal{M}_{22}$, where

$$\mathcal{M}_{21} = \left\{(x, y) \in \mathbb{R}_+^2 | x \in X_3^2, y \in Y_3^2\right\}, \tag{36}$$

with

$$X_3^2 = \left[\frac{\mathrm{AT}}{\theta_1 + a\theta_2}, \frac{\mathrm{AT}\beta}{(\theta_1 + a\theta_2)\beta - (\sqrt{v\beta} - 1)b\theta_2}\right],$$
$$Y_3^2 = \left[0, \frac{\sqrt{v\beta} - 1}{\beta}\right], \tag{37}$$

and

$$\mathcal{M}_{22} = \left\{(x, y) \in \mathbb{R}_+^2 | x \in X_4^2, y \in Y_4^2\right\}, \tag{38}$$

with

$$X_4^2 = \left(\frac{\mathrm{AT}\beta}{(\theta_1 + a\theta_2)\beta - (\sqrt{v\beta} - 1)b\theta_2}, x_S\right],$$
$$Y_4^2 = \left(\frac{\sqrt{v\beta} - 1}{\beta}, y_S\right]. \tag{39}$$

Hence, the phase set corresponding to the impulsive set $\mathcal{M}_2 = \mathcal{M}_{21} \cup \mathcal{M}_{22}$ can be expressed as $\mathcal{N}_{23} \cup \mathcal{N}_{24}$, where

$$\mathcal{N}_{23} = \left\{(x^+, y^+) \in \mathbb{R}_+^2 | x^+ \in X_5^2, y^+ \in Y_5^2\right\}, \tag{40}$$

with

$$X_{23}^{0}=\left(\frac{\mathrm{AT}(1-P_{\mathrm{AT}})\beta}{(\theta_1+a\theta_2)\beta-(\sqrt{v\beta}-1)b\theta_2},\frac{\mathrm{AT}(1-P_{\mathrm{AT}})}{\theta_1+a\theta_2}\right],\ X_5^2=X_D^l\cap X_{23}^0,$$
$$Y_{23}^{0}=\left[\frac{2\sqrt{v\beta}-1}{\beta},v\right],\ Y_5^2=Y_D^l\cap Y_{23}^0, \tag{41}$$

$$\mathcal{N}_{24}=\left\{(x^+,y^+)\in\mathbb{R}_+^2|x^+\in X_6^2,y^+\in Y_6^2\right\}, \tag{42}$$

with

$$X_{24}^{0}=\left(\frac{\mathrm{AT}(1-P_{\mathrm{AT}})\beta}{(\theta_1+a\theta_2)\beta-(\sqrt{v\beta}-1)b\theta_2},(1-P_{\mathrm{AT}})x_S\right],$$
$$X_6^2=X_D^l\cap X_{24}^0, \tag{43}$$

$$Y_{24}^{0}=\left(\frac{2\sqrt{v\beta}-1}{\beta},y_S+\frac{v}{1+\beta y_S}\right],$$
$$Y_6^2=Y_D^l\cap Y_{24}^0. \tag{44}$$

For Case (A), if $\mathrm{AT}/\theta_1\le d/c$, then the solution from the phase set does not reach the interval $(y_{G_2},a/b]$. It is also important to note that if $y_T=a/b$ and $A_{G_2}=0$, then $y_{G_2}=a/b$. For Case (B), it can be seen from the vector field of system (1) that if the closed orbit is tangent or does not touch the curve Γ_{PS}, then there must be a trajectory that is tangent to the curve Γ_{PS} at a point (x_T,y_T), and the trajectory intersects the curve Γ_{IS} at lower point G_2. This proves that the impulsive set in this case is defined by $\mathscr{M}_1$, as shown in Figure 1(b).

If the closed trajectory is tangent to Γ_{IS} at point $S=(x_S,y_S)$ and intersects the curve Γ_{PS} at two points, then it can be seen that for any solution from the phase set, it is impossible to reach the interval $(y_S,a/b]$. The above theory shows that nonlinear terms of the controlling measure combined with nonlinear action threshold make impulse system (1) quite complicated, and it is very difficult to analyze each situation in detail. □

4. Poincaré Map

Poincaré map [40–42] plays a very helpful role in examining the qualitative behavior of a dynamical system, most prominently the asymptotic stability of periodic or almost periodic orbits. Based on the impulse and phase sets discussed above, the following related theorem for Poincaré map can be obtained.

Theorem 1. *For the impulsive points of model (1), the Poincaré map for Cases* $(A)$and(B) *has the following form.*

(A) $AT/\theta_1\le d/c$*:*

$$y_{i+1}^{+}=\begin{cases}\psi(y_i^+),y_i^+\in Y_1^1,\text{if }\dfrac{\sqrt{v\beta}-1}{\beta}\le 0,\\ \psi(y_i^+),y_i^+\in Y_2^1,\text{if }\dfrac{\sqrt{v\beta}-1}{\beta}\ge y_{G_2},\\ \psi(y_i^+),y_i^+\in Y_5^1\cup Y_6^1,\text{if }0<\dfrac{\sqrt{v\beta}-1}{\beta}<y_{G_2}.\end{cases} \tag{45}$$

(B) $d/c<AT/\theta_1$*:*

$$y_{i+1}^{+}=\begin{cases}\psi(y_i^+),y_i^+\in Y_1^2,\text{if }\dfrac{\sqrt{v\beta}-1}{\beta}\le 0,\\ \psi(y_i^+),y_i^+\in Y_2^2,\text{if }\dfrac{\sqrt{v\beta}-1}{\beta}\ge y_S,\\ \psi(y_i^+),y_i^+\in Y_5^2\cup Y_6^2,\text{if }0<\dfrac{\sqrt{v\beta}-1}{\beta}<y_S,\end{cases} \tag{46}$$

where

$$\psi(y_i^+)=-\frac{a}{b}W\left[-\frac{b}{a}y_i^+\exp\left(-\frac{b}{a}y_i^++\frac{A_l}{a}\right)\right]+\frac{v}{1-\beta a/bW\left[-b/ay_i^+\exp\left(-b/ay_i^++A_l/a\right)\right]}. \tag{47}$$

Proof. Suppose that a trajectory initiating from (x_0^+,y_0^+) repeats k (finite or infinite) times pulse action. Let the points of the impulse set be represented by $p_i=(x_i,y_i)$, and after the pulse action, the corresponding points of phase set are represented by $p_i^+=(x_i^+,y_i^+)$. If $p_0^+=(x_i^+,y_i^+)\in\Gamma_{\mathrm{PS}}$ and $p_1=(x_{i+1},y_{i+1})\in\Gamma_{\mathrm{IS}}$ are on the same trajectory above, then the coordinates of the two points satisfy the following trajectory equation:

$$d\ln x_i^+ - d\ln x_{i+1} + \mathrm{cx}_{i+1} - \mathrm{cx}_i^+ = a\ln\frac{y_{i+1}}{y_i^+} - b\left(y_{i+1} - y_i^+\right). \tag{48}$$

Solving the above equation for y_{i+1}, we get

$$y_{i+1} = -\left(\frac{a}{b}\right)W\left[-\frac{b}{a}y_i^+\exp\left(-\frac{b}{a}y_i^+ + \frac{A_1}{a}\right)\right], \tag{49}$$

where

$$A_l = d\ln x_i^+ - d\ln x_{i+1} + \mathrm{cx}_{i+1} - \mathrm{cx}_i^+, \tag{50}$$

and therefore

$$\psi\left(y_i^+\right) = -\frac{a}{b}W\left[-\frac{b}{a}y_i^+\exp\left(-\frac{b}{a}y_i^+ + \frac{A_1}{a}\right)\right] + \upsilon/1 - \frac{\beta a}{b}W\left[-\frac{b}{a}y_i^+\exp\left(-\frac{b}{a}y_i^+ + \frac{A_l}{a}\right)\right] = y_{i+1}^+. \tag{51}$$

From above equation, we can see that the Poincaré map given in (47) depends on both the Lambert W function and the sign of A_l.

Case. (A). If $A_l \le 0$, then for $y_i^+ \ge 0$, the above expressions defined in (9) and (10) are well defined. Further, if we define $g(y) = -b/ay\exp(-b/ay)$, then it is easy to prove that $g(y)$ achieved its minimum value $-e^{-1}$ at $y = a/b$. Therefore, $-b/ay\exp(-b/ay)\exp(A_l/a) \in [-e^{-1}, 0)$ for all $A_l \le 0$ and $y > 0$. This denotes that the Poincaré map defined relative to Case (A) is (7).

Table 1: The exact impulsive and phase sets for system (1) under Cases (A) and (B).

Cases		Condition	Impulsive set	Phase set
(A)	(i)	$\frac{\mathrm{AT}}{\theta_1} \le \frac{d}{c}$	$\mathscr{M}_1$	$\mathscr{N}_{11}$
	(ii)			$\mathscr{N}_{12}$
	(iii)			$\mathscr{N}_{13} \cup \mathscr{N}_{14}$
(B)	(i)	$\frac{\mathrm{AT}}{\theta_1} \le \frac{d}{c}$	$\mathscr{M}_2$	$\mathscr{N}_{21}$
	(ii)			$\mathscr{N}_{22}$
	(iii)			$\mathscr{N}_{23} \cup \mathscr{N}_{24}$

For Case (B), if $A_l > 0$, then $-b/ay\exp(-b/ay)\exp(A_l/a) \ge -\exp(-1)$. From this, we obtain the following:

$$\left(\frac{b}{a}\right)y\exp\left(-y\frac{b}{a}\right) \le \exp\left(-\left[1 + \frac{A_l}{a}\right]\right). \tag{52}$$

This solution further simplifies as $y \in (0, y_{K_2}] \cup [y_{K_1}, (\theta_1 + a\theta_2)/b\theta_2 + b\theta_2\upsilon/b\theta_2 + \beta(\theta_1 + a\theta_2))$, and from Lemma 2 we know that

$$y_{K_2} = -\frac{a}{b}W\left(-\frac{b}{a}y_S e^{-b/ay_S - A_{K_2}/a}\right) \text{ and } y_{K_1} = -\frac{a}{b}W\left(-1, -\frac{b}{a}y_S e^{-b/ay_S - A_{K_1}/a}\right). \tag{53}$$

Hence, in the same way, the Poincaré map domain for all remaining cases provided in Section 3 and Table 1 can be found. This finalized the proof. □

5. Characteristics of Poincaré Map

To discuss the existence as well as the stability for the order-1 periodic solution of problem (1), we first analyze the different characteristics of Poincaré map for the above existing cases. For this, we define an important point $G = (x_G, y_G) = (\mathrm{AT}\beta/(\theta_1 + a\theta_2)\beta - (\sqrt{\upsilon\beta} - 1)b\theta_2, \sqrt{\upsilon\beta} - 1/\beta)$ which will be used in the following discussion. If $G \in \Gamma_{\mathrm{IS}}$, then after one time pulse, the corresponding impulse point can be presented as G^+: $(x_{G^+}, y_{G^+}) = (\mathrm{AT}(1 - P_{\mathrm{AT}})\ \beta/(\theta_1 + a\theta_2)\beta - (\sqrt{\upsilon\beta} - 1)b\theta_2, 2\sqrt{\upsilon\beta} - 1/\beta)$.

Theorem 2. *The Poincaré map $\psi(y_i^+)$ for Cases (A) and (B) provided in Table 2 satisfies different properties as follows:*

(A) $AT/\theta_1 \le d/c$ and $A_l \le 0$.

(i) It shows increasing behavior on $[0, y_T]$ and decreasing behavior on $[y_T, \theta_1 + a\theta_2/b\theta_2 + b\theta_2\upsilon/b\theta_2 + \beta(\theta_1 + a\theta_2))$ for $\sqrt{\upsilon\beta} - 1/\beta \le 0$.

(ii) It is increasing on $[y_T, \theta_1 + a\theta_2/b\theta_2 + b\theta_2\upsilon/b\theta_2 + \beta(\theta_1 + a\theta_2))$ and decreasing on $[0, y_T]$ for $\sqrt{\upsilon\beta} - 1/\beta \ge y_{G_2}$.

(iii) It is decreasing on $[0, y_{n_2}]$ and $[y_T, y_{n_1}]$ and increasing on $[y_{n_2}, y_T]$ and $[y_{n_1}, \theta_1 + a\theta_2/b\theta_2 + b\theta_2\upsilon/b\theta_2 + \beta(\theta_1 + a\theta_2))$ for $0 < \sqrt{\upsilon\beta} - 1/\beta < y_{G_2}$, where $y_{n_2} = \min\{y^+ : \psi(y^+) = y_{G^+}\}$, $y_{n_1} = \max\{y^+ : \psi(y^+) = y_{G^+}\}$.

(B) $d/c < AT/\theta_1$ and $A_l > 0$.

(i) It shows increasing behavior over the closed interval $[0, y_{K_2}]$ and decreasing behavior on $[y_{K_1}, \theta_1 + a\theta_2/b\theta + b\theta_2\upsilon/b\theta_2 + \beta(\theta_1 + a\theta_2)$ for $\sqrt{\upsilon\beta} - 1/\beta \le 0$.

(ii) It is increasing on $[y_{K_1}, \theta_1 + a\theta_2/b\theta_2 + b\theta_2\upsilon/b\theta_2 + \beta(\theta_1 + a\theta_2))$ and decreasing on $[0, y_{K_2}]$ for $\sqrt{\upsilon\beta} - 1/\beta \ge y_S$.

Table 2: The domain of the Poincaré map for Cases (A) and (B).

Cases		Condition	A_l	$\psi(y_i^+)$
(A)	(i)	$\mathrm{AT}/\theta_1 \le d/c$	$A_l \le 0$	$y_i^+ \in Y_1^1$
	(ii)			$y_i^+ \in Y_2^1$
	(iii)			$y_i^+ \in Y_5^1 \cup Y_6^1$
(B)	(i)	$\mathrm{AT}/\theta_1 \le d/c$	$A_l > 0$	$y_i^+ \in Y_1^2$
	(ii)			$y_i^+ \in Y_2^2$
	(iii)			$y_i^+ \in Y_5^2 \cup Y_6^2$

(iii) It is decreasing on $[0, y_{N_2}]$ *and* $[y_{K_1}, y_{N_1}]$ *and increasing on* $[y_{N_2}, y_{K_2}]$ *and* $[y_{N_1}, \theta_1 + a\theta_2/b\theta_2 + b\theta_2 v/b\theta_2 + \beta(\theta_1 + a\theta_2))$ *for* $0 < \sqrt{v\beta} - 1/\beta < y_S$, *where* $y_{N_2} = \min\{y^+ : \psi(y^+) = y_{G^+}\}$, $y_{N_1} = \max\{y^+ : \psi(y^+) = y_{G^+}\}$.

Proof. Assuming that $q_i^+ = (x_i^+, y_i^+) \in \Gamma_{PS}$, the solution initiating from q_i^+ intersects the curve Γ_{IS} at $q_{i+1} = (x_{i+1}, y_{i+1})$. If q_i^+ and q_{i+1} lie in one trajectory, then y_{i+1} is established by y_i^+ and can be expressed as $y_{i+1} = F(y_i^+)$. The corresponding vector field relative of the system given in (1) confirms that the domain of consideration of Poincaré map $\psi(y_i^+)$ for Case $(A)(i)$ is defined by $[0, y_T] \cup [y_T, \theta_1 + a\theta_2/b\theta_2 + b\theta_2 v/b\theta_2 + \beta(\theta_1 + a\theta_2))$. Furthermore, for this case, the corresponding impulsive function F has increasing behavior over the closed interval $[0, y_T]$. Therefore, based on the definition of $\psi(y_i^+)$, it is increasing on $[0, y_T]$ and decreasing on $[y_T, \theta_1 + a\theta_2/b\theta_2 + b\theta_2 v/b\theta_2 + \beta(\theta_1 + a\theta_2))$. The function F is decreasing upon $[0, y_T]$ in Case $(A)(ii)$, which shows that $\psi(y_i^+)$ is decreasing over the interval $[0, y_T]$ and increasing over the closed interval $[y_T, \theta_1 + a\theta_2/b\theta_2 + b\theta_2 v/b\theta_2 + \beta(\theta_1 + a\theta_2))$. For Case $(A)(iii)$, F is decreasing over $[0, y_G]$ and increasing upon $[y_G, y_T]$. Therefore, $\psi(y_i^+)$ is decreasing on $[0, y_{N_2}]$ and $[y_{K_1}, y_{N_1}]$ and increasing on $[y_{N_2}, y_{K_2}]$ and $[y_{N_1}, \theta_1 + a\theta_2/b\theta_2 + b\theta_2 v/b\theta_2 + \beta(\theta_1 + a\theta_2))$.

By using the same methods as above, we can prove that the monotonicities of the Poincaré map for Cases $(B)(i)$, (ii), (iii) in Theorem 2 are true. □

Lemma 3. *If* $A_l > 0$ *and* $v > 0$, *then the inequality*

$$\psi(y_i^+) > y_i^+, \text{for all } y_i^+ \in \left(0, y_{K_2}\right), \tag{54}$$

is fulfilled for the corresponding Poincaré map shown by $\psi(y_i^+)$.

Proof. Let a solution originate from $p_0^+ = (x_i^+, y_i^+)$, and it touches the curve Γ_{IS} at point $p_1 = (x_{i+1}, y_{i+1})$. We assume that $y_i^+, y_{i+1} < a/b$; then,

$$\begin{aligned} a \ln y_{i+1} - \mathrm{by}_{i+1} + d \ln x_{i+1} - \mathrm{cx}_{i+1} &= a \ln y_i^+ - \mathrm{by}_i^+ \\ &\quad + d \ln x_i^+ - \mathrm{cx}_i^+. \end{aligned} \tag{55}$$

From (55), we get

$$-\frac{b}{a} y_{i+1} e^{(-b/a y_{i+1})} = -\frac{b}{a} y_i^+ e^{(-b/a y_i^+ + A_l/a)}. \tag{56}$$

If $A_l > 0$, then we get the inequality

$$-\frac{b}{a} y_{i+1} e^{(-b/a y_{i+1})} < -\frac{b}{a} y_i^+ e^{(-b/a y_i^+)}. \tag{57}$$

Let $f(y) = -y \exp(-y)$; then, $f'(y) > 0$ if $y > 1$ and $f'(y) < 0$ if $y \in (0, 1)$. The inequality $y_{i+1} > y_i^+$ is satisfied for all $b/a y_i^+, b/a y_{i+1} \in (0, 1)$. We also know that $y_{i+1}^+ = y_{i+1} + v$ and $\psi(y_i^+) = y_{i+1}^+$. Hence, we deduce that $\psi(y_i^+) > y_i^+$ for all $y_i^+ \in (0, y_{K_2})$.

In light of the above explained properties of Poincaré map, the existence of the fixed point of Poincaré map $\psi(y_i^+)$ for $v > 0$ is discussed in following section. □

6. Characteristics of Boundary Periodic Solution

In Section 4, the formula for Poincaré map $\psi(y_i^+)$ has been attained. We will use this formula to study the existence of fixed point, where the fixed point is indicated as y^*, satisfying $\psi(y^*) = y^*$, such as

$$y^* = -\frac{a}{b} W \times \left[\left(-\frac{b}{a}\right) y^* \exp\left(-\frac{b}{a} y^* + \frac{A_l}{a}\right)\right] + \frac{v}{1 - \beta a/bW\left[-b/a y^* \exp\left(-b/a y^* + A_l/a\right)\right]}. \tag{58}$$

For $v = 0$, we get the following equation from above:

$$y^* = -\left(\frac{a}{b}\right) W\left[-\frac{b}{a} y^* \exp\left(-\frac{b}{a} y^* + \frac{A_l}{a}\right)\right]. \tag{59}$$

If $A_l = 0$, the fixed point shown by y^* of the respective Poincaré map $\psi(y_i^+)$ becomes

$$y^* = -\left(\frac{a}{b}\right) W\left[-\frac{b}{a} y^* \exp\left(-\frac{b}{a} y^*\right)\right]. \tag{60}$$

This shows that if $v = 0$, $A_l = 0$, then every point is the fixed point of $\psi(y_i^+)$. If $v = 0$, $A_l \neq 0$, then y^* (a fix point) of the $\psi(y_i^+)$ fulfils

$$y^* = -\left(\frac{a}{b}\right) W\left[-\frac{b}{a} y^* \exp\left(-\frac{b}{a} y^* + \frac{A_l}{a}\right)\right]. \tag{61}$$

In this case, $\psi(y^*) = y^*$ holds $\Leftrightarrow y^* = 0$. Thus, we deduced that $y^* = 0$ is a unique fixed point for system (1).

In the following result, we present the conditions of global stability for boundary order-1 periodic solution. To demonstrate it, we first discuss an important lemma [43, 44].

Lemma 4. *The T-periodic solution* $(x, y) = (\zeta(t), \xi(t))$ *of system*

$$\begin{cases} \dfrac{\mathrm{d}x}{\mathrm{d}t} = C(x, y), \dfrac{\mathrm{d}y}{\mathrm{d}t} = D(x, y), \text{if } \theta(x, y) \neq 0, \\ x^{+} = x + \varepsilon(x, y), y^{+} = y + \varepsilon(x, y), \text{if } \theta(x, y) = 0, \end{cases} \tag{62}$$

is orbitally asymptotically stable if the Floquet multiplier μ_2 *satisfies* $|\mu_2| < 1$, *where*

$$\mu_2 = \prod_{j=1}^{k} \Delta_j \exp\left(\int_0^T \left[\frac{\partial C}{\partial x}(\zeta(t), \xi(t)) + \frac{\partial D}{\partial y}(\zeta(t), \xi(t)) \right] \mathrm{d}t \right), \tag{63}$$

with

$$\Delta_j = \frac{C_+ (\partial\varepsilon/\partial y \partial\theta/\partial x - \partial\varepsilon/\partial x \partial\theta/\partial y + \partial\theta/\partial x) + D_+ (\partial\epsilon/\partial x \partial\theta/\partial y - \partial\epsilon/\partial y \partial\theta/\partial x + \partial\theta/\partial y)}{C\partial\theta/\partial x + B\partial\theta/\partial y}, \tag{64}$$

and θ *is continuously differentiable corresponding to both* x, y. $C, D, \partial\epsilon/\partial x, \partial\epsilon/\partial y, \partial\varepsilon/\partial x, \partial\varepsilon/\partial y, \partial\theta/\partial x$ *and* $\partial\theta/\partial y$ *are evaluated at* $(\zeta(t_j), \xi(t_j))$, $C_+ = C(\zeta(t_j^+), \xi(t_j^+))$ *and* $D_+ = D(\zeta(t_j^+), \xi(t_j^+))$, *and* t_j $(j, k \in \mathbb{N}$, $\mathbb{N}$ *is the set of non-negative integers) is the time of the j-th jump.*

Theorem 3. *If* $A_l = 0$ *and* $v = 0$, *then the fixed point* y^* *of Poincaré map* $\psi(y_i^+)$ *is stable in the phase set. If* $A_l < 0$ *and* $v = 0$, *then* $(x^T(t), 0)$ *is globally asymptotically stable. If* $A_l > 0$ *and* $v = 0$, *then it is unstable.*

Proof. If $v = 0$, $A_l = 0$, then y^* in the phase set is a fixed point of the Poincaré map $\psi(y_i^+)$. This case confirms the stable solution of the problem but is not asymptotically stable. We first show that when $y(t) = 0$ if and only if $v = 0$, and then boundary order-1 periodic solution exists for system (1). For $y(t) = 0$, system (1) is converted into the subsystem given below:

$$\begin{cases} \dfrac{\mathrm{d}x(t)}{\mathrm{d}t} = a \times x(t), \quad x(t) < \dfrac{\mathrm{AT}}{\theta_1 + a\theta_2}, \\ x(t^+) = x(t)\left(1 - \dfrac{\delta x(t)}{x(t) + \alpha}\right), \quad x(t) = \dfrac{\mathrm{AT}}{\theta_1 + a\theta_2}, \end{cases} \tag{65}$$

The first equation of the subsystem (14), combining with the respective initial condition shown as $x(0^+) = (1 - P_{\mathrm{AT}})\mathrm{AT}/\theta_1 + a\theta_2$, where $P_{\mathrm{AT}} = \delta x(t)/x(t) + \alpha$, gives us the solution

$$x(t) = (1 - P_{\mathrm{AT}}) \frac{\mathrm{AT}}{\theta_1 + a\theta_2} \exp(\mathrm{at}). \tag{66}$$

Taking the equation $\mathrm{AT}/\theta_1 + a\theta_2 = (1 - P_{\mathrm{AT}})\mathrm{AT}/\ \theta_1 + a\theta_2 \exp(\mathrm{aT})$ and evaluating it for T, we get $T = -1/a\ln(1 - P_{\mathrm{AT}})$. This shows that T-periodic boundary order-1 solution exists for system (1) as

$$\left(x^T(t), 0\right) = \left((1 - P_{\mathrm{AT}}) \frac{\mathrm{AT}}{\theta_2 + a\theta_2} \exp(\mathrm{at}), 0 \right). \tag{67}$$

Next, we show that $(x^T(t), 0)$ is asymptotically stable. For this, we apply Lemma 4 and present the following.

Method 1.

$$\begin{gathered} C(x, y) = (a - \mathrm{by})x, D(x, y) = y(\mathrm{cx} - d), \\ \varepsilon(x, y) = -P_{\mathrm{AT}} x, \varepsilon(x, y) = \frac{v}{1 + \beta y}, \theta(x, y) = (\theta_1 + a\theta_2)x - b\theta_2 \mathrm{xy} - \mathrm{AT}, \\ \left(x^T(T), y^T(T)\right) = \left(\frac{\mathrm{AT}}{\theta_1 + a\theta_2}, 0 \right), \left(x^T(T^+), y^T(T^+)\right) = \left((1 - P_{\mathrm{AT}}) \frac{\mathrm{AT}}{\theta_1 + a\theta_2}, 0 \right). \end{gathered} \tag{68}$$

From the above, we get

$$\frac{\partial C}{\partial x} = a - \mathrm{by}, \frac{\partial D}{\partial y} = \mathrm{cx} - d, \frac{\partial \varepsilon}{\partial x} = \frac{-\delta x^2 + 2\delta\alpha x}{(x+\alpha)^2}, \frac{\partial \varepsilon}{\partial x} = \frac{\upsilon\beta}{(1+\beta y)^2},$$
$$\frac{\partial \theta}{\partial x} = \theta_1 + a\theta_2 - b\theta_2 y, \frac{\partial \theta}{\partial y} = -b\theta_2 x, \frac{\partial \varepsilon}{\partial y} = \frac{\partial \varepsilon}{\partial y} = 0, \tag{69}$$

$$\begin{aligned}\Delta_1 &= \frac{C_+(\partial\varepsilon/\partial y\partial\theta/\partial x - \partial\varepsilon/\partial x\partial\theta/\partial y + \partial\theta/\partial x) + D_+(\partial\varepsilon/\partial x\partial\theta/\partial y - \partial\varepsilon/\partial y\partial\theta/\partial x + \partial\theta/\partial y)}{C\partial\theta/\partial x + D\partial\theta/\partial y} \\ &= \frac{C^+\left(x^T(T^+), y^T(T^+)\right)(\theta_1 + a\theta_2 - b\theta_2 y) + D^+\left(x^T(T^+), y^T(T^+)\right)(P_{\mathrm{AT}} b\theta_2 x - b\theta_2 x)}{C\left(x^T(T), y^T(T)\right)(\theta_1 + a\theta_2 - b\theta_2 y) - D\left(x^T(T), y^T(T)\right)(b\theta_2 x)} \\ &= (1 - P_{\mathrm{AT}}).\end{aligned} \tag{70}$$

Based on the above information, the Floquet multiplier denoted by μ_2 is defined as

$$\begin{aligned}\mu_2 &= \Delta_1 \exp\left(\int_0^T \left[\frac{\partial C}{\partial x}\left(x^T(t), y^T(t)\right) + \frac{\partial D}{\partial y}\left(x^T(t), y^T(t)\right)\right]\mathrm{d}t\right) \\ &= (1 - P_{\mathrm{AT}})\exp\left(\ln\frac{1}{1 - P_{\mathrm{AT}}} + \frac{A_l}{a}\right) \\ &= \exp\left(\frac{A_l}{a}\right).\end{aligned} \tag{71}$$

If $A_l < 0$ and $\upsilon = 0$, then we get $|\mu_2| < 1$. This indicates that for the problem described in (1), the boundary order-1 periodic solution $(x^T(t), 0)$ is orbitally stable asymptotically. If $A_l > 0$, the sequence y_k^+ of pulse points is increasing strictly and additionally will be free from more pulse action only after limited time pulse effects.

Method 2. The asymptotic stability of boundary order-1 periodic solution can also be discussed directly from Poincaré map portrayed in (47). Let $\upsilon = 0$; then,

$$\psi(y_i^+) = -\frac{a}{b}W\left[-\frac{b}{a}y_i^+\left(\exp\left(-\frac{b}{a}y_i^+ + \frac{A_l}{a}\right)\right)\right]. \tag{72}$$

Taking the derivative of (72), we get

$$\begin{aligned}\left.\frac{d\psi(y_i^+)}{\mathrm{d}y_i^+}\right|y_i^+ = y^* &= \left.\frac{d}{\mathrm{d}y_i^+}\right|_{y_i^+ = y^*}\left(-\frac{a}{b}W\left[-\frac{b}{a}y_i^+\left(\exp\left(-\frac{b}{a}y_i^+ + \frac{A_l}{a}\right)\right)\right]\right) \\ &= \frac{-a/bW\left[-b/ay^*\left(\exp\left(-b/ay^* + A_l/a\right)\right)\right]}{1 + W\left[-b/ay^*\left(\exp\left(-b/ay^* + A_l/a\right)\right)\right]}\left(1/y^* - b/a\right) = h(y^*).\end{aligned} \tag{73}$$

The boundary order-1 periodic solution is stable $\Leftrightarrow |h(y^*)| < 1$. By utilizing the limit of $h(y^*)$, we get

$$\lim_{y^* \longrightarrow 0} h(y^*) = e^{A_l/a}. \tag{74}$$

This denotes that if $y^* \longrightarrow 0$, then $|h(y^*)| < 1$ for $A_l < 0$, and hence $(x^T(t), 0)$ is asymptotically stable.

In the following, we show the global attractivity of the boundary order-1 periodic solution $(x^T(t), 0)$. Let $p_0^+ = (\mathrm{AT}(1 - P_{\mathrm{AT}})/\theta_1 + a\theta_2, y_1^+) \in L_3$ and $p_1 = (\mathrm{AT}/\theta_1 + a\theta_2, y_2) \in L_2$ be the points of the same trajectory; then,

$$A_l = d\ln(1 - P_{\mathrm{AT}}) + c\frac{\mathrm{AT}}{\theta_1 + a\theta_2}P_{\mathrm{AT}} = a\ln\frac{y_2}{y_1^+} - b(y_2 - y_1^+). \tag{75}$$

Let $A_l \neq 0$; then, from (75), it is clear that $y_2 \neq y_1^+$. If $f(y) = a\ln y - by$, then $f(y) = a/y - b$. This indicates that if $y < a/b$, then $f(y)$ is monotonically increasing.

If $A_l < 0$, then $a\ln y_2/y_1^+ - b(y_2 - y_1^+) < 0$. Since $v = 0$, the inequality becomes $a\ln y_2/y_1 - b(y_2 - y_1) < 0$. This shows that $y_2 < y_1$. Therefore, *if* $A_l \leq 0$, then the impulsive sequence $\{y_k^+\}_{k=0}^{\infty}$ is monotonically decreasing and $\lim_{k\longrightarrow\infty} y_k^+ = y^*$. These kinds of information affirm that the boundary order-1 periodic solution is globally attractive. In the same way as above, we can prove that if $A_l > 0$, then $y_2 > y_1$. Therefore, the sequence y_k^+ will be free from impulsive effect after finite time pulse actions, as shown in Figure 2(b). Hence, from all the above outcomes, it can be concluded that if $A_l < 0$, then the boundary order-1 periodic solution, i.e., $(x^T(t), 0)$, is globally asymptotically stable.

The numerical calculation in Figure 2(a) shows that if $A_l < 0$, then the boundary order-1 periodic solution is stable while Figure 2(b) confirms that if $A_l \geq 0$, then it is unstable. □

7. Existence of Order-1 Periodic Solution

In this section, we will discuss and analyze the order-1 periodic solution for system (1) when $v > 0$.

Theorem 4. *For Case* $(A)(i)(or(ii))$*, the fixed point of Poincaré map* $\psi(y_i^+)$ *exists, and therefore an order-1 periodic solution exists for system (1).*

Proof. For Case $(A)(i)$, the trajectory Γ_1 is tangent to the curve Γ_{PS} at point (x_T, y_T) and intersects the curve Γ_{IS} at lower point G_2. If $\psi(y_T) = y_{G_2^+} = y_T$, then the curve $\widehat{TG_2}$ forms an order-1 periodic solution for system (1).

For Case $(A)(i)$, if $y_{G_2^+} > y_T$ or $y_{G_2^+} < y_T$, then the solution originating from the point G_2^+ touches the curve Γ_{PS} at a point $G_3 = (x_{G_3}, y_{G_3})$ with $y_{G_3} < y_{G_2}$. The pulse action is applied and the point G_3 maps to a point $G_3^+ = (x_{G_3^+}, y_{G_3^+})$, and $y_{G_3^+} = F(y_{G_3})$. For Case $(A)(i)$, F is increasing on $[0, y_{G_2}]$. Therefore, $y_{G_3^+} = \psi(y_{G_2^+})$ satisfies the inequality

$$\psi\left(y_{G_2^+}\right) < y_{G_2^+}. \tag{76}$$

The point $\psi_v(\mathrm{AT}(1 - P_{\mathrm{AT}})/\theta_1 + a\theta_2, v)$ being the lowest impulsive point satisfies

$$\psi(v) > v. \tag{77}$$

Inequalities (17) and (18) confirm that a fixed point of the Poincaré map exists, and therefore an order-1 periodic solution exists for system (1).

For Case $(A)(ii)$, F is decreasing on $[0, y_{G_2}]$. If $y_{G_2^+} > y_T$ or $y_{G_2^+} < y_T$, we get

$$\psi\left(y_{G_2^+}\right) > y_{G_2^+}. \tag{78}$$

Moreover, the highest impulsive point is $\psi_v(\mathrm{AT}(1 - P_{\mathrm{AT}})/\theta_1 + a\theta_2, v)$, and we get

$$\psi(v) < v. \tag{79}$$

Inequalities (19) and (20) confirm that there exists a fixed point for the Poincaré map, and therefore an order-1 periodic solution exists for system (1). This completes the proof. □

Theorem 5. *For Case* $(A)(iii)$*, the fixed point of Poincaré map* $\psi(y_i^+)$ *exists, and therefore an order-1 periodic solution exists for system (1).*

Proof. If $y_{G_2^+} = y_T$, then the curve $\widehat{TG_2}$ forms an order-1 periodic solution for the problem given in system (1). If $y_{G_2^+} \neq y_T$, then the following two cases are taken into consideration.

$$(1)\ y_{G_2^+} \geq v,\ (2)\ y_{G_2^+} < v. \tag{80}$$

For Case (1), if $y_{G_2^+} > y_T$, then we can write

$$\psi(y_T) > y_T. \tag{81}$$

As G_2^+ is the lowest impulsive point, it satisfies

$$\psi\left(y_{G_2^+}\right) < y_{G_2^+}. \tag{82}$$

Thus, inequalities (21) and (22) confirm that we can find a fixed point of Poincaré map $\psi(y_i^+)$.

If $y_{G_2^+} < y_T$, then we can write

$$\psi(y_T) < y_T. \tag{83}$$

Moreover, if G^+ is the least impulsive point, then it leads to the following:

$$\psi(y_{G^+}) \geq y_{G^+}. \tag{84}$$

Thus, the above two inequalities (83) and (84) confirm that there exists a fixed point of Poincare map $\psi(y_i^+)$.

For Case (2), if $y_{G_2^+} > y_T$, then $\psi(y_T) > y_T$. On the other hand, if the highest impulsive point is $\psi_v(\mathrm{AT}(1 - P_{\mathrm{AT}})/\theta_1 + a\theta_2, v)$, then $\psi(v) < v$. The above two inequalities affirm that there exists a fixed point of the Poincaré map $\psi(y_i^+)$.

If $y_{G_2^+} < y_T$, then $\psi(y_T) < y_T$. Moreover, as G^+ is the least impulsive point, we get $\psi(y_{G^+}) \geq y_{G^+}$. It confirms that there exists a fixed point for the map shown by $\psi(y_i^+)$, and hence an order-1 periodic solution exists for system (1). □

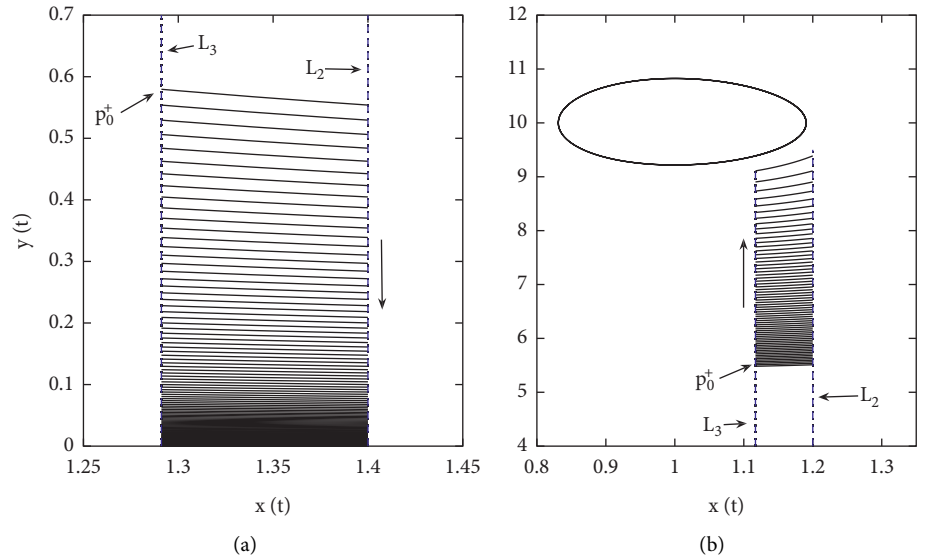

FIGURE 2: (a) The stable boundary order-1 periodic solution where $L_2 = 1.4$ and $A_l = -0.050, c = 0.50, d = 1.20$. (b) The unstable boundary order-1 periodic solution with $L_2 = 1.20$ and $A_l = 0.0030, d = 0.20, c = 0.20$. The rest of the parameter values are fixed with $a = 1, \delta = 0.3, b = 0.1, \alpha = 4, \beta = 1, \upsilon = 0$.

Theorem 6. *For Case $(B)(i)(or(ii))$, if $y_{S^+} > y_{K_1}$, then the fixed point of Poincaré map $\psi(y_i^+)$ exists, and therefore an order-1 periodic solution exists for system (1).*

Proof. For Case $(B)(i)$, we know that there exists a curve Γ_2, which is tangent to Γ_{IS} at point $S = (x_S, y_S)$ and intersects the curve Γ_{PS} at two points K_1 and K_2. If $y_{S^+} = y_{K_1}$, then the curve $\widehat{K_1 S}$ forms an order-1 periodic solution for the problem stated in (1).

Further, for Case $(B)(i)$, if $y_{S^+} > y_{K_1}$, then the point demoted by S^+ lies above the point K_1, and we get

$$\psi\left(y_{K_1}\right) > y_{K_1}. \tag{85}$$

In addition, the solution initiating from the point S^+ meets the curve Γ_{IS} at a point S_1 which lies below the point S, i.e., $y_{S_1} < y_S$. As F is increasing on $[0, y_S]$, we have $F(y_{S_1}) < F(y_S)$, i.e., $y_{S_1}^+ < y_S^+$. All the above results affirm that the Poincaré map for Case $(B)(i)$ satisfies

$$\psi\left(y_{S^+}\right) < y_{S^+}. \tag{86}$$

Inequalities (25) and (26) confirm that a fixed point in (y_{K_1}, y_{T^+}) will exist. Hence, an order-1 periodic solution exists for problem (1).

If $y_{S^+} < y_{K_1}$, then after a one time impulsive effect, the solution will directly map to the interval $[\upsilon, y_{S^+}]$. Thus, if $y_{K_2} \geq \upsilon$, then according to inequality (1), any trajectory originating from y^+ with $\upsilon \leq y^+ \leq y_{K_2}$ will intersect the curve Γ_{IS} and experience a limited time of pulse actions and at last enter into Int Γ_2 and will be free from more pulse action. If $y_{K_2} < \upsilon < y_{S^+}$, then each solution curve of problem (1) will map to the Int Γ_2 after a one time impulsive effect. Hence, if $y_{S^+} < y_{K_1}$, then a fixed point does not exist.

For Case (B) (ii), if $y_{S^+} > y_{K_1}$, then $\psi(y_{K_1}) > y_{K_1}$. We also know that the function F is decreasing on $[0, y_S]$. So, the solution y^+ initiating from $[0, y_{K_2}] \cup [y_{K_1}, \theta_1 + a\theta_2/b\theta_2 + b\theta_2\upsilon/b\theta_2 + \beta(\theta_1 + a\theta_2))$ will map to the interval $[y_{S^+}, \upsilon]$ after a one time impulsive effect. Therefore, the trajectory originating from the point $\psi_\upsilon(\mathrm{AT}(1 - P_{\mathrm{AT}})/\theta_1 + a\theta_2, \upsilon)$ will satisfy $\psi(\upsilon) < \upsilon$. From the above inequalities, it follows that the fixed point exists in the interval (y_{K_1}, υ). □

Theorem 7. *For Case $(B)(iii)$, if $y_{S^+} > y_{K_1}$, then the fixed point of Poincaré map $\psi(y_i^+)$ exists, and therefore an order-1 periodic solution exists for system (1).*

Proof. If $y_{S^+} = y_{K_1}$, then for system (1), the curve $\widehat{K_1 S}$ forms an order-1 periodic solution. If $y_{S^+} \neq y_{K_1}$, then we consider the following two cases.

$$(1)\ y_{S^+} \geq \upsilon,\ (2)\ y_{S^+} < \upsilon. \tag{87}$$

For Case (1), if $y_{T^+} > y_{K_1}$, then $\psi(y_{K_1}) > y_{K_1}$. Moreover, according to the exact domain of the Poincaré map $\psi(y_i^+)$, the impulsive point S_1^+ of S^+ lies below the point S^+, i.e., $S_1^+ < S^+$ for $y_{S^+} \geq \upsilon$. Therefore, inequality $\psi(y_{S^+}) < y_{S^+}$ is true, which shows that the fixed point exists in the interval $[y_{K_1}, y_{S^+}]$.

If $y_{S^+} < y_{K_1}$, then applying the same techniques as those given in Theorem 6, it can easily be shown there must exist a finite number of pulse effects for any solution of system (1). Furthermore, the solution enters into Int Γ_2 and becomes free from more pulse actions.

For Case (2), if $y_{S^+} > y_{K_1}$, then $\psi(y_{K_1}) > y_{K_1}$ holds true. We also know that the highest impulsive point is $\psi_\upsilon(\mathrm{AT}(1 - P_{\mathrm{AT}})/\theta_1 + a\theta_2, \upsilon)$ because $y_{S^+} < \upsilon$. Therefore, we get $\psi(\upsilon) < \upsilon$, and hence the theorem is true.

If $y_{S^+} < y_{K_1}$, then any trajectory of system (1) tends into Int Γ_2 only after finite pulse effects. This completes the proof. □

8. Stability of Order-1 Periodic Solution

The monotonicities of Poincaré map $\psi(y_i^+)$ and existence of its fixed point were discussed in previous sections. Now, based on these, we will discuss the stability of fixed point of Poincaré map $\psi(y_i^+)$ for system (1).

Theorem 8. *For Case $(A)(i)$, if the fixed point of Poincaré map $\psi(y_i^+)$ is unique and one of the following two conditions is satisfied, then the corresponding fixed point denoted by y^* is stable globally.*

(a) If $\psi(y_T) < y_T$.

(b) If $\psi(y_T) > y_T$ and $\psi^2(y_i^+) > y_i^+$ for $y_i^+ \in [y_T, y^*)$.

Proof. From Theorem 4, we know that for Case $(A)(i)$, the fixed point of Poincaré map $\psi(y_i^+)$ exists. Let the fixed point y^* be unique; then, the global stability can be discussed as follows:

(a) If $\psi(y_T) < y_T$, then $y_i^+ < \psi(y_i^+) < y^*$ for all $y_i^+ \in [0, y^*)$. This means that as j increases, $\psi^j(y_i^+)$ increases monotonically and satisfies $\lim_{j\longrightarrow+\infty} \psi^j(y_i^+) = y^*$. If $y_i^+ \in (y^*, \theta_1 + a\theta_2/b\theta_2 + b\theta_2 v/b\theta_2 + \beta(\theta_1 + a\theta_2)]$, then we take two cases. (1) If $y_i^+ \in (y^*, y_T]$, then according to the relation $y^* < \psi(y_i^+) < y_i^+$, $\psi(y_i^+)$ decreases monotonically, i.e., $y^* < \psi^j(y_i^+) < \psi^{j-1}(y_i^+)$ for all $j \geq 1$ and we get $\lim_{j\longrightarrow+\infty} \psi^j(y_i^+) = y^*$. (2) If $y_i^+ \in (y_T, \theta_1 + a\theta_2/b\theta_2 + b\theta_2 v/b\theta_2 + \beta(\theta_1 + a\theta_2))$, then $\psi(y_i^+) \in (0, y_T)$ and $\lim_{j\longrightarrow+\infty} \psi^{1+j}(y_i^+) = y^*$. Therefore, the conclusion in (a) is true.

(b) If $\psi(y_T) > y_T$, then we take three intervals: (1) $y_i^+ \in [y_T, y^*)$; (2) $y_i^+ \in [0, y_T)$; (3) $y_i^+ \in (y^*, \theta_1 + a\theta_2/b\theta_2 + b\theta_2 v/b\theta_2 + \beta(\theta_1 + a\theta_2))$. For interval (1), since $y_T \leq y_i^+ < y^*$ and Poincaré map $\psi(y_i^+)$ is monotonically decreasing in this interval, it is easy to get $(y_T) \geq \psi(y_i^+) > y^*$. At the same time, by using the second condition $\psi^2(y_i^+) > y_i^+$, we get $y_i^+ < \psi^2(y_i^+) < y^*$. This means that for all $j \geq 1$, $\psi^{2(j-1)}(y_i^+) < \psi^{2j}(y_i^+) < y^*$. This shows that $\psi^{2j}(y_i^+)$ increases monotonically, and $\lim_{j\longrightarrow+\infty} \psi^{2j}(y_i^+) = y^*$.

For intervals (2) and (3), using the same method as those in (1), we can prove that there must exist $n \geq 1$ such that $\psi^n(y_i^+) \in [y_T, y^*]$, and hence the fixed point of Poincaré map $\psi(y_i^+)$ is globally stable under conditions (2) and (3). This completes the proof. □

Theorem 9. *For Case $(A)(ii)$, if the fixed point y^* of Poincaré map $\psi(y_i^+)$ is unique and one of the following two conditions is true, then y^* is globally stable.*

(a) If $\psi(y_T) > y_T$.

(b) If $\psi(y_T) < y_T$ and $\psi^2(y_i^+) < y_i^+$ for $y_i^+ \in (y^*, y_T]$.

Proof. Theorem 4 shows that for Case (A)(ii), there exists a fixed point of the map $\psi(y_i^+)$. Assuming that the fixed point is unique, we have the following conclusions regarding its stability:

(a) From Theorem 2, it is clear that the Poincaré map is monotonically increasing in the interval $[y_T, \theta_1 + a\theta_2/b\theta_2 + b\theta_2 v/b\theta_2 + \beta(\theta_1 + a\theta_2))$ and monotonically decreasing in the interval $[0, y_T]$. If $\psi(y_T) > y_T$, then the fixed point satisfies $y^* > y_T$ for any $y_i^+ \in [y_T, y^*)$ and $\psi^{j_1}(y_i^+)$ increases with the increasing value of j_1 such that $\lim_{j\longrightarrow+\infty} \psi^{j_1}(y_i^+) = y^*$ for all $y_i^+ \in (y^*, \theta_1 + a\theta_2/b\theta_2 + b\theta_2 v/b\theta_2 + \beta(\theta_1 + a\theta_2))$. $\psi^{j_2}(y_i^+)$ decreases as j_2 increases, and $\lim_{j\longrightarrow+\infty} \psi^{j_2}(y_i^+) = y^*$.

For all $y_i^+ \in (0, y_T)$, there is $\psi(y_i^+) \in (y_T, \theta_1 + a\theta_2/b\theta_2 + b\theta_2 v/b\theta_2 + \beta(\theta_1 + a\theta_2))$; therefore, $\lim_{j\longrightarrow+\infty} \psi^{1+j_1}(y_i^+) = y^*$ or $\lim_{j\longrightarrow+\infty} \psi^{1+j_2}(y_i^+) = y^*$. In summary, the only fixed point y^* is globally stable.

(b) The Poincaré map $\psi(y_i^+)$ is monotonically decreasing in the interval $[0, y_T]$, and for $y_i^+ \in (y^*, y_T]$, the condition $\psi^2(y_i^+) < y_i^+$ is satisfied. So, it is easy to get $y^* < \psi^4(y_i^+) < \psi^2(y_i^+)$. By induction, there is a relation $y^* < \psi^{2j}(y_i^+) < \psi^{2(j-1)}(y_i^+)$ for all $j \geq 1$. This shows that $\psi^{2j}(y_i^+)$ monotonically decreases with increasing value of j, and $\lim_{j\longrightarrow+\infty} \psi^{2j}(y_i^+) = y^*$. In addition, for all $y_i^+ \in (0, y^*) \cup (y_T, \theta_1 + a\theta_2/b\theta_2 + b\theta_2 v/b\theta_2 + \beta(\theta_1 + a\theta_2))$, there must exist $l \geq 1$ such that $\psi^l(y_i^+) \in (y^*, y_T]$, and hence $\lim_{j\longrightarrow+\infty} \psi^{l+2j}(y_i^+) = y^*$. □

Theorem 10. *For Case $(A)(iii)$, if the fixed point y^* is unique and one of the following conditions is true, then it is globally stable.*

(a) If $\psi(y_{n_i}) > y_{n_i}$ $i = 1, 2$.

(b) If $\psi(y_{n_i}) < y_{n_i}$ $i = 1, 2$, and $\psi^2(y_i^+) < y_i^+$ for all $y_i^+ \in (y^*, y_{n_2}]$.

(c) If $\psi(y_T) > y_T$, $\psi(y_{n_2}) > y_{n_2}$, and $\psi(y_{n_1}) < y_{n_1}$, for $y_i^+ \in (y^*, y_{n_1}]$ when $y^* < \psi^2(y_i^+) < y_i^+$.

(d) If $\psi(y_T) < y_T$, $\psi(y_{n_2}) > y_{n_2}$, and $\psi(y_{n_1}) < y_{n_1}$.

Proof. Theorem 5 shows that there exists a fixed point of Poincaré map $\psi(y_i^+)$ for Case (A)(iii). Moreover, if y^* is unique, then its global stability can be described as follows:

(a) If $\psi(y_{n_i}) > y_{n_i}$ for $i = 1, 2$, then we take three intervals: (1) $[y_{n_1}, y^*)$; (2) $(y^*, \theta_1 + a\theta_2/b\theta_2 + b\theta_2 v/b\theta_2 + \beta(\theta_1 + a\theta_2))$; (3) $(0, y_{n_1})$. For all $y_i^+ \in [y_{n_1}, y^*)$, we get $y_i^+ < \psi(y_i^+) < y^*$. The Poincaré map $\psi(y_i^+)$ is monotonically increasing in the interval $[y_{n_1}, \theta_1 + a\theta_2/b\theta_2 + b\theta_2 v/b\theta_2 + \beta(\theta_1 + a\theta_2))$, and $\psi(y_i^+) < \psi^2(y_i^+) < y^*$. By induction, we get $\psi^{j-1}(y_i^+) < \psi^j(y_i^+) < y^*$ for all $j \geq 1$, which means that $\psi^j(y_i^+)$ monotonically increases as j increases, and $\lim_{j\longrightarrow+\infty} \psi^j(y_i^+) = y^*$, $y_i^+ \in [y_{n_1}, y^*)$.

For all $y_i^+ \in (y^*, \theta_1 + a\theta_2/b\theta_2 + b\theta_2 v/b\theta_2 + \beta(\theta_1 + a\theta_2))$, we get $y^* < \psi(y_i^+) < y_i^+$. From the

monotonicity of $\psi(y_i^+)$, we have $y^* < \psi^2(y_i^+) < \psi(y_i^+)$, which means that $\psi^j(y_i^+)$ decreases with increasing value of j and $\lim_{j\longrightarrow+\infty}\psi^j(y_i^+) = y^*$ for all $y_i^+ \in (y^*, \theta_1 + a\theta_2/b\theta_2 + b\theta_2 v/b\theta_2 + \beta(\theta_1 + a\theta_2))$. For all $y_i^+ \in (0, y_{n_1})$, it is easy to get $\psi(y_i^+) \in (y_{n_1}, \theta_1 + a\theta_2/b\theta_2 + b\theta_2 v/b\theta_2 + \beta(\theta_1 + a\theta_2))$, and according to the previous conclusion, we get $\lim_{j\longrightarrow+\infty}\psi^{1+j}(y_i^+) = y^*$. Therefore, the result in Case (a) is true.

(b) If $\psi(y_{n_i})) < y_{n_i}$ for $i = 1, 2$, then we take two cases: (1) $y_i^+ \in (y^*, y_{n_2}]$; (2) $y_i^+ \in (0, y^*) \cup (y_{n_2}, \theta_1 + a\theta_2/b\theta_2 + b\theta_2 v/b\theta_2 + \beta(\theta_1 + a\theta_2))$. For all $y_i^+ \in (y^*, y_{n_2}]$ and according to the monotonicity of the Poincaré map, $\psi(y_i^+)$ satisfies $\psi^2(y_i^+) < y_i^+$. From this, it is easy to get $y^* < \psi^4(y_i^+) < \psi^2(y_i^+)$. By induction, the inequality $y^* < \psi^{2j}(y_i^+) < \psi^{2(j-1)}(y_i^+)$ for all $j \geq 1$ holds, which means that as j increases, the mapping $\psi^{2j}(y_i^+)$ monotonically decreases, and $\lim_{j\longrightarrow+\infty}\psi^{2j}(y_i^+) = y^*$ for all $y_i^+ \in (y^*, y_{n_2}]$. For all $y_i^+ \in (0, y^*) \cup (y_{n_2}, +\infty)$, there exists $k \geq 1$, such that $\psi^k(y_i^+) \in [y^*, y_{n_2})$. From this, we get $\lim_{j\longrightarrow+\infty}\psi^{k+2j}(y_i^+) = y^*$ for all $y_i^+ \in (0, y^*) \cup (y_{n_2}, \theta_1 + a\theta_2/b\ \ \theta_2 + b\theta_2 v/b\theta_2 + \beta(\theta_1 + a\theta_2))$. All the above conclusions indicate that Case (b) is true.

(c) We again take two conditions: (1) $y_i^+ \in (y^*, y_{n_1}]$; (2) $y_i^+ \in (0, y^*) \cup (y_{n_1}, \theta_1 + a\theta_2/b\theta_2 + b\theta_2 v/b\theta_2 + \beta(\theta_1 + a\theta_2))$. For all $y_i^+ \in (y^*, y_{n_1}]$, the Poincaré map $\psi(y_i^+)$ is monotonically decreasing, and the inequality $y^* < \psi^2(y_i^+) < y_i^+$ is satisfied. We can easily get the relationship $y^* < \psi^4(y_i^+) < \psi^2(y_i^+)$, and by induction, $y^* < \psi^{2j}(y_i^+) < \psi^{2(j-1)}(y_i^+)$ for all $j \geq 1$. This means that as j increases, the mapping $\psi^{2j}(y_i^+)$ monotonically decreases, and $\lim_{j\longrightarrow+\infty}\psi^{2j}(y_i^+) = y^*$. For all $y_i^+ \in (0, y^*) \cup (y_{n_1}, +\infty)$, there must exist $l \geq 1$, such that $\psi^l(y_i^+) \in [y^*, y_{n_1}]$. Therefore, we get $\lim_{j\longrightarrow+\infty}\psi^{l+2j}(y_i^+) = y^*$ for all $y_i^+ \in (0, y^*) \cup (y_{n_1}, \theta_1 + a\theta_2/b\theta_2 + b\theta_2 v/b\theta_2 + \beta(\theta_1 + a\theta_2))$, which means that Case (c) is true.

(d) If the conditions given in statement are satisfied, we consider two intervals: (1) $y_i^+ \in [y_{n_2}, y_T]$; (2) $y_i^+ \in (0, y_{n_2}) \cup (y_T, \theta_1 + a\ \ \theta_2/b\theta_2 + b\theta_2 v/b\theta_2 + \beta(\theta_1 + a\theta_2))$. If $y_i^+ \in [y_{n_2}, y_T]$, then according to the monotonicity of the Poincaré map $\psi(y_i^+)$, $\psi^{j_1}(y_i^+)$ monotonically increases as j_1 increases, and $\lim_{j\longrightarrow+\infty}\psi^{j_1}(y_i^+) = y^*$. If $y_i^+ \in (y^*, y_T]$, then $\psi^{j_2}(y_i^+)$ monotonically decreases as j_2 increases, and $\lim_{j\longrightarrow+\infty}\psi^{j_2}(y_i^+) = y^*$. For all $y_i^+ \in (0, y_{n_2}) \cup (y_T, \theta_1 + a\theta_2/\ b\theta_2 + b\theta_2 v/\ b\theta_2 + \beta(\theta_1 + a\theta_2))$, it is easy to know that there must exist a positive integer k, such that $\psi^k(y_i^+) \in [y_{n_2}, y_T]$, and at the same time, $\lim_{j\longrightarrow+\infty}\psi^{k+j_1}(y_i^+) = y^*$ or $\lim_{j\longrightarrow+\infty}\psi^{k+j_2}(y_i^+) = y^*$. Hence, the Case (d) is true. □

Theorem 11. *For Case $(B)(i)$, if $\psi(y_{K_1}) > y_{K_1}$, then the fixed point y^* of Poincaré map $\psi(y_i^+)$ is globally asymptotically stable provided that $\psi^2(y_i^+) > y_i^+$ for all $y_i^+ \in [y_{K_1}, y^*)$.*

Proof. From Theorem 6, we know that for Case $(B)(i)$, a fixed point of Poincaré map $\psi(y_i^+)$ exists.

According to the inequality given in Lemma 3, $\psi(y_i^+) > y_i^+$ for all $y_i^+ \in (0, y_{K_2})$. At the same time, the inequality $\psi(0) = v > 0$ is satisfied. So, the fixed point y^* does not lie in the interval $[0, y_{K_2}]$. This shows that the unique fixed point belongs to the interval $[y_{K_1}, \theta_1 + a\theta_2/b\theta_2 + b\theta_2 v/b\theta_2 + \beta(\theta_1 + a\theta_2))$.

If $y_{K_1} \leq y_i^+ < y^*$, then from the monotonicity of the mapping $\psi(y_i^+)$, we get $\psi(y_{K_1}) \geq \psi(y_i^+) > y^*$. By applying the inequality $\psi^2(y_i^+) > y_i^+$ for all $y_i^+ \in [y_{K_1}, y^*)$, we get $y_i^+ < \psi^2(y_i^+) < y^*$. By induction, there exists a relationship $\psi^{2(j-1)}(y_i^+) < \psi^{2j}(y_i^+) < y^*$ for all $j \geq 1$. This means that as j increases, $\psi^{2j}(y_i^+)$ increases monotonically, and hence $\lim_{j\longrightarrow+\infty}\psi^{2j}(y_i^+) = y^*$. □

Theorem 12. *For Case $(B)(ii)$, if $\psi(y_{K_1}) > y_{K_1}$, then the fixed point of Poincaré map $\psi(y_i^+)$ is globally stable.*

Proof. From Theorem 6, there exists a fixed point of Poincaré map $\psi(y_i^+)$ for Case (B)(ii). Using the same method as in Theorem 11, there is no fixed point on the interval $[0, y_{K_2}]$, and y^* is located in the interval $(y_{K_1}, \theta_1 + a\theta_2/b\theta_2 + b\theta_2 v/b\theta_2 + \beta(\theta_1 + a\theta_2))$. Moreover, under the uniqueness of y^*, the global stability can be described as follows.

For Case (B)(ii), the Poincaré map $\psi(y_i^+)$ is monotonically decreasing in the interval $[0, y_{K_2}]$ and monotonically increasing in the interval $[y_{K_1}, \theta_1 + a\theta_2/b\theta_2 + b\theta_2 v/b\theta_2 + \beta(\theta_1 + a\theta_2))$. If $y_i^+ \in [y_{K_1}, y^*)$, then according to the relationship $y_i^+ < \psi(y_i^+) < y^*$, it is obvious that $\psi^j(y^+)$ increases monotonically towards y^* as j increases, i.e., $\lim_{j\longrightarrow+\infty}\psi^j(y_i^+) = y^*$. For all $y_i^+ \in (y^*, \theta_1 + a\theta_2/b\theta_2 + b\theta_2 v/b\theta_2 + \beta(\theta_1 + a\theta_2))$, according to the relationship $y^* < \psi(y_i^+) < y_i^+$ and properties of Poincaré map $\psi(y_i^+)$, we know that $\psi^j(y_i^+)$ monotonically decreases with the increasing value of j, and $\lim_{j\longrightarrow+\infty}\psi^j(y_i^+) = y^*$.

If $y_i^+ \in [0, y_{K_2}]$, then there must exist some $l \geq 1$ such that $\psi(y_i^+) \in [y_{K_1}, \theta_1 + a\theta_2/b\theta_2 + b\theta_2 v/b\theta_2 + \beta(\theta_1 + a\theta_2))$, and therefore $\lim_{j\longrightarrow+\infty}\psi^{1+j}(y_i^+) = y^*$. Hence, the result in Theorem 12 is correct. □

Theorem 13. *For Case $(B)(iii)$, if $\psi(y_{K_1}) > y_{K_1}$, then the unique fixed point y^* of Poincaré map $\psi(y_i^+)$ exists. If one of the conditions (a) and (b) given below is true, then y^* is globally stable.*

(a) If $\psi(y_{N_i}) > y_{N_i}$ $i = 1, 2$.

(b) If $y_{K_1} \leq \psi(y_{N_2}) = \psi(y_{N_1}) \leq y_{N_1}$, and $\psi^2(y_i^+) > y_i^+$ for all $y_i^+ \in [y_{K_1}, y^*)$.

Proof. For Case (B)(iii), if $\psi(y_{K_1}) > y_{K_1}$, then from Lemma 3 and Theorem 7, we know that Poincaré mapping $\psi(y_i^+)$ has at least one fixed point y^* belonging to the interval $[y_{K_1}, \theta_1 + a\theta_2/b\theta_2 + b\theta_2 v/b\theta_2 + \beta(\theta_1 + a\theta_2))$. Under the uniqueness of y^*, the global stability can be demonstrated as follows:

(a) If $\psi(y_{N_i}) > y_{N_i}$ $i = 1, 2$, then only y^* exists in the interval $[y_{N_1}, \theta_1 + a\theta_2/b\theta_2 + b\theta_2 v/b\theta_2 + \beta(\theta_1 + a\theta_2))$. From Theorem 2, we can see that Poincaré map $\psi(y_i^+)$ is monotonically increasing in the interval $[y_{N_1}, \theta_1 + a\theta_2/b\theta_2 + b\theta_2 v/b\theta_2 + \beta(\theta_1 + a\theta_2))$. For any $y_i^+ \in [y_{N_1}, y^*)$, we get $y_i^+ < \psi(y_i^+) < y^*$, which shows that $\psi^j(y_i^+)$ for $j \geq 1$ increases monotonically, and $\lim_{j\longrightarrow+\infty}\psi^j(y_i^+) = y^*$. For any $y_i^+ \in (y^*, \theta_1 + a\theta_2/b\theta_2 + b\theta_2 v/b\theta_2 + \beta(\theta_1 + a\theta_2)]$, we get the relation $y^* < \psi(y_i^+) < y_i^+$. Therefore, from the monotonicity of $\psi(y_i^+)$, $\psi^j(y_i^+)$ monotonically decreases with increasing value of j, and we get $\lim_{j\longrightarrow+\infty}\psi^j(y_i^+) = y^*$. For all $y_i^+ \in [0, y_{K_2}] \cup [y_{K_1}, y_{N_1})$, it is obvious that there exists an integer $l \geq 0$, such that $\psi^l(y_i^+) \in [y_{N_1}, \theta_1 + a\theta_2/\ b\theta_2 + b\theta_2 v/b\theta_2 + \beta(\theta_1 + a\theta_2))$. Hence, for all $y_i^+ \in [0, y_{K_2}] \cup [y_{K_1}, y_{N_1})$, we get $\lim_{j\longrightarrow+\infty}\psi^{l+j}(y_i^+) = y^*$.

All these results show that if $\psi(y_{N_i}) > y_{N_i}$ $i = 1, 2$, then the unique fixed point y^* of the mapping $\psi(y_i^+)$ is globally stable.

(b) If $y_{K_1} \leq \psi(y_{N_2}) = \psi(y_{N_1}) \leq y_{N_1}$, then combined with the inequality $\psi(y_{K_1}) > y_{K_1}$ given in the statement, it is clear that there exists only one y^* in the interval $(y_{K_1}, y_{N_1}]$. The mapping $\psi(y_i^+)$ monotonically decreases in the interval $[y_{K_1}, y^*)$, i.e., for all $y_i^+ \in [y_{K_1}, y^*)$, we have $\psi(y_{K_1}) \geq \psi(y_i^+) > y^*$. In addition, by applying the condition $\psi^2(y_i^+) > y_i^+$, we get $y_i^+ < \psi^2(y_i^+) < y^*$. Hence, we get $\psi^{2(j-1)}(y_i^+) < \psi^{2j}(y_i^+) < y^*$ for $j \geq 1$. This shows that $\psi^{2j}(y_i^+)$ monotonically increases with the increasing value of j and $\lim_{j\longrightarrow+\infty}\psi^{2j}(y_i^+) = y^*$ for all $y_i^+ \in [y_{K_1}, y^*)$.

If $y_i^+ \in (0, y_{K_2}) \cup (y^*, \theta_1 + a\theta_2/b\theta_2 + b\theta_2 v/b\theta_2 + \beta(\theta_1 + a\theta_2))$ and $y_{K_1} \leq \psi(y_{N_2}) = \psi(y_{N_1}) \leq y_{N_1}$, then there must exist $l \geq 1$ such that $\psi^l(y_i^+) \in [y_{K_1}, y^*]$. By using the same way as above, we get $\lim_{j\longrightarrow+\infty}\psi^{l+2j}(y_i^+) = y^*$ for all $y_i^+ \in [0, y_{K_2}] \cup (y^*, \theta_1 + a\theta_2/b\theta_2 + b\theta_2 v/b\theta_2 + \beta(\theta_1 + a\theta_2))$.

Therefore, if $y_{K_1} \leq \psi(y_{N_2}) = \psi(y_{N_1}) \leq y_{N_1}$ and $\psi^2(y_i^+) > y_i^+$ for all $y_i^+ \in [y_{K_1}, y^*)$, then the fixed point y^* is globally stable. □

9. Conclusions

The IPM strategy is a dynamic management system. From a mathematical perspective, this is actually an optimal control problem under multiple objectives. The IPM approach's purpose is to monitor the number of pest populations in real time and decide whether to implement a control strategy based on the size of the population. The state-dependent impulsive differential equation [20, 45–47] is needed to truly characterize the IPM strategy and the dynamic evolution of pest-natural system. Moreover, in recent years, researchers have proposed a variety of state-dependent pest-natural enemy feedback control systems.

The change rate of pest population plays an important role in state-dependent prey-predator ecological system. There are two fundamental circumstances in the previous studies which require high attention. First, the pest population is comparatively high and the change rate is little; second, the population of pest is small, but the change rate is high. A crucial issue illustrated by these two situations is that when the pest population is large, the growth rate is small or even negative at this time. In this case, even if the IPM strategy is not implemented, the number of pests may not exceed EIL. Another situation is that although the number of pests is not large, the growth rate of the pest population is very large. If the control strategy is not implemented in time, it may lead to a large outbreak of pests. Next, the IPM process needs precise checking of the pest populations, and consequently suitable integrated control strategies can be prepared. The pest killing rate should be a function of their density, whereas the releasing quantity of natural enemies should be a function of their density. Based on this, a feasible new nonlinear state-feedback system with nonlinear ratio-dependent AT is proposed.

The use of nonlinear pulse as state-dependent feedback control with nonlinear ratio-dependent AT is more reasonable and closer to reality in a biological sense, but the impulsive model becomes very difficult because of the existence of two population quantities in the control actions. By including the densities of pest and its natural enemy in controlling measures, we can develop the pest control model based on the practical importance according to the growth direction of agriculture and forestry. Corresponding analytical techniques and numerical methods were developed, the dynamic behavior of the system was examined, and the important role of the main conclusions in integrated pest control was given.

To avoid the complexity, in this paper, we proposed the simple Lotka–Volterra impulsive mathematical model. Our aim is to reveal how nonlinear pulse control with nonlinear ratio-dependent AT affects the whole dynamics and concentrate on the biological implications. The definition and properties of Poincaré map for phase-concentrated pulse points in various cases are discussed and studied. The existence, uniqueness, and global stability of boundary and interior periodic solutions of order 1 for model (1) are analyzed by using the definition of Poincaré map. In the present paper, some basic techniques were used for the qualitative analysis of nonlinear pulsed model with nonlinear ratio-depended AT, which can be widely used in the study of feedback control systems with critical conditions, such as the blood glucose-insulin regulation system.

Data Availability

The data used to support the findings of this study are included within the article.

Conflicts of Interest

The authors declare that they have no conflicts of interest.

Acknowledgments

Basem Al Alwan would like to thank the Deanship of Scientific Research at King Khalid University, Abha, K.S.A., for funding this work through a research group program under grant no. RGP.2/204/42.

References

[1] S. Tang, L. Chen, and L. Chen, "Modelling and analysis of integrated pest management strategy," *Discrete & Continuous Dynamical Systems - B*, vol. 4, no. 3, pp. 759–768, 2004.

[2] S. Tang, G. Tang, and R. A. Cheke, "Optimum timing for integrated pest management: modelling rates of pesticide application and natural enemy releases," *Journal of Theoretical Biology*, vol. 264, no. 2, pp. 623–638, 2010.

[3] S. Tang, J. Liang, Y. Tan, and R. A. Cheke, "Threshold conditions for integrated pest management models with pesticides that have residual effects," *Journal of Mathematical Biology*, vol. 66, no. 1-2, pp. 1–35, 2013.

[4] V. Lakshmikantham, D. D. Bainov, and P. S. Simeonov, *Theory of Impulsive Diferential Equations*, World Scientific, Singapore, 1989.

[5] P. Wang, W. Qin, and G. Tang, "Modelling and analysis of a host-parasitoid impulsive ecosystem under resource limitation," *Complexity*, vol. 2019, Article ID 9365293, 12 pages, 2019.

[6] S. Saha and G. Samanta, "Modeling of insect-pathogen dynamics with biological control," *Mathematical Biology and Bioinformatics*, vol. 15, no. 2, pp. 268–294, 2020.

[7] J. C. van Lenteren and J. Woets, "Biological and integrated pest control in greenhouses," *Annual Review of Entomology*, vol. 33, no. 1, pp. 239–269, 1988.

[8] L. Nie, J. Peng, Z. Teng, and L. Hu, "Existence and stability of periodic solution of a Lotka-Volterra predator-prey model with state dependent impulsive effects," *Journal of Computational and Applied Mathematics*, vol. 224, no. 2, pp. 544–555, 2009.

[9] L. Nie, Z. Teng, L. Hu, and J. Peng, "Existence and stability of periodic solution of a predator-prey model with state-dependent impulsive effects," *Mathematics and Computers in Simulation*, vol. 79, no. 7, pp. 2122–2134, 2009.

[10] Y. Tian, K. Sun, and L. Chen, "Modelling and qualitative analysis of a predator-prey system with state-dependent impulsive effects," *Mathematics and Computers in Simulation*, vol. 82, no. 2, pp. 318–331, 2011.

[11] L. Zhao, L. Chen, and Q. Zhang, "The geometrical analysis of a predator-prey model with two state impulses," *Mathematical Biosciences*, vol. 238, no. 2, pp. 55–64, 2012.

[12] T. Zhang, X. Meng, R. Liu, and T. Zhang, "Periodic solution of a pest management Gompertz model with impulsive state feedback control," *Nonlinear Dynamics*, vol. 78, no. 2, pp. 921–938, 2014.

[13] A. Mondal, A. K. Pal, and G. P. Samanta, "Analysis of a delayed eco-epidemiological pest-plant model with infected pest," *Biophysical Reviews and Letters*, vol. 14, no. 3, pp. 141–170, 2019.

[14] M. B. Thomas, "Ecological approaches and the development of "truly integrated" pest management," *Proceedings of the National Academy of Sciences*, vol. 96, no. 11, pp. 5944–5951, 1999.

[15] S. U. Karaagac, *Insecticide Resistance*, InTech Press, London, 2012.

[16] P. DeBach and D. Rosen, *Biological Control by Natural Enemies*, Cambridge University Press, Cambridge, 1991.

[17] J. Grasman, O. A. van Herwaarden, L. Hemerik, and J. C. van Lenteren, "A two-component model of host-parasitoid interactions: determination of the size of inundative releases of parasitoids in biological pest control," *Mathematical Biosciences*, vol. 169, no. 2, pp. 207–216, 2001.

[18] A. Maiti, A. K. Pal, and G. P. Samanta, "Usefulness of b of pests in tea: a mathematical model," *Mathematical Modelling of Natural Phenomena*, vol. 3, no. 4, pp. 96–113, 2008.

[19] A. Maiti, B. Patra, and G. P. Samanta, "Sterile insect release method as a control measure of insect pests: a mathematical model," *Journal of Applied Mathematics and Computing*, vol. 22, no. 3, pp. 71–86, 2006.

[20] S. Tang, Y. Xiao, and R. A. Cheke, "Multiple attractors of host-parasitoid models with integrated pest management strategies: eradication, persistence and outbreak," *Theoretical Population Biology*, vol. 73, no. 2, pp. 181–197, 2008.

[21] S. Tang, Y. Xiao, L. Chen, and R. Cheke, "Integrated pest management models and their dynamical behaviour," *Bulletin of Mathematical Biology*, vol. 67, no. 1, pp. 115–135, 2005.

[22] J. C. V. Lenteren, "Integrated pest management in protected crops," in *Integrated Pest Management*, D. Dent, Ed., pp. 311–343, Chapman & Hall, London, 1995.

[23] J. C. V. Lenteren, *Environmental Manipulation Advantageous to Natural Enemies of Pests*, V. Delucchi, Ed., pp. 123–166, Integrated Pest Management, Parasitis, Geneva, 1987.

[24] Y. N. Xiao and F. V. D. Bosch, "The dynamics of an eco-epidemic model with biological control," *Ecological Modelling*, vol. 168, no. 1-2, pp. 203–214, 2003.

[25] H. J. Barclay, "Models for pest control using predator release, habitat management and pesticide release in combination," *Journal of Applied Ecology*, vol. 19, no. 2, pp. 337–348, 1982.

[26] W. Znegui, H. Gritli, and S. Belghith, "Stabilization of the passive walking dynamics of the compass-gait biped robot by developing the analytical expression of the controlled Poincaré map," *Nonlinear Dynamics*, vol. 101, no. 8, pp. 1061–1091, 2020.

[27] W. Znegui, H. Gritli, and S. Belghith, "A new Poincaré map for investigating the complex walking behavior of the compass-gait biped robot," *Applied Mathematical Modelling*, vol. 94, pp. 534–557, 2021.

[28] H. Gritli and S. Belghith, "Walking dynamics of the passive compass-gait model under OGY-based state-feedback control: analysis of local bifurcations via the hybrid Poincaré map," *Chaos, Solitons & Fractals*, vol. 98, pp. 72–87, 2017.

[29] W. Znegui, H. Gritli, and S. Belghith, "Design of an explicit expression of the Poincaré map for the passive dynamic walking of the compass-gait biped model," *Chaos, Solitons & Fractals*, vol. 130, no. 12, 2020.

[30] H. Gritli, F. Turki, and S. Belghith, "State-feedback control via LMI approach of a 1-DOF disturbed impacting mechanical oscillator under double-side rigid constraints," in *Proceedings of the International Conference on Advanced Systems and Electric Technologies (IC ASET)*, pp. 441–448, IEEE, Hammamet, Tunisia, 22 March 2018.

[31] F. Turki, H. Gritli, and S. Belghith, "Robust position control of a two-sided 1-DoF impacting mechanical oscillator subject to an external persistent disturbance by means of a state-Feedback controller," *Complexity*, vol. 2019, Article ID 9174284, 14 pages, 2019.

[32] G. P. Samanta, "Analysis of a delayed epidemic model with pulse vaccination," *Chaos, Solitons & Fractals*, vol. 66, pp. 74–85, 2014.

[33] J. Wang, H. Cheng, X. Meng, and B. G. S. A. Pradeep, "Geometrical analysis and control optimization of a predator-prey model with multi state-dependent impulse," *Advances in Difference Equations*, vol. 2017, Article ID 252, 2017.

[34] Q. Xiao and B. Dai, "Periodic solutions generated by impulses for state-dependent impulsive differential equation," *Discrete*

Dynamics in Nature and Society, vol. 2015, Article ID 816325, 7 pages, 2015.

[35] L. Feng and Z. Liu, "An impulsive periodic predator-prey Lotka-Volterra type dispersal system with mixed functional responses," *Journal of Applied Mathematics and Computing*, vol. 45, no. 1-2, pp. 235–257, 2014.

[36] M. Kogan, "Integrated pest management: historical perspectives and contemporary developments," *Annual Review of Entomology*, vol. 43, no. 1, pp. 243–270, 1998.

[37] S. Tang and R. A. Cheke, "State-dependent impulsive models of integrated pest management (IPM) strategies and their dynamic consequences," *Journal of Mathematical Biology*, vol. 50, no. 3, pp. 257–292, 2005.

[38] Y. Tian, S. Tang, and R. A. Cheke, "Nonlinear state-dependent feedback control of a pest-natural enemy system," *Nonlinear Dynamics*, vol. 94, no. 3, pp. 2243–2263, 2018.

[39] I. U. Khan, S. Y. Tang, and B. Tang, "The state-dependent impulsive model with action threshold depending on the pest density and its changing rate," *Complexity*, vol. 2019, Article ID 6509867, 15 pages, 2019.

[40] S. H. M. J. Houben, J. M. L. Maubach, and R. M. M. Mattheij, "An accelerated Poincaré-map method for autonomous oscillators," *Applied Mathematics and Computation*, vol. 140, no. 2-3, pp. 191–216, 2003.

[41] R. Efrem, "Numerical approximation of Poincaré maps," *Romanistisches Jahrbuch*, vol. 4, no. 1, pp. 101–106, 2008.

[42] M. Henon, "On the numerical computation of Poincar maps," *Physica D: Nonlinear Phenomena*, vol. 5, no. 2-3, pp. 412–414, 1982.

[43] P. S. Simeonov and D. D. Bainov, "Orbital stability of periodic solutions of autonomous systems with impulse effect," *International Journal of Systems Science*, vol. 19, no. 12, pp. 2561–2585, 1988.

[44] D. Bainov and P. Simeonov, *Impulsive Differential Equations, Periodic Solutions and Applications, Monographs and Surveys in Pure and Applied Mathematics*, Longman Scientific and Technical, New York, 1993.

[45] S. Tang and R. A. Cheke, "Models for integrated pest control and their biological implications," *Mathematical Biosciences*, vol. 215, no. 1, pp. 115–125, 2008.

[46] J. Yang and S. Tang, "Holling type II predator-prey model with nonlinear pulse as state-dependent feedback control," *Journal of Computational and Applied Mathematics*, vol. 291, pp. 225–241, 2016.

[47] S. Y. Tang, X. W. Tan, J. Yang, and J. H. Liang, "Periodic solution bifurcation and spiking dynamics of impacting predator-prey dynamical model," *Int. J. Bif. and Chaos*, vol. 28, no. 12, 2018.

Hindawi
Complexity
Volume 2021, Article ID 2018307, 9 pages
https://doi.org/10.1155/2021/2018307

Research Article

A Fractional-Order Sequential Hybrid System with an Application to a Biological System

Hasib Khan,[1] Hashim M. Alshehri,[2] and Zareen A. Khan[3]

[1]*Department of Mathematics, Shaheed Benazir Bhutto University Sheringal Dir Upper, Sheringal, Khyber Pakhtunkhwa, Pakistan*
[2]*Mathematics Department, Faculty of Sciences, King Abdulaziz University, Jeddah 21521, Saudi Arabia*
[3]*Department of Mathematical Sciences, College of Science, Princess Nourah bint Abdulrahman University, Riyadh, Saudi Arabia*

Correspondence should be addressed to Zareen A. Khan; zakhan@pnu.edu.sa

Received 7 May 2021; Accepted 14 July 2021; Published 23 July 2021

Academic Editor: Constantin Udriste

With the help of Banach's fixed-point approach and the Leray–Schauder alternative theorem, we produced existence results for a general class of fractional differential equations in this paper. The proposed problem is more comprehensive and applicable to real-life situations. As an example of how our problem might be used, we have created a fractional-order COVID-19 model whose solution is guaranteed by our results. We employed a numerical approach to solve the COVID-19 model, and the results were compared for different fractional orders. Our numerical results for fractional orders follow the same pattern as the classical example of order 1, indicating that our numerical scheme is accurate.

1. Introduction

In science and engineering, fractional-order operators have lately been investigated for the modeling of dynamical systems. There are operators based on singular kernels and nonsingular kernels. It is tough to determine which operator is the best at the moment, but researchers are constantly analyzing various operators for new features and uses. We have seen that in the vast majority of cases, researchers must compare their findings to the traditional results in terms of accuracy, stability, and simulations. Atangana and Araz focused on the modeling and existence results of the COVID-19 model [1, 2]. The area of fractional calculus is still open for the researchers to investigate nonlinear models for their theoretical and computational studies with the help of [6–9].

In order to highlight the literature for the existence results and numerical simulations and their applications, we present some examples. Recently, Ahmad et al. [3] discussed a fractional-order COVID-19 model for the existence, uniqueness, and comparative analysis with the existing integer-order model. Babakhani and Daftardar-Gejji [4] studied a boundary value problem of fractional order for the existence of results and presented some applications of their results. Tuan et al. [5] gave some theoretical and computational studies of a fractional-order COVID-19 model for the existence and numerical simulations by the help of Haar wavelets approach. Zhang et al. [10] investigated an impulsive integrodifferential equation for the existence of results and applications.

Boundary value problems (BVPs) with lower-order fractional derivatives and either constant or linear boundary conditions are considered in the majority of these papers. However, there are many cases where nonlinear circumstances at the boundary and differential equations are possible. For example, in case of head flow problems, there are possibilities to have some source or sink on both sides of the boundary (at $x = 0$ and $x = 1$) which may be nonlinear functions and a controller at $x = \zeta_0\,(0 < \zeta_0 < 1)$. Okuonghae and Omame [11] studied a nonlinear system of hybrid fractional differential equations (FDEs) for the existence and applications of solutions. The purpose of this paper is to

investigate existence results for BVPs involving nonlinear boundary conditions at both ends; that is, we study the following class of two-point BVPs:

$$ {}^{c}\mathscr{D}^{\vartheta_i}\left[{}^{c}\mathscr{D}^{\omega_i^{**}}u_i^*(t)-\sum_{1}^{m}h_i\left(t,u_i^*(t)\right)\right]=-f_i\left(t,u_i^*(t)\right),\quad t\in I=[0,1],u_i^*(0)=0,u_i^*(1)=0, \tag{1} $$

where the fractional orders $0<\vartheta_i\le 1$ and $0\le\omega_i^{**}\le 1$, the functions $u_i^*\colon \mathrm{I}\longrightarrow\mathscr{R}_e$ are fractional-order differentiable functions for $i=1,2,\ldots,m$, and $f_i\colon \mathrm{I}\times\mathscr{R}_e\longrightarrow\mathscr{R}_e-\{0\}$ and $h_i\colon \mathrm{I}\times\mathscr{R}_e\longrightarrow\mathscr{R}_e\,(i=1,2,\ldots,m)$ satisfy the Caratheodory conditions. The fractional-order derivatives ${}^{c}\mathscr{D}^{\vartheta c}\mathscr{D}^{\omega_i^{**}}$ are in Caputo's sense. To the best of our knowledge, existence, uniqueness, and stability results had never been studied for BVP (1). Such situation may have importance in application point of view and also in theoretical development and can be studied in the work of Dhage in [12–14] and the reference therein.

2. Existence Criteria

Lemma 1. *For integrable functions f_i and h_i on I, problem (1) has integral representation given by*

$$ u_i^*(t)=\int_0^1 K_{\omega_i,\vartheta_i}(s,t)f_i\left(s,u_i^*(s)\right)\mathrm{d}s, \tag{2} $$

where $K_{\omega_i}(s,t)$ is Green's function given by

$$ K_{\omega_i,\vartheta_i}(s,t)=\frac{1}{\Gamma\left(\omega_i^{**}+\vartheta_i\right)}\begin{cases}(1-s)^{\omega_i^{**}+\vartheta_i-1}; & t\le s,\\ (1-s)^{\omega_i^{**}+\vartheta_i-1}-(t-s)^{\omega_i^{**}+\vartheta_i-1}, & s\le t,\end{cases} \tag{3} $$

for $i=1,2,\ldots,m$.

Proof. Applying integral (I^{ϑ_i}) to problem (1), we obtain

$$ {}^{c}\mathscr{D}^{\omega_i^{**}}u_i^*(t)-\sum_{1}^{m}I^{\omega_i}h_i\left(t,u_i^*(\delta_i)\right)=-I^{\vartheta_i}f_i\left(t,u_i^*(t)\right)+C_1, \tag{4} $$

for $i=1,2,\ldots,m$. By the help of $u_i^*(0)=0$, we have $C_1=0$ and hence, we obtain

$$ {}^{c}\mathscr{D}^{\omega_i^{**}}u_i^*(t)=\sum_{1}^{m}h_i\left(t,u_i^*(\delta_i)\right)-I^{\vartheta_i}f_i\left(t,u_i^*(t)\right). \tag{5} $$

Now, applying I^{ϑ_i}, for $i=1,2,\ldots,m$ on (5), we have

$$ u_i^*(t)=\sum_{1}^{m}\mathscr{I}^{\omega_i^{**}}h_i\left(t,u_i^*(\delta_i)\right)-I^{\vartheta_i+\omega_i^{**}}f_i\left(t,u_i^*(t)\right)+K_1. \tag{6} $$

By the use of initial condition $u_i^*(1)=0$, for $i=1,2,\ldots,m$ and (6), we have $K_1=I^{\vartheta_i+\omega_i^{**}}f_i(t,u_i^*(t))|_{t=1}$. Ultimately, we have the following solution:

$$ \begin{aligned} u_i^*(t)&=I^{\vartheta_i+\omega_i^{**}}f_i\left(t,u_i^*(t)\right)|_{t=1}-I^{\vartheta_i+\omega_i^{**}}f_i\left(t,u_i^*(t)\right)\\ &=\frac{1}{\Gamma\left(\vartheta_i+\omega_i^{**}\right)}\int_0^1(1-s)^{\vartheta_i+\omega_i^{**}-1}f_i\left(s,u_i^*(s)\right)\mathrm{d}s-\frac{1}{\Gamma\left(\vartheta_i+\omega_i^{**}\right)}\int_0^t(t-s)^{\vartheta_i+\omega_i^{**}-1}f_i\left(s,u_i^*(s)\right)\mathrm{d}s\\ &=\int_0^1 K_{\omega_i,\vartheta_i}(t,s)f_i\left(s,u_i^*(s)\right)\mathrm{d}s. \end{aligned} \tag{7} $$

$K_{\omega_i,\vartheta_i}(s,t)$ are Green's functions defined in (3), for $i=1,2,\ldots,m$. □

Here, we introduce a Banach's space $\mathscr{B}=\{f_i(t)\colon f_i(t)\in\mathscr{C}([0,1],\mathbb{R}),\text{for}\,t\in[0,1]\}$, with a norm

$\|f_i\| = \max_{t\in[0,1]} f_i(t)$, for $i = 1, 2, \ldots, m$. Let us a define an operator $\mathcal{T}_i$: $\mathcal{C}([0,1], \mathbb{R}) \longrightarrow \mathcal{C}([0,1], \mathbb{R})$, for $i = 1, 2, \ldots, m$, such that

$$\begin{aligned}\mathcal{T}_i u_i^*(t) &= I^{\vartheta_i+\omega_i^{**}} f_i(t, u_i^*(t))|_{t=1} - I^{\vartheta_i+\omega_i^{**}} f_i(t, u_i^*(t)) \\ &= \frac{1}{\Gamma(\vartheta_i+\omega_i^{**})}\int_0^1 (1-s)^{\vartheta_i+\omega_i^{**}-1} f_i(s, u_i^*(s))\mathrm{d}s - \frac{1}{\Gamma(\vartheta_i+\omega_i^{**})}\int_0^t (t-s)^{\vartheta_i+\omega_i^{**}-1} f_i(s, u_i^*(s))\mathrm{d}s \\ &= \int_0^1 K_{\omega_i,\vartheta_i}(t,s) f_i(s, u_i^*(s))\mathrm{d}s,\end{aligned} \tag{8}$$

where $K_{\omega_i,\vartheta_i}(s,t)$ are Green's functions defined in (3), for $i = 1, 2, \ldots, m$. Then, the solutions of fractional-order system (1) are the fixed points of the operator $\mathcal{T}_i$ defined in (8).

Also, with the help of (3), Green's functions $K_{\omega_i}(s,t) > 0$ for the following cases. For $t \le s$, we have $K_{\omega_i}(s,t) = (1-s)^{\omega_i^{**}+\vartheta_i-1}$, which is obviously positive. And for $t \ge s$, we have $K_{\omega_i}(s,t) = (1-s)^{\omega_i^{**}+\vartheta_i-1} - (t-s)^{\omega_i^{**}+\vartheta_i-1}$. Since $(1-s) \ge (t-s)$, for all $t, s \in [0,1]$, and as per our assumption $\omega_i^{**} + \vartheta_i > 1$, we have $(1-s)^{\omega_i^{**}+\vartheta_i-1} \ge (t-s)^{\omega_i^{**}+\vartheta_i-1}$. Ultimately, Green's functions are positive.

Lemma 2. *Let $f_i \in \mathcal{C} = \mathcal{C}([0,1] \times \mathcal{R}_e, \mathcal{R}_e)$ be continuous functions for all $i = 1, 2, \ldots, m$ and there exist some positive constants $\lambda_i \in \mathcal{R}_e$, for $u_l^*, u_j^* \in \mathcal{C}$ and $t \in [0,k]$, such that*

$$\left|f_i(t, u_l^*) - f_i\left(t, u_j^*\right)\right| \le \lambda_i \left|u_l^* - u_j^*\right|, \tag{9}$$

for all $i = 1, 2, \ldots, m$ and $\beta_i = \lambda_i(1 + k^{\vartheta_i+\omega_i^{**}})(\lambda_i\eta_i + \wp)/\Gamma(\vartheta_i + \omega_i^{**} + 1) < 1$, for $i = 1, 2, \ldots, m$. Then, the system of fractional order (1) has a unique solution.

Proof. Let us consider $\sup_{t\in[0,k]}|f_i(t,0)| = \wp < \infty$ and $\mathcal{S}_{\eta_i} = \{u \in \mathcal{C}([0,k], \mathcal{R}_e): \|u\| < \eta_i\}$, where $\max_{t\in[0,k]}\lambda_i$, for $i = 1, 2, \ldots, m$ and $k \ge 1$.

For $u_i^* \in \mathcal{S}_{\eta_i}$, for $i = 1, 2, \ldots, m$ and $t \in [0,k]$, we have

$$\begin{aligned}\left|f_i(t, u_i^*(t))\right| &= \left|f_i(t, u_i^*(t)) - f_i(t,0) + f_i(t,0)\right| \\ &\le \left|f_i(t, u_i^*(t)) - f_i(t,0)\right| + \left|f_i(t,0)\right| \\ &\le \lambda_i\left|u_i^*(t)\right| + \left|f_i(t,0)\right| \\ &\le \lambda_i\eta_i + \wp.\end{aligned} \tag{10}$$

With the help of (8) and (10), for $i = 1, 2, \ldots, m$, we obtain

$$\begin{aligned}\left|\mathcal{T}_i u_i^*(t)\right| &= \left|\frac{1}{\Gamma(\vartheta_i+\omega_i^{**})}\int_0^1 (1-s)^{\vartheta_i+\omega_i^{**}-1} f_i(s, u_i^*(s))\mathrm{d}s - \frac{1}{\Gamma(\vartheta_i+\omega_i^{**})}\int_0^t (t-s)^{\vartheta_i+\omega_i^{**}-1} f_i(s, u_i^*(s))\mathrm{d}s\right| \\ &\le \frac{1}{\Gamma(\vartheta_i+\omega_i^{**})}\int_0^1 (1-s)^{\vartheta_i+\omega_i^{**}-1}\left|f_i(s, u_i^*(s))\right|\mathrm{d}s + \frac{1}{\Gamma(\vartheta_i+\omega_i^{**})}\int_0^t (t-s)^{\vartheta_i+\omega_i^{**}-1}\left|f_i(s, u_i^*(s))\right|\mathrm{d}s \\ &\le \frac{\lambda_i\eta_i+\wp}{\Gamma(\vartheta_i+\omega_i^{**})}\int_0^1 (1-s)^{\vartheta_i+\omega_i^{**}-1}\mathrm{d}s + \frac{\lambda_i\eta_i+\wp}{\Gamma(\vartheta_i+\omega_i^{**})}\int_0^t (t-s)^{\vartheta_i+\omega_i^{**}-1}\mathrm{d}s \\ &= \frac{\lambda_i\eta_i+\wp}{\Gamma(\vartheta_i+\omega_i^{**}+1)}\left(1 + t^{\vartheta_i+\omega_i^{**}}\right) \\ &\le \frac{\left(1+k^{\vartheta_i+\omega_i^{**}}\right)(\lambda_i\eta_i+\wp)}{\Gamma(\vartheta_i+\omega_i^{**}+1)}.\end{aligned} \tag{11}$$

This implies $\mathscr{T}_i\mathscr{S}_{\eta_i} \subset \mathscr{S}_{\eta_i}$. Furthermore, we assume $u_l^*, u_j^* \in \mathscr{C}([0,k], \mathscr{R}_e)$; for all $t \in [0,k]$, we have

$$\begin{aligned}\left|\mathscr{T}_i u_l^*(t) - \mathscr{T}_i u_j^*(t)\right| &= \frac{1}{\Gamma\left(\vartheta_i + \omega_i^{**}\right)} \int_0^1 (1-s)^{\vartheta_i+\omega_i^{**}-1} \left|f_i\left(s, u_l^*(s)\right) - f_i\left(s, u_j^*(s)\right)\right| \mathrm{d}s \\ &\quad + \frac{1}{\Gamma\left(\vartheta_i + \omega_i^{**}\right)} \int_0^t (t-s)^{\vartheta_i+\omega_i^{**}-1} \left|f_i\left(s, u_l^*(s)\right) - f\left(s, u_j^*(s)\right)\right| \mathrm{d}s \\ &\leq \frac{\lambda_i\left(\left|u_l^* - u_j^*\right|\right)}{\Gamma\left(\vartheta_i + \omega_i^{**}\right)} \int_0^1 (1-s)^{\vartheta_i+\omega_i^{**}-1} \mathrm{d}s + \frac{\lambda_i\left(\left|u_l^* - u_j^*\right|\right)}{\Gamma\left(\vartheta_i + \omega_i^{**}\right)} \int_0^t (t-s)^{\vartheta_i+\omega_i^{**}-1} \mathrm{d}s \\ &\leq \frac{\lambda_i\left(1 + k^{\vartheta_i+\omega_i^{**}}\right)}{\Gamma\left(\vartheta_i + \omega_i^{**} + 1\right)} \left|u_l^* - u_j^*\right| \leq \beta_i \left|u_l^* - u_j^*\right|,\end{aligned} \tag{12}$$

for $i = 1, 2, \ldots, m$. Ultimately, the operator is a contraction and by Banach's fixed-point theorem, the system of fractional order (1) has a unique solution. □

Theorem 1. *Assume that the $f_i \in \mathscr{C}([0,k] \times \mathscr{R}_e, \mathscr{R}_e)$, for $i = 1, 2, \ldots, m$. Then, fractional-order system (1) has a solution provided that the assumptions of Lemma 2 are satisfied.*

Proof. However, in Lemma 2, we have studied that the operator $\mathscr{T}_i$ is a bounded operator and $\mathscr{T}_i\mathscr{S}_{\eta_i} \subset \mathscr{S}_{\eta_i}$. Now, in order to prove the existence of solution of problem (1), we move towards the equicontinuity of the $\mathscr{T}_i$. For this, let us assume $t_1, t_2 \in [0,k]$ with $t_2 > t_1$, and consider

$$\begin{aligned}\left|\mathscr{T}_i u_i^*(t_2) - \mathscr{T}_i u_i^*(t_1)\right| &= \left|\frac{1}{\Gamma\left(\vartheta_i + \omega_i^{**}\right)} \int_0^{t_2} (t_2-s)^{\vartheta_i+\omega_i^{**}-1} f_i(s, u_i^*(s)) \mathrm{d}s - \frac{1}{\Gamma\left(\vartheta_i + \omega_i^{**}\right)} \int_0^{t_1} (t_1-s)^{\vartheta_i+\omega_i^{**}-1} f_i(s, u_i^*(s)) \mathrm{d}s\right| \\ &\leq \frac{\lambda_i\eta_i + \wp}{\Gamma\left(\vartheta_i + \omega_i^{**} + 1\right)} \left(\int_0^{t_2} (t_2-s)^{\vartheta_i+\omega_i^{**}-1} \mathrm{d}s - \int_0^{t_1} (t_1-s)^{\vartheta_i+\omega_i^{**}-1} \mathrm{d}s\right) = \frac{\lambda_i\eta_i + \wp}{\Gamma\left(\vartheta_i + \omega_i^{**} + 1\right)} \left(t_2^{\vartheta_i+\omega_i^{**}} - t_1^{\vartheta_i+\omega_i^{**}}\right).\end{aligned} \tag{13}$$

This implies $|\mathscr{T}_i u_i^*(t_2) - \mathscr{T}_i u_i^*(t_1)| \longrightarrow 0$ as $t_2 \longrightarrow t_1$. This implies that the operator $\mathscr{T}_i$ is equicontinuous. Next, we show that $\mathscr{A} = \{u^* \in \mathscr{C}([0,k], \mathscr{R}_e)\colon u^* = \hbar\mathscr{T}_i(u^*), \text{for } \hbar \in [0,1]\}$ is bounded. For this, consider

$$\begin{aligned}\left\|u^*\right\| = \left|\hbar\mathscr{T}_i u_i^*(t)\right| &= \hbar\left|\frac{1}{\Gamma\left(\vartheta_i + \omega_i^{**}\right)} \int_0^1 (1-s)^{\vartheta_i+\omega_i^{**}-1} f_i\left(s, u_i^*(s)\right) \mathrm{d}s - \frac{1}{\Gamma\left(\vartheta_i + \omega_i^{**}\right)} \int_0^t (t-s)^{\vartheta_i+\omega_i^{**}-1} f_i\left(s, u_i^*(s)\right) \mathrm{d}s\right| \\ &\leq \frac{\hbar}{\Gamma\left(\vartheta_i + \omega_i^{**}\right)} \int_0^1 (1-s)^{\vartheta_i+\omega_i^{**}-1} \left|f_i\left(s, u_i^*(s)\right) - f_i(s,0) + f_i(s,0)\right| \mathrm{d}s \\ &\quad + \frac{\hbar}{\Gamma\left(\vartheta_i + \omega_i^{**}\right)} \int_0^t (t-s)^{\vartheta_i+\omega_i^{**}-1} \left|f_i\left(s, u_i^*(s)\right) - f_i(s,0) + f_i(s,0)\right| \mathrm{d}s \\ &\leq \frac{\hbar\left(\lambda_i\left\|u^*\right\| + \wp\right)}{\Gamma\left(\vartheta_i + \omega_i^{**}\right)} \int_0^1 (1-s)^{\vartheta_i+\omega_i^{**}-1} \mathrm{d}s + \frac{\hbar\left(\lambda_i\left\|u^*\right\| + \wp\right)}{\Gamma\left(\vartheta_i + \omega_i^{**}\right)} \int_0^t (t-s)^{\vartheta_i+\omega_i^{**}-1} \mathrm{d}s \leq \frac{\hbar\left(1 + k^{\vartheta_i+\omega_i^{**}}\right)\left(\lambda_i\left\|u^*\right\| + \wp\right)}{\Gamma\left(\vartheta_i + \omega_i^{**} + 1\right)}.\end{aligned} \tag{14}$$

By the help of (14), we have

$$\|u^*\| \leq \frac{\hbar\left(1+k^{\vartheta_i+\omega_i^{**}}\right)\wp}{\Gamma\left(\vartheta_i+\omega_i^{**}+1\right)-\hbar\left(1+k^{\vartheta_i+\omega_i^{**}}\right)\lambda_i}, \tag{15}$$

for $i = 1, 2, \ldots, m$. Hence, by (15), we have that the set $\mathscr{A}$ is bounded. Therefore, by Leray–Schauder alternative theorem, operator $\mathscr{T}_i$ has at least one fixed point which is the solution of fractional-order system (1). □

3. Hyers–Ulam Stability

In this section, we are presenting the Hyers–Ulam stability analysis for hybrid fractional differential equation (8).

Definition 1. Fractional integral system (8) is said to be Hyers–Ulam stable, if there exists a constant $\zeta > 0$, such that for a given $\varphi > 0$ and for each solution u_i^* of the inequality

$$\left\|u_i^* - \mathscr{T}_i u_i^*\right\|_1 < \varphi, \tag{16}$$

there exists a solution $\overline{u_i^*}(t)$ of integral system (8),

$$\overline{u}_i^*(t) = \mathscr{T}_i \overline{u}_i^*(t), \tag{17}$$

such that

$$\left\|u_i^* - \overline{u}_i^*\right\| < \varphi\zeta. \tag{18}$$

Theorem 2. *Assume that $f_i \in \mathscr{C}([[0,k]\times\mathscr{R}_e, \mathscr{R}_e)$, for $i = 1, 2, \ldots, m$. Then, fractional-order system (1) is Hyers–Ulam stable provided that the assumptions of Lemma 2 are satisfied.*

Proof. Let $u_i^* \in \mathscr{C}$ satisfy the inequality (16) and $\overline{u_i^*} \in \mathscr{C}$ be a solution of BVP (1) satisfying integral system (8). By the help of (16) and (17), consider the following norm:

$$\left\|u_i^* - \overline{u}_i^*\right\| = \left\|u_i^* - \mathscr{T}_i u_i^* + \mathscr{T}_i u_i^* - \overline{u}_i^*\right\| \leq \left\|u_i^* - \mathscr{T}_i u_i^*\right\| + \left\|\mathscr{T}_i u_i^* - \mathscr{T}_i \overline{u}_i^*\right\| \leq \varphi_i + \lambda_i\left\|u_i^* - \overline{u}_i^*\right\|, \tag{19}$$

for $i = 1, 2, \ldots, m$. This further implies that

$$\left\|u_i^* - \overline{u}_i^*\right\| \leq \frac{\varphi}{1-\lambda_i}, \tag{20}$$

with $\zeta_i = 1/1 - \lambda_i$, for $i = 1, 2, \ldots, m$. Therefore, system (8) is Hyers–Ulam stable which implies the stability of fractional-order system (1). □

4. Application

In this section, we give a specific example of fractional-order system (1) which is a fractional-order extension of the COVID-19 model given in [15]:

$$\begin{aligned}
\mathscr{D}_0^{\vartheta_1}\mathcal{S} &= \Lambda^* - \frac{\alpha^*\mathcal{S}\mathcal{I}_1}{1+m\mathcal{I}_1^2} - \frac{\beta^*\mathcal{S}\mathcal{I}_2}{1+k\mathcal{I}_2^2} - \delta^*\mathcal{S},\\
\mathscr{D}_0^{\vartheta_2}\mathrm{E}_1 &= \frac{\alpha^*\mathcal{S}\mathcal{I}_1}{1+m\mathcal{I}_1^2} - (\gamma_1^*+\delta^*)\mathrm{E}_1,\\
\mathscr{D}_0^{\vartheta_3}\mathrm{E}_2 &= \frac{\beta^*\mathcal{S}\mathcal{I}_2}{1+k\mathcal{I}_2^2} - (\gamma_2^*+\delta^*)\mathrm{E}_2,\\
\mathscr{D}_0^{\vartheta_4}\mathcal{I}_1 &= \gamma_1^*\mathrm{E}_1 - (\mu_1^*+\delta^*)\mathcal{I}_1,\\
\mathscr{D}_0^{\vartheta_5}\mathcal{I}_2 &= \gamma_2^*\mathrm{E}_2 - (\mu_2^*+\delta^*)\mathcal{I}_2,\\
\mathscr{D}_0^{\vartheta_6}\mathcal{R} &= \mu_1^*\mathcal{I}_1 + \mu_2^*\mathcal{I}_2 - \delta^*\mathcal{R}.
\end{aligned} \tag{21}$$

Here, $\vartheta_i \in (0,1]$, for $i = 1, 2, \ldots, 6$, $(u_1^*, u_2^*, \ldots, u_6^*) = (\mathcal{S}, \mathscr{E}_1, \mathscr{E}_2, \mathcal{I}_1, \mathcal{I}_2, \mathcal{R})$, $f_1 = \Lambda^* - \alpha^*\mathcal{S}\mathcal{I}_1/1 + m\mathcal{I}_1^2 - \beta^*\mathcal{S}\mathcal{I}_2/1 + k\mathcal{I}_2^2 - \delta^*\mathcal{S}$, $f_2 = \alpha^*\mathcal{S}\mathcal{I}_1/1 + m\mathcal{I}_1^2 - (\gamma_1^*+\delta^*)\mathscr{E}_1$, $f_3 = \beta^*\mathcal{S}\mathcal{I}_2/1 + k\mathcal{I}_2^2 - (\gamma_2^*+\delta^*)\mathscr{E}_2$, $f_4 = \gamma_1^*\mathscr{E}_1 - (\mu_1^*+\delta^*)\mathcal{I}_1$, $f_5 = \gamma_2^*\mathscr{E}_2 - (\mu_2^*+\delta^*)\mathcal{I}_2$, and $f_6 = \mu_1^*\mathcal{I}_1 + \mu_2^*\mathcal{I}_2 - \delta^*\mathcal{R}$.

Fractional-order model (21) has six compartments. $\mathcal{S}(t)$ represents the susceptible class, $\mathscr{E}_1(t)$ and $\mathscr{E}_2(t)$ are latent individuals, $\mathcal{I}_1(t)$ and $\mathcal{I}_2(t)$ are infected individuals, and $\mathcal{R}(t)$ is the recovered class. The parameters include the following: Λ is the recruitment rate, $1/\delta$ is the average life of the population, α is the infection rate of strain 1, β is the infection rate of strain 2, $1/\mu_1$ is the average infection period for strain 1, $1/\mu_2$ is the average infection period for strain 2, $1/\gamma_1$ is the average latency rate for strain 1, $1/\gamma_2$ is the average latency rate for strain 2, m is the psychological effect of strain 1, and k is the psychological effect of strain 2.

The existence of solution of (21) is ensured by Theorem 1. The stability of (21) is also ensured by Theorem 2. Now, we give the numerical scheme for the simulation of (21) as follows. By applying the fractional-order Riemann–Liouville integral operator for the equispace intervals of $[0, k]$, we get the following form:

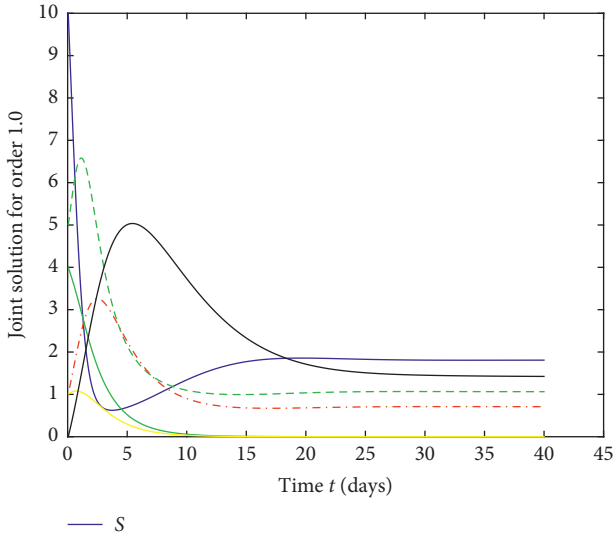

Figure 1: Joint solution of (21) for order 1.0.

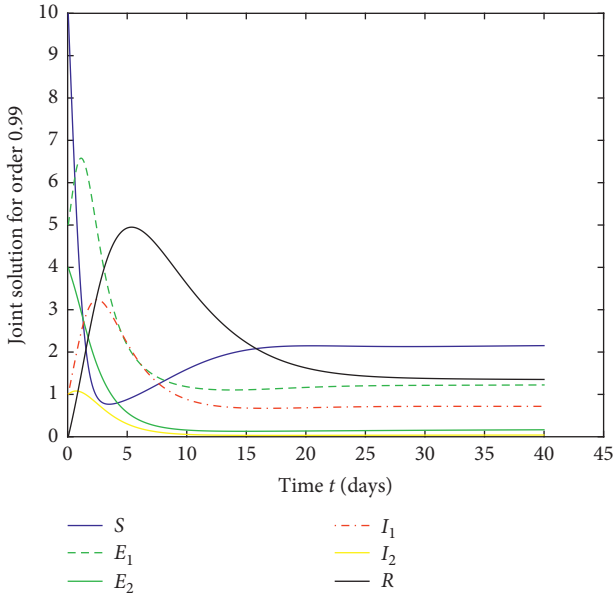

Figure 2: Joint solution of (21) for order 0.99.

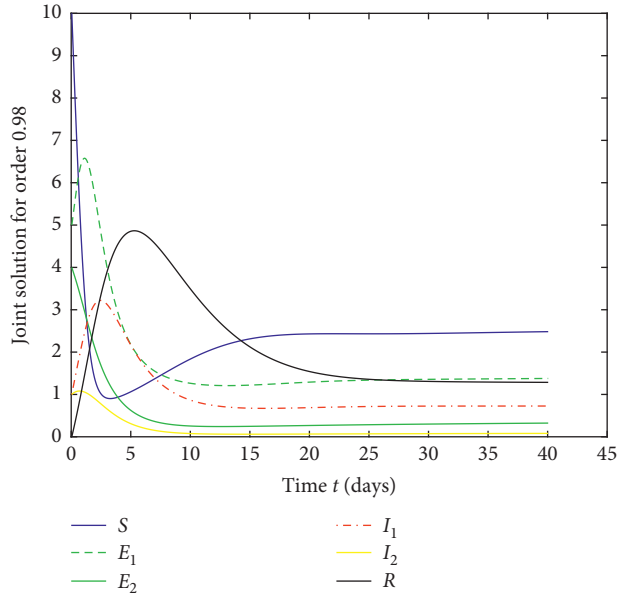

Figure 3: Joint solution of (21) for order 0.98.

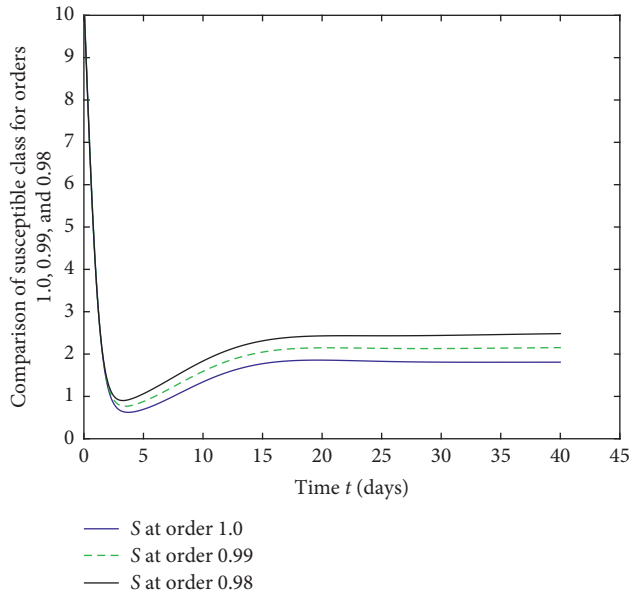

Figure 4: Comparison of $S(t)$ for orders 1.0, 0.99, and 0.98.

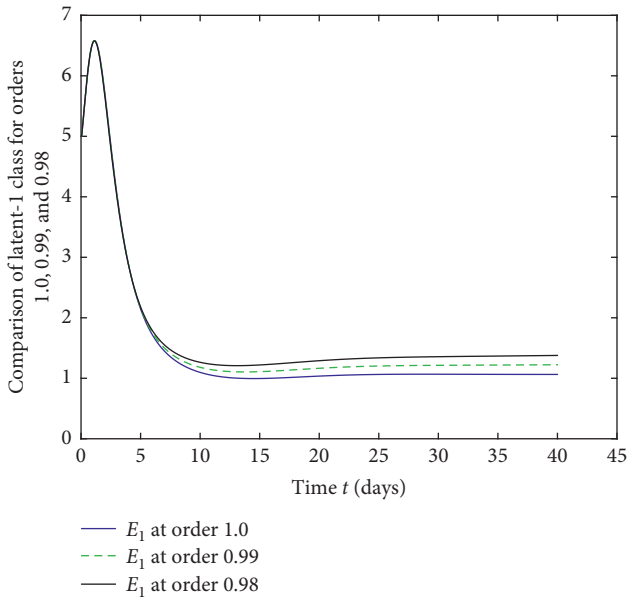

Figure 5: Comparison of $E_1(t)$ for orders 1.0, 0.99, and 0.98.

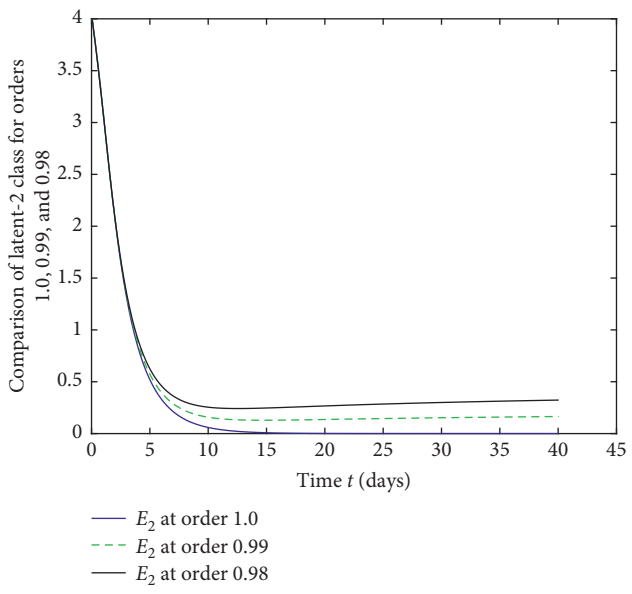

Figure 6: Comparison of $I_1(t)$ for orders 1.0, 0.99, and 0.98.

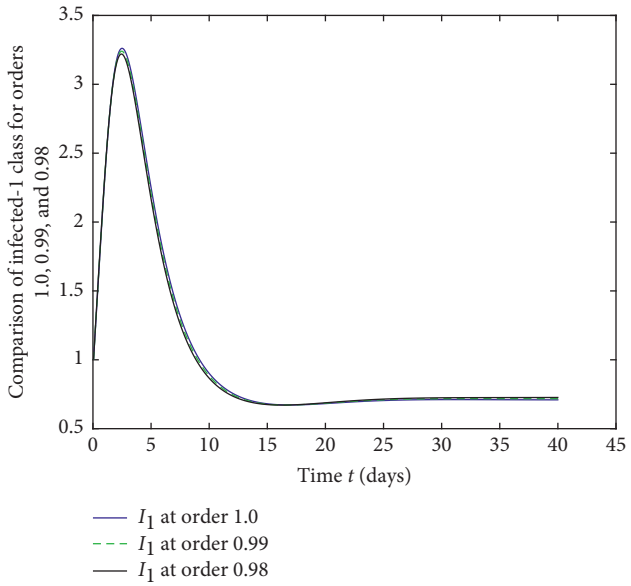

Figure 7: Comparison of $E_2(t)$ for orders 1.0, 0.99, and 0.98.

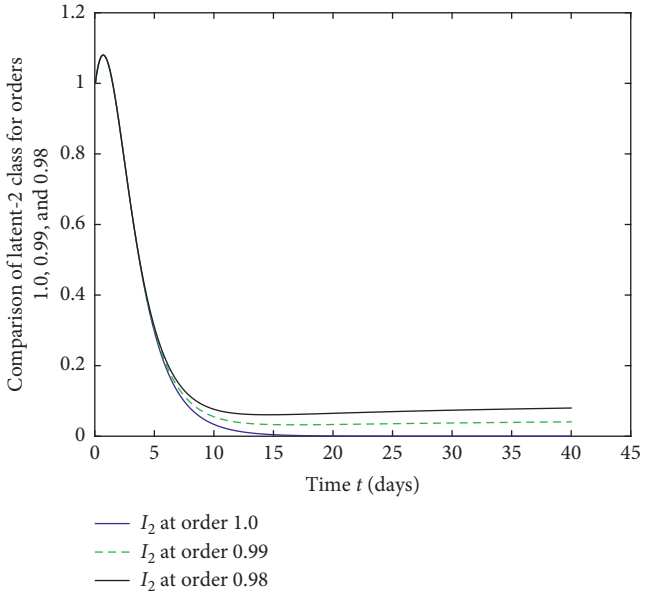

Figure 8: Comparison of $R(t)$ for orders 1.0, 0.99, and 0.98.

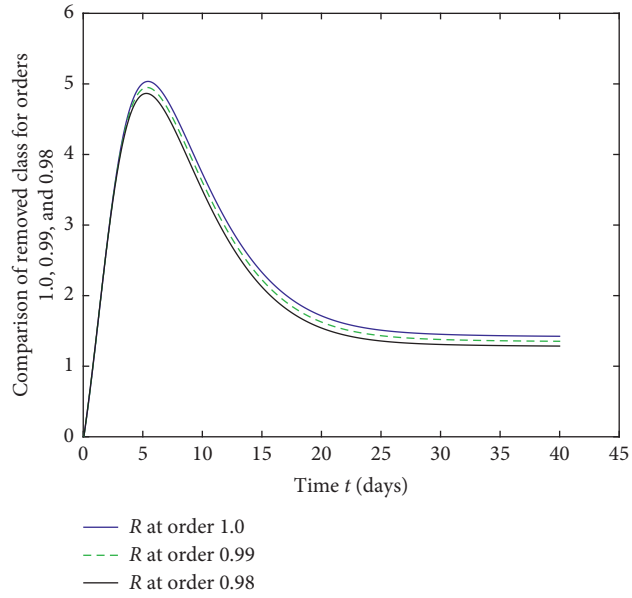

Figure 9: Comparison of $I_2(t)$ for orders 1.0, 0.99, and 0.98.

$$
\begin{aligned}
\mathcal{S}_{n+1} &= \mathcal{S}_0 + \frac{h^{\vartheta_1}}{\Gamma(\vartheta_1+1)} \times \sum_{k=0}^{n} \left((n-k+1)^{\vartheta_1} - (n-k)^{\vartheta_1} \right) \left(\Lambda^* - \frac{\alpha^* \mathcal{S}_n \mathcal{I}_{1_n}}{1+m\mathcal{I}_{1_n}^2} - \frac{\beta^* \mathcal{S}_n \mathcal{I}_{2_n}}{1+k\mathcal{I}_{2_n}^2} - \delta^* \mathcal{S}_n \right), \\
\varepsilon_{1_n} &= \varepsilon_0 + \frac{h^{\vartheta_2}}{\Gamma(\vartheta_2+1)} \times \sum_{k=0}^{n} \left((n-k+1)^{\vartheta_2} - (n-k)^{\vartheta_2} \right) \left(\frac{\alpha^* \mathcal{S}_n \mathcal{I}_{1_n}}{1+m\mathcal{I}_{1_n}^2} - (\gamma_1^* + \delta^*) \mathrm{E}_{1_n} \right), \\
\varepsilon_{2_n} &= \varepsilon_{2_0} + \frac{h^{\vartheta_3}}{\Gamma(\vartheta_3+1)} \times \sum_{k=0}^{n} \left((n-k+1)^{\vartheta_3} - (n-k)^{\vartheta_3} \right) \left(\frac{\beta^* \mathcal{S}_n \mathcal{I}_{2_n}}{1+k\mathcal{I}_{2_n}^2} - (\gamma_2^* + \delta^*) \mathrm{E}_{2_n} \right), \\
\mathcal{I}_{1_n} &= \mathcal{I}_{1_0} + \frac{h^{\vartheta_4}}{\Gamma(\vartheta_4+1)} \times \sum_{k=0}^{n} \left((n-k+1)^{\vartheta_4} - (n-k)^{\vartheta_4} \right) \left(\gamma_1^* \mathrm{E}_{1_n} - (\mu_1^* + \delta^*) \mathcal{I}_{1_n} \right), \\
\mathcal{I}_{2_n} &= \mathcal{I}_{2_0} + \frac{h^{\vartheta_5}}{\Gamma(\vartheta_5+1)} \times \sum_{k=0}^{n} \left((n-k+1)^{\vartheta_5} - (n-k)^{\vartheta_5} \right) \left(\gamma_2^* \mathrm{E}_{2_n} - (\mu_2^* + \delta^*) \mathcal{I}_{2_n} \right), \\
\mathcal{R}_n &= \mathcal{R}_0 + \frac{h^{\vartheta_6}}{\Gamma(\vartheta_6+1)} \times \sum_{k=0}^{n} \left((n-k+1)^{\vartheta_6} - (n-k)^{\vartheta_6} \right) \left(\mu_1^* \mathcal{I}_{1_n} + \mu_2^* \mathcal{I}_{2_n} - \delta^* \mathcal{R}_n \right).
\end{aligned}
\tag{22}
$$

5. Computational Results

Here, we test the numerical scheme given in (22) for the numerical results of fractional-order COVID-19 model (21), considering the parametric values, and $\vartheta_i = 1.0, 0.99$, and 0.98, for $i = 1, 2, \ldots, 6$, and the initial values $\mathcal{S}(0) = 10, \mathcal{E}_1(0) = 5, \mathcal{E}_2(0) = 4, \mathcal{I}_1(0) = 1, \mathcal{I}_2(0) = 1$, and $\mathcal{R}(0) = 0$.

In Figure 1, we have given the numerical solution of COVID-19 model (21) for the order 1.0. Also, Figures 2 and 3 are the solutions for the fractional orders 0.99 and 0.98, respectively. These graphs show that the fractional-order solutions of model (21) are similar in behavior as to the solution of the classical model of the order 1.0. This shows the accuracy of our scheme given in (22).

In Figure 4, we have given a comparative study of the susceptible class which has a decrease in the early 5 days and later on a slight increase and then a stability is observed for the orders 1.0, 0.99, and 0.98. In Figure 5, we have given a comparative study of the $E_1(t)$ for the orders 1.0, 0.99, and 0.98. We have observed that the behavior of the fractional-order results are similar to the classical integer order and in this class, there is a slight increase and then there is a rapid decrease up to 10 days. This decrease is converted into the infected class, and we observe a rapid increase in the $I_1(t)$ class and then

there is a gradual decrease of up to 14 days as given in Figure 6.

In Figure 7, we have given a comparative study of the $E_2(t)$ for the orders 1.0, 0.99, and 0.98. We have observed that the behavior of the fractional-order results are similar to the classical integer order and in this class, there is a rapid decrease of up to 10 days. This decrease is converted into the infected class, and we observed a rapid increase in the $R(t)$ class and then there is a gradual decrease of up to 20 days as given in Figure 8. In Figure 9, we have presented a computational analysis of $\mathcal{I}_2$ class.

All the numerical computations are for the comparative study of COVID-19 model (21) and we have noticed the behavior of the joint solution as well as the individual comparison of the compartments for the orders 1.0, 0.99, and 0.98.

6. Conclusion

In this article, we have considered a very important class of fractional-order system of sequential differential equations (1), for the existence and stability results based on the classical fixed-point approach, and have observed that under certain necessary assumptions, suggested problem (1) has a unique solution as well as Hyers–Ulam stability. Such problems are widely applicable in the real-world situations. In the example section, we have given a COVID-19 model as a particular case of system (1). The existence of solution of (21) is ensured by Theorem 1. The Hyers–Ulam stability of (21) is guaranteed by Theorem 2. For the numerical solution of example (21), we obtained numerical scheme (22) and the scheme was tested with the real data given in the literature [15]. All the computational results ensured that the numerical simulations for fractional-order system (21) are of the same behavior as to the classical case for the order 1.

Data Availability

The data used to support the findings of this study are included within the article.

Conflicts of Interest

The authors declare no conflicts of interest regarding the publication of this paper.

Authors' Contributions

All the authors have equal contributions in this article.

Acknowledgments

This research was funded by the Deanship of Scientific Research at Princess Nourah Bint Abdulrahman University through the Fast-Track Research Funding Program to support publication in the top journal (Grant no. 42-FTTJ-64).

References

[1] A. Atangana and S. I. Araz, "Mathematical model of COVID-19 spread in Turkey and South Africa: theory, methods and applications," *Advances in Difference Equations*, vol. 2020, p. 658, 2020.

[2] A. Atangana and S. I. Araz, "Nonlinear equations with global differential and integral operators: existence, uniqueness with application to epidemiology," *Results in Physics*, vol. 20, Article ID 103593, 2020.

[3] S. Ahmad, A. Ullah, Q. M. Al-Mdallal, H. Khan, K. Shah, and A. Khan, "Fractional order mathematical modeling of COVID-19 transmission. Chaos," *Solitons & Fractals*, vol. 139, Article ID 110256, 2020.

[4] A. Babakhani and V. Daftardar-Gejji, "Existence of positive solutions of nonlinear fractional differential equations," *Journal of Mathematical Analysis and Applications*, vol. 278, no. 2, pp. 434–442, 2003.

[5] N. H. Tuan, H. Mohammadi, and S. Rezapour, "A mathematical model for COVID-19 transmission by using the Caputo fractional derivative," *Chaos, Solitons & Fractals*, vol. 140, Article ID 110107, 2020.

[6] Z. A. Khan, "Hadamard type fractional differential equations for the system of integral inequalities on time scales," *Integral Transforms and Special Functions*, vol. 31, no. 5, pp. 412–423, 2020.

[7] Z. A. Khan, K. Shah, A. Khan, and H. Khan, "Nonlinear discrete fractional sum inequalities related to the theory of discrete fractional calculus with applications," *Journal of Function Spaces*, vol. 2021, Article ID 8734535, 8 pages, 2021.

[8] K. Deimling, *Nonlinear Functional Analysis*, Springer-Verlag, New York, NY, USA, 1985.

[9] P. Samui, J. Mondal, and S. Khajanchi, "A mathematical model for COVID-19 transmission dynamics with a case study of India," *Chaos, Solitons, and Fractals*, vol. 140, Article ID 110173, 2020.

[10] S. Zhang, "The existence of a positive solution for a nonlinear fractional differential equation," *Journal of Mathematical Analysis and Applications*, vol. 252, no. 2, pp. 804–812, 2000.

[11] D. Okuonghae and A. Omame, "Analysis of a mathematical model for COVID-19 population dynamics in Lagos, Nigeria," *Chaos, Solitons, and Fractals*, vol. 139, Article ID 110032, 2020.

[12] B. C. Dhage, "Quadratic perturbations of periodic boundary value problems of second order ordinary differential equations," *Differential Equations & Applications*, vol. 2, no. 4, pp. 465–486, 2010.

[13] B. Dhage, "Periodic boundary value problems of first order Caratheodory and discontinuous differential equations," *Nonlinear Functional Analysis and Applications*, vol. 13, no. 2, pp. 323–352, 2008.

[14] B. Dhage, "Basic results in the theory of hybrid differential equations with mixed perturbations of second type," *Functional Differential Equations*, vol. 19, pp. 1–20, 2012.

[15] A. Meskaf, O. Khyar, J. Danane, and K. Allali, "Global stability analysis of a two-strain epidemic model with non-monotone incidence rates," *Chaos, Solitons & Fractals*, vol. 133, Article ID 109647, 2020.

Hindawi
Complexity
Volume 2021, Article ID 9963031, 38 pages
https://doi.org/10.1155/2021/9963031

Research Article

Dynamics of a Predator-Prey Population in the Presence of Resource Subsidy under the Influence of Nonlinear Prey Refuge and Fear Effect

Sudeshna Mondal,[1] **G. P. Samanta**,[1] **and Juan J. Nieto**[2]

[1]*Department of Mathematics, Indian Institute of Engineering Science and Technology, Shibpur, Howrah 711103, India*
[2]*Instituto de Matemáticas, Universidade de Santiago de Compostela, Santiago de Compostela 15782, Spain*

Correspondence should be addressed to G. P. Samanta; gpsamanta@math.iiests.ac.in

Received 6 March 2021; Revised 7 May 2021; Accepted 11 June 2021; Published 5 July 2021

Academic Editor: Eberhard O. Voit

In this work, our aim is to investigate the impact of a non-Kolmogorov predator-prey-subsidy model incorporating nonlinear prey refuge and the effect of fear with Holling type II functional response. The model arises from the study of a biological system involving arctic foxes (predator), lemmings (prey), and seal carcasses (subsidy). The positivity and asymptotically uniform boundedness of the solutions of the system have been derived. Analytically, we have studied the criteria for the feasibility and stability of different equilibrium points. In addition, we have derived sufficient conditions for the existence of local bifurcations of codimension 1 (transcritical and Hopf bifurcation). It is also observed that there is some time lag between the time of perceiving predator signals through vocal cues and the reduction of prey's birth rate. So, we have analyzed the dynamical behaviour of the delayed predator-prey-subsidy model. Numerical computations have been performed using MATLAB to validate all the analytical findings. Numerically, it has been observed that the predator, prey, and subsidy can always exist at a nonzero subsidy input rate. But, at a high subsidy input rate, the prey population cannot persist and the predator population has a huge growth due to the availability of food sources.

1. Introduction

In the ecological system, the predator-prey interaction is one of the most significant tools which is comparatively easy to observe in the field. But fear of the predator felt by the prey (indirect effect) also plays a vital role since its effect is stronger than direct predation [1, 2]. The cost of fear can reduce the reproduction rate of prey because it affects the physiological condition of prey population. As a result, the prey species may get a long-term loss. In support of this, it is mentioned that, in the Greater Yellowstone Ecosystem, wolves (*Canis lupus*) affect the reproductive physiology of elk (*Cervus elaphus*) [3]. When the prey species recognize the predator signal (chemical/vocal), they spend more time to become keenly watchful to detect danger rather than in foraging. So, the birth rate of the scared prey reduces and adopts some survival mechanisms like starvation [1, 2]. For examples, some birds react to the sound of predator with antipredator defenses [1, 2] and they flee from their nests at the first sign of danger [2]. This antipredator behaviour may affect survival and reproduction of the birds [2]. It has been experimentally investigated that, in the absence of direct killing, the reproduction of the offspring of song sparrows (*Melospiza melodia*) could be reduced by 40% as a result of impact of feeling fear created by the predator [4]. So, this reduction caused by the antipredator behaviour affects the birth rate and survival of offspring. Thus, the cost of fear (apart from direct predation) should be introduced in a predator-prey interaction. Mathematical formulation of the impact of fear on the two species prey-predator system has been initiated by Wang et al. [5] in 2016 introducing fear factor: $f(k, y) = (1/(1 + ky))$. It involves a parameter k

denoting the level of fear to represent the antipredator behaviour of the prey. Some research works have already been done on the ecological system under the influence of predation fear felt by prey species [6–17]. Moreover, the impact of fear in a two-species predator-prey model with prey refuge was analyzed by many researchers [11, 18, 19].

In evolutionary biology, prey refuge is a concept which helps an organism to protect themselves from predation by hiding in an area inaccessible to the predator, for example, in a wolf-ungulate system, ungulates may seek refuge by migrating to areas outside the core territories of wolves. Also, it has many significant roles on the dynamics of predator-prey interactions: prey refuge may decrease the chance of extinction of prey. Researchers have mainly used the dynamic nature of predator-prey model with linear prey refuge (that is, mx amounts of prey are unavailable to the predator, where $m \in (0, 1)$ is the coefficient of refuge and x is the biomass of prey species) with Volterra response [20–22]. Recently, Mondal and Samanta have studied the dynamics of the predator-prey system with prey refuge dependent on both species (that is, mxy amounts of prey are free from the predator risk, where $0 < 1 - my < 1$, m is prey refuge coefficient, x is the biomass of prey population, and y is the biomass of predator population) in the presence of additional food (for details, see [23]). In 2020, Mondal and Samanta [11] have also analyzed the dynamics of predator-prey interaction having nonlinear prey refuge function $\Phi(x, y) = (mxy/(a + y))$ which is the amount of prey that are free from predation, where a is half saturation constant and y is the biomass of predator population.

Many experimental studies suspect that the introduction of resource subsidies may disrupt otherwise stable food web linkages [24–26]. Such concept is significant for resource management purposes. It is learnt that reintroduced wolves in Yellowstone Park switch to bison when their preferred ungulate prey, namely, elk, are rare in the concerned ecosystem [27]. Mathematically, the influence of resource subsidy on the predator-prey model has been initiated in the work of Nevai and Van Gorder [28]. They have discussed how different subsidy input rate may affect the prey and predator population to persist in the ecosystem.

Generalist predator can consume more than one food source: either multiple prey population or a combination of prey population and resource subsidy. There are many rich theoretical research on ecological systems involving generalist predator [29–31]. Also, there are a variety of real-life applications for such systems [32–34]. From literature surveys, it has been shown that generalist predator can persist in an ecosystem even if one particular prey species is going towards extinction [29–31].

In 2012, Nevai and Van Gorder [28] first extended the Kolmogorov model to a non-Kolmogorov predator-prey-subsidy model. It has been observed that the predator-prey-subsidy model occurs in the arctic foxes (predator), lemmings (prey), and seal carcasses (subsidy). Motivated by the works of Das and Samanta [35], Nevai and Van Gorder [28], and Xu et al. [36], we have analyzed the dynamical behaviour of a mathematical model of non-Kolmogorov form that includes the three components (predator, prey, and subsidy) with the impacts of nonlinear prey refuge function and the fear effect felt by the prey in the presence of the predator. To the best of our knowledge, there does not exist any mathematical model to explore the impact of fear effect incorporating nonlinear prey refuge function in predator-prey-subsidy interaction.

The organization of this work is structured as follows: in Section 2, a mathematical model has been formulated with the influences of nonlinear prey refuge and fear effect. Section 3 shows that the proposed model is well-behaved. In Section 4, feasibility criteria and stability of all the equilibria of the proposed system (in absence of delay) have been studied. The equilibria can change their stability nature through transcritical and Hopf bifurcation which are also analyzed in this section. Generally, the reduction of prey's birth rate due to the effect of fear will not be an instantaneous biological process but deviated through some time lag, so the study of time-delay τ is very meaningful to obtain the more realistic dynamics. So, Section 5 deals with the dynamic behaviour of the delayed system for two equilibrium points E_3 (subsidy free) and E^* (interior), respectively. Section 6 provides the numerical computations which support the analytical calculations. Section 7 provides a brief conclusion about the system dynamics.

2. Model Formulation

In 2020, Mondal and Samanta [11] analyzed the dynamics of a delayed predator-prey interaction incorporating nonlinear prey refuge function under the influence of fear effect and additional food. Motivated by the work of Mondal and Samanta [11], we have first considered a predator-prey-subsidy model with nonlinear prey refuge function where the prey and subsidy occur in the same habitat and they are both consumed by a single generalist predator according to the following differential equations:

$$\begin{aligned}
\frac{dx}{dt} &= rx - d_1 x - a_1 x^2 - \frac{a_2(1-(my/(a+y)))xy}{b_1 + w + (1-(my/(a+y)))x}, \quad x(0) > 0,\\
\frac{dw}{dt} &= A - d_2 w - \frac{a_3 wy}{b_1 + w + (1-(my/(a+y)))x}, \quad w(0) > 0,\\
\frac{dy}{dt} &= \frac{c_1 a_2(1-(my/(a+y)))xy}{b_1 + w + (1-(my/(a+y)))x} + \frac{c_2 a_3 wy}{b_1 + w + (1-(my/(a+y)))x} - d_3 y, \quad y(0) > 0,
\end{aligned} \tag{1}$$

where x is prey population, w denotes the population of the subsidy, and y is the generalist predator which exploits both the prey and subsidy. For example, wolves (predator) consume both deer (prey) and salmon carcasses (subsidy) [37].

The term $(1-(my/(a+y)))x$ represents the quantity of prey available to the predator, i.e., $(mxy/(a+y))$ amounts of prey are free from predation risk where $(mxy/(a+y))$ is designated as nonlinear prey refuge function. Also, we have modeled the dynamics of a generalist predator with Holling type II [38–41] response function in the presence of nonlinear prey refuge function.

All parameters are positive (except $A \geq 0$) and biologically meaningful. Parameters are described in Table 1.

Apart from direct consumption, feeling of fear among the individuals of the prey species in presence of predator is very common in predator-prey interaction which changes life-history, behavioural responses, and reproduction capability of prey species. In ecology, effect of fear is a common factor, but there does not exist any considerable attention to introduce the impact of fear in the mathematical modeling. Experimental studies indicate that the feeling of fear among the individuals of the prey species in presence of predator reduces the prey's birth rate. So, birth rate of prey species r is multiplied by a monotone decreasing function $f(k,y) = (1/(1+ky))$, where $k(\geq 0)$ is a level of fear [5]. The fear function $f(k,y)$ satisfies the following conditions:

(1) $f(0,y) = 1$: when there is no fear effect on the prey species, the birth rate of the prey is not reduced

(2) $f(k,0) = 1$: when there is no predator, the birth rate of the prey species is not reduced in the presence of fear effect

(3) $(\partial f(k,y)/\partial k) < 0$: when fear effect increases, the birth rate of the prey reduces

(4) $(\partial f(k,y)/\partial y) < 0$: when predator species increases, prey population reduces

Our main focus is to analyze the dynamic nature of the predator-prey-subsidy model with the influence of nonlinear prey refuge and fear effect. So, system (1) can be modified in the following aspects:

$$\begin{aligned}
\frac{dx}{dt} &= \frac{rx}{1+ky} - d_1 x - a_1 x^2 - \frac{a_2(1-(my/(a+y)))xy}{b_1 + w + (1-(my/(a+y)))x},\\
\frac{dw}{dt} &= A - d_2 w - \frac{a_3 wy}{b_1 + w + (1-(my/(a+y)))x},\\
\frac{dy}{dt} &= \frac{c_1 a_2(1-(my/(a+y)))xy}{b_1 + w + (1-(my/(a+y)))x} + \frac{c_2 a_3 wy}{b_1 + w + (1-(my/(a+y)))x} - d_3 y,
\end{aligned} \tag{2}$$

with initial conditions:

$$\begin{aligned}
x(0) &> 0,\\
w(0) &> 0,\\
y(0) &> 0.
\end{aligned} \tag{3}$$

Throughout the analysis of this work, we have taken $c_1 > c_2$ which is biologically meaningful.

3. Positivity and Uniform Boundedness

Theorem 1. *Every solution of system (2) with (3) uniquely exists and is positive for all $t \geq 0$.*

Proof. Solution $(x(t), w(t), y(t))$ of (2) with (3) exists and is unique on $[0,\xi)$, where $(0 < \xi \leq +\infty)$ [42].

From (2) with (3),

$$\begin{aligned}
x(t) &= x(0)\exp\left[\int_0^t \left\{\frac{r}{1+ky(\theta)} - d_1 - a_1 x(\theta) - \frac{a_2(1-(my(\theta)/(a+y(\theta))))y(\theta)}{b_1 + w(\theta) + (1-(my(\theta)/(a+y(\theta))))x(\theta)}\right\}d\theta\right] > 0,\\
y(t) &= y(0)\exp\left[\int_0^t \left\{\frac{c_1 a_2(1-(my(\theta)/(a+y(\theta))))x(\theta)}{b_1 + w(\theta) + (1-(my(\theta)/(a+y(\theta))))x(\theta)} + \frac{c_2 a_3 w(\theta)}{b_1 + w(\theta) + (1-(my(\theta)/(a+y(\theta))))x(\theta)} - d_3\right\}d\theta\right] > 0.
\end{aligned} \tag{4}$$

Table 1: Description of biologically meaningful parameters.

Parameters	Descriptions
r	Birth rate of the prey
d_1	Natural death rate of the prey
d_2	The subsidy decay rate
a_1	Mortality rate due to intraspecific competition among the individuals of the prey population
a_2	Consumption rate of the predator
a_3	Maximum rate at which the predator consumes the subsidy
b_1	Handling time assumed to be uniform over all food sources
c_1	Conversion rate of the energy that the predator obtains from the target prey
c_2	Conversion rate of the energy that the predator obtains from the subsidy
A	Subsidy input rate
m	Coefficient of prey refuge ($m \in (0,1)$)
d_3	Mortality rate of the predator
a	Half saturation constant for refuge function

Now, we claim that $w(t) > 0$ for all $t \in [0, \xi)$. If it does not hold then there exists $t_1 \in [0, \xi)$ such that $w(t_1) = 0$, $\dot{w}(t) \le 0$, and $w(t) > 0$ on $[0, t_1)$. From the second equation of (2),

$$w(t_1) = w(0)\exp\left[-\int_0^{t_1}\left(d_2 + \frac{a_3 y(\theta)}{b_1 + w(\theta) + (1 - (my(\theta)/(a + y(\theta))))x(\theta)}\right)\mathrm{d}(\theta)\right] + \int_0^{t_1} A\left[\exp\left(\int_{t_1}^{u}\left(d_2 + \frac{a_3 y(\theta)}{b_1 + w(\theta) + (1 - (my(\theta)/(a + y(\theta))))x(\theta)}\right)\mathrm{d}(\theta)\right)\right]\mathrm{d}u > 0, \tag{5}$$

a contradiction with $w(t_1) = 0$. So, $w(t) > 0, \forall t \in [0, \xi)$.

Hence, solutions of (2) stay positive for all $t \ge 0$. □

Theorem 2. *All solutions of system (2) which start in $\mathbb{R}^3_+$ are asymptotically uniformly bounded.*

Proof. Case 1: if $r > d_1$, from the first equation of (2),

$$\begin{aligned}\frac{\mathrm{d}x}{\mathrm{d}t} &\le \frac{rx}{1 + ky} - d_1 x - a_1 x^2 \\ &\le rx - d_1 x - a_1 x^2 \left[\text{since } \frac{rx}{1 + ky} \le rx\right] \\ &= (r - d_1)x\left(1 - \frac{x}{(r - d_1)/a_1}\right),\end{aligned} \tag{6}$$

$$\therefore \limsup_{t \longrightarrow +\infty} x(t) \le \frac{r - d_1}{a_1}, \quad \text{since } r > d_1.$$

Let us take $P = x + w + (y/c_1)$.

Differentiating both sides with respect to t, we obtain

$$\begin{aligned}
\frac{dP}{dt} &= \frac{dx}{dt} + \frac{dw}{dt} + \frac{1}{c_1}\frac{dy}{dt} \\
&= \frac{rx}{1+ky} - d_1x - a_1x^2 + A - d_2w - \frac{a_3wy(a+y)}{(b_1+w)(a+y)+(a+(1-m)y)x} \\
&\quad + \frac{(c_2/c_1)a_3wy(a+y)}{(b_1+w)(a+y)+(a+(1-m)y)x} - \frac{d_3y}{c_1} \\
&\le rx - d_1x - a_1x^2 + A - d_2w - d_3\frac{y}{c_1} - \frac{a_3wy(a+y)}{(b_1+w)(a+y)+(a+(1-m)y)x}\left(1 - \frac{c_2}{c_1}\right) \\
&\le 2(r-d_1)x - a_1x^2 + A - (r-d_1)x - d_2w - d_3\frac{y}{c_1}\,[\text{since } c_1 > c_2] \\
&= -a_1\left(x - \frac{r-d_1}{a_1}\right)^2 + \frac{(r-d_1)^2}{a_1} + A - \left\{(r-d_1)x + d_2w + d_3\frac{y}{c_1}\right\} \\
&\le \frac{(r-d_1)^2}{a_1} + A - \left\{(r-d_1)x + d_2w + d_3\frac{y}{c_1}\right\}, \\
\therefore \frac{dP}{dt} &\le \frac{(r-d_1)^2}{a_1} + A - \left\{(r-d_1)x + d_2w + d_3\frac{y}{c_1}\right\}.
\end{aligned} \tag{7}$$

Let

$$\eta = \min\{r-d_1, d_2, d_3\}, \quad \text{when } r > d_1. \tag{8}$$

Then,

$$\frac{dP}{dt} + \eta P \le \frac{(r-d_1)^2}{a_1} + A. \tag{9}$$

Using the Gronwall inequality, we obtain

$$\begin{aligned}
0 < P(x(t), w(t), y(t)) &\le \frac{\left((r-d_1)^2/a_1\right) + A}{\eta}\left(1 - e^{-\eta t}\right) + e^{-\eta t}P(x(0), w(0), y(0)), \\
\therefore 0 < P(x(t), w(t), y(t)) &\le \frac{\left((r-d_1)^2/a_1\right) + A}{\eta}, \quad \text{as } t \longrightarrow \infty.
\end{aligned} \tag{10}$$

Thus, all solutions of system (2) enter into the region:

$$\Omega = \left\{(x, w, y) \in \mathbb{R}_+^3 : 0 < x(t) \le \frac{r-d_1}{a_1}; 0 < P(x(t), w(t), y(t)) \le \frac{\left((r-d_1)^2/a_1\right) + A}{\eta}\right\}. \tag{11}$$

Case 2: if $r < d_1$, from the first equation of (2) we obtain $\lim_{t\longrightarrow\infty} x(t) = 0$.

Now, from the second and third equations of (2), we have

$$\frac{dw}{dt} + \frac{1}{c_2}\frac{dy}{dt} = A - d_2w + \frac{(c_1/c_2)a_2(1-(my/(a+y)))xy}{b_1 + w + (1-(my/(a+y)))x} - d_3\frac{y}{c_2}. \tag{12}$$

For large t,

$$\frac{dw}{dt}+\frac{1}{c_2}\frac{dy}{dt}=A-d_2w-d_3\frac{y}{c_2}\left[\because \lim_{t\longrightarrow\infty} x(t)=0\right]. \quad (13)$$

Let

$$\eta'=\min\{d_2,d_3\}. \quad (14)$$

Then,

$$\frac{d}{dt}\left(w+\frac{y}{c_2}\right)+\eta'\left(w+\frac{y}{c_2}\right)\le A. \quad (15)$$

Using Gronwall inequality, we obtain

$$0<w(t)+\frac{y(t)}{c_2}\le\frac{A}{\eta'}\left(1-e^{-\eta' t}\right)+e^{-\eta' t}\left(w(0)+\frac{y(0)}{c_2}\right),$$

$$\therefore 0<w(t)+\frac{y(t)}{c_2}\le\frac{A}{\eta'},\quad \text{as } t\longrightarrow\infty. \quad (16)$$

Hence, the theorem. □

4. Equilibrium Points and Stability Analysis

4.1. Equilibria

4.1.1. Trivial Equilibrium Point. Extinction: $E_0(0,0,0)$.

4.1.2. Axial Equilibrium Points

(i) Subsidy only: $E_1(0,(A/d_2),0)$

(ii) Prey only: $E_2((r-d_1)/a_1,0,0)$ exists if $r>d_1$ and $A=0$

4.1.3. Planer Equilibrium Points

(i) Subsidy free: $E_3(\overline{x},0,\overline{y})$ exists if $A=0$, $\overline{x}>0$, and $\overline{y}>0$ where $\overline{x}$ and $\overline{y}$ can be obtained by solving the equations:

$$\frac{r}{1+ky}-d_1-a_1x-\frac{a_2(1-(my/(a+y)))y}{b_1+(1-(my/(a+y)))x}=0,$$

$$\frac{c_1a_2(1-(my/(a+y)))x}{b_1+(1-(my/(a+y)))x}-d_3=0, \quad (17)$$

and we get

$$\overline{y}=\frac{a\{d_3b_1-\overline{x}(c_1a_2-d_3)\}}{(1-m)(c_1a_2-d_3)\overline{x}-d_3b_1},\quad m\neq 1, \quad (18)$$

where $\overline{x}$ is a positive root of the equation:

$$B_0x^4+B_1x^3+B_2x^2+B_3x+B_4=0. \quad (19)$$

Here,

$$\begin{aligned}
B_0&=a_1(1-m)(1-m-ak)(c_1a_2-d_3)^2,\\
B_1&=a_1b_1d_3(1-m)(ak-1)(c_1a_2-d_3)-a_1b_1d_3(1-m-ak)(c_1a_2-d_3)+d_1(1-m)(1-m-ak)(c_1a_2-d_3)^2\\
&\quad -r(1-m)^2(c_1a_2-d_3)^2,\\
B_2&=b_1d_1d_3(1-m)(ak-1)(c_1a_2-d_3)-a_1b_1^2d_3^2(ak-1)-b_1d_1d_3(1-m-ak)(c_1a_2-d_3)\\
&\quad -\frac{d_3}{c_1}(1-m-ak)(c_1a_2-d_3)^2+2b_1d_3r(1-m)(c_1a_2-d_3),\\
B_3&=-b_1^2d_3^2r+\frac{b_1d_3^2}{c_1}(1-m-ak)(c_1a_2-d_3)-\frac{b_1d_3^2}{c_1}(ak-1)(c_1a_2-d_3)-b_1^2d_1d_3^2(ak-1),\\
B_4&=\frac{b_1^2d_3^3}{c_1}(ak-1),
\end{aligned} \quad (20)$$

and $\overline{y}=(a\{d_3b_1-\overline{x}(c_1a_2-d_3)\}/((1-m)(c_1a_2-d_3)\overline{x}-d_3d_1))$ exists if $(1-m)(c_1a_2-d_3)\overline{x}<d_3b_1<(c_1a_2-d_3)\overline{x}$ and $c_1a_2>d_3$.

(ii) Prey free: $E_4(0,\widehat{w}=(d_3b_1/(c_2a_3-d_3)),\widehat{y}=((A-d_2\widehat{w})(b_1+\widehat{w})/a_3))$ exists if $c_2a_3>d_3$ and $\widehat{y}>0$.

(iii) Predator free: $E_5((r-d_1)/a_1,(A/d_2),0)$ exists if $r>d_1$.

4.1.4. Interior (Coexistence) Equilibrium Point. Solving the following system of equations,

$$\frac{r}{1+ky} - d_1 - a_1x - \frac{a_2(1-(my/(a+y)))y}{b_1 + w + (1-(my/(a+y)))x} = 0,$$

$$A - d_2w - \frac{a_3wy}{b_1 + w + (1-(my/(a+y)))x} = 0, \tag{21}$$

$$\frac{c_1a_2(1-(my/(a+y)))x}{b_1 + w + (1-(my/(a+y)))x} + \frac{c_2a_3w}{b_1 + w + (1-(my/(a+y)))x} - d_3 = 0,$$

we can obtain $E^*(x^*, w^*, y^*)$ using the software MATHEMATICA with the following existence conditions:

(1) $d_3 < \min\{c_1a_2, c_2a_3\}$

(2) $0 < w^* < \min\{(A/d_2), d_3b_1/(c_2a_3 - d_3)\}$

(3) $r > d_1 + a_1x^* + (\{b_1d_3 - (c_2a_3 - d_3)w^*\}(A - d_2w^*)/a_3x^*w^*(c_1a_2 - d_3))$ (otherwise, predator population goes into extinction)

4.2. Stability Analysis. Now, we will study the stability conditions of all equilibria for the proposed system (2).

The Jacobian matrix $J_0(0,0,0)$ at $E_0(0,0,0)$ is given by

$$J_0(0,0,0) = \begin{bmatrix} r-d_1 & 0 & 0 \\ 0 & -d_2 & 0 \\ 0 & 0 & -d_3 \end{bmatrix}. \tag{22}$$

The eigenvalues of $J_0(0,0,0)$ are $r - d_1$, $-d_2 (<0)$, and $-d_3 (<0)$. Then. we have stated the following theorem.

Theorem 3. *Trivial equilibrium point $E_0(0,0,0)$ is locally asymptotically stable (LAS) if $r < d_1$ and unstable if $r > d_1$.*

The Jacobian matrix $J_1(0, (A/d_2), 0)$ at $E_1(0, (A/d_2), 0)$ is as follows:

$$J_1\left(0, \frac{A}{d_2}, 0\right) = \begin{bmatrix} r-d_1 & 0 & 0 \\ 0 & -d_2 & -\dfrac{a_3(A/d_2)}{b_1 + (A/d_2)} \\ 0 & 0 & -d_3 + \dfrac{c_2a_3(A/d_2)}{b_1 + (A/d_2)} \end{bmatrix}. \tag{23}$$

We see that

$$\begin{aligned} &r - d_1, \\ &-d_2 (<0), \\ &-d_3 + \frac{c_2a_3(A/d_2)}{b_1 + (A/d_2)}, \end{aligned} \tag{24}$$

are the eigenvalues of the matrix $J_1(0, (A/d_2), 0)$. Thus, we have the following theorem.

Theorem 4. *Axial equilibrium point (subsidy only) $E_1(0, (A/d_2), 0)$ is locally asymptotically stable if $r < d_1$ and $(c_2a_3(A/d_2)/b_1 + (A/d_2)) < d_3$ and unstable if either $\{r > d_1, (c_2a_3(A/d_2)/b_1 + (A/d_2)) < d_3\}$ or $\{r < d_1, (c_2a_3(A/d_2)/b_1 + (A/d_2)) > d_3\}$ or $\{r > d_1, (c_2a_3(A/d_2)/b_1 + (A/d_2)) > d_3\}$.*

The Jacobian matrix $J_2((r-d_1)/a_1, 0, 0)$ at $E_2((r-d_1)/a_1, 0, 0)$ is given by

$$J_2\left(\frac{r-d_1}{a_1}, 0, 0\right) = \begin{bmatrix} -r + d_1 & 0 & \dfrac{r-d_1}{a_1}\left(-rk - \dfrac{a_2}{b_1 + ((r-d_1)/a_1)}\right) \\ 0 & -d_2 & 0 \\ 0 & 0 & -d_3 + \dfrac{c_1a_2((r-d_1)/a_1)}{b_1 + ((r-d_1)/a_1)} \end{bmatrix}. \tag{25}$$

The eigenvalues of $J_2((r-d_1)/a_1, 0, 0)$ are $-r+d_1 (<0)$, $-d_2 (<0)$ or $-d_3 + (c_1a_2((r-d_1)/a_1)/b_1 + ((r-d_1)/a_1))$. Thus. we have stated the following theorem.

Theorem 5. *Axial equilibrium point (prey only)* $E_2((r-d_1)/a_1, 0, 0)$ *is locally asymptotically stable if*

$$\frac{c_1a_2((r-d_1)/a_1)}{b_1+((r-d_1)/a_1)} < d_3 \Longrightarrow 0 < r < d_1 + a_1\left(\frac{b_1d_3}{c_1a_2-d_3}\right) \text{ with } c_1a_2 > d_3. \tag{26}$$

If $r > d_1 + a_1(b_1d_3/(c_1a_2-d_3))$ *with* $c_1a_2 > d_3$, *then* $E_2((r-d_1)/a_1, 0, 0)$ *is unstable.*

The Jacobian matrix $J_3(\overline{x}, 0, \overline{y})$ at $E_3(\overline{x}, 0, \overline{y})$ is as follows:

$$J_3(\overline{x}, 0, \overline{y}) = \begin{bmatrix} b_{11} & b_{12} & b_{13} \\ b_{21} & b_{22} & b_{23} \\ b_{31} & b_{32} & b_{33} \end{bmatrix}, \tag{27}$$

where

$$\begin{aligned}
b_{11} &= \overline{x}\left\{-a_1 + \frac{a_2\overline{y}(a+(1-m)\overline{y})^2}{\{b_1(a+\overline{y})+[a+(1-m)\overline{y}]\overline{x}\}^2}\right\},\\
b_{12} &= \frac{a_2\overline{x}\overline{y}[a+(1-m)\overline{y}](a+\overline{y})}{\{b_1(a+\overline{y})+[a+(1-m)\overline{y}]\overline{x}\}^2},\\
b_{13} &= \overline{x}\left\{-\frac{rk}{(1+k\overline{y})^2} - \frac{a_2[a+2(1-m)\overline{y}]}{b_1(a+\overline{y})+[a+(1-m)\overline{y}]\overline{x}} + \frac{a_2\overline{y}[a+(1-m)\overline{y}][b_1+(1-m)\overline{x}]}{\{b_1(a+\overline{y})+[a+(1-m)\overline{y}]\overline{x}\}^2}\right\},\\
b_{21} &= 0,\\
b_{22} &= -d_2 - \frac{a_3\overline{y}}{b_1+(1-(m\overline{y}/(a+\overline{y})))\overline{x}},\\
b_{23} &= 0,\\
b_{31} &= \overline{y}\left\{\frac{c_1a_2[a+(1-m)\overline{y}]}{b_1(a+\overline{y})+[a+(1-m)\overline{y}]\overline{x}} - \frac{c_1a_2[a+(1-m)\overline{y}]^2\overline{x}}{\{b_1(a+\overline{y})+[a+(1-m)\overline{y}]\overline{x}\}^2}\right\},\\
b_{32} &= \frac{c_2a_3\overline{y}(a+\overline{y})}{b_1(a+y^*)+[a+(1-m)\overline{y}]\overline{x}},\\
b_{33} &= \overline{y}\left\{\frac{c_1a_2(1-m)\overline{x}}{b_1(a+\overline{y})+[a+(1-m)\overline{y}]\overline{x}} - \frac{c_1a_2[a+(1-m)\overline{y}]\overline{x}[b_1+(1-m)\overline{x}]}{\{b_1(a+\overline{y})+[a+(1-m)\overline{y}]\overline{x}\}^2}\right\}.
\end{aligned} \tag{28}$$

The characteristic equation corresponding to $J_3(\overline{x}, 0, \overline{y})$ is expressed as

$$\lambda^3 + B_1\lambda^2 + B_2\lambda + B_3 = 0, \tag{29}$$

where $B_1 = -(b_{11}+b_{22}+b_{33})$, $B_2 = b_{22}b_{33} + b_{11}b_{33} - b_{13}b_{31} + b_{11}b_{22}$, and $B_3 = -b_{22}(b_{11}b_{33} - b_{13}b_{31})$.

Theorem 6. *Subsidy-free equilibrium point* $E_3(\overline{x}, 0, \overline{y})$ *is locally asymptotically stable if* $b_{11} < 0$, $b_{33} < 0$, *and* $b_{13} < 0$.

The Jacobian matrix $J_4(0, \widehat{w}, \widehat{y})$ corresponding to $E_4(0, \widehat{w}, \widehat{y})$ is given by

$$J_4(0, \widehat{w}, \widehat{y}) = \begin{bmatrix} c_{11} & c_{12} & c_{13} \\ c_{21} & c_{22} & c_{23} \\ c_{31} & c_{32} & c_{33} \end{bmatrix}, \tag{30}$$

where

$$
\begin{aligned}
c_{11} &= \frac{r}{1+k\widehat{y}} - d_1 - \frac{a_2[a+(1-m)\widehat{y}]\widehat{y}}{(b_1+\widehat{w})(a+\widehat{y})},\\
c_{12} &= 0,\\
c_{13} &= 0,\\
c_{21} &= \frac{a_3(1-m)(a+\widehat{y})\widehat{w}\widehat{y}^2}{[(b_1+\widehat{w})(a+\widehat{y})]^2},\\
c_{22} &= -d_2 - \frac{a_3\widehat{y}(a+\widehat{y})}{(b_1+\widehat{w})(a+\widehat{y})},\\
c_{23} &= -\frac{a_3\widehat{w}(a+2\widehat{y})}{(b_1+\widehat{w})(a+\widehat{y})} + \frac{a_3\widehat{y}\widehat{w}(a+\widehat{y})(b_1+\widehat{w})}{[(b_1+\widehat{w})(a+\widehat{y})]^2},\\
c_{31} &= \frac{c_1a_2\widehat{y}[a+(1-m)\widehat{y}]}{(b_1+\widehat{w})(a+\widehat{y})},\\
c_{32} &= \frac{c_2a_3\widehat{y}(a+\widehat{y})}{(b_1+\widehat{w})(a+\widehat{y})} - \frac{c_2a_3\widehat{w}\widehat{y}(a+\widehat{y})^2}{[(b_1+\widehat{w})(a+\widehat{y})]^2} = \frac{c_2a_3\widehat{y}b_1}{[(b_1+\widehat{w})(a+\widehat{y})]^2},\\
c_{33} &= \frac{c_2a_3\widehat{w}\widehat{y}}{(b_1+\widehat{w})(a+\widehat{y})} - \frac{c_2a_3\widehat{w}\widehat{y}(a+\widehat{y})(b_1+\widehat{w})}{[(b_1+\widehat{w})(a+\widehat{y})]^2} = 0.
\end{aligned}
\tag{31}
$$

The characteristic equation corresponding to $J_4(0,\widehat{w},\widehat{y})$ is expressed as

$$\lambda^3 + C_1\lambda^2 + C_2\lambda + C_3 = 0, \tag{32}$$

where

$$
\begin{aligned}
C_1 &= -(c_{11}+c_{22}),\\
C_2 &= -c_{23}c_{32} + c_{11}c_{22},\\
C_3 &= +c_{11}c_{23}c_{32}.
\end{aligned}
\tag{33}
$$

Theorem 7. *Prey-free equilibrium point $E_4(0,\widehat{w},\widehat{y})$ is locally asymptotically stable if $c_{11}<0$ and $c_{23}<0$.*

The Jacobian matrix $J_5((r-d_1)/a_1, (A/d_2), 0)$ corresponding to $E_5((r-d_1)/a_1, (A/d_2), 0)$ is given by

$$J_5\left(\frac{r-d_1}{a_1}, \frac{A}{d_2}, 0\right) = \begin{bmatrix} d_{11} & d_{12} & d_{13}\\ d_{21} & d_{22} & d_{23}\\ d_{31} & d_{32} & d_{33}\end{bmatrix}, \tag{34}$$

where

$$
\begin{aligned}
d_{11} &= -r + d_1,\\
d_{12} &= 0,\\
d_{13} &= \frac{r-d_1}{a_1}\left[-rk - \frac{a_2}{b_1 + (A/d_2) + ((r-d_1)/a_1)}\right],\\
d_{21} &= 0,\\
d_{22} &= -d_2,\\
d_{23} &= -\frac{a_3(A/d_2)}{b_1 + (A/d_2) + ((r-d_1)/a_1)},\\
d_{31} &= d_{32} = 0,\\
d_{33} &= \frac{c_1a_2((r-d_1)/a_1)}{b_1 + (A/d_2) + ((r-d_1)/a_1)} + \frac{c_2a_3(A/d_2)}{b_1 + (A/d_2) + ((r-d_1)/a_1)} - d_3.
\end{aligned}
\tag{35}
$$

The characteristic equation corresponding to $J_5((r-d_1)/a_1, (A/d_2), 0)$ is expressed as

$$\lambda^3 + D_1\lambda^2 + D_2\lambda + D_3 = 0, \tag{36}$$

where

$$
\begin{aligned}
D_1 &= -(d_{11}+d_{22}+d_{33}),\\
D_2 &= d_{22}d_{33} + d_{11}d_{33} + d_{11}d_{22},\\
D_3 &= -d_{11}d_{22}d_{33}.
\end{aligned}
\tag{37}
$$

Theorem 8. *Predator free equilibrium point* $E_5((r-d_1)/a_1, (A/d_2), 0)$ *is locally asymptotically stable if*

$$\frac{c_1a_2\left((r-d_1)/a_1\right)}{b_1+(A/d_2)+\left((r-d_1)/a_1\right)}+\frac{c_2a_3\left(A/d_2\right)}{b_1+(A/d_2)+\left((r-d_1)/a_1\right)}<d_3\Longrightarrow 0<r<d_1+a_1\left\{\frac{b_1d_3-(c_2a_3-d_3)(A/d_2)}{c_1a_2-d_3}\right\}, \tag{38}$$

provided $d_3<\min\{c_1a_2, c_2a_3\}$ *and* $0<(A/d_2)<(b_1d_3/(c_2a_3-d_3))$.

The Jacobian matrix $J^*(x^*, w^*, y^*)$ corresponding to $E^*(x^*, w^*, y^*)$ is as follows:

$$J^*(x^*, w^*, y^*)=\begin{bmatrix} a_{11} & a_{12} & a_{13}\\ a_{21} & a_{22} & a_{23}\\ a_{31} & a_{32} & a_{33}\end{bmatrix}, \tag{39}$$

where

$$a_{11}=x^*\left[-a_1+\frac{a_2(a+(1-m)y^*)^2y^*}{\left[(b_1+w^*)(a+y^*)+(a+(1-m)y^*)x^*\right]^2}\right],$$

$$a_{12}=\frac{a_2(a+(1-m)y^*)(a+y^*)x^*y^*}{\left[(b_1+w^*)(a+y^*)+(a+(1-m)y^*)x^*\right]^2},$$

$$a_{13}=\left[-\frac{rkx^*}{(1+ky^*)^2}-\frac{a_2(a+2(1-m)y^*)x^*}{(b_1+w^*)(a+y^*)+(a+(1-m)y^*)x^*}+\frac{a_2(a+(1-m)y^*)x^*y^*(b_1+w^*+(1-m)x^*)}{\left[(b_1+w^*)(a+y^*)+(a+(1-m)y^*)x^*\right]^2}\right],$$

$$a_{21}=\frac{a_3(a+y^*)(a+(1-m)y^*)w^*y^*}{\left[(b_1+w^*)(a+y^*)+(a+(1-m)y^*)x^*\right]^2},$$

$$a_{22}=-d_2-\frac{a_3(a+y^*)y^*}{(b_1+w^*)(a+y^*)+(a+(1-m)y^*)x^*}+\frac{a_3(a+y^*)^2w^*y^*}{\left[(b_1+w^*)(a+y^*)+(a+(1-m)y^*)x^*\right]^2},$$

$$a_{23}=-\frac{a_3(a+2y^*)w^*}{(b_1+w^*)(a+y^*)+(a+(1-m)y^*)x^*}+\frac{a_3(a+y^*)(b_1+w^*+(1-m)x^*)}{\left[(b_1+w^*)(a+y^*)+(a+(1-m)y^*)x^*\right]^2},$$

$$a_{31}=\frac{c_1a_2(a+(1-m)y^*)y^*}{(b_1+w^*)(a+y^*)+(a+(1-m)y^*)x^*}-\frac{c_1a_2(a+(1-m)y^*)^2x^*y^*}{\left[(b_1+w^*)(a+y^*)+(a+(1-m)y^*)x^*\right]^2}$$
$$-\frac{c_2a_3w^*y^*(a+y^*)(a+(1-m)y^*)}{\left[(b_1+w^*)(a+y^*)+(a+(1-m)y^*)x^*\right]^2},$$

$$a_{32}=-\frac{c_1a_2(a+(1-m)y^*)x^*y^*(a+y^*)}{\left[(b_1+w^*)(a+y^*)+(a+(1-m)y^*)x^*\right]^2}+\frac{c_2a_3(a+y^*)y^*}{(b_1+w^*)(a+y^*)+(a+(1-m)y^*)x^*}$$
$$-\frac{c_2a_3w^*y^*(a+y^*)^2}{\left[(b_1+w^*)(a+y^*)+(a+(1-m)y^*)x^*\right]^2},$$

$$a_{33}=\frac{c_1a_2(1-m)x^*y^*+c_2a_3w^*y^*}{(b_1+w^*)(a+y^*)+(a+(1-m)y^*)x^*}-\frac{\left[c_1a_2(a+(1-m)y^*)x^*y^*+c_2a_3w^*y^*(a+y^*)\right](b_1+w^*+(1-m)x^*)}{\left[(b_1+w^*)(a+y^*)+(a+(1-m)y^*)x^*\right]^2}. \tag{40}$$

The characteristic equation corresponding to $J^*(x^*, w^*, y^*)$ is expressed as

$$\lambda^3+A_1\lambda^2+A_2\lambda+A_3=0, \tag{41}$$

where

$$A_1 = -(a_{11} + a_{22} + a_{33}),$$
$$A_2 = a_{22}a_{33} - a_{23}a_{32} + a_{11}a_{33} - a_{13}a_{31} + a_{11}a_{22} - a_{12}a_{21}, \tag{42}$$
$$A_3 = -[a_{11}(a_{22}a_{33} - a_{23}a_{32}) + a_{12}(a_{23}a_{31} - a_{21}a_{33}) + a_{13}(a_{21}a_{32} - a_{22}a_{31})].$$

Theorem 9. *The coexistence equilibrium $E^*(x^*, w^*, y^*)$ is locally asymptotically stable if $A_1 > 0$, $A_3 > 0$, and $A_1A_2 > A_3$, where A_1, A_2, and A_3 are stated in (41).*

4.3. Local Bifurcations of Codimension 1

4.3.1. Transcritical Bifurcation

Theorem 10. *System (2) undergoes a transcritical bifurcation around $E_1(0, (A/d_2), 0)$ if $d_1^{[TC]} = r$ and $(c_2a_3(A/d_2)/(b_1 + (A/d_2))) < d_3$ ([TC] stands for transcritical bifurcation).*

Proof. We apply Sotomayor's theorem [43] to prove the occurrence of a transcritical bifurcation around E_1 with d_1 as bifurcation parameter. For applicability of Sotomayor's theorem, exactly one of the eigenvalues of the Jacobian matrix at E_1 must be zero and other eigenvalues must have negative real parts. So, we need to fulfill the condition $(c_2a_3(A/d_2)/(b_1 + (A/d_2))) < d_3$.

The eigenvectors of $J(E_1) = [v_{ij}]$ and $(J(E_1))^T$ corresponding to the zero eigenvalue of $E_1(0, (A/d_2), 0)$ are obtained as $V = (v_1, v_2, v_3)^T$ and $W = (1, 0, 0)^T$, respectively, where $v_1 = 1$, $v_2 = v_3 = 0$, $v_{11} = 0$, $v_{12} = 0$, $v_{13} = 0$, $v_{21} = 0$, $v_{22} = -d_2$, $v_{23} = 0$, $v_{31} = 0$, $v_{32} = 0$, $v_{33} = -d_3 + (c_2a_3(A/d_2)/(b_1 + (A/d_2)))$.

Compute Δ_1, Δ_2, and Δ_3 as follows:

$$\Delta_1 = W^T \cdot F_{d_1}\left(0, \frac{A}{d_2}, 0; d_1^{[TC]}\right) = (1,0,0) \cdot \begin{pmatrix} \frac{\partial F_1}{\partial d_1} \\ \frac{\partial F_2}{\partial d_1} \\ \frac{\partial F_3}{\partial d_1} \end{pmatrix}_{E_1} = (1,0,0) \cdot \begin{pmatrix} -x \\ 0 \\ 0 \end{pmatrix}_{E_1} = 0, \tag{43}$$

where $F = (F_1, F_2, F_3)^T$ and F_1, F_2, and F_3 are given by

$$F_1 = \frac{rx}{1+ky} - d_1x - a_1x^2 - \frac{a_2(1 - (my/(a+y)))xy}{b_1 + w + (1 - (my/(a+y)))x},$$
$$F_2 = A - d_2w - \frac{a_3wy}{b_1 + w + (1 - (my/(a+y)))x},$$
$$F_3 = \frac{c_1a_2(1 - (my/(a+y)))xy}{b_1 + w + (1 - (my/(a+y)))x} + \frac{c_2a_3wy}{b_1 + w + (1 - (my/(a+y)))x} - d_3y,$$
$$\Delta_2 = W^T \cdot \left[DF_{d_1}\left(0, \frac{A}{d_2}, 0; d_1^{[TC]}\right)V\right] = (1,0,0) \cdot \begin{bmatrix} \frac{\partial^2 F_1}{\partial x\,\partial d_1} & \frac{\partial^2 F_1}{\partial w\,\partial d_1} & \frac{\partial^2 F_1}{\partial y\,\partial d_1} \\ \frac{\partial^2 F_2}{\partial x\,\partial d_1} & \frac{\partial^2 F_2}{\partial w\,\partial d_1} & \frac{\partial^2 F_2}{\partial y\,\partial d_1} \\ \frac{\partial^2 F_3}{\partial x\,\partial d_1} & \frac{\partial^2 F_3}{\partial w\,\partial d_1} & \frac{\partial^2 F_3}{\partial y\,\partial d_1} \end{bmatrix}_{E_1} \cdot \begin{pmatrix} 1 \\ 0 \\ 0 \end{pmatrix}$$

$$= (1,0,0)\cdot\begin{bmatrix}-1 & 0 & 0\\ 0 & 0 & 0\\ 0 & 0 & 0\end{bmatrix}_{E_1}\cdot\begin{pmatrix}1\\0\\0\end{pmatrix} = -1 \neq 0,$$

$$\Delta_3 = W^T\cdot\left[D^2F\left(0,\frac{A}{d_2},0;d_1^{[\mathrm{TC}]}\right)(V,V)\right] = (1,0,0)\cdot D\begin{pmatrix}\frac{\partial F_1}{\partial x}v_1+\frac{\partial F_1}{\partial w}v_2+\frac{\partial F_1}{\partial y}v_3\\ \frac{\partial F_2}{\partial x}v_1+\frac{\partial F_2}{\partial w}v_2+\frac{\partial F_2}{\partial y}v_3\\ \frac{\partial F_3}{\partial x}v_1+\frac{\partial F_3}{\partial w}v_2+\frac{\partial F_3}{\partial y}v_3\end{pmatrix}_{E_1}\cdot\begin{pmatrix}v_1\\v_2\\v_3\end{pmatrix}$$

$$= (1,0,0)\cdot\begin{pmatrix}\frac{\partial^2F_1}{\partial x^2}v_1^2+\frac{\partial^2F_1}{\partial w^2}v_2^2+\frac{\partial^2F_1}{\partial y^2}v_3^2+2\frac{\partial^2F_1}{\partial x\,\partial w}v_1v_2+2\frac{\partial^2F_1}{\partial x\,\partial y}v_1v_3+2\frac{\partial^2F_1}{\partial w\,\partial y}v_2v_3\\ \frac{\partial^2F_2}{\partial x^2}v_1^2+\frac{\partial^2F_2}{\partial w^2}v_2^2+\frac{\partial^2F_2}{\partial y^2}v_3^2+2\frac{\partial^2F_2}{\partial x\,\partial w}v_1v_2+2\frac{\partial^2F_2}{\partial x\,\partial y}v_1v_3+2\frac{\partial^2F_2}{\partial w\,\partial y}v_2v_3\\ \frac{\partial^2F_3}{\partial x^2}v_1^2+\frac{\partial^2F_3}{\partial w^2}v_2^2+\frac{\partial^2F_3}{\partial y^2}v_3^2+2\frac{\partial^2F_3}{\partial x\,\partial w}v_1v_2+2\frac{\partial^2F_3}{\partial x\,\partial y}v_1v_3+2\frac{\partial^2F_3}{\partial w\,\partial y}v_2v_3\end{pmatrix}_{E_1}$$

$$= -2a_1 \neq 0. \tag{44}$$

Therefore, by Sotomayor's theorem [43], system (2) undergoes a transcritical bifurcation at $d_1 = d_1^{[\mathrm{TC}]}$ around the axial equilibrium point E_1. □

Theorem 11. *System (2) exhibits a transcritical bifurcation around* $E_2((r-d_1)/a_1, 0, 0)$ *if*

$$d_3^{[\mathrm{TC}]} = \frac{c_1a_2\left((r-d_1)/a_1\right)}{b_1+\left((r-d_1)/a_1\right)}. \tag{45}$$

Proof. Let us apply Sotomayor's theorem [43] to prove the occurrence of a transcritical bifurcation around E_2 with d_3 as bifurcation parameter. For applicability of Sotomayor's theorem, exactly one of the eigenvalues of the Jacobian matrix at E_2 must be zero and other eigenvalues must have negative real parts.

The eigenvectors of $J(E_2) = [t_{ij}]$ and $(J(E_2))^T$ corresponding to the zero eigenvalue of $E_2((r-d_1)/a_1, 0, 0)$ are obtained as $V = (v_1, v_2, v_3)^T$ and $W = (0,0,1)^T$, respectively, where $v_1 = (1/a_1)[-rk - (a_2/(b_1 + ((r-d_1)/a_1)))] < 0$, $v_2 = 0$, $v_3 = 1$, $t_{11} = -r + d_1$, $t_{12} = 0$, $t_{13} = ((r-d_1)/a_1)[-rk - (a_2/(b_1 + ((r-d_1)/a_1)))]$, $t_{21} = 0$, $t_{22} = -d_2$, $t_{23} = 0$, $t_{31} = 0$, $t_{32} = 0$, $t_{33} = 0$.

Compute Δ_1, Δ_2, and Δ_3 as follows:

$$\Delta_1 = W^T\cdot F_{d_1}\left(\frac{r-d_1}{a_1},0,0;d_3^{[\mathrm{TC}]}\right) = (0,0,1)\cdot\begin{pmatrix}\frac{\partial F_1}{\partial d_3}\\ \frac{\partial F_2}{\partial d_3}\\ \frac{\partial F_3}{\partial d_3}\end{pmatrix}_{E_2} = (0,0,1)\cdot\begin{pmatrix}0\\0\\-y\end{pmatrix}_{E_2} = 0, \tag{46}$$

where $F = (F_1, F_2, F_3)^T$ and F_1, F_2, and F_3 are given by

$$F_1 = \frac{rx}{1+ky} - d_1 x - a_1 x^2 - \frac{a_2(1-(my/(a+y)))xy}{b_1 + w + (1-(my/(a+y)))x},$$

$$F_2 = A - d_2 w - \frac{a_3 wy}{b_1 + w + (1-(my/(a+y)))x},$$

$$F_3 = \frac{c_1 a_2(1-(my/(a+y)))xy}{b_1 + w + (1-(my/(a+y)))x} + \frac{c_2 a_3 wy}{b_1 + w + (1-(my/(a+y)))x} - d_3 y,$$

$$\Delta_2 = W^T \cdot \left[DF_{d_3}\left(\frac{r-d_1}{a_1}, 0, 0; d_3^{[TC]}\right)V \right] = (0,0,1) \cdot \begin{bmatrix} \frac{\partial^2 F_1}{\partial x\,\partial d_3} & \frac{\partial^2 F_1}{\partial w\,\partial d_3} & \frac{\partial^2 F_1}{\partial y\,\partial d_3} \\ \frac{\partial^2 F_2}{\partial x\,\partial d_3} & \frac{\partial^2 F_2}{\partial w\,\partial d_3} & \frac{\partial^2 F_2}{\partial y\,\partial d_3} \\ \frac{\partial^2 F_3}{\partial x\,\partial d_3} & \frac{\partial^2 F_3}{\partial w\,\partial d_3} & \frac{\partial^2 F_3}{\partial w\,\partial d_3} \end{bmatrix}_{E_2} \cdot \begin{pmatrix} v_1 \\ v_2 \\ v_3 \end{pmatrix}$$

$$= (0,0,1) \cdot \begin{bmatrix} 0 & 0 & 0 \\ 0 & 0 & 0 \\ 0 & 0 & -1 \end{bmatrix}_{E_2} \cdot \begin{pmatrix} v_1 \\ v_2 \\ v_3 \end{pmatrix} = -v_3 = -1 \neq 0, \tag{47}$$

$$\Delta_3 = W^T \cdot \left[D^2 F\left(\frac{r-d_1}{a_1}, 0, 0; d_3^{[TC]}\right)(V,V) \right] = (0,0,1) \cdot D \begin{pmatrix} \frac{\partial F_1}{\partial x}v_1 + \frac{\partial F_1}{\partial w}v_2 + \frac{\partial F_1}{\partial y}v_3 \\ \frac{\partial F_2}{\partial x}v_1 + \frac{\partial F_2}{\partial w}v_2 + \frac{\partial F_2}{\partial y}v_3 \\ \frac{\partial F_3}{\partial x}v_1 + \frac{\partial F_3}{\partial w}v_2 + \frac{\partial F_3}{\partial y}v_3 \end{pmatrix}_{E_2} \cdot \begin{pmatrix} v_1 \\ v_2 \\ v_3 \end{pmatrix}$$

$$= (0,0,1) \cdot \begin{pmatrix} \frac{\partial^2 F_1}{\partial x^2}v_1^2 + \frac{\partial^2 F_1}{\partial w^2}v_2^2 + \frac{\partial^2 F_1}{\partial y^2}v_3^2 + 2\frac{\partial^2 F_1}{\partial x\,\partial w}v_1 v_2 + 2\frac{\partial^2 F_1}{\partial x\,\partial y}v_1 v_3 + 2\frac{\partial^2 F_1}{\partial w\,\partial y}v_2 v_3 \\ \frac{\partial^2 F_2}{\partial x^2}v_1^2 + \frac{\partial^2 F_2}{\partial w^2}v_2^2 + \frac{\partial^2 F_2}{\partial y^2}v_3^2 + 2\frac{\partial^2 F_2}{\partial x\,\partial w}v_1 v_2 + 2\frac{\partial^2 F_2}{\partial x\,\partial y}v_1 v_3 + 2\frac{\partial^2 F_2}{\partial w\,\partial y}v_2 v_3 \\ \frac{\partial^2 F_3}{\partial x^2}v_1^2 + \frac{\partial^2 F_3}{\partial w^2}v_2^2 + \frac{\partial^2 F_3}{\partial y^2}v_3^2 + 2\frac{\partial^2 F_3}{\partial x\,\partial w}v_1 v_2 + 2\frac{\partial^2 F_3}{\partial x\,\partial y}v_1 v_3 + 2\frac{\partial^2 F_3}{\partial w\,\partial y}v_2 v_3 \end{pmatrix}_{E_2}$$

$$= \frac{2a_2 b_1 c_1 (v_1 - (m/a))}{(b_1 + ((r-d_1)/a_1))^2} \neq 0.$$

Therefore, by Sotomayor's theorem [43], system (2) exhibits a transcritical bifurcation at $d_3 = d_3^{[TC]}$ around the axial equilibrium point E_2. □

Theorem 12. *System (2) undergoes a transcritical bifurcation around $E_4(0, \widehat{w}, \widehat{y})$ if*

$$d_1^{[TC]} = \frac{r}{1+k\widehat{y}} - \frac{a_2[a+(1-m)\widehat{y}]\widehat{y}}{(b_1+\widehat{y})(a+\widehat{y})},$$

$$\frac{c_2 a_3 \widehat{w}\widehat{y}}{(b_1+\widehat{w})(a+\widehat{y})} < \frac{c_2 a_3 \widehat{w}\widehat{y}(a+\widehat{y})(b_1+\widehat{w})}{[(b_1+\widehat{w})(a+\widehat{y})]^2}. \tag{48}$$

Proof. Proof is the same as in Theorem 10. □

Theorem 13. *System (2) undergoes a transcritical bifurcation around* $E_5((r-d_1)/a_1, (A/d_2), 0)$ *if*

$$d_3^{[\mathrm{TC}]} = \frac{c_1 a_2\left((r-d_1)/a_1\right)}{b_1 + (A/d_2) + \left((r-d_1)/a_1\right)} + \frac{c_2 a_3 (A/d_2)}{b_1 + (A/d_2) + \left((r-d_1)/a_1\right)}. \tag{49}$$

Proof. Proof is the same as in Theorem 11. □

4.3.2. Hopf Bifurcation around $E^*(x^*, w^*, y^*)$. Let us consider k as a bifurcation parameter of system (2) where the characteristic equation at E^* is

$$\lambda^3 + A_1(k)\lambda^2 + A_2(k)\lambda + A_3(k) = 0. \tag{50}$$

Then, Hopf bifurcation theorem is stated as follows.

Theorem 14 (Hopf bifurcation theorem [44]). *If* $A_1(k)$, $A_2(k)$, *and* $A_3(k)$ *are the smooth functions of* k *in* $N_\varepsilon(k^{[H]})$, $(\varepsilon > 0)$, $k^{[H]} \in \mathbb{R}$ *for which the characteristic equation (50) has the following:*

(i) A pair of imaginary eigenvalues $\lambda = q_1(k) \pm iq_2(k)$ *with* $q_1(k)$ *and* $q_2(k) \in \mathbb{R}$ *so that they become purely complex at* $k = k^{[H]}$ *and* $(dq_1/dk)|_{k=k^{[H]}} \neq 0$

(ii) The other eigenvalue is negative at $k = k^{[H]}$*; then, a Hopf bifurcation appears around* E^* *at* $k = k^{[H]}$

Theorem 15. *If* $E^*(x^*, w^*, y^*)$ *is locally asymptotically stable, then a Hopf bifurcation is exhibited around* $E^*(x^*, w^*, y^*)$ *when* k *passes through its critical value* $k^{[H]}$ *provided* $A_1(k^{[H]}) > 0$, $A_3(k^{[H]}) > 0$, *and* $A_1(k^{[H]})A_2(k^{[H]}) = A_3(k^{[H]})$ *(*$k^{[H]}$ *is a positive root of equation* $A_1(k)A_2(k) - A_3(k) = 0$*).*

Proof. At $k = k^{[H]}$, we can write equation (50) as

$$\left(\lambda^2 + A_2\right)\left(\lambda + A_1\right) = 0. \tag{51}$$

The roots of equation (51) are $\lambda_1 = i\sqrt{A_2}$, $\lambda_2 = -i\sqrt{A_2}$, and $\lambda_3 = -A_1$. Also A_1, A_2, and A_3 are the smooth functions of k. So, the roots of equation (59) have the form $\lambda_1 = p_1(k) + ip_2(k)$, $\lambda_2 = p_1(k) - ip_2(k)$, and $\lambda_3 = p_3(k)$ where $p_i(k)$ are real functions of k in an open neighborhood of $k^{[H]}$ for $i = 1, 2, 3$. Next, we verify the transversality condition:

$$\frac{\mathrm{d}}{\mathrm{d}k}\left(\mathrm{Re}\lambda_i(k)\right)|_{k=k^{[H]}} \neq 0, \quad i = 1, 2. \tag{52}$$

Putting $\lambda(k) = p_1(k) + ip_2(k)$ in (59), we get

$$p_1(k) + ip_2(k)^3 + A_1(k)p_1(k) + ip_2(k)^2 + A_2(k)\left(p_1(k) + ip_2(k)\right) + A_3(k) = 0. \tag{53}$$

Differentiating both sides with respect to k, we have

$$\begin{aligned} &3\left(p_1(k) + ip_2(k)\right)^2\left(\dot{p}_1(k) + i\dot{p}_2(k)\right) + 2A_1(k)\left(p_1(k) + ip_2(k)\right)\left(\dot{p}_1(k) + i\dot{p}_2(k)\right) \\ &\quad + \dot{A}_1(k)\left(p_1(k) + ip_2(k)\right)^2 + A_2\left(\dot{p}_1(k) + i\dot{p}_2(k)\right) + \dot{A}_2(k)\left(p_1(k) + ip_2(k)\right) + \dot{A}_3(k) = 0. \end{aligned} \tag{54}$$

Comparing real and imaginary parts from both sides, we obtain

$$X_1\dot{p}_1 - X_2\dot{p}_2 + X_3 = 0, \tag{55}$$

$$X_2\dot{p}_1 + X_1\dot{p}_2 + X_4 = 0, \tag{56}$$

where

$$\begin{aligned} X_1 &= 3\left(p_1^2 - p_2^2\right) + 2A_1p_1 + A_2, \\ X_2 &= 6p_1p_2 + 2A_1p_2, \\ X_3 &= \dot{A}_1\left(p_1^2 - p_2^2\right) + \dot{A}_2p_1 + \dot{A}_3 \neq \dot{A}_1\left(p_1^2 - p_2^2\right) + \dot{A}_2p_1 + A_1\dot{A}_2 + A_2\dot{A}_1, \\ &\quad \left[\text{since } A_3 \neq A_1A_2 \text{ in a deleted neighbour hood of } k^{[H]}\right], \end{aligned} \tag{57}$$

and $X_4 = 2\dot{A}_1 p_1 p_2 + \dot{A}_2 p_2$.

Multiplying (55) by X_1 and (56) by X_2 and then adding, we get

$$\left(X_1^2 + X_2^2\right)\dot{p}_1 + X_1X_3 + X_2X_4 = 0 \Longrightarrow \dot{p}_1 = -\left\{\frac{X_1X_3 + X_2X_4}{X_1^2 + X_2^2}\right\}. \tag{58}$$

At $k = k^{[H]}$,

Case 1: $p_1 = 0$, $p_2 = \sqrt{A_2}$. Then, $X_1 = -2A_2$, $X_2 = 2A_1\sqrt{A_2}$, $X_3 \neq A_1\dot{A}_2$, and $X_4 = \dot{A}_2\sqrt{A_2}$. $\therefore X_1X_3 + X_2X_4 \neq 0$.

Case 2: $p_1 = 0$, $p_2 = -\sqrt{A_2}$. Then, $X_1 = -2A_2$, $X_2 = -2A_1\sqrt{A_2}$, $X_3 \neq A_1\dot{A}_2$, and $X_4 = -\dot{A}_2\sqrt{A_2}$. $\therefore X_1X_3 + X_2X_4 \neq 0$.

Also, $\lambda_3 = -A_1(k^{[H]}) < 0$.

Hence, this theorem is proved by virtue of Theorem 14. □

4.3.3. Hopf Bifurcation around $E_3(\overline{x}, 0, \overline{y})$. Let us consider k as a bifurcation parameter of system (2) where the characteristic equation of E_3 is

$$\lambda^3 + B_1(k)\lambda^2 + B_2(k)\lambda + B_3(k) = 0, \tag{59}$$

and then Hopf bifurcation theorem is stated as follows.

Theorem 16 (Hopf bifurcation theorem [44]). *If $B_1(k)$, $B_2(k)$, and $B_3(k)$ are the smooth functions of k in $N_\varepsilon(k^*)$, $(\varepsilon > 0)$, $k^* \in \mathbb{R}$ for which the characteristic equation (59) has the following:*

(i) A pair of imaginary eigenvalues $\lambda = p_1'(k) \pm ip_2'(k)$ with $p_1'(k)$ and $p_2'(k) \in \mathbb{R}$ so that they become purely imaginary at $k = k^*$ and $(dp_1'/dk)|_{k=k^*} \neq 0$

(ii) The other eigenvalue is negative at $k = k^*$; then a Hopf bifurcation occurs around $E_3(\overline{x}, 0, \overline{y})$ at $k = k^*$

Theorem 17. *If $E_3(\overline{x}, 0, \overline{y})$ is locally asymptotically stable, then a Hopf bifurcation appears around subsidy-free equilibrium $E_3(\overline{x}, 0, \overline{y})$ when k passes through its critical value k^* provided $B_1(k^*) > 0$, $B_3(k^*) > 0$, and $B_1(k^*)B_2(k^*) = B_3(k^*)$ (k^* is a positive root of equation $B_1(k)B_2(k) - B_3(k) = 0$).*

Proof. Proof is the same as in Theorem 15. □

5. Delayed Dynamical System

In biological point of view, many processes, both natural and man-made, include time-delay. The study of delay factor makes our system much more realistic than non-delayed system. Also, a delay differential equation reveals much more complicated dynamics than an ordinary differential equation (for details, see [10–13, 23, 45–49]).

In reality, after sensing the vocal cue, individuals of prey species take some time for assessing the predation risk. So, the effect of fear (felt by prey) of predator does not respond spontaneously on the birth rate of prey population; some time lag must be needed. In view of this fact, the predator-prey-subsidy interactions (2) can be modified as follows:

$$\begin{aligned}
\frac{dx}{dt} &= \frac{rx}{1 + ky(t-\tau)} - d_1x - a_1x^2 - \frac{a_2(1 - (my/(a+y)))xy}{b_1 + w + (1 - (my/(a+y)))x},\\
\frac{dw}{dt} &= A - d_2w - \frac{a_3wy}{b_1 + w + (1 - (my/(a+y)))x},\\
\frac{dy}{dt} &= \frac{c_1a_2(1 - (my/(a+y)))xy}{b_1 + w + (1 - (my/(a+y)))x} + \frac{c_2a_3wy}{b_1 + w + (1 - (my/(a+y)))x} - d_3y.
\end{aligned} \tag{60}$$

The initial conditions are assumed as $(i = 1, 2, 3)$

$$\begin{aligned}
&\psi_i(\phi) > 0, \phi \in [-\tau, 0], \quad \text{where } x(\phi) = \psi_1(\phi), w(\phi) = \psi_2(\phi), y(\phi) = \psi_3(\phi),\\
&\text{For biological feasibility: } \psi_1(0) > 0,\ \psi_2(0) > 0, \psi_3(0) > 0.
\end{aligned} \tag{60a}$$

Let us linearize (60) using the following transformations:

$$\begin{aligned}
X &= x - \overline{x},\\
W &= w - 0,\\
Y &= y - \overline{y}.
\end{aligned} \tag{61}$$

It leads to

$$\frac{dU}{dt} = B_1'U(t) + B_2'U(t-\tau), \tag{62}$$

where $U = [X, W, Y]^T$,

$$B_1' = \begin{bmatrix} b_{11} & b_{12} & b_{13}' \\ b_{21} & b_{22} & b_{23} \\ b_{31} & b_{32} & b_{33} \end{bmatrix},$$

$$B_2' = \begin{bmatrix} 0 & 0 & b_{13}'' \\ 0 & 0 & 0 \\ 0 & 0 & 0 \end{bmatrix},$$

$$b_{11} = \overline{x}\left\{-a_1 + \frac{a_2\overline{y}(a+(1-m)\overline{y})^2}{\{b_1(a+\overline{y})+[a+(1-m)\overline{y}]\overline{x}\}^2}\right\},$$

$$b_{12} = \frac{a_2\overline{x}\overline{y}[a+(1-m)\overline{y}](a+\overline{y})}{\{b_1(a+\overline{y})+[a+(1-m)\overline{y}]\overline{x}\}^2},$$

$$b_{13}' = \overline{x}\left\{-\frac{a_2[a+2(1-m)\overline{y}]}{b_1(a+\overline{y})+[a+(1-m)\overline{y}]\overline{x}} + \frac{a_2\overline{y}[a+(1-m)\overline{y}][b_1+(1-m)\overline{x}]}{\{b_1(a+\overline{y})+[a+(1-m)\overline{y}]\overline{x}\}^2}\right\}, \quad (63)$$

$$b_{21} = 0,$$

$$b_{22} = -d_2 - \frac{a_3\overline{y}}{b_1+(1-(m\overline{y}/(a+\overline{y})))\overline{x}},$$

$$b_{23} = 0,$$

$$b_{31} = \overline{y}\left\{\frac{c_1a_2[a+(1-m)\overline{y}]}{b_1(a+\overline{y})+[a+(1-m)\overline{y}]\overline{x}} - \frac{c_1a_2[a+(1-m)\overline{y}]^2\overline{x}}{\{b_1(a+\overline{y})+[a+(1-m)\overline{y}]\overline{x}\}^2}\right\},$$

$$b_{32} = \frac{c_2a_3\overline{y}(a+\overline{y})}{b_1(a+y^*)+[a+(1-m)\overline{y}]\overline{x}},$$

$$b_{33} = \overline{y}\left\{\frac{c_1a_2(1-m)\overline{x}}{b_1(a+\overline{y})+[a+(1-m)\overline{y}]\overline{x}} - \frac{c_1a_2[a+(1-m)\overline{y}]\overline{x}[b_1+(1-m)\overline{x}]}{\{b_1(a+\overline{y})+[a+(1-m)\overline{y}]\overline{x}\}^2}\right\},$$

$$b_{13}'' = -\frac{rk\overline{x}}{(1+k\overline{y})^2}.$$

The characteristic equation corresponding to (62) is

$$\lambda^3 + L_1\lambda^2 + L_2\lambda + L_3 + (M_1\lambda + M_2)e^{-\lambda\tau} = 0, \quad (64)$$

where

$$\begin{aligned} L_1 &= -(b_{11}+b_{22}+b_{33}), \\ L_2 &= b_{22}b_{33} + b_{11}b_{33} - b_{13}'b_{31} + b_{11}b_{22}, \\ L_3 &= -[b_{11}b_{22}b_{33} - b_{13}'b_{22}b_{31}], \\ M_1 &= -b_{13}''b_{31}, \\ M_2 &= b_{13}''b_{31}b_{22}. \end{aligned} \quad (65)$$

If $\tau \neq 0$, E_3 of system (60) is LAS provided equation (64) has no purely imaginary roots and it is also LAS for $\tau = 0$. Further, it has been shown that stability nature of E_3 switches at $\tau = \tau'^*$. Already, it has been derived that E_3 is LAS provided $B_1 > 0$, $B_3 > 0$, and $B_1B_2 > B_3$ for $\tau = 0$ (non-delayed system). Let us discuss if the real part of the roots of equation (64) gradually increases to reach zero and eventually turns to a positive value when τ increases.

Substituting $\lambda = q_1' + iq_2'$ in equation (64), we have

$$\begin{aligned} &(q_1'+iq_2')^3 + L_1(q_1'+iq_2')^2 + L_2(q_1'+iq_2') + L_3 \\ &\quad + (M_1(q_1'+iq_2') + M_2)e^{-q_1'\tau}(\cos(q_2'\tau) - i\sin(q_2'\tau)) = 0. \end{aligned} \quad (66)$$

Equating respective real and complex parts from both sides, we obtain

$$q_1^{'3} - 3q_1'q_2^{'2} + L_1\left(q_1^{'2} - q_2^{'2}\right) + L_2q_1' + L_3 + M_1q_1'e^{-q_1'\tau}\cos\left(q_2'\tau\right) + M_2e^{-q_1'\tau}\cos\left(q_2'\tau\right) + M_1q_2'e^{-q_1'\tau}\sin\left(q_2'\tau\right) = 0, \tag{67}$$

$$3q_1^{'2}q_2' - q_2^{'3} + 2L_1q_1'q_2' + L_2q_2' + M_1q_2'e^{-q_1'\tau}\cos\left(q_2'\tau\right) - M_1q_1'e^{-q_1'\tau}\sin\left(q_2'\tau\right) - M_2e^{-q_1'\tau}\sin\left(q_2'\tau\right) = 0. \tag{68}$$

Now, let us examine whether equation (64) has purely imaginary roots or not. For this purpose, let us take $q_1' = 0$. Then, equations (67) and (68) become

$$M_1q_2'\sin\left(q_2'\tau\right) + M_2\cos\left(q_2'\tau\right) = L_1q_2^{'2} - L_3, \tag{69}$$

$$M_1q_2'\cos\left(q_2'\tau\right) - M_2\sin\left(q_2'\tau\right) = q_2^{'3} - L_2q_2'. \tag{70}$$

Eliminating τ from (69) and (70) (squaring and adding), we get

$$q_2^{'6} + q_2^{'4}\left(L_1^2 - 2L_2\right) + q_2^{'2}\left(L_2^2 - 2L_1L_3 - M_1^2\right) + \left(L_3^2 - M_2^2\right) = 0. \tag{71}$$

Putting $q_2^{'2} = \beta$, we have

$$L(\beta) \equiv \beta^3 + \left(L_1^2 - 2L_2\right)\beta^2 + \left(L_2^2 - 2L_1L_3 - M_1^2\right)\beta + \left(L_3^2 - M_2^2\right) = 0. \tag{72}$$

This is a cubic equation of β. It is noticed that $L(\infty) = \infty$. So, equation (72) has exactly one positive real root if $L(0) < 0$, i.e., if $L_3^2 < M_2^2$.

Let $\beta = \beta_+$ be a positive root of (77); then, $q_2' = \sqrt{\beta_+}$.

Lemma 1 (see [50]). *Consider the exponential polynomial:*

$$\begin{aligned} P(\lambda) \equiv P\left(\lambda, \tau_1, \tau_2, \ldots, \tau_m\right) \equiv {} & \lambda^n + p_1^{(0)}\lambda^{n-1} + \cdots + p_{n-1}^{(0)}\lambda + p_n^{(0)} + \left[p_1^{(1)}\lambda^{n-1} + \cdots + p_{n-1}^{(1)}\lambda + p_n^{(1)}\right]e^{-\lambda\tau_1} + \cdots \\ & + \left[p_1^{(m)}\lambda^{n-1} + \cdots + p_{n-1}^{(m)}\lambda + p_n^{(m)}\right]e^{-\lambda\tau_m}, \end{aligned} \tag{73}$$

where $\tau_i \geq 0\,(i = 1, 2, \ldots, m)$ and $p_j^{(i)}\,(i = 0, 1, \ldots, m;\ j = 1, 2, \ldots, n)$ are constants. As $(\tau_1, \tau_2, \ldots, \tau_m)$ vary, the sum of the orders of zero of $P(\lambda)$ in the open half plane can change only if a zero appears on or crosses the imaginary axis.

Now, let us discuss the existence of Hopf bifurcation around E_3 with τ as a bifurcation parameter.

Theorem 18. *Suppose E_3 exists and is locally asymptotically stable for system (2) when $\tau = 0$. If $L_3^2 < M_2^2$, then there exists a critical value τ'^* such that E_3 of system (60) is LAS when $\tau \in [0, \tau'^*)$ and unstable when $\tau > \tau'^*$, where*

$$\tau_+^{'(j)} = \frac{\cos^{-1}\left(\left(M_2\left(L_1\beta_+ - L_3\right) + M_1\left(\beta_+^2 - L_2\beta_+\right)\right)/\left(M_2^2 + M_1^2\beta_+\right)\right)}{\sqrt{\beta_+}} + \frac{2\pi j}{\sqrt{\beta_+}}, \quad j = 0, 1, 2, 3, \ldots, \tag{74}$$

and $\tau'^* = \tau_+^{'(0)}$ (minimum value). Also, system (60) exhibits Hopf bifurcation around E_3 at $\tau = \tau'^*$ provided $K'M' - L'N' \neq 0$, where

$$
\begin{aligned}
K' &= \left\{-3\beta_+ + L_2 + M_1 \ \cos\left(\sqrt{\beta_+}\,\tau'^*\right) - M_2\tau'^*\cos\left(\sqrt{\beta_+}\,\tau'^*\right) - M_1\sqrt{\beta_+}\,\tau'^*\sin\left(\sqrt{\beta_+}\,\tau'^*\right)\right\},\\
L' &= \left\{-2L_1\sqrt{\beta_+} + M_1\sin\left(\sqrt{\beta_+}\,\tau'^*\right) - M_2\tau'^*\sin\left(\sqrt{\beta_+}\,\tau'^*\right) + M_1\sqrt{\beta_+}\,\tau'^*\cos\left(\sqrt{\beta_+}\,\tau'^*\right)\right\},\\
M' &= \left\{M_2\sqrt{\beta_+}\sin\left(\sqrt{\beta_+}\,\tau'^*\right) - M_1\beta_+\cos\left(\sqrt{\beta_+}\,\tau'^*\right)\right\},\\
N' &= \left\{M_2\sqrt{\beta_+}\cos\left(\sqrt{\beta_+}\,\tau'^*\right) + M_1\beta_+\sin\left(\sqrt{\beta_+}\,\tau'^*\right)\right\}.
\end{aligned}
\tag{75}
$$

Proof. If $L_3^2 < M_2^2$, then (72) has exactly one positive root β_+, i.e., from (69) and (70), $\tau_+^{(j)}$, $j = 0, 1, 2, \ldots$, are obtained as functions of β_+:

$$
\tau_+'^{(j)} = \frac{\cos^{-1}\left(\left(M_2\left(L_1\beta_+ - L_3\right) + M_1\left(\beta_+^2 - L_2\beta_+\right)\right)/\left(M_2^2 + M_1^2\beta_+\right)\right)}{\sqrt{\beta_+}} + \frac{2\pi j}{\sqrt{\beta_+}}, \quad j = 0, 1, 2, 3, \ldots. \tag{76}
$$

If E_3 is locally asymptotically stable, the stability behaviour of E_3 will remain unaltered for $\tau < \tau'^*$ (using Butler's Lemma [51]).

To check the transversality condition, $[(\mathrm{d}/\mathrm{d}\tau)\mathrm{Re}\,\lambda(\tau)]_{\tau=\tau'^*} \neq 0$, let us differentiate (67) and (68) with respect to τ and set $q_1' = 0$ and $\tau = \tau'^*$. The following equations are obtained:

$$
K'\left[\frac{\mathrm{d}}{\mathrm{d}\tau}\left[\mathrm{Re}\{\lambda(\tau)\}\right]\right]_{\tau=\tau'^*} + L'\left[\frac{\mathrm{d}}{\mathrm{d}\tau}\left[\mathrm{Im}\{\lambda(\tau)\}\right]\right]_{\tau=\tau'^*} = M', \tag{77}
$$

$$
-L'\left[\frac{\mathrm{d}}{\mathrm{d}\tau}\left[\mathrm{Re}\{\lambda(\tau)\}\right]\right]_{\tau=\tau'^*} + K'\left[\frac{\mathrm{d}}{\mathrm{d}\tau}\left[\mathrm{Im}\{\lambda(\tau)\}\right]\right]_{\tau=\tau'^*} = N', \tag{78}
$$

where

$$
\begin{aligned}
K' &= \left\{-3\beta_+ + L_2 + M_1 \ \cos\left(\sqrt{\beta_+}\,\tau'^*\right) - M_2\tau'^*\cos\left(\sqrt{\beta_+}\,\tau'^*\right) - M_1\sqrt{\beta_+}\,\tau'^*\sin\left(\sqrt{\beta_+}\,\tau'^*\right)\right\},\\
L' &= \left\{-2L_1\sqrt{\beta_+} + M_1\sin\left(\sqrt{\beta_+}\,\tau'^*\right) - M_2\tau'^*\sin\left(\sqrt{\beta_+}\,\tau'^*\right) + M_1\sqrt{\beta_+}\,\tau'^*\cos\left(\sqrt{\beta_+}\,\tau'^*\right)\right\},\\
M' &= \left\{M_2\sqrt{\beta_+}\sin\left(\sqrt{\beta_+}\,\tau'^*\right) - M_1\beta_+\cos\left(\sqrt{\beta_+}\,\tau'^*\right)\right\},\\
N' &= \left\{M_2\sqrt{\beta_+}\cos\left(\sqrt{\beta_+}\,\tau'^*\right) + M_1\beta_+\sin\left(\sqrt{\beta_+}\,\tau'^*\right)\right\}.
\end{aligned}
\tag{79}
$$

Solving (77) and (78),

$$
\left[\frac{\mathrm{d}[\mathrm{Re}\{\lambda(\tau)\}]}{\mathrm{d}\tau}\right]_{\tau=\tau'^*} = \left[\frac{K'M' - L'N'}{K'^2 + L'^2}\right]. \tag{80}
$$

Now, we have $\mathrm{d}[\mathrm{Re}\{\lambda(\tau)\}]/\mathrm{d}\tau_{\tau=\tau'^*} \neq 0$, if $K'M' - L'N' \neq 0$. Hence, the transversality condition is satisfied and a Hopf bifurcation occurs around E^* when τ passes through its critical value τ'^*. □

Now, linearize system (60) using the transformations $X = x - x^*$, $W = w - w^*$, and $Y = y - y^*$:

$$
\frac{\mathrm{d}U}{\mathrm{d}t} = A_1'U(t) + A_2'U(t-\tau), \tag{81}
$$

where $U = [X, W, Y]^T$,

$$A_1' = \begin{bmatrix} a_{11} & a_{12} & a_{13}' \\ a_{21} & a_{22} & a_{23} \\ a_{31} & a_{32} & a_{33} \end{bmatrix},$$

$$A_2' = \begin{bmatrix} 0 & 0 & a_{13}'' \\ 0 & 0 & 0 \\ 0 & 0 & 0 \end{bmatrix},$$

$$a_{11} = x^*\left[-a_1 + \frac{a_2(a+(1-m)y^*)^2 y^*}{[(b_1+w^*)(a+y^*)+(a+(1-m)y^*)x^*]^2}\right],$$

$$a_{12} = \frac{a_2(a+(1-m)y^*)(a+y^*)x^* y^*}{[(b_1+w^*)(a+y^*)+(a+(1-m)y^*)x^*]^2},$$

$$a_{13}' = \left[-\frac{a_2(a+2(1-m)y^*)x^*}{(b_1+w^*)(a+y^*)+(a+(1-m)y^*)x^*} + \frac{a_2(a+(1-m)y^*)x^* y^*(b_1+w^*+(1-m)x^*)}{[(b_1+w^*)(a+y^*)+(a+(1-m)y^*)x^*]^2}\right],$$

$$a_{21} = \frac{a_3(a+y^*)(a+(1-m)y^*)w^* y^*}{[(b_1+w^*)(a+y^*)+(a+(1-m)y^*)x^*]^2},$$

$$a_{22} = -d_2 - \frac{a_3(a+y^*)y^*}{(b_1+w^*)(a+y^*)+(a+(1-m)y^*)x^*} + \frac{a_3(a+y^*)^2 w^* y^*}{[(b_1+w^*)(a+y^*)+(a+(1-m)y^*)x^*]^2},$$

$$a_{23} = -\frac{a_3(a+2y^*)w^*}{(b_1+w^*)(a+y^*)+(a+(1-m)y^*)x^*} + \frac{a_3(a+y^*)(b_1+w^*+(1-m)x^*)}{[(b_1+w^*)(a+y^*)+(a+(1-m)y^*)x^*]^2},$$

$$a_{31} = \frac{c_1 a_2(a+(1-m)y^*)y^*}{(b_1+w^*)(a+y^*)+(a+(1-m)y^*)x^*} - \frac{c_1 a_2(a+(1-m)y^*)^2 x^* y^*}{[(b_1+w^*)(a+y^*)+(a+(1-m)y^*)x^*]^2} - \frac{c_2 a_3 w^* y^*(a+y^*)(a+(1-m)y^*)}{[(b_1+w^*)(a+y^*)+(a+(1-m)y^*)x^*]^2}$$

$$a_{32} = -\frac{c_1 a_2(a+(1-m)y^*)x^* y^*(a+y^*)}{[(b_1+w^*)(a+y^*)+(a+(1-m)y^*)x^*]^2} + \frac{c_2 a_3(a+y^*)y^*}{(b_1+w^*)(a+y^*)+(a+(1-m)y^*)x^*} - \frac{c_2 a_3 w^* y^*(a+y^*)^2}{[(b_1+w^*)(a+y^*)+(a+(1-m)y^*)x^*]^2},$$

$$a_{33} = \frac{c_1 a_2(1-m)x^* y^* + c_2 a_3 w^* y^*}{(b_1+w^*)(a+y^*)+(a+(1-m)y^*)x^*} - \frac{[c_1 a_2(a+(1-m)y^*)x^* y^* + c_2 a_3 w^* y^*(a+y^*)](b_1+w^*+(1-m)x^*)}{[(b_1+w^*)(a+y^*)+(a+(1-m)y^*)x^*]^2},$$

$$a_{13}'' = -\frac{rkx^*}{(1+ky^*)^2}. \tag{82}$$

The characteristic equation corresponding to (81) is

$$\lambda^3 + R_1\lambda^2 + R_2\lambda + R_3 + (S_1\lambda + S_2)e^{-\lambda\tau} = 0, \tag{83}$$

where

$$\begin{aligned} R_1 &= -(a_{11} + a_{22} + a_{33}),\\ R_2 &= a_{22}a_{33} - a_{23}a_{32} + a_{11}a_{33} - a_{13}'a_{31} + a_{11}a_{22} - a_{12}a_{21},\\ R_3 &= -[a_{11}(a_{22}a_{33} - a_{23}a_{32}) + a_{12}(a_{23}a_{31} - a_{21}a_{33}) + a_{13}'(a_{21}a_{32} - a_{22}a_{31})],\\ S_1 &= -a_{13}''a_{31},\\ S_2 &= -a_{13}''(a_{21}a_{32} - a_{31}a_{22}). \end{aligned} \tag{84}$$

If $\tau \neq 0$, E^* of system (60) is LAS provided equation (83) has no purely imaginary roots and it is LAS for $\tau = 0$. Furthermore, it has to be noted that changes of stability occur at $\tau = \tau^*$. Already, it has been discussed that E^* is LAS when $\tau = 0$ provided $A_1 > 0$, $A_3 > 0$, and $A_1A_2 > A_3$. Here, equation (83) is a transcendental equation, so it contains infinitely many eigenvalues. In this situation, we cannot apply the Routh–Hurwitz criteria to determine the stability of system (60). To understand the stability behaviour, our necessity is to check the sign of the real parts of the eigenvalues of equation (83).

Now, putting $\lambda = q_1 + iq_2$ in equation (83), we have

$$(q_1 + iq_2)^3 + R_1(q_1 + iq_2)^2 + R_2(q_1 + iq_2) + R_3 + (S_1(q_1 + iq_2) + S_2)e^{-q_1\tau}(\cos(q_2\tau) - i\sin(q_2\tau)) = 0. \tag{85}$$

Equating respective real and complex parts from both sides, we get

$$q_1^3 - 3q_1q_2^2 + R_1(q_1^2 - q_2^2) + R_2q_1 + R_3 + S_1q_1e^{-q_1\tau}\cos(q_2\tau) + S_2e^{-q_1\tau}\cos(q_2\tau) + S_1q_2e^{-q_1\tau}\sin(q_2\tau) = 0, \tag{86}$$

$$3q_1^2q_2 - q_2^3 + 2R_1q_1q_2 + R_2q_2 + S_1q_2e^{-q_1\tau}\cos(q_2\tau) - S_1q_1e^{-q_1\tau}\sin(q_2\tau) - S_2e^{-q_1\tau}\sin(q_2\tau) = 0. \tag{87}$$

To check whether (83) has purely imaginary roots or not, set $q_1 = 0$; then, (86) and (87) become

$$S_1q_2\sin(q_2\tau) + S_2\cos(q_2\tau) = R_1q_2^2 - R_3, \tag{88}$$

$$S_1q_2\cos(q_2\tau) - S_2\sin(q_2\tau) = q_2^3 - R_2q_2. \tag{89}$$

Eliminating τ from (88) and (89) (squaring and adding), we get

$$q_2^6 + q_2^4(R_1^2 - 2R_2) + q_2^2(R_2^2 - 2R_1R_3 - S_1^2) + (R_3^2 - S_2^2) = 0. \tag{90}$$

Putting $q_2^2 = \sigma$, we have

$$R'(\sigma) \equiv \sigma^3 + (R_1^2 - 2R_2)\sigma^2 + (R_2^2 - 2R_1R_3 - S_1^2)\sigma + (R_3^2 - S_2^2) = 0. \tag{91}$$

This is a cubic equation of σ. It is noted that $R'(\infty) = \infty$. So, equation (91) has exactly one positive root if $R'(0) < 0$, i.e., if $R_3^2 < S_2^2$.

Let $\sigma = \sigma_+$ be a positive root of (91); then, $q_2 = \sqrt{\sigma_+}$.

Let us study the existence of Hopf bifurcation around E^* with τ as bifurcation parameter.

Theorem 19. *Suppose E^* exists and is locally asymptotically stable for system (2) when $\tau = 0$. If $R_3^2 < S_2^2$, then there exists a critical value τ^* such that E^* of system (60) is LAS when $\tau \in [0, \tau^*)$ and unstable when $\tau > \tau^*$, where*

$$\tau_+^{(j)} = \frac{\cos^{-1}\left(\left(S_2(R_1\sigma_+ - R_3) + S_1(\sigma_+^2 - R_2\sigma_+)\right)/\left(S_2^2 + S_1^2\sigma_+\right)\right)}{\sqrt{\sigma_+}} + \frac{2\pi j}{\sqrt{\sigma_+}}, \quad j = 0, 1, 2, 3, \ldots, \tag{92}$$

and $\tau^* = \tau_+^{(0)}$ (minimum value). Also, a supercritical Hopf bifurcation is exhibited around E^* at $\tau = \tau^*$ provided $K''M'' - L''N'' \neq 0$, where

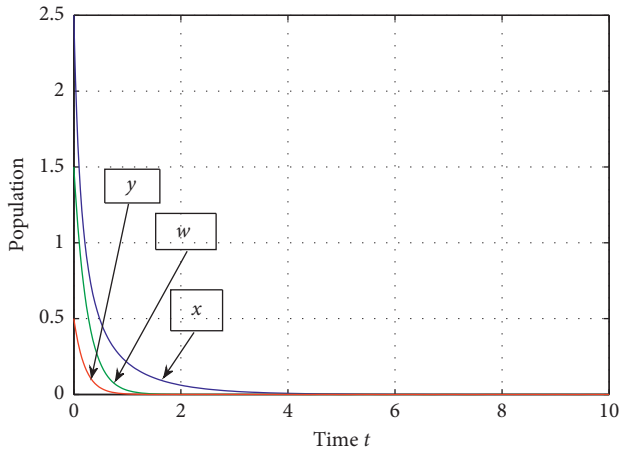

FIGURE 1: Stable behaviour of $E_0(0, 0, 0)$ with respect to time t corresponding to the data set $\{r = 5.5, d_1 = 6.5, d_2 = 4, k = 0.2, d_3 = 5, a_1 = 2, a_2 = 0.3, a_3 = 0.25, b_1 = 1.5, c_1 = 0.7, c_2 = 0.5, A = 0, a = 1.2, m = 0.01\}$.

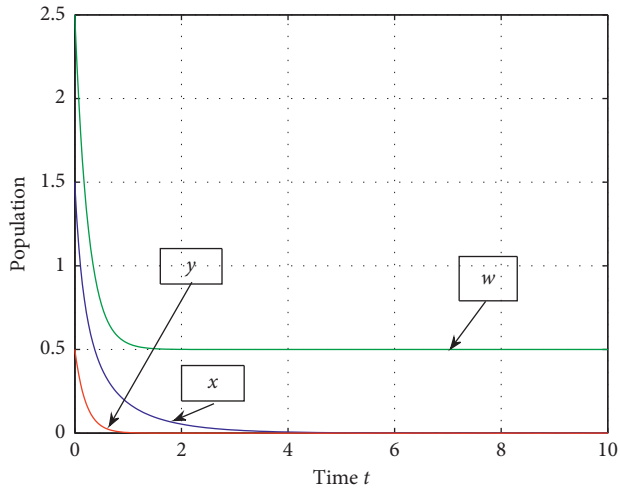

FIGURE 2: Stable behaviour of $E_1(0, 0.5, 0)$ with respect to time t taking the parameters as $\{r = 5.5, d_1 = 6.5, d_2 = 4, k = 0.2, d_3 = 5, a_1 = 2, a_2 = 0.3, a_3 = 0.25, b_1 = 1.5, c_1 = 0.7, c_2 = 0.5, A = 2, a = 1.2, m = 0.01\}$.

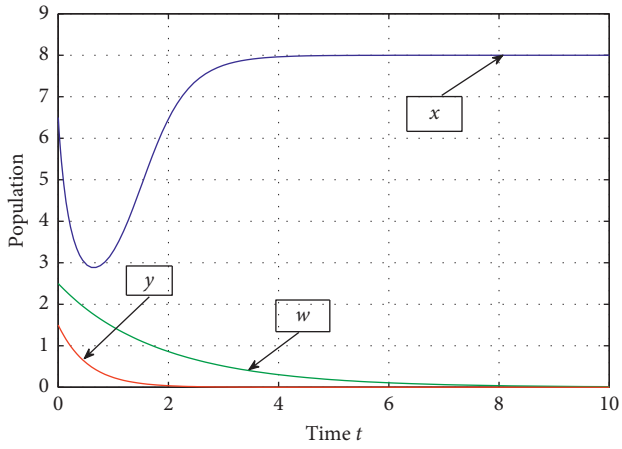

FIGURE 3: Stable nature of $E_2(8, 0, 0)$ with respect to time t regarding the parameters as $\{r = 5.5, d_1 = 1.5, d_2 = 0.52, k = 1.9, d_3 = 2, a_1 = 0.5, a_2 = 0.3, a_3 = 0.25, b_1 = 1.5, c_1 = 0.7, c_2 = 0.5, A = 0, a = 1.2, m = 0.01\}$.

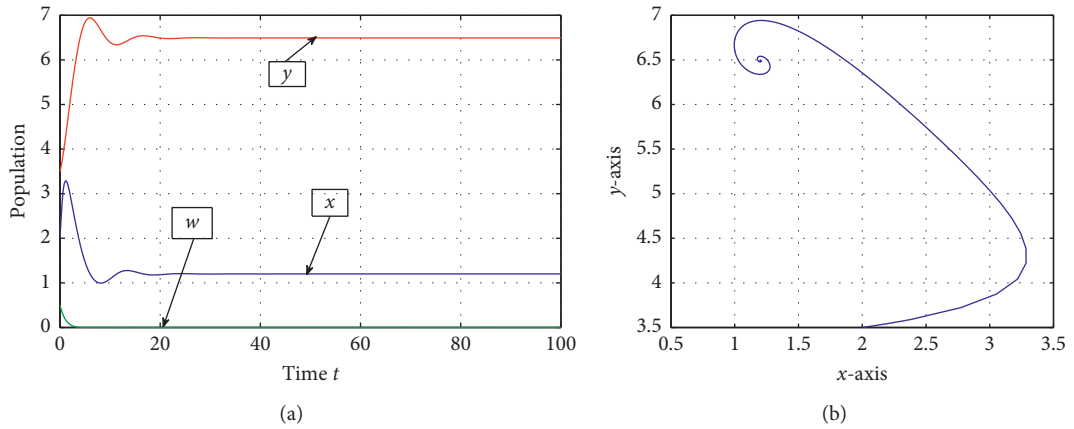

FIGURE 4: (a) Stable nature of $E_3(1.20053, 0, 6.49267)$ with t and (b) stable phase portrait of $E_3(1.20053, 0, 6.49267)$ when $k = 0.2 > k^*$ (threshold value) = 0.019 and other are taken as $\{r = 5.5,\ d_1 = 0.4,\ d_2 = 0.3,\ d_3 = 0.2,\ a_1 = 0.6,\ a_2 = 0.98,\ a_3 = 0.8,\ b_1 = 2.5,\ c_1 = 0.85,\ c_2 = 0.7,\ A = 0,\ a = 1.1,\ m = 0.4\}$.

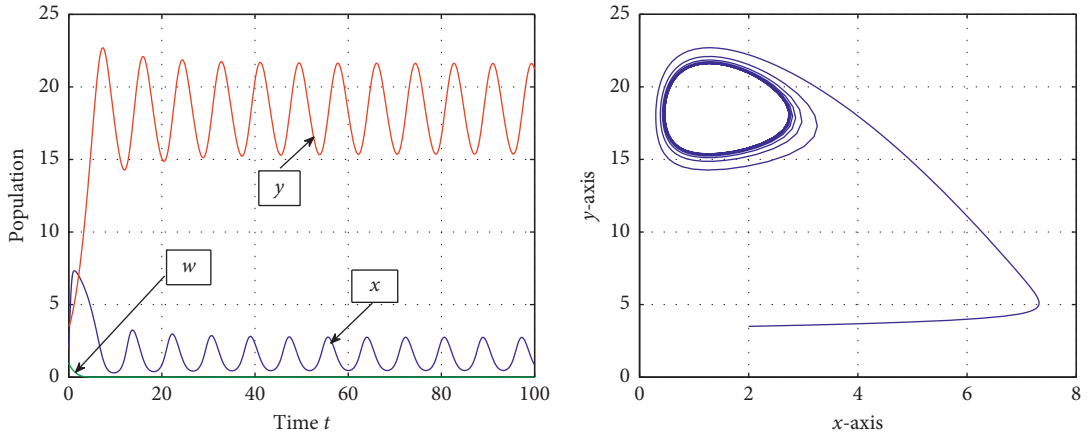

FIGURE 5: (a) Oscillatory behaviour of E_3 with time t and (b) phase diagram (isolated closed orbit) when $k = 0.01 < k^* = 0.019$ and all other parameters are fixed as in Figure 4.

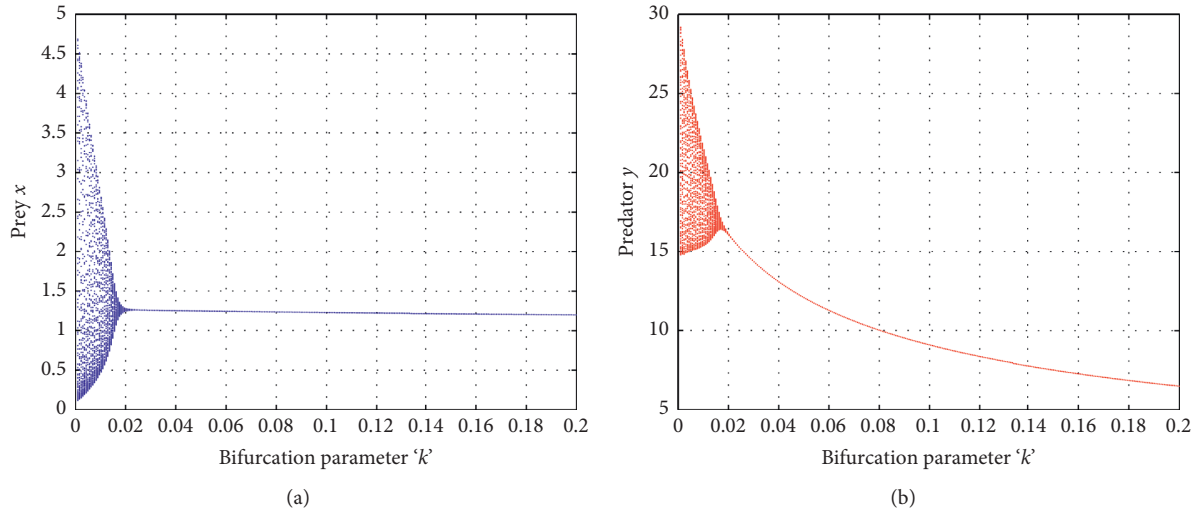

FIGURE 6: Bifurcation diagrams for the Hopf bifurcation around $E_3(1.20053, 0, 6.49267)$ regarding k as bifurcation parameter and others are the same as in Figure 4. (a) Bifurcation diagram of x. (b) Bifurcation diagram of y.

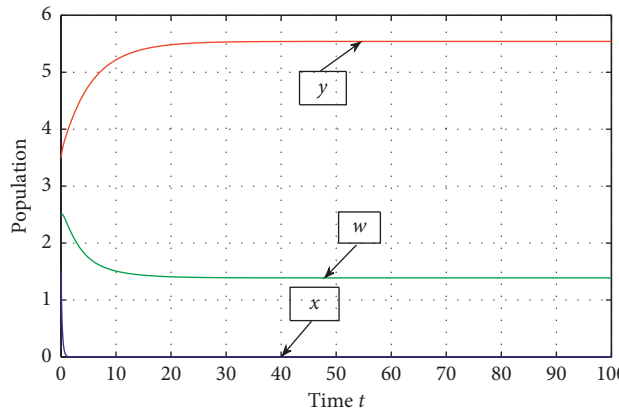

FIGURE 7: Stability nature of $E_4(0, 1.3889, 5.5417)$ with time t regarding the parameters as $\{r = 5.5, d_1 = 6.5, d_2 = 0.3, k = 0.2, d_3 = 0.2, a_1 = 0.6, a_2 = 0.98, a_3 = 0.8, b_1 = 2.5, c_1 = 0.85, c_2 = 0.7, A = 2, a = 1.1, m = 0.01\}$.

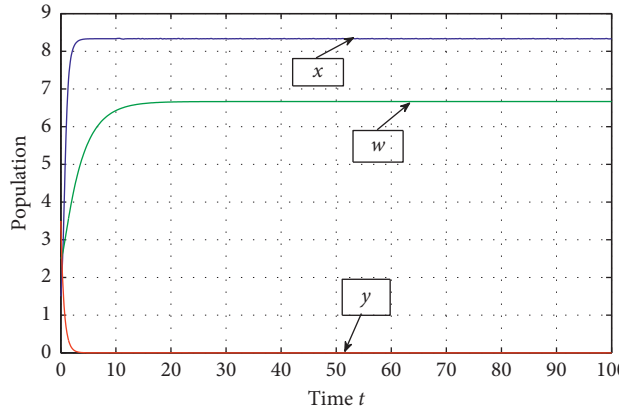

FIGURE 8: Stability nature of $E_5(8.3333, 6.6667, 0)$ with time t regarding the parameters as $\{r = 5.5, d_1 = 0.5, d_2 = 0.3, k = 0.2, d_3 = 2.2, a_1 = 0.6, a_2 = 0.98, a_3 = 0.8, b_1 = 2.5, c_1 = 0.85, c_2 = 0.7, A = 2, a = 1.1, m = 0.01\}$.

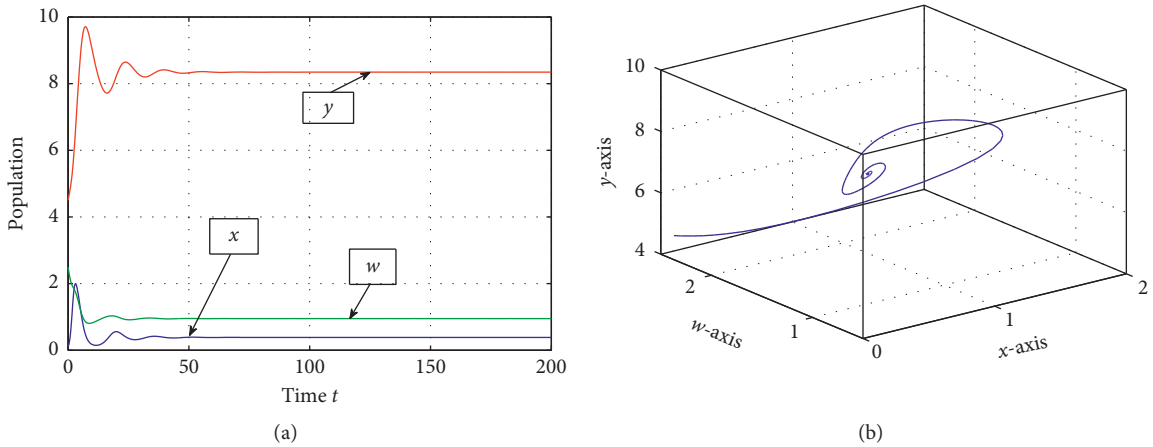

FIGURE 9: (a) Stable nature of E^* $(0.385717, 0.950363, 8.34509)$ with time t and (b) stable phase diagram of E^* $(0.385717, 0.950363, 8.34509)$ when $k = 0.2 > k^{[H]} = 0.025$ and others are chosen as $\{r = 5.5, d_1 = 0.4, d_2 = 0.3, d_3 = 0.2, a_1 = 0.6, a_2 = 0.98, a_3 = 0.8, b_1 = 2.5, c_1 = 0.85, c_2 = 0.7, A = 2, a = 1.1, m = 0.4\}$.

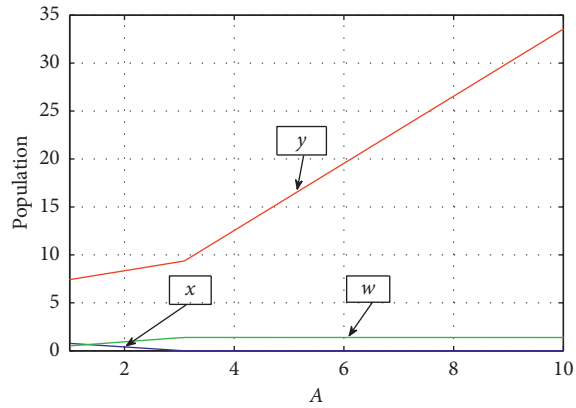

Figure 10: Nature of steady state E^* when subsidy input rate A varies from 1 to 10 and other parameters are fixed as in Figure 9.

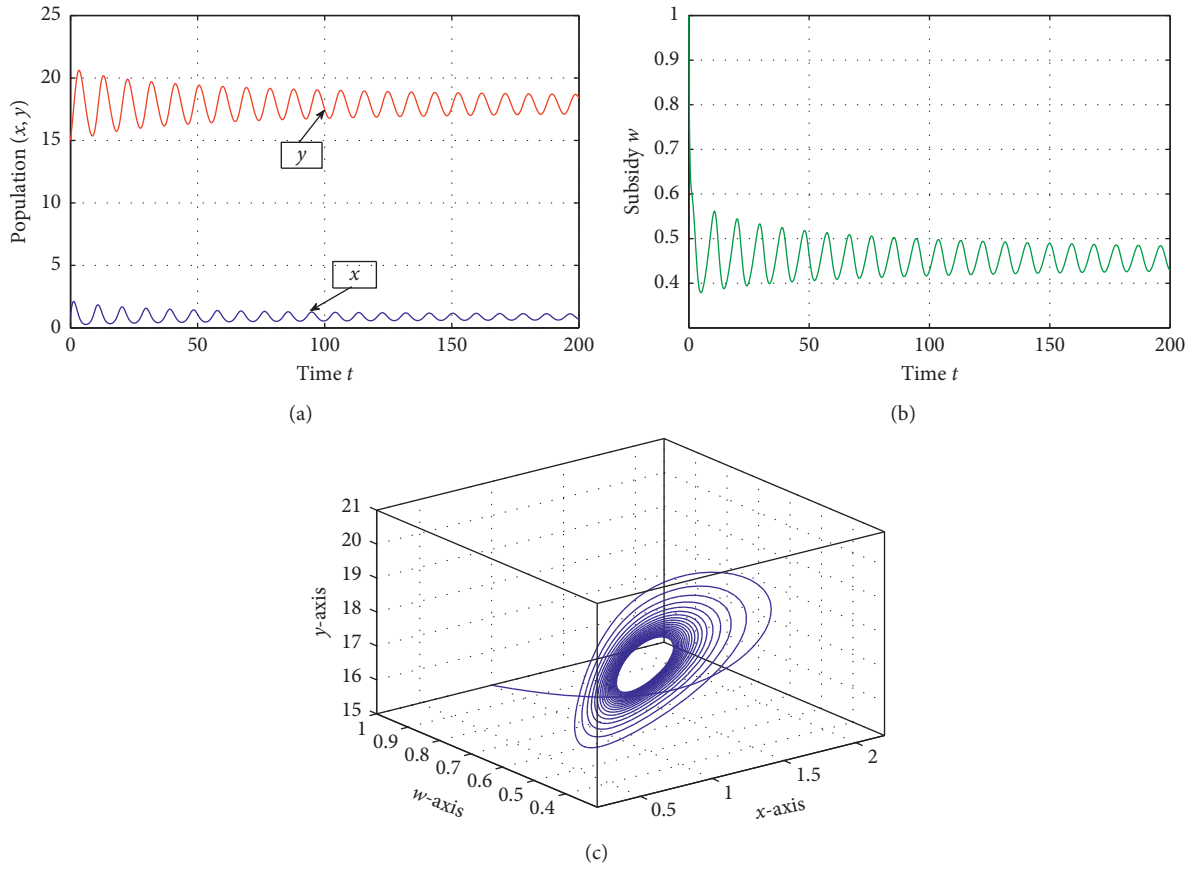

Figure 11: (a), (b) Oscillatory behaviour of E^* with time and (c) isolated closed orbit around E^* when $k = 0.02 < k^{[H]} = 0.025$ and all others are fixed as in Figure 9.

$$\begin{aligned} K'' &= \{-3\sigma_+ + R_2 + S_1 \ \cos(\sqrt{\sigma_+}\,\tau^*) - S_2\tau^*\cos(\sqrt{\sigma_+}\,\tau^*) - S_1\sqrt{\sigma_+}\,\tau^*\sin(\sqrt{\sigma_+}\,\tau^*)\}, \\ L'' &= \{-2R_1\sqrt{\sigma_+} + S_1\sin(\sqrt{\sigma_+}\,\tau^*) - S_2\tau^*\sin(\sqrt{\sigma_+}\,\tau^*) + S_1\sqrt{\sigma_+}\,\tau^*\cos(\sqrt{\sigma_+}\,\tau^*)\}, \\ M'' &= \{S_2\sqrt{\sigma_+}\sin(\sqrt{\sigma_+}\,\tau^*) - S_1\sigma_+\cos(\sqrt{\sigma_+}\,\tau^*)\}, \\ N'' &= \{S_2\sqrt{\sigma_+}\cos(\sqrt{\sigma_+}\,\tau^*) + S_1\sigma_+\sin(\sqrt{\sigma_+}\,\tau^*)\}. \end{aligned} \tag{93}$$

Proof. Proof is similar to that in Theorem 18. □

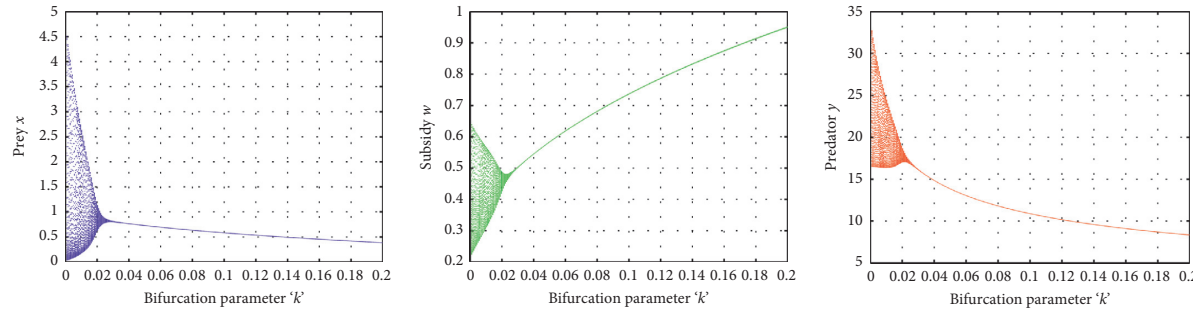

FIGURE 12: Bifurcation diagrams for the Hopf bifurcation around E^* (0.385717, 0.950363, 8.34509) regarding k as bifurcation parameter and others are the same as in Figure 9. (a) Bifurcation diagram of x. (b) Bifurcation diagram of w. (c) Bifurcation diagram of y.

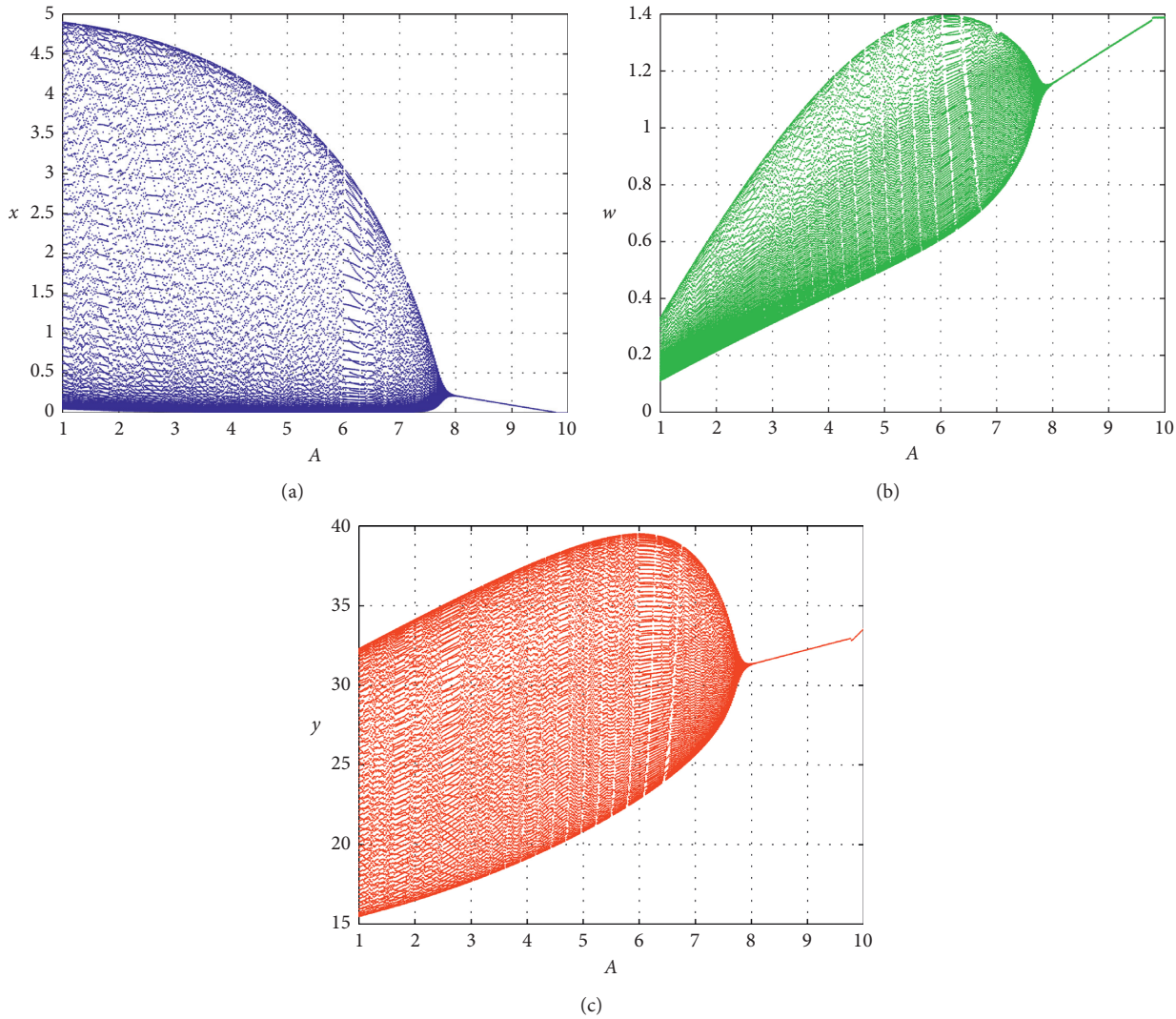

FIGURE 13: Bifurcation diagram with respect to subsidy input rate A when $k = 0$ and the remaining parameters are fixed as in Figure 9. (a) Bifurcation diagram of x. (b) Bifurcation diagram of w. (c) Bifurcation diagram of y.

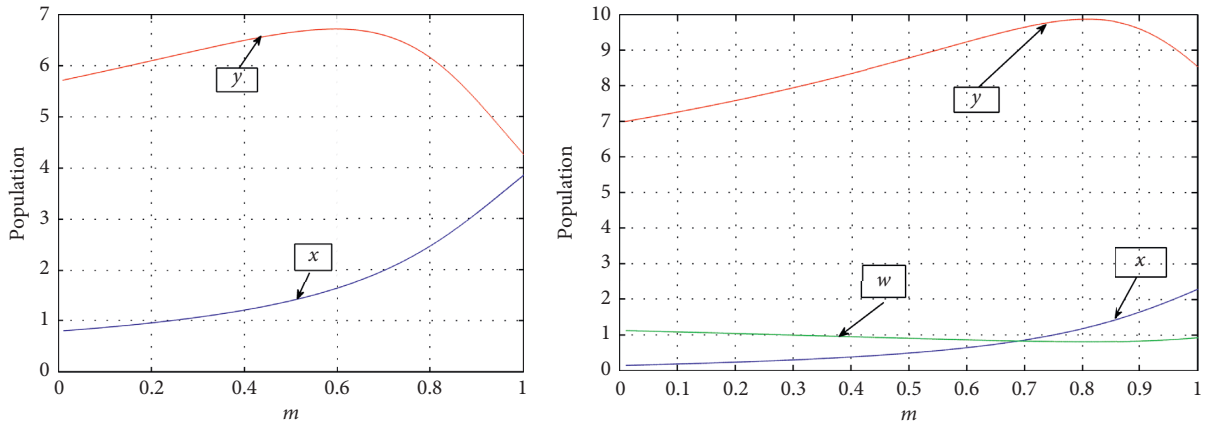

FIGURE 14: Impact of m on the nature of steady states E_3 and E^* when other parameters are fixed as in Figure 9. (a) Nature of steady state E_3 ($A = 0$). (b) Nature of steady state E^* ($A \neq 0$).

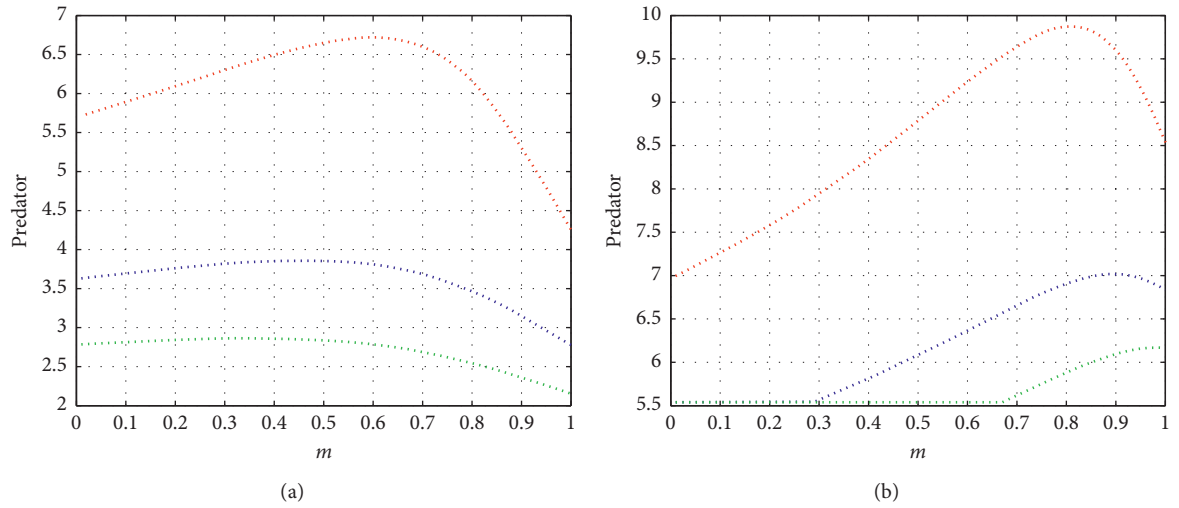

FIGURE 15: Impact of m on the predator's growth for different values of k when others are fixed as in Figure 9. ((i) red color: $k = 0.2$, (ii) blue color: $k = 0.5$, and (iii) green color: $k = 0.8$). (a) Nature at E_3 ($A = 0$). (b) Nature at E^* ($A \neq 0$).

Theorem 20. *Suppose interior (coexistence) equilibrium point E^* exists and is locally asymptotically stable for system (2) when $\tau = 0$. Let equation (91) have exactly two positive roots $\sigma_i, i = 1, 2\,(\sigma_1 > \sigma_2)$ when $R_3^2 > S_2^2$ and $R_2^2 - 2R_1R_3 - S_1^2 < 0$ irrespective of sign of $R_1^2 - 2R_2$. Moreover, let*

$$\tau_j^i = \frac{\cos^{-1}\left(\left(S_2\left(R_1\sigma_i - R_3\right) + S_1\left(\sigma_i^2 - R_2\sigma_i\right)\right)/\left(S_2^2 + S_1^2\sigma_i\right)\right)}{\sqrt{\sigma_i}} + \frac{2\pi j}{\sqrt{\sigma_i}}, \quad i = 1, 2;\ j = 0, 1, 2, 3\ldots,$$
$$\tau_k^+ = \min\left\{\tau_k^i : i = 1, 2\right\}, \tau_k^- = \max\left\{\tau_k^i : i = 1, 2\right\}, \quad k = 0, 1, 2, 3\ldots, \tag{94}$$

then there is a positive integer k such that

$$0 < \tau_0^+ < \tau_0^- < \tau_1^+ < \tau_1^- < \tau_2^+ < \cdots < \tau_{k-1}^- < \tau_k^+, \tag{95}$$

and there are k switches from stability to instability to stability; that is, when

$$\tau \in \left[0, \tau_0^+\right), \left(\tau_0^-, \tau_1^+\right), \left(\tau_1^-, \tau_2^+\right), \ldots, \left(\tau_{k-1}^-, \tau_k^+\right), \tag{96}$$

then E^* is locally asymptotically stable and when

$$\tau \in \left(\tau_0^+, \tau_0^-\right), \left(\tau_1^+, \tau_1^-\right), \left(\tau_2^+, \tau_2^-\right), \ldots, \left(\tau_{k-1}^+, \tau_{k-1}^-\right), \tau > \tau_k^+, \tag{97}$$

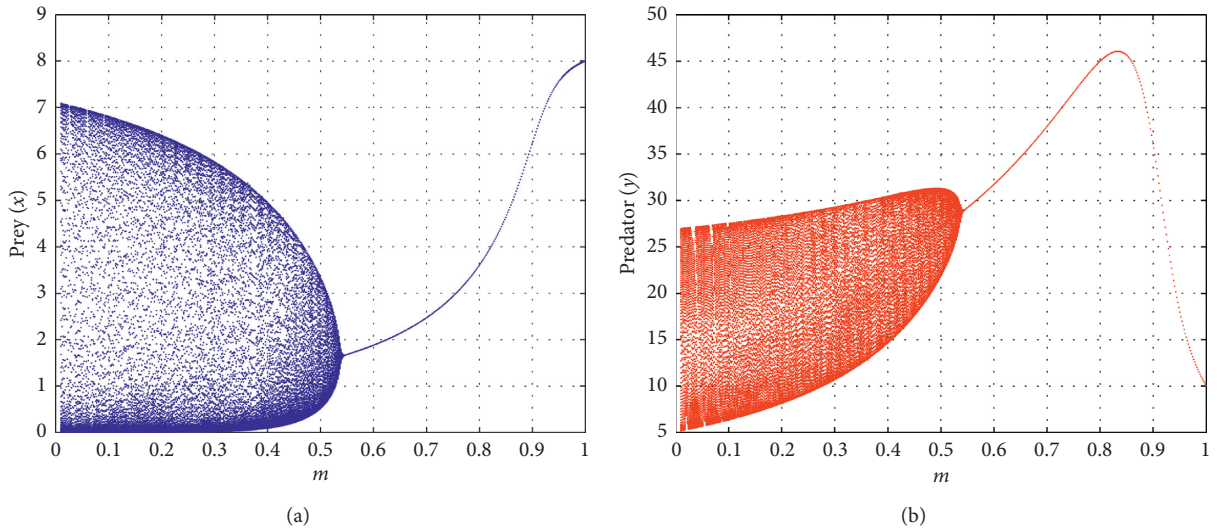

FIGURE 16: Bifurcation diagram around E_3 with respect to coefficient of refuge parameter m when $k = 0$ and the remaining parameters are fixed as in Figure 4. (a) Bifurcation diagram of x. (b) Bifurcation diagram of y.

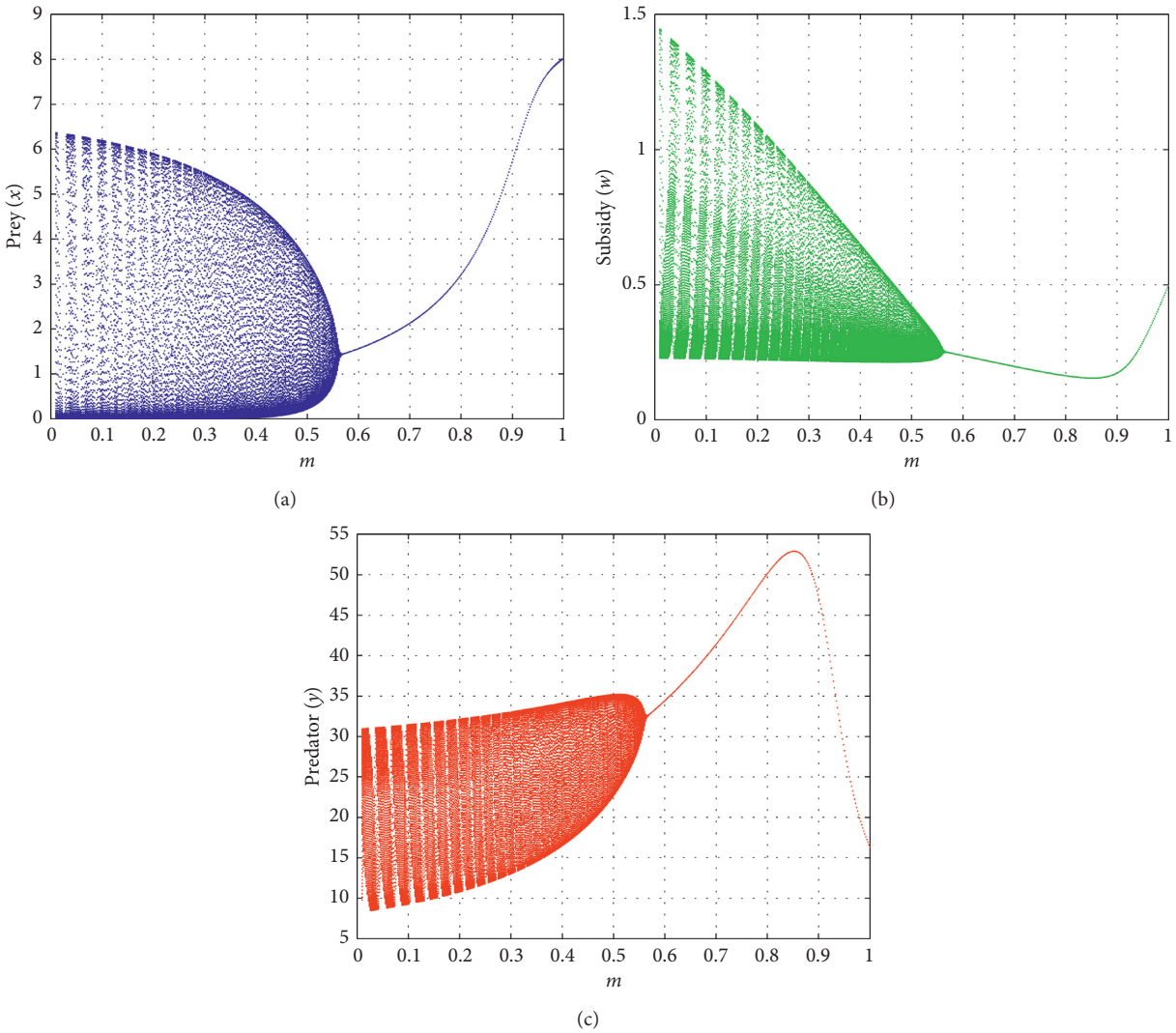

FIGURE 17: Bifurcation diagram around E^* when $k = 0$ and the remaining parameters are fixed as in Figure 9. (a) Bifurcation diagram of x. (b) Bifurcation diagram of w. (c) Bifurcation diagram of y.

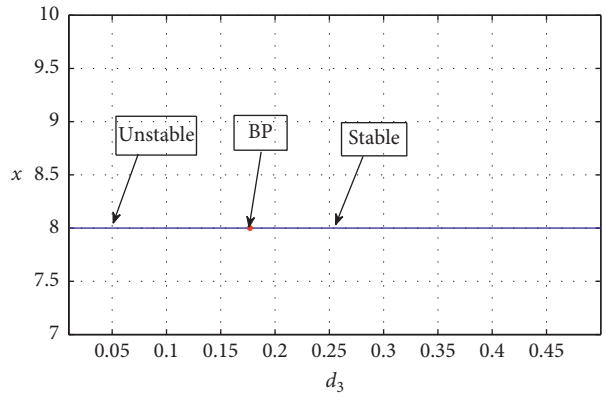

FIGURE 18: Transcritical bifurcation diagram around $E_2(8.0, 0, 0)$ considering d_3 as bifurcation parameter and others parameters are the same as in Figure 3. Here $d_3^{[TC]} = 0.1768$.

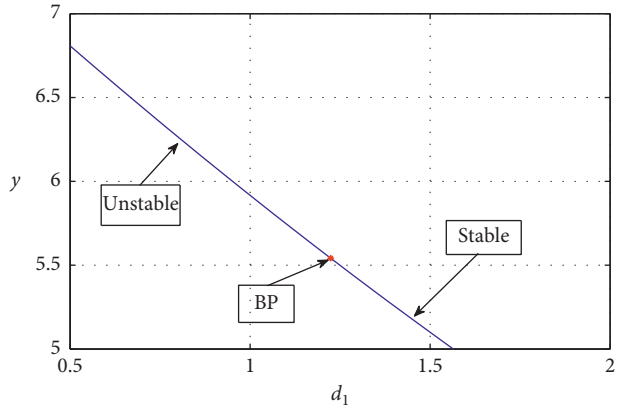

FIGURE 19: Bifurcation diagram for the transcritical bifurcation around $E_4(0, 1.9889, 5.5417)$ considering d_1 as the independent variable and others parameters are the same as in Figure 7. Here, $d_1^{[TC]} = 1.2238$.

then E^* is unstable. Further, at $\tau = \tau_k^{\pm}, k = 0, 1, 2, \ldots$, system (60) experiences Hopf bifurcation provided

$$\begin{aligned} P_k^+ R_k^+ - Q_k^+ S_k^+ &\neq 0, \quad \text{for } k = 0, 1, 2, \ldots, \\ P_k^- R_k^- - Q_k^- S_k^- &\neq 0, \quad \text{for } k = 0, 1, 2, \ldots, \end{aligned} \tag{98}$$

where

$$\begin{aligned} P_k^+ &= \left\{-3\sigma_1 + R_2 + S_1 \cos\left(\sqrt{\sigma_1}\,\tau_k^+\right) - S_2\tau_k^+\cos\left(\sqrt{\sigma_1}\,\tau_k^+\right) - S_1\sqrt{\sigma_1}\,\tau_k^+\sin\left(\sqrt{\sigma_1}\,\tau_k^+\right)\right\}_{k=0,1,2,\ldots}, \\ P_k^- &= \left\{-3\sigma_2 + R_2 + S_1\cos\left(\sqrt{\sigma_2}\,\tau_k^-\right) - S_2\tau_k^-\cos\left(\sqrt{\sigma_2}\,\tau_k^-\right) - S_1\sqrt{\sigma_2}\,\tau_k^-\sin\left(\sqrt{\sigma_2}\,\tau_k^-\right)\right\}_{k=0,1,2,\ldots}, \\ Q_k^+ &= \left\{-2R_1\sqrt{\sigma_1} + S_1\sin\left(\sqrt{\sigma_1}\,\tau_k^+\right) - S_2\tau_k^+\sin\left(\sqrt{\sigma_1}\,\tau_k^+\right) + S_1\sqrt{\sigma_1}\,\tau_k^+\cos\left(\sqrt{\sigma_1}\,\tau_k^+\right)\right\}_{k=0,1,2,\ldots}, \\ Q_k^- &= \left\{-2R_1\sqrt{\sigma_2} + S_1\sin\left(\sqrt{\sigma_2}\,\tau_k^-\right) - S_2\tau_k^-\sin\left(\sqrt{\sigma_2}\,\tau_k^-\right) + S_1\sqrt{\sigma_2}\,\tau_k^-\cos\left(\sqrt{\sigma_2}\,\tau_k^-\right)\right\}_{k=0,1,2,\ldots}, \\ R_k^+ &= \left\{S_2\sqrt{\sigma_1}\sin\left(\sqrt{\sigma_1}\,\tau_k^+\right) - S_1\sigma_1\cos\left(\sqrt{\sigma_1}\,\tau_k^+\right)\right\}_{k=0,1,2,\ldots}, \\ R_k^- &= \left\{S_2\sqrt{\sigma_2}\sin\left(\sqrt{\sigma_2}\,\tau_k^-\right) - S_1\sigma_2\cos\left(\sqrt{\sigma_2}\,\tau_k^-\right)\right\}_{k=0,1,2,\ldots}, \\ S_k^+ &= \left\{S_2\sqrt{\sigma_1}\cos\left(\sqrt{\sigma_1}\,\tau_k^+\right) + S_1\sigma_1\sin\left(\sqrt{\sigma_1}\,\tau_k^+\right)\right\}_{k=0,1,2,\ldots}, \\ S_k^- &= \left\{S_2\sqrt{\sigma_2}\cos\left(\sqrt{\sigma_2}\,\tau_k^-\right) + S_1\sigma_2\sin\left(\sqrt{\sigma_2}\,\tau_k^-\right)\right\}_{k=0,1,2,\ldots}. \end{aligned} \tag{99}$$

Proof. Proof is similar to that in Theorem 18. □

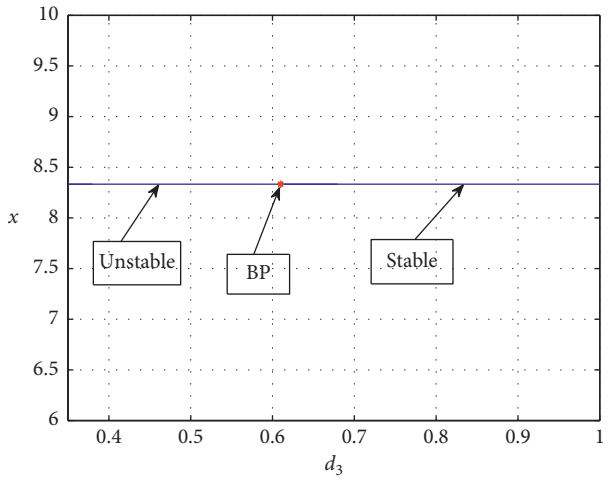

FIGURE 20: Transcritical bifurcation diagram around E_5 (8.3333, 6.6667, 0) considering d_3 as independent variable and others are the same as in Figure 8. Here, $d_3^{[TC]} = 0.61$.

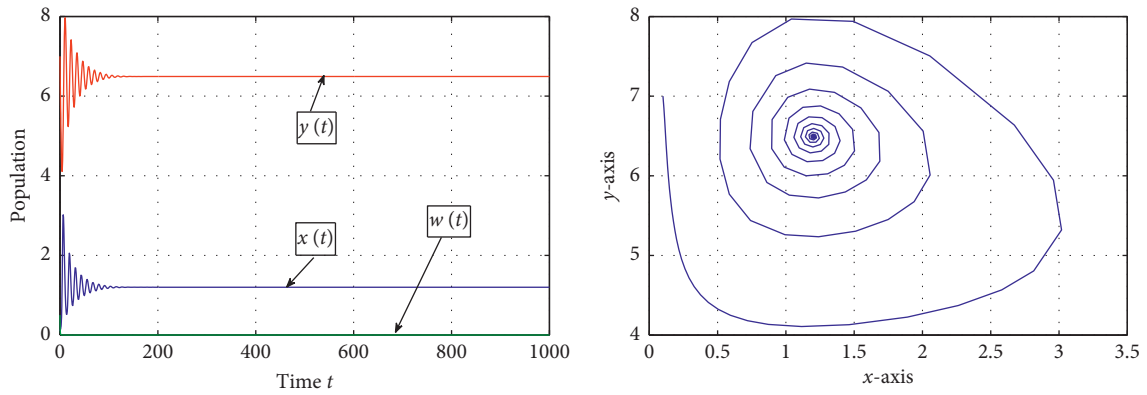

FIGURE 21: (a) Stable nature with time and (b) stable spiral of E_3 (1.20053, 0, 6.49267) when $\tau = 2 < \tau'^* = 2.9272$ corresponding to the data set of Figure 4.

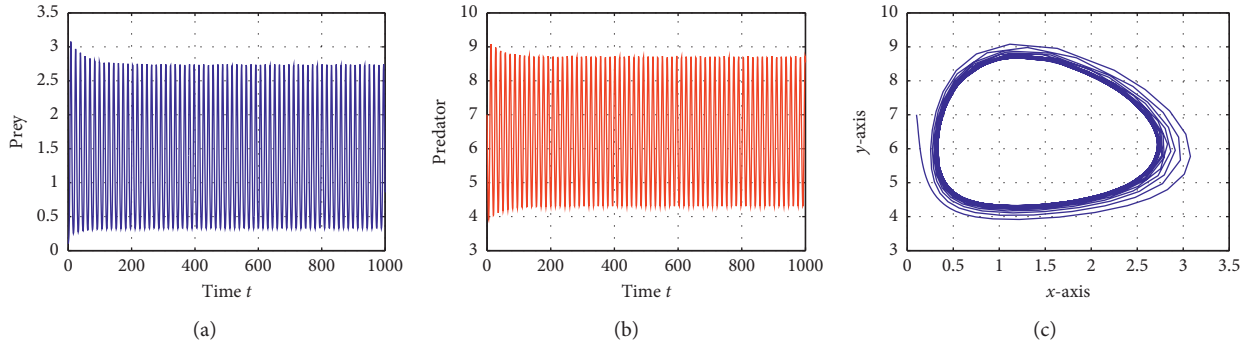

FIGURE 22: (a, b) Oscillatory nature of x, y, respectively, and (c) stable limit cycle around E_3 (1.20053, 0, 6.49267) when $\tau = 3.5 > \tau'^* = 2.9272$ corresponding to the data set of Figure 4. (a) Time series of prey. (b) Time series of predator. (c) Phase diagram.

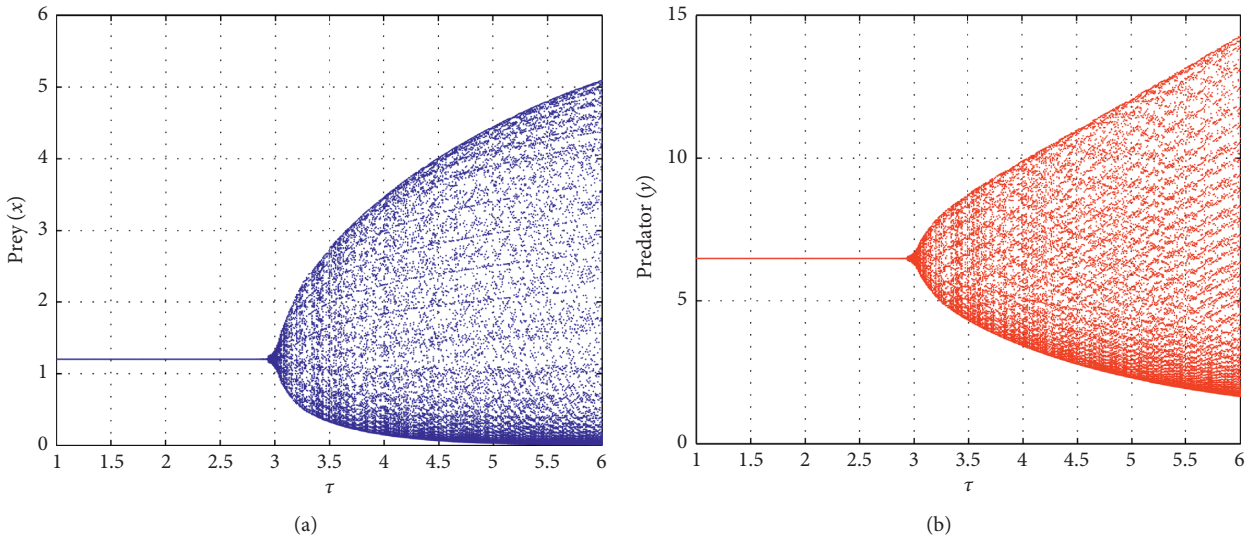

FIGURE 23: Supercritical Hopf bifurcation diagram around $E_3(1.20053, 0, 6.49267)$ considering τ as bifurcation parameter and other parameters are chosen from the data set of Figure 4. (a) Bifurcation diagram of prey. (b) Bifurcation diagram of predator.

6. Numerical Computations

Here, we have illustrated numerical simulations to verify the analytical findings of the proposed system (2). We select a parameter set: $\{r = 5.5,\ d_1 = 6.5,\ d_2 = 4,\ k = 0.2,\ d_3 = 5,\ a_1 = 2, a_2 = 0.3, a_3 = 0.25, b_1 = 1.5, c_1 = 0.7, c_2 = 0.5, A = 0,\ a = 1.2,\ m = 0.01\}$. Under this set of parametric values, the stable nature of $E_0(0, 0, 0)$ is shown in Figure 1. If we take subsidy input rate $A = 2$ and other parametric values are chosen from the data set of Figure 1, then the subsidy only equilibrium $E_1(0, (A/d_2), 0) \equiv E_1(0, 0.5, 0)$ exists and stable nature of $E_1(0, 0.5, 0)$ with time t is depicted in Figure 2. Now, we choose another parameter set: $\{r = 5.5,\ d_1 = 1.5,\ d_2 = 0.52,\ k = 1.9,\ d_3 = 2,\ a_1 = 0.5,\ a_2 = 0.3,\ a_3 = 0.25,\ b_1 = 1.5, c_1 = 0.7, c_2 = 0.5, A = 0, a = 1.2, m = 0.01\}$. Under this set of parametric values, the prey only equilibrium $E_2((r - d_1)/a_1, 0, 0) \equiv E_2(8, 0, 0)$ exists and stable behaviour of $E_2(8, 0, 0)$ is presented in Figure 3. Let us choose the parameters as follows:

$$\{r = 5.5, d_1 = 0.4, d_2 = 0.3, k = 0.2, d_3 = 0.2, a_1 = 0.6, a_2 = 0.98, a_3 = 0.8, b_1 = 2.5, c_1 = 0.85, c_2 = 0.7, a = 1.1, m = 0.4\}. \tag{100}$$

If we take subsidy input rate $A = 0$ and other parameters are taken from set (100), then subsidy-free equilibrium point $E_3(\overline{x}, 0, \overline{y}) \equiv E_3(1.20053, 0, 6.49267)$ exists and is locally asymptotically stable. Stable time series and stable phase diagram are represented in Figure 4. In the same manner, if we change the value of the parameter $k\,(= 0.01)$ and others are the same as in the data set of Figure 4, then it is observed that $E_3(1.20053, 0, 6.49267)$ is unstable accompanied with a limit cycle (see Figure 5). From Figures 4 and 5, it can be easily noted that there must exist a threshold value of k, say $k^* = 0.019$ for which unstable behaviour of E_3 changes to stable spiral. Since the vector fields for $k < k^*$ and $k > k^*$ are qualitatively different, a Hopf bifurcation is created around E_3 taking k as bifurcation parameter (see Figure 6). For the set of parameter values $\{r = 5.5,\ d_1 = 6.5,\ d_2 = 0.3,\ k = 0.2,\ d_3 = 0.2,\ a_1 = 0.6,\ a_2 = 0.98,\ a_3 = 0.8,\ b_1 = 2.5,\ c_1 = 0.85,\ c_2 = 0.7,\ A = 2,\ a = 1.1,\ m = 0.01\}$, prey free equilibrium point $E_4(0, \widehat{w}, \widehat{y}) \equiv E_4(0, 1.3889, 5.5417)$ exists and is stable (see Figure 7). Next, let us take a different set of parameters of system (2): $\{r = 5.5,\ d_1 = 0.5,\ d_2 = 0.3,\ k = 0.2,\ d_3 = 2.2,\ a_1 = 0.6,\ a_2 = 0.98,\ a_3 = 0.8,\ b_1 = 2.5,\ c_1 = 0.85,\ c_2 = 0.7,\ A = 2,\ a = 1.1,\ m = 0.01\}$. Then, predator free equilibrium point $E_5((r - d_1)/a_1, (A/d_2), 0) \equiv E_5(8.3333, 6.6667, 0)$ is locally asymptotically stable. The stable behaviour with time t is shown in Figure 8.

If we take subsidy input rate $A = 2$ and others are fixed as in the data set of Figure 4, then $E^*(x^*, w^*, y^*) \equiv E^*(0.385717, 0.950363, 8.34509)$ exists and is locally asymptotically stable. Figure 9 depicts the stable behaviour of E^*. Comparing Figures 4 and 9, it is observed that subsidy input rate A enhances the value of y component of E^* and decreases the value of x component of E^*. Also, from Figure 10, it is noticed that the prey population is leading towards extinction and the predator population has enormous growth (due to huge supply of food source) at high subsidy input rate (when $A \in (2, 10]$) in the presence of fear felt by prey population. So, it can be concluded that it is not possible to control prey population from extinction in presence of nonlinear prey refuge because they cannot get enough time to protect themselves from

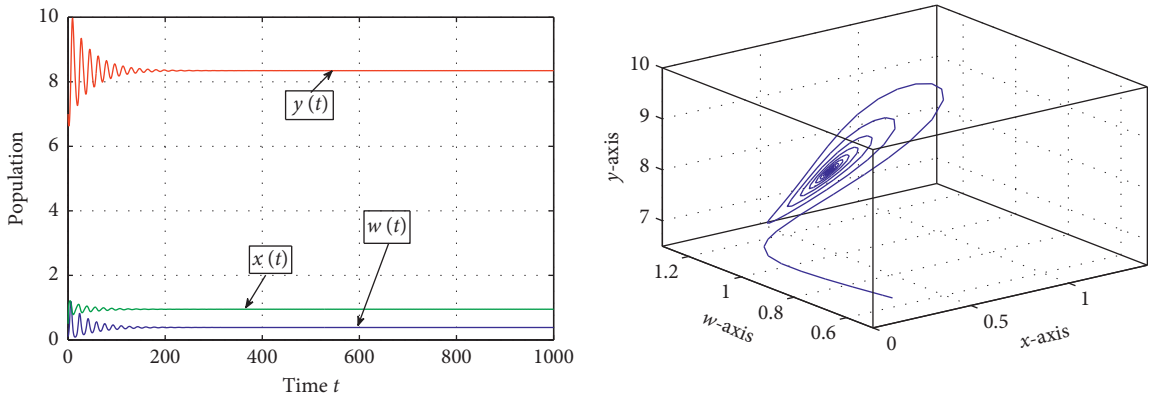

FIGURE 24: (a) Stable behaviour with time and (b) stable trajectory of E^* (0.385717, 0.950363, 8.34509) when $\tau = 2.5 \in [0, \tau_0^+ = 4.0652)$ corresponding to the data set of Figure 9.

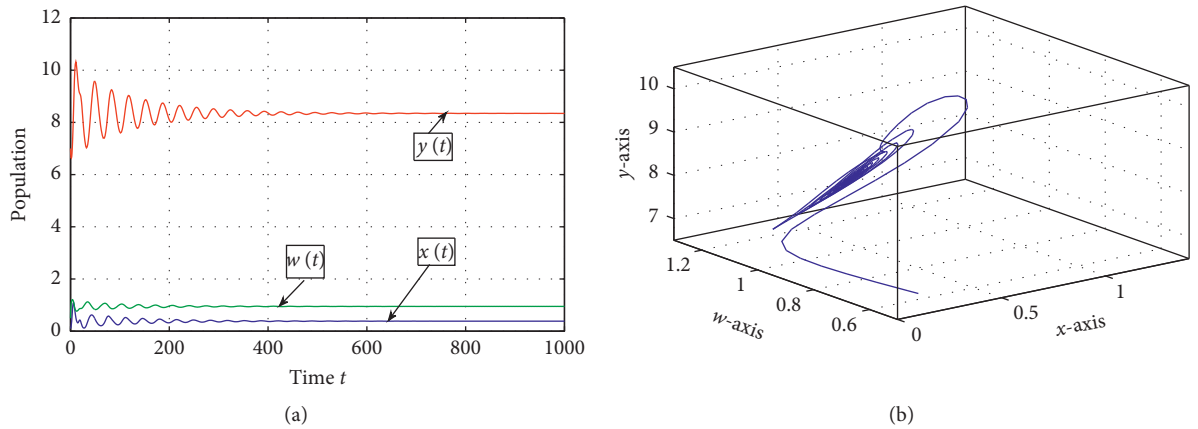

FIGURE 25: (a) Stable nature with time and (b) stable phase portrait of E^* (0.385717, 0.950363, 8.34509) when $\tau = 14.5 \in (\tau_0^- = 10.3836, \tau_1^+ = 22.7845)$ corresponding to the data set of Figure 9.

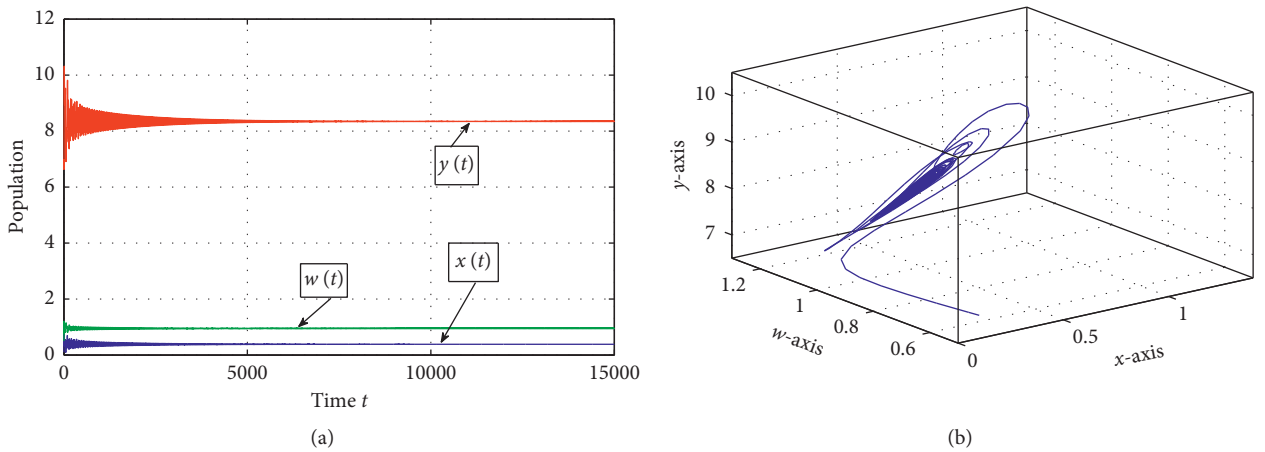

FIGURE 26: (a) Stable behaviour with time and (b) stable trajectory of E^* (0.385717, 0.950363, 8.34509) when $\tau = 39 \in (\tau_1^- = 37.7710, \tau_2^+ = 41.5037)$ corresponding to the data set of Figure 9.

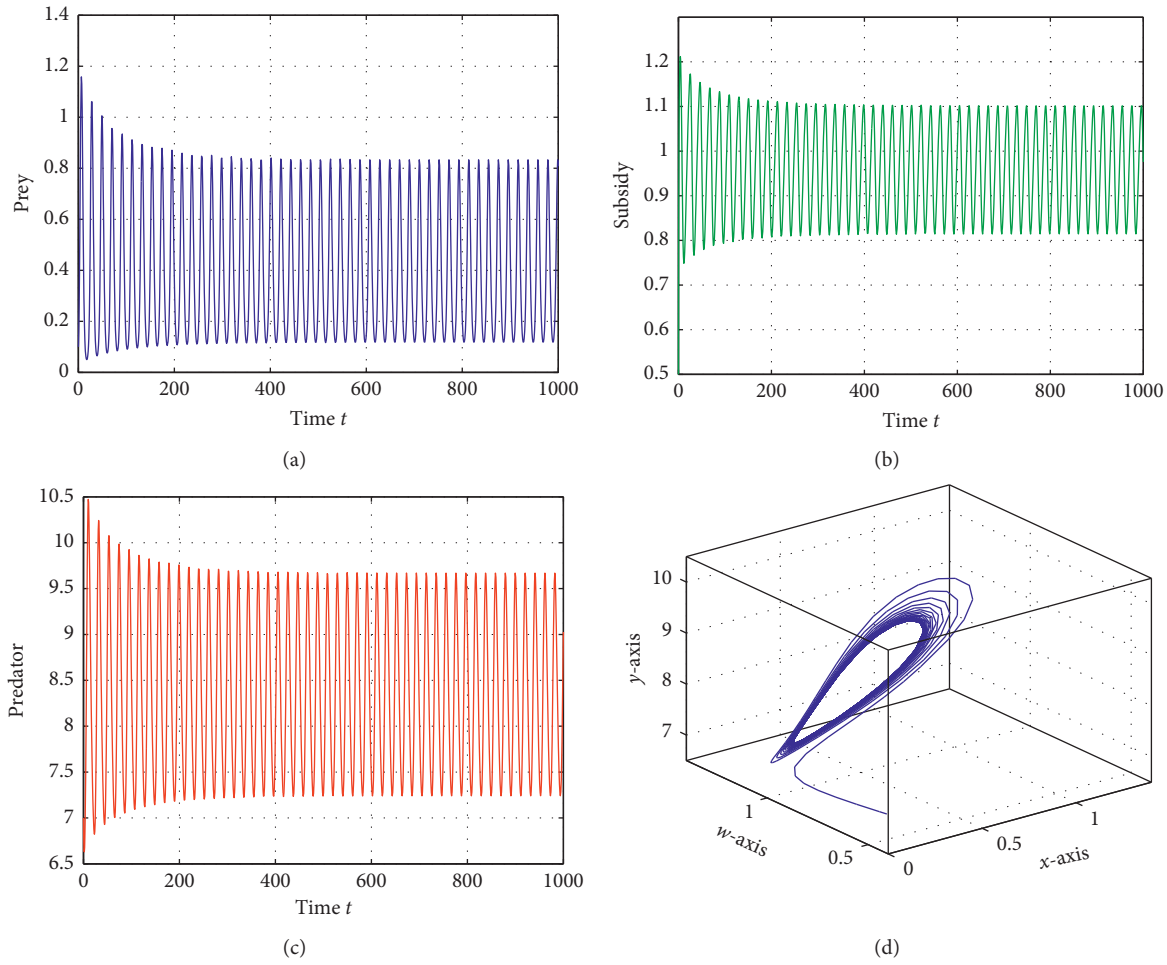

FIGURE 27: (a, b, c) Oscillatory nature of prey, subsidy, and predator, respectively, with time and (d) stable limit cycle around E^* (0.385717, 0.950363, 8.34509) when $\tau = 5 \in (\tau_0^+ = 4.0652, \tau_0^- = 10.3836)$ corresponding to the data set of Figure 9. (a) Oscillation of prey. (b). Oscillation of subsidy. (c) Oscillation of predator. (d) Phase portrait (closed orbit).

predation risk. After extinction of prey species, predator can easily survive with the help of resource subsidy. Thus, the parameter A has great importance in the proposed population dynamics.

Moreover, Figure 11 represents the unstable nature of E^* when $k = 0.02$ and other parametric values are the same as in Figure 9. So, the parameter k has an interesting nature because there exists a threshold value $k^{[H]} = 0.025$ of k for which unstable nature (limit cycle) of E^* switches to stable behaviour (stable spiral) when k passes through its critical value $k^{[H]}$; i.e., the vector fields for $k > k^{[H]}$ and $k < k^{[H]}$ are topologically different. Hence, a Hopf bifurcation occurs around E^* and Figure 12 depicts the corresponding bifurcation diagram taking k as bifurcation parameter. Also, it has to be noted from Figure 13 that, in the absence of fear effect, the oscillatory behaviour of E^* changes to stable nature when subsidy input rate A crosses its critical value $A^* = 7.9$ (approximately) and since predator population has huge growth rate at very large value of subsidy input rate A, the prey population cannot persist in ecosystem in presence nonlinear prey refuge. This phenomenon is very interesting because the prey refuge cannot control the prey population from extinction due to enormous growth of predator when subsidy input rate is very high. In this manner, system (2) is not persistent.

Further, Figure 14 depicts that the nature of steady states E_3 and E^* when $m \in (0, 1)$. Here, the predator population cannot go extinct for large value of coefficient of prey refuge parameter. Also, Figure 15 shows the changes of predator's growth at the steady states E_3 and E^* for three different fear levels k when m varies from 0 to 1. Here, also the predator can persist for large m. From here, it may be concluded that system (2) is always persistent for small subsidy input rate in the presence of nonlinear prey refuge function. Again, Figures 16 and 17, respectively, show that, in the absence of fear effect ($k = 0$), the equilibria E_3 and E^* are approaching towards stable state by excluding the existence of oscillatory behaviour taking m as the bifurcating parameter. In this manner, predator population also survives in ecosystem for large coefficient of prey refuge parameter m.

A "transcritical bifurcation" (BP) occurs at $d_1^{[TC]} = 5.5$ around E_1. At this point, exactly one eigenvalue of the Jacobian matrix is zero and others have negative real parts. Bifurcation diagram 32 depicts that when $d_1 < d_1^{[TC]}$, then E_1

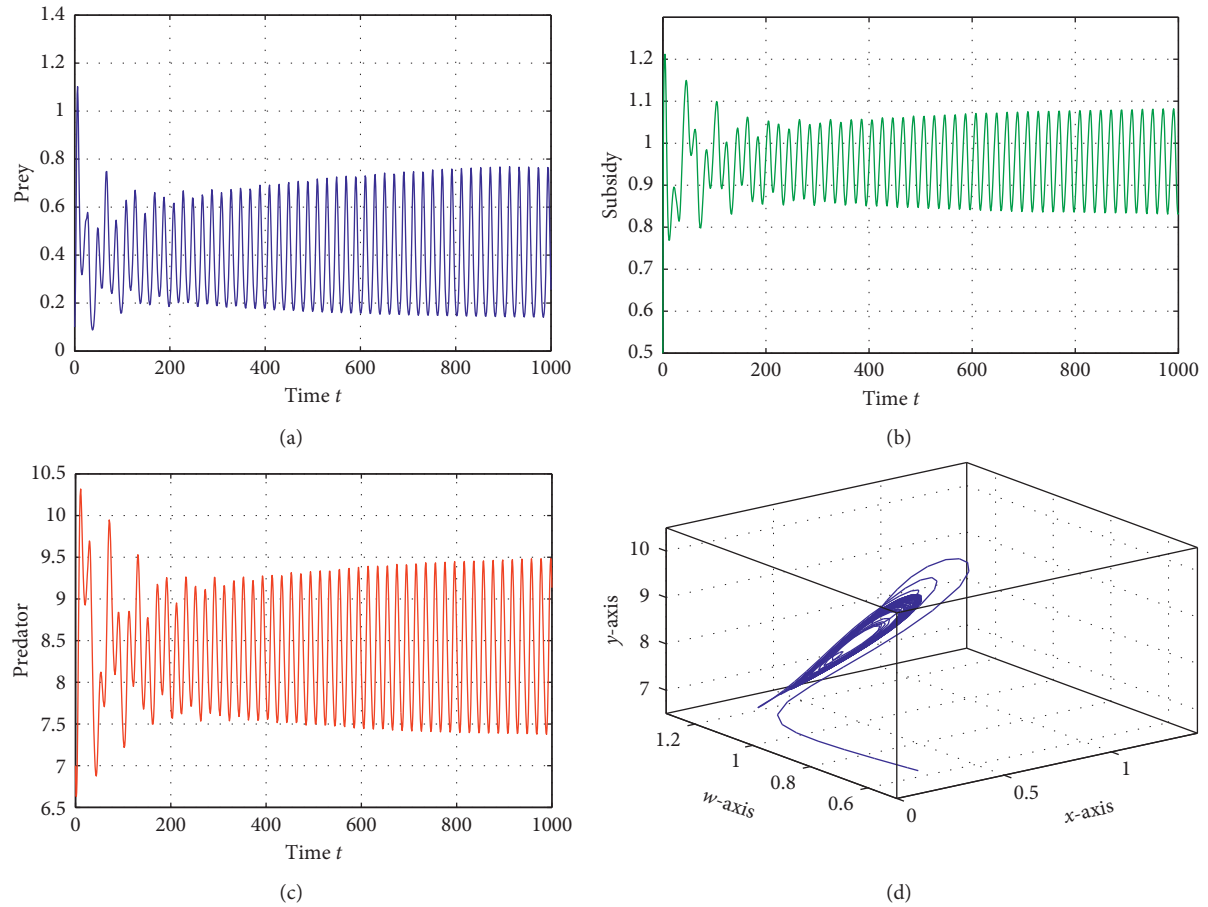

FIGURE 28: (a–c) oscillatory nature of prey, subsidy, and predator, respectively, with time and (d) stable limit cycle around E^* (0.385717, 0.950363, 8.34509) when $\tau = 25 \in (\tau_1^+ = 22.7845, \tau_1^- = 37.7710)$ corresponding to the data set of Figure 9. (a) Oscillation of prey. (b). Oscillation of subsidy. (c) Oscillation of predator. (d) Phase portrait (closed orbit).

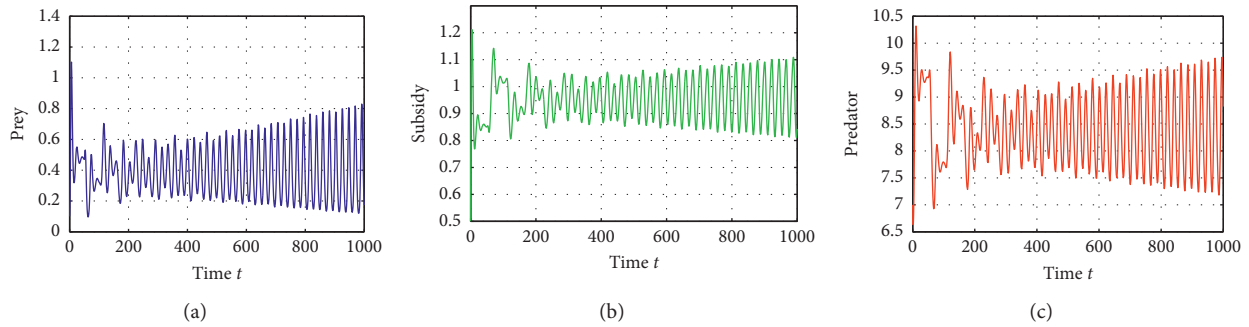

FIGURE 29: (a–c) Oscillatory nature of prey, subsidy, and predator, respectively, with time around E^* (0.385717, 0.950363, 8.34509) when $\tau = 50 > \tau_2^+ = 41.5037$ corresponding to the data set of Figure 9. (a) Oscillation of prey. (b). Oscillation of subsidy. (c) Oscillation of predator.

is unstable, and when $d_1 > d_1^{[TC]}$, then E_1 is stable. Also, Figure 18 exhibits that when $d_3 < d_3^{[TC]} = 0.1768$, then E_2 is unstable, and when $d_3 > d_3^{[TC]} = 0.1768$, then E_2 is stable. So, a transcritical bifurcation is exhibited at $d_3^{[TC]} = 0.1768$ around E_2. Similarly, Figures 19 and 20 depict the transcritical bifurcation diagrams around equilibrium E_4 and E_5 taking d_1 ($d_1^{[TC]} = 1.2238$) and d_3 ($d_3^{[TC]} = 0.61$) as bifurcation parameter, respectively.

6.1. Effect of Time-Delay on Population Dynamics. Now, let us perform the numerical computations to validate the analytical results of the delayed model (60). For the parameter set $\{r = 5.5,\ d_1 = 0.4,\ d_2 = 0.3,\ d_3 = 0.2,\ a_1 = 0.6,\ a_2 = 0.98,\ a_3 = 0.8,\ b_1 = 2.5,\ c_1 = 0.85,\ c_2 = 0.7,\ A = 0,\ a = 1.1, m = 0.4\}$, equation (72) has exactly one positive root 0.2246 (correct up to four decimal places). So, from Theorem 18, the planer equilibrium point E_3 (1.20053, 0, 6.49267) is

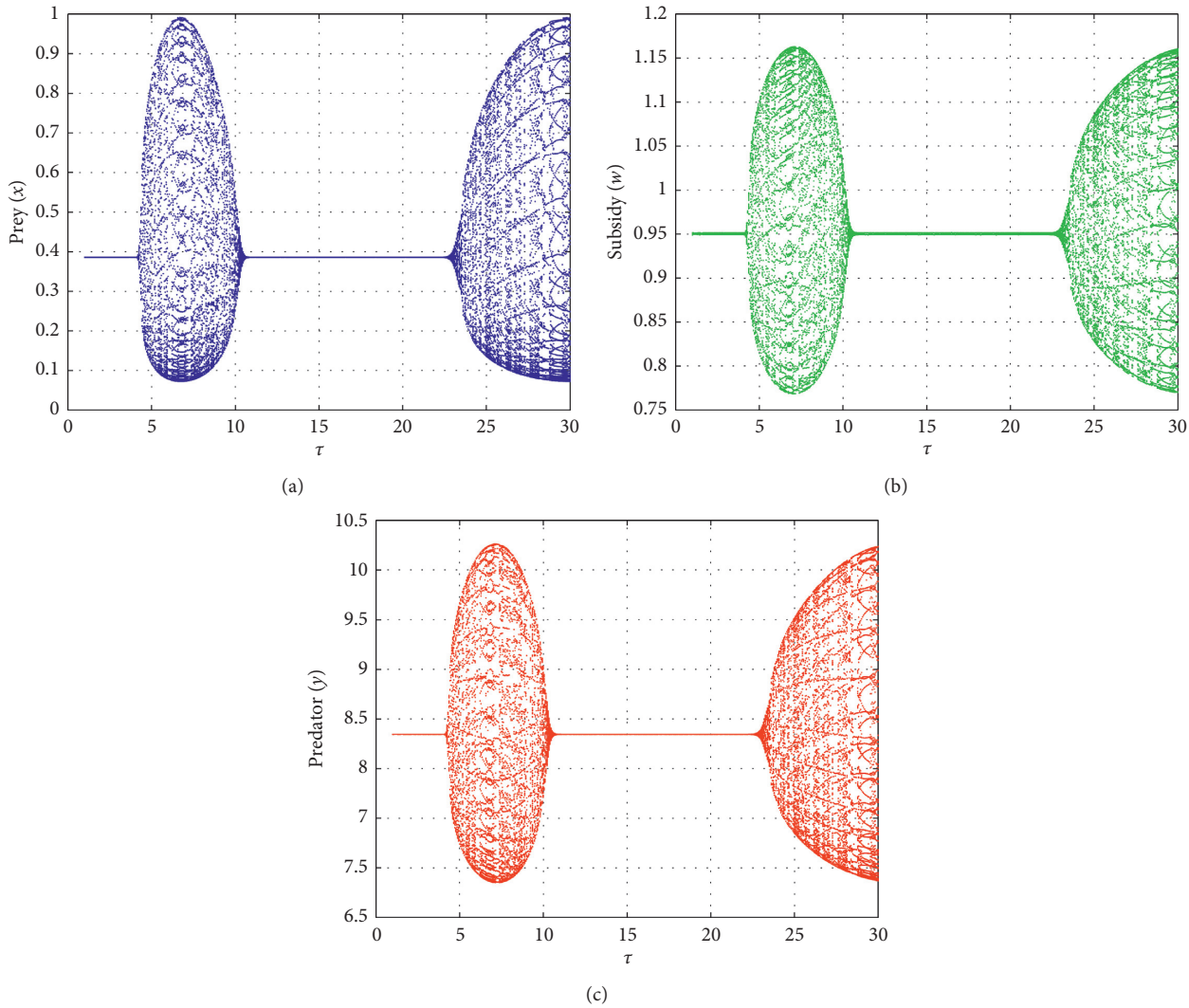

FIGURE 30: Bifurcation diagram around E^* considering τ as independent variable and the remaining parameters are fixed as in dataset of Figure 9. Here, τ runs from 0 to 30. (a) Bifurcation diagram of x. (b) Bifurcation diagram of w. (c) Bifurcation diagram of y.

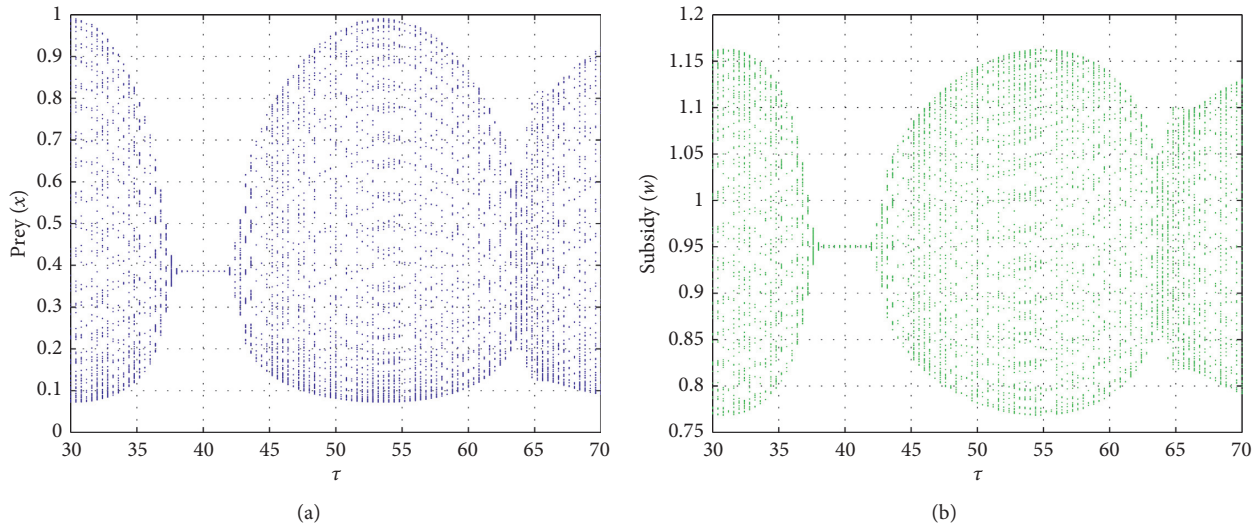

FIGURE 31: Continued.

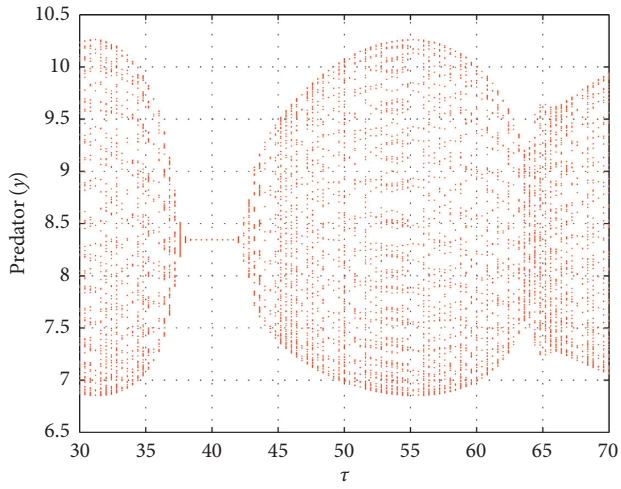

FIGURE 31: Bifurcation diagram around E^* regarding τ as bifurcation parameter when τ runs from 30 to 70 and parameters are chosen from the data set of Figure 9. (a) Bifurcation diagram of x. (b) Bifurcation diagram of w. (c) Bifurcation diagram of y.

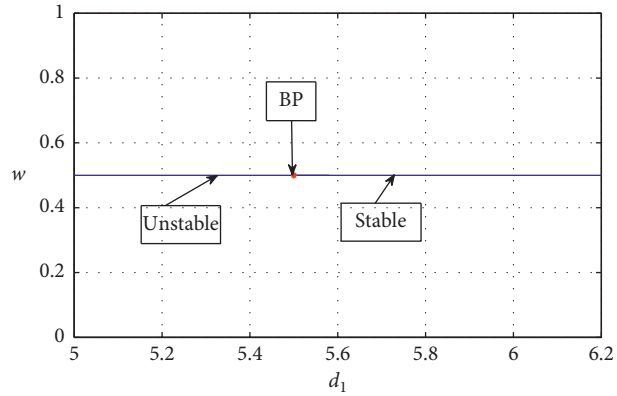

FIGURE 32: Transcritical bifurcation diagram around $E_1(0, 0.5, 0)$ considering d_1 as bifurcation parameter and others parameters are the same as in Figure 2. Here $d_1^{[TC]} = 5.5$.

stable when $\tau \in [0, \tau'^* = 2.9272)$ and unstable when $\tau > \tau'^* = 2.9272$. Stable time series and stable phase trajectory of $E_3(1.20053, 0, 6.49267)$ are shown in Figure 21 when $\tau = 2 < \tau'^* = 2.9272$. Also, Figure 22 depicts the corresponding unstable behaviour of E_3 when $\tau = 3.5 > \tau'^* = 2.9272$. Moreover, Figure 23 presents the supercritical Hopf bifurcation diagram around E_3 taking τ as bifurcation parameter.

For the parameter set $\{r = 5.5,\ d_1 = 0.4,\ d_2 = 0.3,\ d_3 = 0.2,\ a_1 = 0.6,\ a_2 = 0.98,\ a_3 = 0.8,\ b_1 = 2.5,\ c_1 = 0.85,\ c_2 = 0.7,\ A = 2,\ a = 1.1,\ m = 0.4\}$, equation (91) has exactly two positive roots, 0.1127 and 0.0526 (correct up to four decimal places). Then from Theorem 20, we have calculated $\tau_0^+ = 4.0652$, $\tau_0^- = 10.3836$, $\tau_1^+ = 22.7845$, $\tau_1^- = 37.7710$, and $\tau_2^+ = 41.5037$. The interior equilibrium $E^*(0.385717, 0.950363, 8.34509)$ is locally asymptotically stable when $\tau \in [0, 4.0652), (10.3836, 22.7845), (37.7710, 41.5037)$ and unstable when $\tau \in (4.0652, 10.3836), (22.7845, 37.7710)$ and $\tau > 41.5037$. At $\tau = \tau_k^{\pm}, k = 0, 1$ and τ_2^+, Hopf bifurcation appears around E^*. Figures 24–26 depict the stable nature of E^* for $\tau \in [0, 4.0652), (10.3836, 22.7845), (37.7710, 41.5037)$ respectively. Also, unstable behaviour of E^* is presented in Figures 27–29 for $\tau \in (4.0652, 10.3836), (22.7845, 37.7710)$ and $\tau > \tau_2^+ = 41.5037$, respectively. The corresponding bifurcation diagrams are depicted in Figures 30 and 31 .

7. Conclusion

We have analyzed a system for generalist predator which utilizes more than one food source: predator-prey-subsidy model of non-Kolmogorov form introducing nonlinear prey refuge function and the effect of fear felt by prey population. Our main interest is to find the situations such that dynamical stability and instability appear so as to make out more fully how subsidy may influence the predator and their prey. It has been shown that the solutions of system (2) remain positively invariant always and they are asymptotically uniformly bounded. These, in turn, imply that system (2) is biologically well-behaved. Existence

criteria and stable behaviour of all the biologically meaningful equilibria have been discussed. It has to be noted that Hopf bifurcations are exhibited around E_3 (subsidy free) and E^* (interior) of system (2) considering k as a bifurcating parameter (see Figures 4–6, 9, 11, and 12). Also, observing Figures 6 and 12, it can be concluded that high levels of fear can stabilize system (2) by excluding the existence of periodic solutions. These phenomena are biologically significant because prey species are aware after a certain level of fear; i.e., after a certain level of fear, they are not affected as they are aware and show signs of habituation.

Moreover, this work derives transcritical bifurcations (local bifurcation of codimension 1) at the various equilibrium points E_1, E_2, E_4, and E_5, respectively (see Figures 18–20 and 32).

Also, we have discussed numerically the influences of coefficient of prey refuge parameter m on the nature of the equilibrium points E_3 (zero subsidy input rate) and E^* (fixed small subsidy input rate) irrespective of fear level k. Noting Figures 14–17, it is observed that both the prey and predator species always persist in ecosystem due to continuous increment of coefficient of prey refuge. But Figures 10 and 13 depict that, irrespective of fear level, a highly subsidized predator should indeed drive the prey population towards extinction regardless of whether the prey and subsidy arise in the same habitat. This phenomenon is ecologically meaningful because the prey population cannot get enough time to protect themselves from predation risk for enormous growth of predator at high subsidy input rate. So, the prey population is leading towards extinction, but the predator species can easily survive in ecosystem with the help of resource subsidy. Thus, the study of system (2) is ecologically very significant.

In reality, fear effect does not instantaneously reduce the birth of a prey population, but some time lag should be needed to create an impact on the birth rate of the prey population. We have considered that there is a time-delay on the impact of fear to the birth rate of prey, from the instance it perceives the fear of predator through any means. So, the incorporation of time-delay makes system (60) more realistic. It is noted that delay parameter τ has a significant role because there exists a threshold value τ'^* such that stable behaviour of planer equilibrium point E_3 (in the absence of subsidy input rate) switches to oscillatory nature when τ passes through its threshold value τ'^*; i.e., the vector fields for $\tau < \tau'^*$ and $\tau > \tau'^*$ are qualitatively different. So, system (60) exhibits a supercritical Hopf bifurcation around E_3 considering τ as bifurcation parameter (see Figures 21–23). Also, a rigorous study of the stability and bifurcation of interior equilibrium point E^* has been performed. Our analysis describes that the delay within a certain specified range could maintain the stable behaviour of E^*. On the other hand, the delay could drive the system into an unstable state. Hence, the study of the time-delay parameter has a regulatory impact on the whole system.

Data Availability

The data used to support the findings of the study are available within the article.

Conflicts of Interest

The authors declare that they have no conflicts of interest.

Acknowledgments

The authors are grateful to Dr. Eberhard O. Voit (editor) for his careful reading, valuable comments, and helpful suggestions, which have helped them to improve the presentation of this work significantly. This research was completed during the visit of Prof. G.P. Samanta to the Institute of Mathematics of the University of Santiago de Compostela. This work has been partially supported by the Agencia Estatal de Investigacion (AEI) of Spain, cofinanced by the European Fund for Regional Development (FEDER) corresponding to the 2014–2020 multiyear financial framework project MTM2016-75140-P and by Xunta de Galicia under grant ED431C 2019/02.

References

[1] S. Creel and D. Christianson, "Relationships between direct predation and risk effects," *Trends in Ecology & Evolution*, vol. 23, no. 4, pp. 194–201, 2008.

[2] W. Cresswell, "Predation in bird populations," *Journal of Ornithology*, vol. 152, no. S1, pp. 251–263, 2010.

[3] S. Creel, D. Christianson, S. Liley, and J. A. Winnie, "Predation risk affects reproductive physiology and demography of elk," *Science*, vol. 315, no. 5814, p. 960, 2007.

[4] L. Y. Zanette, A. F. White, M. C. Allen, and M. Clinchy, "Perceived predation risk reduces the number of offspring songbirds produce per year," *Science*, vol. 334, no. 6061, pp. 1398–1401, 2011.

[5] X. Wang, L. Zanette, and X. Zou, "Modelling the fear effect in predator-prey interactions," *Journal of Mathematical Biology*, vol. 73, no. 5, pp. 1179–1204, 2016.

[6] A. Das and G. P. Samanta, "Modeling the fear effect on a stochastic prey-predator system with additional food for the predator," *Journal of Physics A: Mathematical and Theoretical*, vol. 51, Article ID 465601, 2018.

[7] A. Das and G. P. Samanta, "Modelling the fear effect in a two-species predator-prey system under the influence of toxic substances," *Rendiconti del Circolo Matematico di Palermo Series 2*, vol. 70, 2021.

[8] M. Das and G. P. Samanta, "A prey-predator fractional order model with fear effect and group defense," *International Journal of Dynamics and Control*, vol. 9, no. 1, pp. 334–349, 2020.

[9] M. Das and G. P. Samanta, "A delayed fractional order food chain model with fear effect and prey refuge," *Mathematics and Computers in Simulation*, vol. 178, pp. 218–245, 2021.

[10] S. Mondal, A. Maiti, and G. P. Samanta, "Effects of fear and additional food in a delayed predator-prey model," *Biophysical Reviews and Letters*, vol. 13, no. 04, pp. 157–177, 2018.

[11] S. Mondal and G. P. Samanta, "Dynamics of a delayed predator-prey interaction incorporating nonlinear prey refuge under the influence of fear effect and additional food," *Journal of Physics A: Mathematical and Theoretical*, vol. 53, no. 29, Article ID 295601, 2020.

[12] S. Mondal and G. P. Samanta, "Time-delayed predator-prey interaction with the benefit of antipredation response in presence of refuge," *Zeitschrift fur Naturforschung A*, vol. 76, no. 1, pp. 23–42, 2021.

[13] S. Mondal and G. P. Samanta, "Impact of fear on a predator-prey system with prey-dependent search rate in deterministic and stochastic environment," *Nonlinear Dynamics*, vol. 104, pp. 2931–2959, 2021.

[14] D. Sahoo and G. P. Samanta, "Comparison between two tritrophic food chain models with multiple delays and anti-predation effect," *International Journal of Biomathematics*, vol. 14, no. 3, Article ID 2150008, 2021.

[15] D. Sahoo and G. P. Samanta, "Impact of fear effect in a two prey-one predator system with switching behaviour in predation," *Differential Equations and Dynamical Systems*, vol. 29, 2021.

[16] X. Wang and X. Zou, "Modeling the fear effect in predator-prey interactions with adaptive avoidance of predators," *Bulletin of Mathematical Biology*, vol. 79, pp. 1325–1359, 2017.

[17] Y. Wang and X. Zou, "On a predator–prey system with digestion delay and anti-predation strategy," *Journal of Nonlinear Science*, vol. 30, pp. 1432–1467, 2020.

[18] S. Samaddar, M. Dhar, and P. Bhattacharya, "Effect of fear on prey-predator dynamics: Exploring the role of prey refuge and additional food," *Chaos: An Interdisciplinary Journal of Nonlinear Science*, vol. 30, no. 6, Article ID 063129, 2020.

[19] H. Zhang, Y. Cai, S. Fu, and W. Wang, "Impact of the fear effect in a prey-predator model incorporating a prey refuge," *Applied Mathematics and Computation*, vol. 356, pp. 328–337, 2019.

[20] J. Ghosh, B. Sahoo, and S. Poria, "Prey-predator dynamics with prey refuge providing additional food to predator," *Chaos, Solitons & Fractals*, vol. 96, pp. 110–119, 2017.

[21] E. González-Olivares, B. González-Yañez, R. Becerra-Klix, and R. Ramos-Jiliberto, "Multiple stable states in a model based on predator-induced defenses," *Ecological Complexity*, vol. 32, pp. 111–120, 2017.

[22] T. K. Kar, "Stability analysis of a prey-predator model incorporating a prey refuge," *Communications in Nonlinear Science and Numerical Simulation*, vol. 10, no. 6, pp. 681–691, 2005.

[23] S. Mondal and G. P. Samanta, "Dynamics of an additional food provided predator-prey system with prey refuge dependent on both species and constant harvest in predator," *Physica A: Statistical Mechanics and Its Applications*, vol. 534, Article ID 122301, 2019.

[24] C. T. Darimont, P. C. Paquet, and T. E. Reimchen, "Spawning salmon disrupt trophic coupling between wolves and ungulate prey in coastal British Columbia," *BMC Ecol*, vol. 8, pp. 1–12, 2008.

[25] J. Halaj and D. H. Wise, "Impact of a detrital subsidy on trophic cascades in a terrestrial grazing food web," *Ecology*, vol. 83, no. 11, pp. 3141–3151, 2002.

[26] J.-A. Henden, R. A. Ims, N. G. Yoccoz, P. Hellstorm, and A. Angerbjorn, "Strength of asymmetric competition between predators in food webs ruled by fluctuating prey: The case of foxes in tundra," *Oikos*, vol. 119, no. 1, pp. 27–34, 2010.

[27] R. A. Garrott, J. E. Bruggeman, M. S. Becker, S. T. Kalinowski, and P. J. White, "Evaluating prey switching in wolf-ungulate systems," *Ecological Applications*, vol. 17, no. 6, pp. 1588–1597, 2007.

[28] A. L. Nevai and R. A. Van Gorder, "Effect of resource subsidies on predator-prey population dynamics: a mathematical model," *Journal of Biological Dynamics*, vol. 6, no. 2, pp. 891–922, 2012.

[29] A. Erbach, F. Lutscher, and G. Seo, "Bistability and limit cycles in generalist predator-prey dynamics," *Ecological Complexity*, vol. 14, pp. 48–55, 2013.

[30] A. Morozov and S. Petrovskii, "Feeding on multiple sources: towards a universal parameterization of the functional response of a generalist predator allowing for switching," *PLoS One*, vol. 8, no. 9, Article ID e74586, 2013.

[31] P. Sunde, K. Thorup, L. B. Jacobsen, and C. Rahbek, "Weather conditions drive dynamic habitat selection in a generalist predator," *PLoS ONE*, vol. 9, no. 2, Article ID e88221, 2014.

[32] E. L. Clare, E. E. Fraser, H. E. Braid, M. B. Fenton, and P. D. N. Hebert, "Species on the menu of a generalist predator, the eastern red bat (Lasiurus borealis): using a molecular approach to detect arthropod prey," *Molecular Ecology*, vol. 18, no. 11, pp. 2532–2542, 2009.

[33] F. Díaz-Ruiz, M. Delibes-Mateos, J. L. García-Moreno, J. María López-Martín, C. Ferreira, and P. Ferreras, "Biogeographical patterns in the diet of an opportunistic predator: the red foxVulpes vulpesin the Iberian Peninsula," *Mammal Review*, vol. 43, no. 1, pp. 59–70, 2013.

[34] J. D. Willson and W. A. Hopkins, "Prey morphology constrains the feeding ecology of an aquatic generalist predator," *Ecology*, vol. 92, no. 3, pp. 744–754, 2011.

[35] A. Das and G. P. Samanta, "Modelling the effect of resource subsidy on a two-species predator-prey system under the influence of environmental noises," *International Journal of Dynamics and Control*, vol. 9, 2021.

[36] Y. Xu, A. L. Krause, and R. A. Van Gorder, "Generalist predator dynamics under Kolmogorov versus non-Kolmogorov models," *Journal of Theoretical Biology*, vol. 486, Article ID 110060, 2020.

[37] L. G. Adams, S. D. Farley, C. A. Stricker et al., "Are inland wolf-ungulate systems influenced by marine subsidies of pacific salmon?" *Ecological Applications*, vol. 20, no. 1, pp. 251–262, 2010.

[38] C. S. Holling, "The components of predation as revealed by a study of small-mammal predation of the european pine sawfly," *The Canadian Entomologist*, vol. 91, no. 5, pp. 293–320, 1959.

[39] C. S. Holling, "Some characteristics of simple types of predation and parasitism," *The Canadian Entomologist*, vol. 91, no. 7, pp. 385–398, 1959.

[40] C. S. Holling, "The functional response of predators to prey density and its role in mimicry and population regulation," *Memoirs of the Entomological Society of Canada*, vol. 97, no. S45, pp. 5–60, 1965.

[41] K. Sarkar, S. Khajanchi, P. C. Mali, and J. J. Nieto, "Rich dynamics of a predator-prey system with different kinds of functional responses," *Complexity*, vol. 2020, Article ID 4285294, 2020.

[42] J. K. Hale, *Theory of Functional Differential Equations*, Springer-Verlag, New York, NY, USA, 1977.

[43] L. Perko, *Differential Equations and Dynamical Systems*, Springer, Berlin, Germany, 2001.

[44] J. D. Murray, *Mathematical Biology*, Springer, Berlin, Germany, 1993.

[45] S. Khajanchi and J. J. Nieto, "Mathematical modeling of tumor-immune competitive system, considering the role of time delay," *Applied Mathematics and Computation*, vol. 340, pp. 180–205, 2019.

[46] Y. Kuang, *Delay Differential Equation with Application in Population Dynamics*, Academic Press, New York, NY, USA, 1993.

[47] S. Mondal and G. P. Samanta, "Dynamical behaviour of a two-prey and one-predator system with help and time delay," *Energy, Ecology and Environment*, vol. 5, no. 1, pp. 12–33, 2020.

[48] S. Mondal and G. P. Samanta, "Pelican-Tilapia interaction in Salton sea: an eco-epidemiological model with strong Allee effect and additional food," *Modeling Earth Systems and Environment*, vol. 7, 2021.

[49] D. Sahoo, S. Mondal, and G. P. Samanta, "Interaction among toxic phytoplankton with viral infection and zooplankton in presence of multiple time delays," *International Journal of Dynamics and Control*, vol. 9, no. 1, pp. 308–333, 2021.

[50] S. Ruan and J. Wei, "On the zeros of transcendental functions with applications to stability of delay differential equations with two delays," *Dynamics of Continuous, Discrete and Impulsive Systems Series B: Applications and Algorithms*, vol. 10, pp. 863–874, 2003.

[51] H. Freedman and V. Rao, "The trade-off between mutual interference and time lags in predator-prey systems," *Bulletin of Mathematical Biology*, vol. 45, no. 6, pp. 991–1004, 1983.

Hindawi
Complexity
Volume 2021, Article ID 9934070, 12 pages
https://doi.org/10.1155/2021/9934070

Research Article

A New Fractional Model for Cancer Therapy with M1 Oncolytic Virus

Majda El Younoussi,[1] **Zakaria Hajhouji**,[1] **Khalid Hattaf**,[1,2] **and Noura Yousfi**[1]

[1]*Laboratory of Analysis, Modeling and Simulation (LAMS), Faculty of Sciences Ben M'sik, Hassan II University of Casablanca, P.O Box 7955 Sidi Othman, Casablanca, Morocco*
[2]*Centre Régional des Métiers de l'Education et de la Formation (CRMEF), Derb Ghalef, Casablanca 20340, Morocco*

Correspondence should be addressed to Khalid Hattaf; k.hattaf@yahoo.fr

Received 18 April 2021; Revised 22 May 2021; Accepted 28 May 2021; Published 7 June 2021

Academic Editor: Constantin Udriste

The aim of this work is to propose and analyze a new mathematical model formulated by fractional differential equations (FDEs) that describes the dynamics of oncolytic M1 virotherapy. The well-posedness of the proposed model is proved through existence, uniqueness, nonnegativity, and boundedness of solutions. Furthermore, we study all equilibrium points and conditions needed for their existence. We also analyze the global stability of these equilibrium points and investigate their instability conditions. Finally, we state some numerical simulations in order to exemplify our theoretical results.

1. Introduction

Cancer is a collection of related diseases where some of the body's cells divide continuously and spread into surrounding tissues. Cancer is caused by certain changes to genes. It can start almost anywhere in the human body. Old or damaged cells survive when they should die; new cells form when the body does not need them. These extra cells can divide continuously and may form tumors. A tumor becomes dangerous when it begins to form extensions to neighboring areas (metastasis) [1]. This is why it is important to detect cancer as early as possible in order to avoid this migration. Cancer treatment is adapted according to each situation. There are different cancer treatments used alone or in combination, such as surgery, radiotherapy, chemotherapy, hormone therapy, immunotherapy, and virotherapy. Virotherapy is one of the new therapies; it consists in using a virus after having reprogrammed it. This virus is called oncolytic virus. Oncolytic viruses infect and destroy cancer cells; they use the cell's genetic machinery to make copies of themselves and subsequently spread to surrounding uninfected cells [2].

According to a medical experiment, in vitro, in vivo, and ex vivo studies showed potent oncolytic efficacy and high tumor tropism of alphavirus M1, which is a naturally occurring and a selective oncolytic virus targeting zinc-finger antiviral protein (ZAP) deficient cancer cells [3]. To model the role of the M1 virus in oncolytic virotherapy, Wang et al. [4] proposed a nonlinear system governed by ordinary differential equations (ODEs) that describe the growth of normal cells, tumor cells, and the M1 virus with limited nutrients. Elaiw et al. [5] extended the model presented in [4] by including spatial effects and anti-tumor immune response mediated by cytotoxic T lymphocyte (CTL) cells. The results in [5] indicated that the immune response has a negative impact on oncolytic M1 virotherapy, and it reduced its efficiency.

On the other hand, all the above mathematical models neglected the memory effect by considering only integer-order derivatives. However, fractional-order derivative provides an excellent tool for describing memory and hereditary properties which exist in most biological systems. For instance, Cole [6] proved that the membranes of cells of the biological organism have fractional-order electrical conductance since the memory means that the system's response is dependent not only on the current state but on its complete history. Therefore, the classical integer-order

derivative does not reflect this memory effect because it is a local operator, unlike the fractional derivative.

The main purpose of this study is to develop a mathematical model governed by fractional-order differential equations (FDEs) to study the effect of memory on the dynamics of oncolytic M1 virotherapy. So, the rest of the paper is outlined as follows: the next section is devoted to the formulation of the model, including the well-posedness and the existence of equilibria. Section 3 focuses on stability analysis. Section 4 deals with numerical simulations in order to illustrate our main analytical results. Finally, a brief conclusion is given in Section 5.

2. Model Formulation and Preliminaries

In this section, we propose the following FDE model:

$$\begin{cases} D^{\alpha}S(t) = A - dS(t) - \beta_1 S(t)N(t) - \beta_2 S(t)T(t), \\ D^{\alpha}N(t) = r_1\beta_1 S(t)N(t) - (d+\varepsilon_1)N(t), \\ D^{\alpha}T(t) = r_2\beta_2 S(t)T(t) - (d+\varepsilon_2)T(t) - \beta_3 T(t)V(t), \\ D^{\alpha}V(t) = B + r_3\beta_3 T(t)V(t) - (d+\varepsilon_3)V(t), \end{cases} \tag{1}$$

where $S(t)$, $N(t)$, $T(t)$, and $V(t)$ are the concentrations of nutrient, normal cells, tumor cells, and M_1 virus at time t, respectively. The parameters A and B are the recruitment rates of nutrient and M_1 virus, respectively. Also, B represents the minimum effective dosage of medication. The normal and tumor cells consume the nutrient at rates $\beta_1 SN$ and $\beta_2 ST$, respectively. The growth rate of normal cells as a result of consuming the nutrient is given by $r_1\beta_1 SN$, while the growth rate of tumor cells is given by $r_2\beta_2 ST$. The virus infects and kills tumor cells at rate $\beta_3 TV$, and it replicates at rate $r_3\beta_3 TV$. The parameter d is the washout constant rate of nutrient and bacteria. The parameters ε_1, ε_2, and ε_3 are the natural death rates of normal cells, tumor cells, and M_1 virus, respectively. The operator D^{α} denotes the Caputo fractional derivative with $\alpha \in (0,1]$ that describes the memory effect.

It is important to note that the ODE mathematical model verifying potent oncolytic efficacy of M1 virus [4] is a special case of our model presented by system (1), and it suffices to take $\alpha = 1$. Furthermore, to prove that our model is biologically well-posed, we assume that the initial conditions of (1) satisfy:

$$\begin{aligned} S(0) = \phi_1(0) \geq 0, N(0) = \phi_2(0) \geq 0, T(0) = \phi_3(0) \\ \geq 0, V(0) = \phi_4(0) \geq 0. \end{aligned} \tag{2}$$

Theorem 1. *If the initial conditions (2) are given, then there exists a unique solution of system (1) defined on* $[0,+\infty)$. *Moreover, this solution remains nonnegative and bounded for all* $t \geq 0$.

Proof. It is not hard to show that the vector function of system (1) satisfies the first condition of Lemma 4 in [7]. It remains to prove the second condition. Let

$$X(t) = \begin{pmatrix} S(t) \\ N(t) \\ T(t) \\ V(t) \end{pmatrix}, \quad Y = \begin{pmatrix} A \\ 0 \\ 0 \\ B \end{pmatrix}. \tag{3}$$

Then

$$D^{\alpha}X(t) = Y + A_1 X(t) + A_2 S(t)X(t) + A_3 T(t)X(t), \tag{4}$$

where

$$A_1 = \begin{pmatrix} -d & 0 & 0 & 0 \\ 0 & -(d+\varepsilon_1) & 0 & 0 \\ 0 & 0 & -(d+\varepsilon_2) & 0 \\ 0 & 0 & 0 & -(d+\varepsilon_3) \end{pmatrix},$$

$$A_2 = \begin{pmatrix} 0 & -\beta_1 & -\beta_2 & 0 \\ 0 & r_1\beta_1 & 0 & 0 \\ 0 & 0 & r_2\beta_2 & 0 \\ 0 & 0 & 0 & 0 \end{pmatrix}, \tag{5}$$

$$A_3 = \begin{pmatrix} 0 & 0 & 0 & 0 \\ 0 & 0 & 0 & 0 \\ 0 & 0 & 0 & -\beta_3 \\ 0 & 0 & 0 & r_3\beta_3 \end{pmatrix}.$$

Thus,

$$\left\|D^{\alpha}X(t)\right\| \leq \|Y\| + \left(\left\|A_1\right\| + \left\|A_2\right\|\|S\| + \left\|A_3\right\|\|T\|\right)\|X\|. \tag{6}$$

This implies that the second condition of Lemma 4 in [7] is satisfied. Then system (1) has a unique solution on $[0,+\infty)$.

On the other hand and according to (1), we have

$$\begin{aligned} D^{\alpha}S(t)|_{S=0} &= A > 0, \\ D^{\alpha}N(t)|_{N=0} &= 0 \geq 0, \\ D^{\alpha}T(t)|_{T=0} &= 0 \geq 0, \\ D^{\alpha}V(t)|_{V=0} &= B > 0. \end{aligned} \tag{7}$$

By Lemmas 5 and 6 in [7], we deduce that the solution of (1) is nonnegative.

It remains to prove the boundedness of solutions. Then we consider the following function:

$$F(t) = r_1 r_2 r_3 S(t) + r_2 r_3 N(t) + r_1 r_3 T(t) + r_1 V(t). \tag{8}$$

Hence,

$$\begin{aligned} D^{\alpha}F(t) &= r_1r_2r_3A + r_1B - r_1r_2r_3dS(t) - r_2r_3(d+\varepsilon_1)N(t) \\ &\quad - r_1r_3(d+\varepsilon_2)T(t) - r_1(d+\varepsilon_3)V(t) \\ &\le r_1(r_2r_3A + B) - dF(t). \end{aligned} \tag{9}$$

Then

$$F(t) \le F(0)E_{\alpha}(-\mathrm{d}t^{\alpha}) + \frac{r_1}{d}(r_2r_3A + B)(1 - E_{\alpha}(-\mathrm{d}t^{\alpha})). \tag{10}$$

Since $0 \le E_{\alpha}(-\mathrm{d}t^{\alpha}) \le 1$, we have

$$F(t) \le F(0) + \frac{r_1}{d}(r_2r_3A + B), \tag{11}$$

which implies that S, N, T, and V are bounded. This completes the proof.

Now, we establish the equilibrium points of our model. It is obvious that any equilibrium point of system (1) satisfies the following algebraic equations:

$$A - \mathrm{d}S - \beta_1SN - \beta_2ST = 0, \tag{12}$$

$$r_1\beta_1SN - (d+\varepsilon_1)N = 0, \tag{13}$$

$$r_2\beta_2ST - (d+\varepsilon_2)T - \beta_3TV = 0, \tag{14}$$

$$B + r_3\beta_3TV - (d+\varepsilon_3)V = 0. \tag{15}$$

From (13), we have $N = 0$ or $S = (d+\varepsilon_1)/r_1\beta_1$. Similarly, equation (14) leads to $T = 0$ or $r_2\beta_2S = d + \varepsilon_2 + \beta_3V$:

(i) For $N = 0$ and $T = 0$, we have $S = (A/d)$ and $V = B/(d+\varepsilon_3)$. Then system (1) has an equilibrium point of the form $E_0(S_0, 0, 0, V_0)$, where $S_0 = (A/d)$ and $V_0 = B/((d+\varepsilon_3))$.

(ii) For $N \neq 0$ and $T = 0$, we have $S = (d+\varepsilon_1)/r_1\beta_1$, $V = B/(d+\varepsilon_3)$ and $N = (d/\beta_1)(\mathscr{A}_1 - 1)$, where

$$\mathscr{A}_1 = \frac{Ar_1\beta_1}{d(d+\varepsilon_1)}. \tag{16}$$

This number reflects the ability of absorbing nutrients by normal cells. It is called absorbing number [4]. When $\mathscr{A}_1 > 1$, system (1) has another equilibrium $E_1(S_1, N_1, 0, V_1)$, where $S_1 = (d+\varepsilon_1)/r_1\beta_1$, $N_1 = (d/\beta_1)(\mathscr{A}_1 - 1)$, and $V_1 = B/(d+\varepsilon_3)$.

(iii) For $N = 0$ and $T \neq 0$, we have $S = (\beta_3V + d + \varepsilon_2)/r_2\beta_2$, $T = (-d/\beta_2) + (Ar_2/\beta_3V + d + \varepsilon_2)$, and

$$a_1V^2 + a_2V + a_3 = 0, \tag{17}$$

where

$$\begin{aligned} a_1 &= \beta_3[r_3\beta_3d + \beta_2(d+\varepsilon_3)], \\ a_2 &= \frac{a_1}{\beta_3}(d+\varepsilon_2) - \beta_2\beta_3(B + r_2r_3A), \\ a_3 &= -B\beta_2(d+\varepsilon_2). \end{aligned} \tag{18}$$

Since $a_1 > 0$ and $a_3 < 0$, we have $\delta = a_2^2 - 4a_1a_3 \ge 0$. Thus equation (17) has two roots given by

$$V_{\pm} = \frac{-a_2 \pm \sqrt{\delta}}{2a_1}. \tag{19}$$

Clearly, $V_+ > 0$ and $V_- < 0$. As $V > 0$, we have $V = V_+$.

It is obvious that $S > 0$. However, $T > 0$ implies that $\mathscr{A}_2 > 1 + (B\beta_3/(d+\varepsilon_2)(d+\varepsilon_3))$, where

$$\mathscr{A}_2 = \frac{Ar_2\beta_2}{d(d+\varepsilon_2)}. \tag{20}$$

This number reflects the ability of absorbing nutrients by tumor cells. It can be called the absorbing number of nutrients by tumor cells. Hence, system (1) has another equilibrium point when $\mathscr{A}_2 > 1 + (B\beta_3/(d+\varepsilon_2)(d+\varepsilon_3))$. This equilibrium point is denoted by $E_2(S_2, 0, T_2, V_2)$, where

$$\begin{aligned} V_2 &= V_+, \\ S_2 &= \frac{\beta_3V_2 + d + \varepsilon_2}{r_2\beta_2}, \\ T_2 &= \frac{-d}{\beta_2} + \frac{Ar_2}{\beta_3V_2 + d + \varepsilon_2}. \end{aligned} \tag{21}$$

(iv) For $N \neq 0$ and $T \neq 0$, we have $S = (d+\varepsilon_1)/r_1\beta_1$ and $V = (d+\varepsilon_2/\beta_3)((\mathscr{A}_2/\mathscr{A}_1) - 1)$ as $V > 0$ implies that $\mathscr{A}_2 > \mathscr{A}_1$. From (15), we get $T = (-B + (d+\varepsilon_3)V)/r_3\beta_3V$. Similarly, $T > 0$ leads to $\mathscr{A}_2 > \mathscr{A}_1 + (ABr_1\beta_1\beta_3/d(d+\varepsilon_3)(d+\varepsilon_2)(d+\varepsilon_1))$. Substituting S and T in (12), we obtain

$$N = \frac{(d+\varepsilon_2)((\mathscr{A}_2/\mathscr{A}_1)-1)[Ar_1r_3\beta_1\beta_3 - r_3\beta_3 d(d+\varepsilon_1) - \beta_2(d+\varepsilon_1)(d+\varepsilon_3)]}{r_3\beta_1\beta_3(d+\varepsilon_1)(d+\varepsilon_2)((\mathscr{A}_2/\mathscr{A}_1)-1)} + \frac{B\beta_2\beta_3}{r_3\beta_1\beta_3(d+\varepsilon_2)((\mathscr{A}_2/\mathscr{A}_1)-1)}. \tag{22}$$

Furthermore, $N > 0$ implies that

$$\mathscr{A}_1 + \frac{\beta_2 B}{r_3 d(d+\varepsilon_2)((\mathscr{A}_2/\mathscr{A}_1)-1)} > 1 + \frac{\beta_2(d+\varepsilon_3)}{r_3\beta_3 d}. \tag{23}$$

Thus, system (1) has another equilibrium point when $\mathscr{A}_2 > \mathscr{A}_1$:

$$\mathscr{A}_1 + \frac{\beta_2 B}{r_3 d(d+\varepsilon_2)((A_2/A_1)-1)} > 1 + \frac{\beta_2(d+\varepsilon_3)}{r_3\beta_3 d}, \qquad \mathscr{A}_2 > \mathscr{A}_1 + \frac{ABr_1\beta_1\beta_3}{d(d+\varepsilon_3)(d+\varepsilon_2)(d+\varepsilon_1)}. \tag{24}$$

This equilibrium point is denoted by $E_3(S_3, N_3, T_3, V_3)$, where

$$S_3 = \frac{d+\varepsilon_1}{r_1\beta_1},$$

$$V_3 = \frac{d+\varepsilon_2}{\beta_3}((\mathscr{A}_2/\mathscr{A}_1)-1),$$

$$N_3 = \frac{(d+\varepsilon_2)((\mathscr{A}_2/\mathscr{A}_1)-1)[Ar_1r_3\beta_1\beta_3 - r_3\beta_3 d(d+\varepsilon_1) - \beta_2(d+\varepsilon_1)(d+\varepsilon_3)]}{r_3\beta_1\beta_3(d+\varepsilon_1)(d+\varepsilon_2)((\mathscr{A}_2/\mathscr{A}_1)-1)} + \frac{B\beta_2\beta_3}{r_3\beta_1\beta_3(d+\varepsilon_2)((\mathscr{A}_2/\mathscr{A}_1)-1)}, \tag{25}$$

$$T_3 = \frac{-B + (d+\varepsilon_3)V_3}{r_3\beta_3 V_3}.$$

All the above cases are summerized in the following result. □

Theorem 2. *Let $\mathscr{A}_1$ and $\mathscr{A}_2$ be defined by (16) and (20). Then*

(i) System (1) always has a competition-free equilibrium $E_0(S_0, 0, 0, V_0)$.

(ii) System (1) has a tumor-free equilibrium $E_1(S_1, N_1, 0, V_1)$ when $\mathscr{A}_1 > 1$.

(iii) System (1) has a treatment failure equilibrium $E_2(S_2, 0, T_2, V_2)$ when $\mathscr{A}_2 > 1 + (B\beta_3/(d+\varepsilon_2)(d+\varepsilon_3))$.

(iv) System (1) has a partial success equilibrium $E_3(S_3, N_3, T_3, V_3)$ when

$$\mathscr{A}_2 > \mathscr{A}_1 + \frac{ABr_1\beta_1\beta_3}{d(d+\varepsilon_3)(d+\varepsilon_2)(d+\varepsilon_1)}, \qquad \mathscr{A}_1 + \frac{\beta_2 B}{r_3 d(d+\varepsilon_2)((\mathscr{A}_2/\mathscr{A}_1)-1)} > 1 + \frac{\beta_2(d+\varepsilon_3)}{r_3\beta_3 d}. \tag{26}$$

3. Stability Analysis

In this section, we focus on the stability analysis of the equilibria E_0, E_1, E_2, and E_3.

Theorem 3. *The competition-free equilibrium E_0 is globally asymptotically stable for $\mathscr{A}_2 \le 1 + (B\beta_3/(d+\varepsilon_2)(d+\varepsilon_3))$ and $\mathscr{A}_1 \le 1$, and it is unstable if $\mathscr{A}_2 > 1 + (B\beta_3/(d+\varepsilon_2)(d+\varepsilon_3))$ or $\mathscr{A}_1 > 1$.*

Proof. In order to show the first part of this theorem, we consider the following Lyapunov functional:

$$L_0(t) = S_0\phi\left(\frac{S(t)}{S_0}\right) + \frac{1}{r_1}N(t) + \frac{1}{r_2}T(t) + \frac{1}{r_2 r_3}V_0\phi\left(\frac{V(t)}{V_0}\right), \tag{27}$$

where $\phi(x) = x - \ln(x) - 1$ for $x > 0$.

Based on the property of fractional derivatives given in [8], we get

$$
\begin{aligned}
D^{\alpha}L_0 &\leq \left(1-\frac{S_0}{S}\right)D^{\alpha}S+\frac{1}{r_1}D^{\alpha}N+\frac{1}{r_2}D^{\alpha}T+\frac{1}{r_2r_3}\left(1-\frac{V_0}{V}\right)D^{\alpha}V\\
&=\left(1-\frac{S_0}{S}\right)(A-\mathrm{d}S-\beta_1SN-\beta_2ST)\\
&\quad+\frac{1}{r_1}(r_1\beta_1SN-(d+\varepsilon_1)N)\\
&\quad+\frac{1}{r_2}(r_2\beta_2ST-(d+\varepsilon_2)T-\beta_3TV)\\
&\quad+\frac{1}{r_2r_3}\left(1-\frac{V_0}{V}\right)(B+r_3\beta_3TV-(d+\varepsilon_3)V).
\end{aligned}
\tag{28}
$$

By $S_0=(A/d)$ and $V_0=B/(d+\varepsilon_3)$, we obtain

$$
\begin{aligned}
D^{\alpha}L_0 &\leq \mathrm{d}S_0\left(1-\frac{S}{S_0}\right)\left(1-\frac{S_0}{S}\right)+\beta_1S_0N+\beta_2S_0T-\frac{d+\varepsilon_1}{r_1}N-\frac{d+\varepsilon_2}{r_2}T\\
&\quad+\frac{d+\varepsilon_3}{r_2r_3}V_0\left(1-\frac{V}{V_0}\right)\left(1-\frac{V_0}{V}\right)-\frac{\beta_3}{r_2}TV_0\\
&=\frac{-d}{S}(S-S_0)^2+\left(\beta_1S_0-\frac{d+\varepsilon_1}{r_1}\right)N+\left(\beta_2S_0-\frac{d+\varepsilon_2}{r_2}-\frac{\beta_3V_0}{r_2}\right)T\\
&\quad-\frac{d+\varepsilon_3}{r_2r_3}\frac{(V-V_0)^2}{V}\\
&=\frac{-d}{S}(S-S_0)^2+\frac{d+\varepsilon_1}{r_1}(\mathscr{A}_1-1)N\\
&\quad+\frac{d+\varepsilon_2}{r_2}\left(\mathscr{A}_2-1-\frac{B\beta_3}{(d+\varepsilon_2)(d+\varepsilon_3)}\right)T-\frac{d+\varepsilon_3}{r_2r_3}\frac{(V-V_0)^2}{V}.
\end{aligned}
\tag{29}
$$

Then $D^{\alpha}L_0\leq 0$ when $\mathscr{A}_1\leq 1$ and $\mathscr{A}_2\leq 1+(B\beta_3/(d+\varepsilon_2)(d+\varepsilon_3))$. Clearly, $D^{\alpha}L_0=0$ if and only if $S=S_0$, $N=0$, $T=0$, and $V=V_0$. Then the largest invariant set contained in $\{(S,N,T,V)|D^{\alpha}L_0(t)=0\}$ is the singleton $\{E_0\}$. By LaSalle's invariance principale [9], we deduce that E_0 is globally asymptotically stable for $\mathscr{A}_1\leq 1$ and $\mathscr{A}_2\leq 1+(B\beta_3/(d+\varepsilon_2)(d+\varepsilon_3))$.

It remains to investigate the dynamical property of E_0 in case when $\mathscr{A}_1>1$ or $\mathscr{A}_2>1+(B\beta_3/(d+\varepsilon_2)(d+\varepsilon_3))$. For this purpose, we compute the characteristic equation at E_0 that is given by

$$
(\lambda-\lambda_1)(\lambda-\lambda_2)(\lambda-\lambda_3)(\lambda-\lambda_4)=0,
\tag{30}
$$

where

$$
\begin{aligned}
\lambda_1&=-d,\\
\lambda_2&=-d-\varepsilon_3,\\
\lambda_3&=(d+\varepsilon_2)\left(\mathscr{A}_2-1-\frac{B\beta_3}{(d+\varepsilon_2)(d+\varepsilon_3)}\right),\\
\lambda_4&=(d+\varepsilon_1)(\mathscr{A}_1-1).
\end{aligned}
\tag{31}
$$

We have $\lambda_1<0$, $\lambda_2<0$, $\lambda_3>0$ if $\mathscr{A}_2>1+(B\beta_3/(d+\varepsilon_2)(d+\varepsilon_3))$, and $\lambda_4>0$ if $\mathscr{A}_1>1$. Consequently, E_0 is unstable if $\mathscr{A}_1>1$ or $\mathscr{A}_2>1+(B\beta_3/(d+\varepsilon_2)(d+\varepsilon_3))$. □

Theorem 4. *Suppose that $\mathscr{A}_1 > 1$. Then the tumor-free equilibrium E_1 is globally asymptotically stable if*

$$\mathscr{A}_2 \le \mathscr{A}_1 + \frac{ABr_1\beta_1\beta_3}{d(d+\varepsilon_1)(d+\varepsilon_2)(d+\varepsilon_3)}, \tag{32}$$

and it is unstable if

$$\mathscr{A}_2 > \mathscr{A}_1 + \frac{ABr_1\beta_1\beta_3}{d(d+\varepsilon_1)(d+\varepsilon_2)(d+\varepsilon_3)}. \tag{33}$$

Proof. Consider the following Lyapunov functional:

$$L_1(t) = S_1\phi\left(\frac{S(t)}{S_1}\right) + \frac{1}{r_1}N_1\phi\left(\frac{N(t)}{N_1}\right) + \frac{1}{r_2}T(t) + \frac{1}{r_2r_3}V_1\phi\left(\frac{V(t)}{V_1}\right). \tag{34}$$

Then

$$\begin{aligned} D^\alpha L_1 \le{}& \left(1-\frac{S_1}{S}\right)(A - \mathrm{d}S - \beta_1 SN - \beta_2 ST) \\ &+ \frac{1}{r_1}\left(1-\frac{N_1}{N}\right)(r_1\beta_1 SN - (d+\varepsilon_1)N) \\ &+ \frac{1}{r_2}(r_2\beta_2 ST - (d+\varepsilon_2)T - \beta_3 TV) \\ &+ \frac{1}{r_2r_3}\left(1-\frac{V_1}{V}\right)(B + r_3\beta_3 TV - (d+\varepsilon_3)V). \end{aligned} \tag{35}$$

By $V_1 = B/(d+\varepsilon_3)$ and $S_1 = (d+\varepsilon_1)/r_1\beta_1$, we obtain

$$\begin{aligned} D^\alpha L_1 \le{}& \mathrm{d}S_1\left(1-\frac{S_1}{S}\right)\left(1-\frac{S}{S_1}\right) + \beta_1 S_1 N_1\left(2-\frac{S_1}{S}-\frac{S}{S_1}\right) \\ &+ \left(\beta_1 S_1 - \frac{d+\varepsilon_1}{r_1}\right)N + \left(\beta_2\frac{d+\varepsilon_1}{r_1\beta_1} - \frac{d+\varepsilon_2}{r_2} - \frac{\beta_3 B}{r_2(d+\varepsilon_3)}\right)T \\ &+ \frac{B}{r_2r_3}\left(2-\frac{V_1}{V}-\frac{V}{V_1}\right) \\ ={}& -(d+\beta_1 N_1)\frac{(S-S_1)^2}{S} - \frac{B}{r_2r_3}\frac{(V-V_1)^2}{VV_1} \\ &+ \frac{d(d+\varepsilon_1)(d+\varepsilon_2)}{Ar_1r_2\beta_1}\left(\mathscr{A}_2 - \mathscr{A}_1 - \frac{ABr_1\beta_1\beta_3}{d(d+\varepsilon_1)(d+\varepsilon_2)(d+\varepsilon_3)}\right)T. \end{aligned} \tag{36}$$

Then $D^\alpha L_1 \le 0$ when

$$\mathscr{A}_2 \le \mathscr{A}_1 + \frac{ABr_1\beta_1\beta_3}{d(d+\varepsilon_1)(d+\varepsilon_2)(d+\varepsilon_3)}. \tag{37}$$

Obviously, $D^\alpha L_1 = 0$ if and only if $S = S_1, N = N_1, T = 0$, and $V = V_1$. Then the largest invariant set contained in $\{(S,N,T,V) | D^\alpha L_1(t) = 0\}$ is the singleton E_1. By LaSalle's invariance principle, we deduce that E_1 is globally asymptotically stable for

$$\mathscr{A}_2 \le \mathscr{A}_1 + \frac{ABr_1\beta_1\beta_3}{d(d+\varepsilon_1)(d+\varepsilon_2)(d+\varepsilon_3)}. \tag{38}$$

On the contrary, the characteristic equation at E_1 is given by

$$(d+\varepsilon_1+\lambda)(r_2\beta_2 S_1 - d - \varepsilon_2 - \beta_3 V_1 - \lambda)f(\lambda) = 0, \tag{39}$$

where

$f(\lambda) = (d+\lambda+\beta_1 N_1)(d+\varepsilon_1+\lambda - r_1\beta_1 S_1) + r_1\beta_1^2 N_1 S_1$.

One of the eigenvalues of (39) is

$$\lambda_1 = r_2\beta_2 S_1 - d - \varepsilon_2 - \beta_3 V_1 = \frac{d(d+\varepsilon_1)(d+\varepsilon_2)}{Ar_1\beta_1}\left(\mathscr{A}_2 - \mathscr{A}_1 - \frac{ABr_1\beta_1\beta_3}{d(d+\varepsilon_1)(d+\varepsilon_2)(d+\varepsilon_3)}\right). \tag{40}$$

We observe that $\lambda_1 > 0$ if

$$\mathscr{A}_2 > \mathscr{A}_1 + \frac{ABr_1\beta_1\beta_3}{d(d+\varepsilon_1)(d+\varepsilon_2)(d+\varepsilon_3)}. \tag{41}$$

Thus, E_1 is unstable when

$$\mathscr{A}_2 > \mathscr{A}_1 + \frac{ABr_1\beta_1\beta_3}{d(d+\varepsilon_1)(d+\varepsilon_2)(d+\varepsilon_3)}. \tag{42}$$

□

Theorem 5. *Suppose that* $\mathscr{A}_2 > 1 + (B\beta_3/(d+\varepsilon_2)(d+\varepsilon_3))$ *and* $(\mathscr{A}_2/\mathscr{A}_1) > 1$. *Then the treatment failure equilibrium* E_2 *is globally asymptotically stable if*

$$1 + \frac{\beta_2(d+\varepsilon_3)}{r_3\beta_3 d} \geq \mathscr{A}_1 + \frac{B\beta_2}{r_3 d(d+\varepsilon_2)((\mathscr{A}_2/\mathscr{A}_1)-1)}, \tag{43}$$

and becomes unstable if

$$1 + \frac{\beta_2(d+\varepsilon_3)}{r_3\beta_3 d} < \mathscr{A}_1 + \frac{B\beta_2}{r_3 d(d+\varepsilon_2)((\mathscr{A}_2/\mathscr{A}_1)-1)}. \tag{44}$$

Proof. Consider the following Lyapunov functional:

$$L_2(t) = S_2\phi\left(\frac{S(t)}{S_2}\right) + \frac{1}{r_1}N(t) + \frac{1}{r_2}T_2\phi\left(\frac{T(t)}{T_2}\right) + \frac{1}{r_2 r_3}V_2\phi\left(\frac{V(t)}{V_2}\right). \tag{45}$$

Then

$$\begin{aligned} D^\alpha L_2 &\leq \mathrm{d}S_2\left(1 - \frac{S_2}{S}\right)\left(1 - \frac{S}{S_2}\right) + \beta_2 S_2 T_2\left(2 - \frac{S_2}{S} - \frac{S}{S_2}\right) \\ &\quad + \left(\beta_1 S_2 - \frac{d+\varepsilon_1}{r_1}\right)N \\ &\quad + \left(\beta_2 S_2 - \frac{d+\varepsilon_2}{r_2} - \frac{\beta_3}{r_2}V_2\right)T \\ &\quad + \frac{B}{r_2 r_3}\left(2 - \frac{V_2}{V} - \frac{V}{V_2}\right) \\ &= -(d+\beta_2 T_2)\frac{(S-S_2)^2}{S} + \beta_1(S_2 - S_3)N - \frac{B}{r_2 r_3}\frac{(V-V_2)^2}{VV_2}. \end{aligned} \tag{46}$$

By computation, we find

$$\begin{aligned} S_2 - S_3 &= Ar_1\beta_1 r_3\beta_3(d+\varepsilon_2)\left(\frac{A_2}{A_1} - 1\right) + B\beta_2\beta_3(d+\varepsilon_1) \\ &\quad - \beta_2(d+\varepsilon_1)(d+\varepsilon_2)(d+\varepsilon_3)\left(\frac{A_2}{A_1} - 1\right) \\ &\quad - r_3\beta_3 d(d+\varepsilon_1)(d+\varepsilon_2)\left(\frac{A_2}{A_1} - 1\right). \end{aligned} \tag{47}$$

Thus, $S_2 - S_3 \leq 0$ implies that

$$\mathscr{A}_1 + \frac{B\beta_2}{r_3 d(d+\varepsilon_2)((\mathscr{A}_2/\mathscr{A}_1)-1)} \leq 1 + \frac{\beta_2(d+\varepsilon_3)}{r_3\beta_3 d}. \tag{48}$$

Consequently, $D^\alpha L_2 \leq 0$ when

$$\mathscr{A}_1 + \frac{B\beta_2}{r_3 d(d+\varepsilon_2)((\mathscr{A}_2/\mathscr{A}_1)-1)} \leq 1 + \frac{\beta_2(d+\varepsilon_3)}{r_3\beta_3 d}. \tag{49}$$

Clearly, $D^\alpha L_2 = 0$ if and only if $S = S_2$, $N = 0$, $T = T_2$, and $V = V_2$. Then the largest invariant set contained in $\{(S,N,T,V) | D^\alpha L_2(t) = 0\}$ is the singleton $\{E_2\}$. By LaSalle's invariance principle, we deduce that E_2 is globally asymptotically stable for

$$1 + \frac{\beta_2(d+\varepsilon_3)}{r_3\beta_3 d} \geq \mathscr{A}_1 + \frac{B\beta_2}{r_3 d(d+\varepsilon_2)((\mathscr{A}_2/\mathscr{A}_1)-1)}. \tag{50}$$

On the other side, the characteristic equation at E_2 is given by

$$(r_1\beta_1 S_2 - d - \varepsilon_1 - \lambda)g(\lambda) = 0, \tag{51}$$

where

$$g(\lambda) = (d + \beta_2 T_2 + \lambda)\left[(d + \varepsilon_2 + \lambda + \beta_3 V_2 - r_2\beta_2 S_2)(r_3\beta_3 T_2 - d - \varepsilon_3 - \lambda) - r_3\beta_3^2 T_2 V_2\right] + r_2\beta_2^2 S_2 T_2 (r_3\beta_3 T_2 - d - \varepsilon_3 - \lambda). \tag{52}$$

One of the eigenvalues of (51) is

$$\lambda_2 = r_1\beta_1 S_2 - d - \varepsilon_1 = r_1\beta_1 (S_2 - S_3). \tag{53}$$

We can observe from the proof of part (a) that $\lambda_2 > 0$ if

$$1 + \frac{\beta_2 (d + \varepsilon_3)}{r_3\beta_3 d} < \mathscr{A}_1 + \frac{B\beta_2}{r_3 d (d + \varepsilon_2)((\mathscr{A}_2/\mathscr{A}_1) - 1)}. \tag{54}$$

Thus, E_2 is unstable when

$$1 + \frac{\beta_2 (d + \varepsilon_3)}{r_3\beta_3 d} < \mathscr{A}_1 + \frac{B\beta_2}{r_3 d (d + \varepsilon_2)((\mathscr{A}_2/\mathscr{A}_1) - 1)}. \tag{55}$$

□

Theorem 6. *The partial success equilibrium E_3 is globally asymptotically stable if*

$$\mathscr{A}_2 > \mathscr{A}_1 + \frac{ABr_1\beta_1\beta_3}{d(d + \varepsilon_1)(d + \varepsilon_2)(d + \varepsilon_3)},$$
$$\mathscr{A}_1 + \frac{B\beta_2}{r_3 d (d + \varepsilon_2)((\mathscr{A}_2/\mathscr{A}_1) - 1)} > 1 + \frac{\beta_2 (d + \varepsilon_3)}{r_3\beta_3 d}. \tag{56}$$

Proof. Consider the following Lyapunov functional

$$L_3(t) = S_3\phi\left(\frac{S(t)}{S_3}\right) + \frac{1}{r_1}N_3\phi\left(\frac{N(t)}{N_3}\right) + \frac{1}{r_2}T_3\phi\left(\frac{T(t)}{T_3}\right) + \frac{1}{r_2 r_3}V_3\phi\left(\frac{V(t)}{V_3}\right). \tag{57}$$

Then

$$D^\alpha L_3 \le \left(1 - \frac{S_3}{S}\right)(A - dS - \beta_1 SN - \beta_2 ST) + \frac{1}{r_1}\left(1 - \frac{N_3}{N}\right)(r_1\beta_1 SN - (d + \varepsilon_1)N) + \frac{1}{r_2}\left(1 - \frac{T_3}{T}\right)(r_2\beta_2 ST - (d + \varepsilon_2)T - \beta_3 TV) + \frac{1}{r_2 r_3}\left(1 - \frac{V_3}{V}\right)(B + r_3\beta_3 TV - (d + \varepsilon_3)V). \tag{58}$$

By $A = dS_3 + \beta_2 S_3 T_3 + \beta_1 S_3 N_3$, $(\beta_3/r_2)T_3 V_3 = (d + \varepsilon_3/r_2 r_3)V_3 - (B/r_2 r_3)$, $\beta_1 S_3 N_3 = (d + \varepsilon_1/r_1)N_3$, and $\beta_2 S_3 T_3 = (d + \varepsilon_2/r_2)T_3 + (\beta_3/r_2)T_3 V_3$, we get

$$D^\alpha L_3 \le dS_3\left(1 - \frac{S_3}{S}\right)\left(1 - \frac{S}{S_3}\right) + \beta_2 S_3 T_3\left(2 - \frac{S_3}{S} - \frac{S}{S_3}\right) + \left(\beta_1 S_3 - \frac{d + \varepsilon_1}{r_1}\right)N + \left(\beta_2 S_3 - \frac{d + \varepsilon_2}{r_2} - \frac{\beta_3}{r_2}V_3\right)T + \beta_1 S_3 N_3\left(2 - \frac{S_3}{S} - \frac{S}{S_3}\right) + \frac{B}{r_2 r_3}\left(2 - \frac{V_3}{V} - \frac{V}{V_3}\right) = -(d + \beta_2 T_3 + \beta_1 N_3)\frac{(S - S_3)^2}{S} - \frac{B}{r_2 r_3}\frac{(V - V_3)^2}{VV_3}. \tag{59}$$

Therefore $D^\alpha L_3 \le 0$, with equality if and only if $S = S_3$ and $V = V_3$. By a simple computation, we show that $D^\alpha L_3 = 0$ if and only if $S = S_3$, $N = N_3$, $T = T_3$ and $V = V_3$. It follows from LaSalle's invariance principale that E_3 is globally asymptotically stable under the conditions that this point exists. ■ □

4. Numerical Simulations

In this section, we give some numerical simulations to illustrate and validate our theoretical results, and we present some biological interpretations. We choose the time interval from $t = 0$ to $t = 400$ with a step size $\Delta t = 0.1$. We take $A = 0.02$, $d = 0.02$, $B = 0.01$, $r_1 = 0.8$, and $r_3 = 0.5$. The parameters $\beta_1, \beta_2, \beta_3, \varepsilon_1, \varepsilon_2, \varepsilon_3$, and r_2 of model (1) are taken as free parameters.

First, we take $\beta_1 = 0.03$, $\beta_2 = 0.03$, $\beta_3 = 0.1$, $\varepsilon_1 = 0.04$, $\varepsilon_2 = 0.01$, $\varepsilon_3 = 0.008$, and $r_2 = 0.8$. These values give $\mathscr{A}_1 = 0.4$, $\mathscr{A}_2 = 0.8$, and $1 + (B\beta_3/(d + \varepsilon_2)(d + \varepsilon_3)) = 2.1905$. Thus, $\mathscr{A}_1 < 1$ and $\mathscr{A}_2 < 1 + (B\beta_3/(d + \varepsilon_2)(d + \varepsilon_3))$. According to Theorem 1, the equilibrium $E_0(1, 0, 0, 0.3571)$ is globally asymptotically stable which consists with our numerical simulation in Figure 1. This may reflect an extreme competition between normal and tumor cells, leading to the extinction of normal cells and eradicating tumor cells by the M1 virus, giving rise to patient death.

Next, we take $\beta_1 = 0.1$, $\beta_2 = 0.03$, $\beta_3 = 0.1$, $\varepsilon_1 = 0.008$, $\varepsilon_2 = 0.01$, $\varepsilon_3 = 0.006$, and $r_2 = 0.8$. For this case, we obtain

$$\mathscr{A}_1 = 2.8571,$$
$$\mathscr{A}_2 = 0.8,$$
$$\mathscr{A}_1 + \frac{ABr_1\beta_1\beta_3}{d(d + \varepsilon_1)(d + \varepsilon_2)(d + \varepsilon_3)} = 6.5201. \tag{60}$$

Thus we get

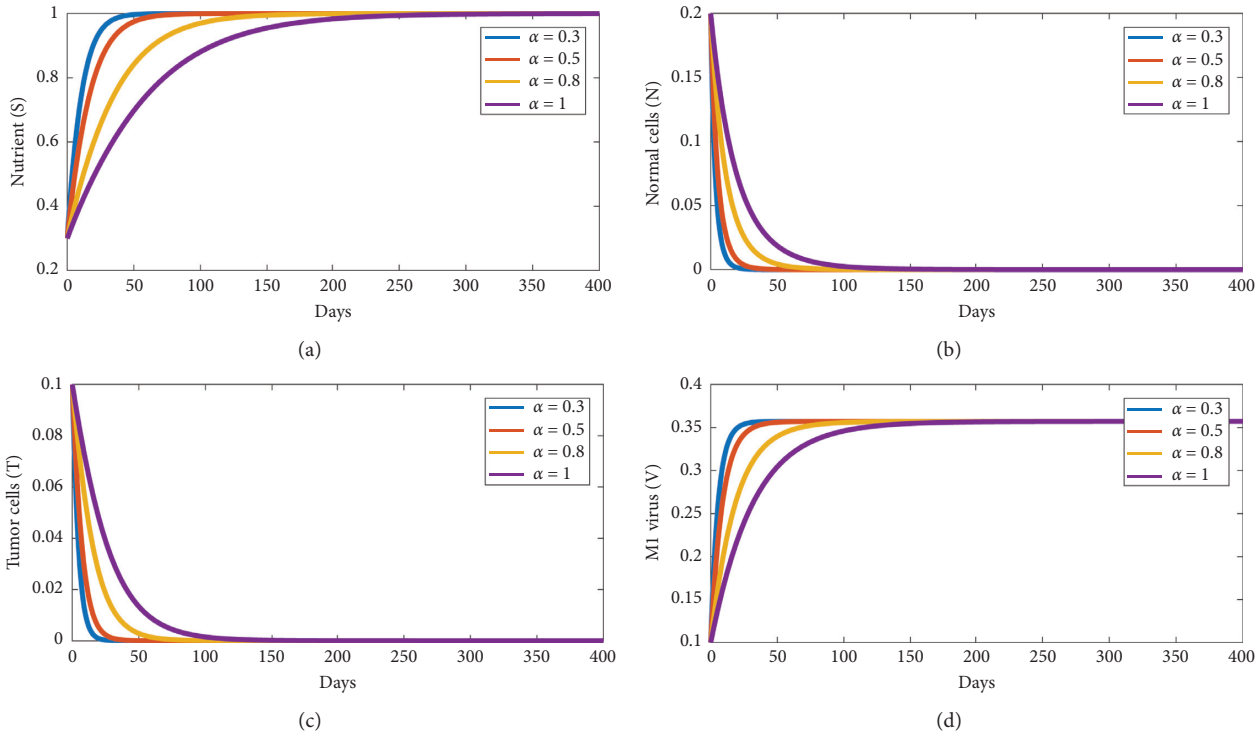

Figure 1: Stability of the competition-free equilibrium E_0.

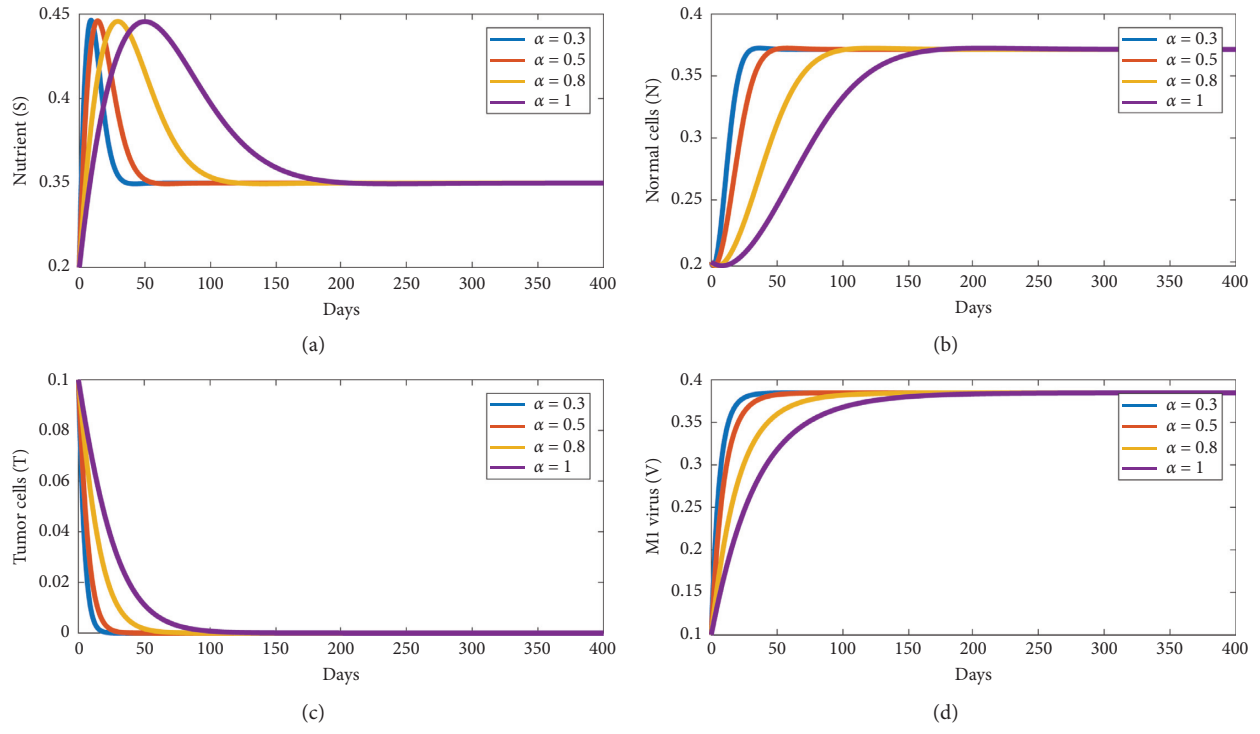

Figure 2: Stability of the tumor-free equilibrium E_1.

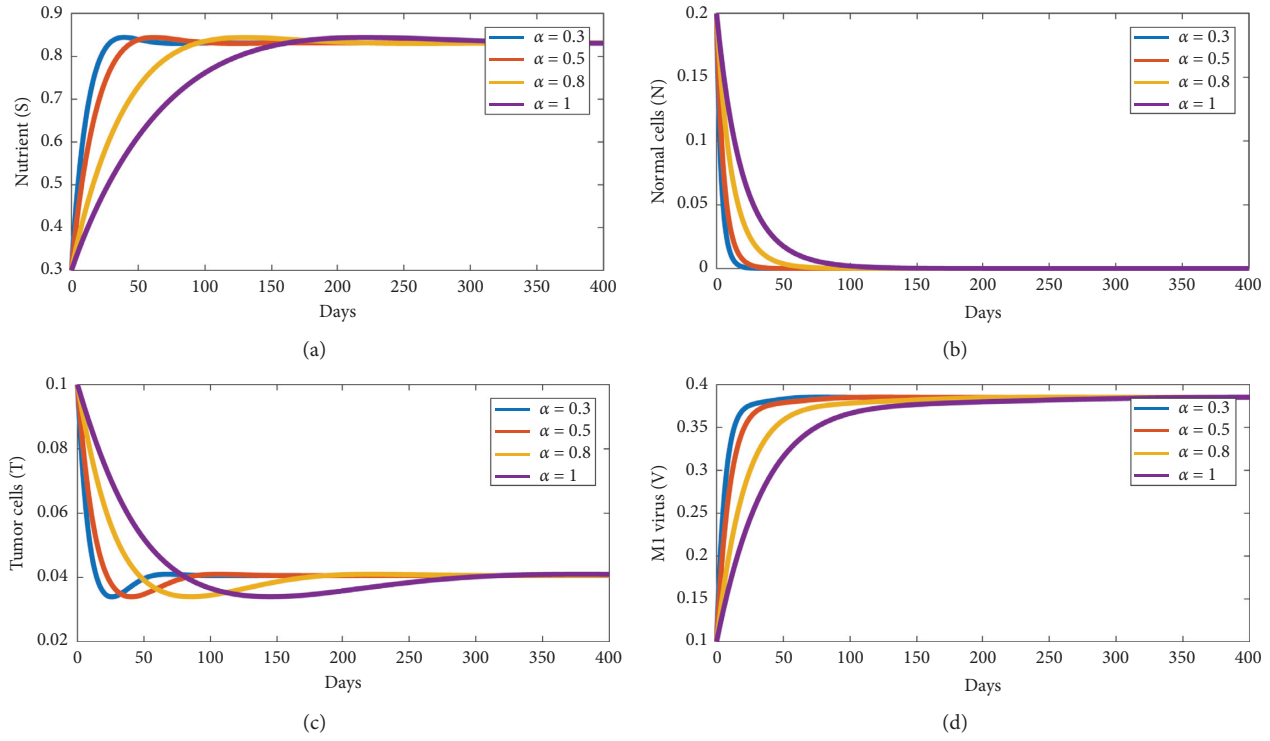

Figure 3: Stability of the treatment failure equilibrium E_2.

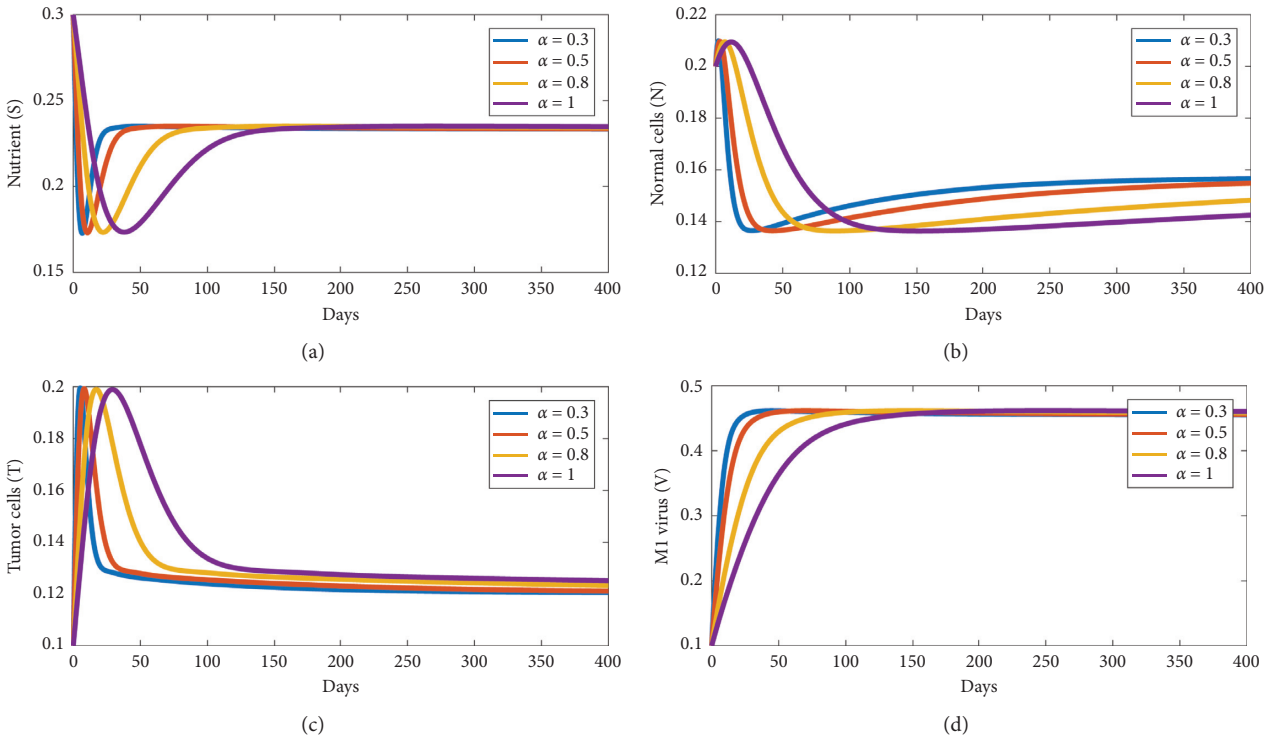

Figure 4: Stability of the partial success equilibrium E_3.

$$\mathscr{A}_1 > 1,$$
$$\mathscr{A}_2 \le \mathscr{A}_1 + \frac{ABr_1\beta_1\beta_3}{d(d+\varepsilon_1)(d+\varepsilon_2)(d+\varepsilon_3)}. \tag{61}$$

In agreement with Theorem 4, the tumor-free equilibrium $E_1(0.35, 0.3714, 0, 0.3846)$ is globally asymptotically stable as exhibited in Figure 2. In this situation, we notice that the M1 virotherapy successfully eliminates tumor cells, and then normal cells have been restored. Consequently, the patient's health will be improved.

In Figure 3, we assume that $\beta_1 = 0.03$, $\beta_2 = 0.1$, $\beta_3 = 0.1$, $\varepsilon_1 = 0.04$, $\varepsilon_2 = 0.008$, $\varepsilon_3 = 0.008$, and $r_2 = 0.8$. Thus,

$$\mathscr{A}_2 = 2.8571 > 2.2755 = 1 + \frac{B\beta_3}{(d+\varepsilon_2)(d+\varepsilon_3)},$$
$$\frac{\mathscr{A}_2}{\mathscr{A}_1} = 7.1429 > 1,$$
$$1 + \frac{\beta_2(d+\varepsilon_3)}{r_3\beta_3 d} = 3.8 \ge 0.9814 = \mathscr{A}_1 + \frac{B\beta_2}{r_3 d(d+\varepsilon_2)((\mathscr{A}_2/\mathscr{A}_1)-1)}. \tag{62}$$

We can see that the equilibrium $E_2(0.8313, 0, 0.0406, 0.385)$ is globally asymptotically stable that agrees with our result in Theorem 5. Biologically, our treatment fails in eliminating the tumor cells as that normal cells are lost. Hence, the patient's health is in danger.

Finally, we choose $\beta_1 = 0.15$, $\beta_2 = 0.35$, $\beta_3 = 0.1$, $\varepsilon_1 = 0.008$, $\varepsilon_2 = 0.008$, $\varepsilon_3 = 0.008$, and $r_2 = 0.9$. We get

$$\mathscr{A}_2 = 11.25 > 4.2857 = \mathscr{A}_1,$$
$$\mathscr{A}_2 > 9.7522 = \mathscr{A}_1 + \frac{ABr_1\beta_1\beta_3}{d(d+\varepsilon_1)(d+\varepsilon_2)(d+\varepsilon_3)}, \tag{63}$$
$$1 + \frac{\beta_2(d+\varepsilon_3)}{r_3\beta_3 d} = 10.8 < 11.978 = \mathscr{A}_1 + \frac{B\beta_2}{r_3 d(d+\varepsilon_2)((\mathscr{A}_2/\mathscr{A}_1)-1)}.$$

In agreement with Theorem 6, the equilibrium $E_3(0.2333, 0.1571, 0.1204, 0.455)$ is globally asymptotically stable as shown in Figure 4. Here, our treatment partially reduces tumor cells and increases normal cells' levels. However, the treatment cannot wholly eliminate tumor cells, but it can prolong the patient's life.

5. Conclusion

In this paper, we have studied the dynamics of an oncolytic M1 virotherapy model, considering the memory effect denoted by the Caputo fractional derivative. The well-posedness of the proposed model was proved through nonnegativity and boundedness of solutions. We found that the model has four possible equilibrium points, namely, the competition-free equilibrium E_0, the tumor-free equilibrium E_1, the treatment failure equilibrium E_2, and the partial success equilibrium E_3. By constructing suitable Lyapunov functionals, the global stability of E_0 is determined by two threshold parameters that are the absorbing number of nutrients by normal cells $\mathscr{A}_1$ and the absorbing number of nutrients by tumor cells $\mathscr{A}_2$, when $\mathscr{A}_1 \le 1$ and $\mathscr{A}_2 \le 1 + (B\beta_3/(d+\varepsilon_2)(d+\varepsilon_3))$, E_0 is globally asymptotically stable, and these conditions determine when normal and tumor cells are lost, which may not be useful to test the viability of treatment. The tumor-free equilibrium E_1 exists and is globally asymptotically stable if $\mathscr{A}_1 > 1$ and

$$\mathscr{A}_2 \le \mathscr{A}_1 + \frac{ABr_1\beta_1\beta_3}{d(d+\varepsilon_1)(d+\varepsilon_2)(d+\varepsilon_3)}, \tag{64}$$

and these conditions show that the M1 virus succeeds to eliminate the tumor, which is helpful in improving virotherapy. The treatment failure equilibrium E_2 exists and is globally asymptotically stable if

$$\mathscr{A}_2 > \mathscr{A}_1,$$

$$\mathscr{A}_2 > 1 + \frac{B\beta_3}{(d+\varepsilon_2)(d+\varepsilon_3)}, \tag{65}$$

$$1 + \frac{\beta_2(d+\varepsilon_3)}{r_3\beta_3 d} \geq \mathscr{A}_1 + \frac{B\beta_2}{r_3 d(d+\varepsilon_2)((\mathscr{A}_2/\mathscr{A}_1)-1)},$$

and these conditions refer to the failure of the treatment, as indicated by his name. The partial success equilibrium E_3 exists and is globally asymptotically stable if

$$\mathscr{A}_2 > \mathscr{A}_1 + \frac{ABr_1\beta_1\beta_3}{d(d+\varepsilon_1)(d+\varepsilon_2)(d+\varepsilon_3)},$$

$$1 + \frac{\beta_2(d+\varepsilon_3)}{r_3\beta_3 d} < \mathscr{A}_1 + \frac{B\beta_2}{r_3 d(d+\varepsilon_2)((\mathscr{A}_2/\mathscr{A}_1)-1)}. \tag{66}$$

These results indicate the partial success of M1 virus in decreasing tumor cells and increasing normal cells, which can reduce the tumor's size and stabilize the disease progression.

From the above analytical results, we remark that the Caputo fractional derivative's memory does not affect the stability analysis of equilibria. Based on the numerical simulations, we observe that the fractional order affects the speed of convergence and the time for arriving to equilibria (Figures 1–4).

The results obtained in this study are based on the fractional derivative in sense of Caputo with singular kernel. It will be more interesting to model the dynamics of oncolytic M1 virotherapy by using the new generalized fractional derivative with nonsingular kernel [10]. Moreover, we will extend our model presented in (1) by taking into account other biological factors such as diffusion [11, 12] and immunity [13, 14].

Data Availability

The data used to support the findings of this study are available from the corresponding author upon request.

Conflicts of Interest

The authors declare that they have no conflicts of interest.

References

[1] National Cancer Institute, "What is cancer?," 2019, https://www.cancer.gov/about-cancer/understanding/what-is-cancer.

[2] Cancer Research Institute, "How oncolytic virus therapy is changing cancer treatment?," 2012, https://www.cancerresearch.org/immunotherapy/treatment-types/oncolytic-virus-therapy.

[3] Y. Lin, H. Zhang, J. Liang et al., "Identification and characterization of alphavirus M1 as a selective oncolytic virus targeting ZAP-defective human cancers," *Proceedings of the National Academy of Sciences*, vol. 111, no. 42, pp. E4504–E4512, 2014.

[4] Z. Wang, Z. Guo, and H. Peng, "A mathematical model verifying potent oncolytic efficacy of M1 virus," *Mathematical Biosciences*, vol. 276, pp. 19–27, 2016.

[5] A. M. Elaiw, A. D. Hobiny, and A. D. Al Agha, "Global dynamics of reaction-diffusion oncolytic M1 virotherapy with immune response," *Applied Mathematics and Computation*, vol. 367, Article ID 124758, 2020.

[6] K. S. Cole, "Electric conductance of biological systems," *Cold Spring Harbor Symposia on Quantitative Biology*, vol. 1, pp. 107–116, 1933.

[7] A. Boukhouima, K. Hattaf, and N. Yousfi, "Dynamics of a fractional order HIV infection model with specific functional response and cure rate," *International Journal of Differential Equations*, vol. 2017, Article ID 8372140, 8 pages, 2017.

[8] C. Vargas-De-León, "Volterra-type Lyapunov functions for fractional-order epidemic systems," *Communications in Nonlinear Science and Numerical Simulation*, vol. 24, no. 1–3, pp. 75–85, 2015.

[9] J. Huo, H. Zhao, and L. Zhu, "The effect of vaccines on backward bifurcation in a fractional order HIV model," *Nonlinear Analysis: Real World Applications*, vol. 26, pp. 289–305, 2015.

[10] K. Hattaf, "A new generalized definition of fractional derivative with non-singular kernel," *Computation*, vol. 8, no. 2, pp. 1–9, 2020.

[11] K. Hattaf and N. Yousfi, "Global stability for fractional diffusion equations in biological systems," *Complexity*, vol. 2020, Article ID 5476842, 6 pages, 2020.

[12] A. M. Elaiw and A. D. Al Agha, "A reaction-diffusion model for oncolytic M1 virotherapy with distributed delays," *The European Physical Journal Plus*, vol. 135, no. 1, pp. 1–40, 2020.

[13] A. M. Elaiw and N. H. AlShamrani, "Analysis of a within-host HIV/HTLV-I co-infection model with immunity," *Virus Research*, vol. 295, Article ID 198204, 2021.

[14] K. Hattaf, "Global stability and Hopf bifurcation of a generalized viral infection model with multi-delays and humoral immunity," *Physica A: Statistical Mechanics and Its Applications*, vol. 545, Article ID 123689, 2020.